frontiers | Research Topics

Nutrition and flavor during food processing: Change patterns and mechanisms

Edited by
Peng Wang, Yu-Chung Chang and Dandan Pu

Published in
Frontiers in Nutrition

ISSN 1664-8714
ISBN 978-2-8325-4878-3
DOI 10.3389/978-2-8325-4878-3

About Frontiers

Frontiers is more than just an open access publisher of scholarly articles: it is a pioneering approach to the world of academia, radically improving the way scholarly research is managed. The grand vision of Frontiers is a world where all people have an equal opportunity to seek, share and generate knowledge. Frontiers provides immediate and permanent online open access to all its publications, but this alone is not enough to realize our grand goals.

Frontiers journal series

The Frontiers journal series is a multi-tier and interdisciplinary set of open-access, online journals, promising a paradigm shift from the current review, selection and dissemination processes in academic publishing. All Frontiers journals are driven by researchers for researchers; therefore, they constitute a service to the scholarly community. At the same time, the *Frontiers journal series* operates on a revolutionary invention, the tiered publishing system, initially addressing specific communities of scholars, and gradually climbing up to broader public understanding, thus serving the interests of the lay society, too.

Dedication to quality

Each Frontiers article is a landmark of the highest quality, thanks to genuinely collaborative interactions between authors and review editors, who include some of the world's best academicians. Research must be certified by peers before entering a stream of knowledge that may eventually reach the public - and shape society; therefore, Frontiers only applies the most rigorous and unbiased reviews. Frontiers revolutionizes research publishing by freely delivering the most outstanding research, evaluated with no bias from both the academic and social point of view. By applying the most advanced information technologies, Frontiers is catapulting scholarly publishing into a new generation.

What are Frontiers Research Topics?

Frontiers Research Topics are very popular trademarks of the *Frontiers journals series*: they are collections of at least ten articles, all centered on a particular subject. With their unique mix of varied contributions from Original Research to Review Articles, Frontiers Research Topics unify the most influential researchers, the latest key findings and historical advances in a hot research area.

Find out more on how to host your own Frontiers Research Topic or contribute to one as an author by contacting the Frontiers editorial office: frontiersin.org/about/contact

Nutrition and flavor during food processing: Change patterns and mechanisms

Topic editors

Peng Wang — Shaanxi Normal University, China

Yu-Chung Chang — Washington State University, United States

Dandan Pu — Beijing Technology and Business University, China

Citation

Wang, P., Chang, Y.-C., Pu, D., eds. (2024). *Nutrition and flavor during food processing: Change patterns and mechanisms*. Lausanne: Frontiers Media SA. doi: 10.3389/978-2-8325-4878-3

Table of contents

frontiers | Frontiers in Nutrition

TYPE Original Research
PUBLISHED 23 June 2023
DOI 10.3389/fnut.2023.1198456

OPEN ACCESS

EDITED BY
Dandan Pu,
Beijing Technology and Business University, China

REVIEWED BY
Jie Luo,
Hunan Agricultural University, China
Liana Claudia Salanta,
University of Agricultural Sciences and Veterinary Medicine Cluj-Napoca, Romania
Malgorzata Ziarno,
Warsaw University of Life Sciences, Poland

*CORRESPONDENCE
Yongqiang Cheng
✉ chengyq@cau.edu.cn
Tianying Yu
✉ tyyu@ytu.edu.cn

RECEIVED 01 April 2023
ACCEPTED 29 May 2023
PUBLISHED 23 June 2023

CITATION
Gan J, Kong X, Wang K, Chen Y, Du M, Xu B, Xu J, Wang Z, Cheng Y and Yu T (2023) Effect of fermentation using different lactic acid bacteria strains on the nutrient components and mineral bioavailability of soybean yogurt alternative.
Front. Nutr. 10:1198456.
doi: 10.3389/fnut.2023.1198456

Effect of fermentation using different lactic acid bacteria strains on the nutrient components and mineral bioavailability of soybean yogurt alternative

Jing Gan[1], Xiao Kong[1], Kuaitian Wang[1,2], Yuhang Chen[1,2], Mengdi Du[1], Bo Xu[1], Jingru Xu[1], Zhenhua Wang[1], Yongqiang Cheng[2]* and Tianying Yu[1]*

[1]Center for Mitochondria and Healthy Aging, College of Life Science, Yantai University, Yantai, Shandong, China, [2]Beijing Key Laboratory of Functional Food from Plant Resources, College of Food Science and Nutrition Engineering, China Agricultural University, Beijing, China

Introduction: Analysis of the composition of yogurt alternatives (YAs) during fermentation provides critical information for evaluating its quality and nutritional attributes.

Method: We investigated the effects of homotypic (HO) and heterotypic (HE) lactic acid bacteria on the nutritional and mineral bioavailabilities of soybean YA (SYA) during fermentation.

Result: The acidic amino acid (Glu, Asp) and organic acid contents in HO-fermented YA were increased from 2.93, 1.71, and 7.43 mg/100 g to 3.23, 1.82, and 73.47 mg/100 g, respectively. Moreover, both HO and HE lactic acid bacteria fermentation enhanced mineral absorptivity. They altered the molecular speciation of minerals from a large molecular type (2,866 Da) to a small molecular type (1,500 Da), which was manifested in a time-dependent manner. Furthermore, YA substantially increased the bone mass in a zebrafish osteoporosis model, further highlighting the potential of lactic acid bacterial fermentation for mineral bioavailability.

Discussion: This study provides a foundation for understanding the effects of fermentation conditions on the composition and bioavailability of minerals in YA and can assist in its production.

KEYWORDS

mineral, speciation analysis, absorptivity, zebrafish model, fermentation, yogurt alternative

1. Introduction

Soybean milk, obtained by crushing and pressing the water-soaked soybean, is a popular soybean-derived food (1). Daily intake of soybean milk has a favorable effect on cardiovascular, glycemic status, and blood pressure (2, 3). Soybean milk, is considered an alternative to cow's milk and is widely consumed in populations suffering from lactose intolerance and milk proteins allergies (4).

Soybean milk is a primary source of mineral elements that play essential roles in sustaining life and supporting fundamental body functions (5–10). For example, calcium regulates the

activity of intracellular enzymes and participates in neuronal conduction via ion channels. Magnesium is required for enzymatic activity and is critical for DNA and RNA synthesis, reproduction, and protein synthesis. Ferric iron is a trace mineral involved in oxygen transport and cellular respiration. Calcium, magnesium, and phosphorus are involved in bone tissue formation. Generally, efficient absorption is essential for performing functional activities in the body (11), but the speciation of minerals limits their absorption in the gastrointestinal environment (12). A previous study demonstrated that the absorptivity differed among the carbonate, pyruvate, and citrate/malate formulations of calcium. Among these, the carbonate and pyruvate formulations were more effective in calcium supplementation (13). Several studies have shown that organic trace elements improve membrane permeability at a higher rate than inorganic forms due to their higher lipophilicity, making them better absorbed and utilized (14). However, Liu et al. reported that bioactive gelatin peptide-chelated calcium had a higher utilization rate and absorptivity than inorganic and organic calcium (15). Nonetheless, studies have also shown that major anti-absorptive factors such as phytate, oxalate, uric acid, and dietary fiber in soy milk decrease the absorption of the minerals (16). Furthermore, (17-18) showed that minerals in food, such as Na and K, Ca and Mg, Mn and Fe, and Fe and Cu, might inhibit their absorption and utilization rates. This mutual inhibition effect between minerals has been speculated to be related to their shared absorption through cell membranes. Therefore, understanding the forms of mineral elements in foods can improve their bioavailability of mineral elements.

In recent years, yogurt alternatives fermented by lactic acid bacteria have effectively enhanced the number of bioactive ingredients and flavors in soy milk and have attracted increasing attention. In our preliminary experiments, we found that the absorption rate of calcium significantly increased in yogurt alternatives, which could be related to changes in the mineral element morphology during fermentation. However, it is not clear whether the absorptivity of other mineral elements besides calcium increases during fermentation. Furthermore, the relationship between bacterial strains, mineral morphology, and absorption remains unclear. Health problems are highly related to diet and nutritional habits (19). Therefore, we speculated that systematic research to elucidate the effects of speciation on mineral absorption in yogurt alternatives produced using different strains could provide better insights.

To test this speculation, the present study aimed to investigate the absorptivity and speciation of minerals in YAs produced using different strains of lactic acid bacteria. Here, we prepared two YA samples by fermenting soybean milk with two different lactic acid bacteria and analyzed their absorptivity *in vitro* and *in vivo*. The molecular weight distribution and the speciation of minerals in the YA samples were characterized by protein structural changes, amino acid production of the strains, and the release of organic acids during fermentation.

2. Materials and methods

2.1. Starter cultures and soybean

Pure freeze-dried thermophilic yogurt cultures for the direct-to-vat set form, *Lactiplantibacillus plantarum* CICC 21022 and *Enterococcus faecalis* ATCC19433were screened in our laboratory. Briefly, 5 g of pickled Chinese cabbage was washed five times with sterile water. Serial decimal dilutions were obtained, plated on MRS agar supplemented with 2% calcium carbonate, and then incubated under aerobic and anaerobic conditions at 37°C for 48 h. Gram-positive, catalase-negative isolates were considered presumptive lactic acid bacteria. Subsequently, the 16S rDNA segments were amplified and sequenced to identify the structure of lactic acid bacteria. Soybean was purchased from the Chinese Academy of Agricultural Sciences. Fetal bovine serum (FBS), Dulbecco's Modified Eagle's medium (DMEM), and other reagents used for cell culture were purchased from Corning (NY, USA). All other reagents were either analytical grade or pure (Solarbio Life Sciences, Beijing, China).

2.2. Preparation of soybean milk and soy yougurt

YA was successfully prepared using a previously reported method (20) with slight modifications. Briefly, soybeans were soaked in water at a ratio of 1:3 (soybean: water) at room temperature for 12 h, followed by hot grinding (a volume 12 times higher than that for soybeans) and remove soybean residue through a 100 mesh sieve. After adding 2% (w/v) sugar in 100 ml soybean milk, the soybean milk was sterilized using high-pressure sterilization at 220 bar for 15 min. For the fermentation process, the *Lactiplantibacillus plantarum* CICC 21022 and *Enterococcus faecalis* ATCC19433 were cultured with 7.512×10^7 CFU/ml, following incubate at 37°C at facultative anaerobic conditions for 12 h, the SYA was collected and stored at −20°C for subsequent use.

2.3. Microbiological analysis

The amount [colony-forming units per ml (CFU/ml)] of *L. plantarum* and *E. faecalis* populations was determined by plating the aliquots of the serial dilution on MRS agar, and incubating at 37°C for 48 h at facultative anaerobic conditions. The aliquots of the serial dilution was plated on MRS agar, and incubated at 37°C for 48 h under the conditions described above. The colony-forming units per ml (CFU/ml) of *L. plantarum* and *E. faecalis* populations was determined following the official microbiological methods.

2.4. Analysis of protein composition during fermentation

2.4.1. Detection of protein content and amino acid profile

The total soluble protein content was determined using bicinchoninic acid (BCA) assay. All samples were combined with 6 M HCl and left to hydrolyze for 4 h at 110°C. An automatic amino acid analyzer (835–50, Hitachi LA8080) was used to determine the amino acid composition. Briefly, 1 g of soybean milk or YAs fermented by different lactic acid bacteria was dissolved in 25 ml ultrapure water. Subsequently, 0.5 ml potassium ferrocyanide (106 g/L) and zinc sulfate (300 g/L) each were added to the solution and allowed to flow statically for 1 h. The separation was performed using a CAPCELL PAK C18

column (150 mm × 4.6 mm × 3 μm) and sodium dihydrogen phosphate solution (20 mmol/L) mobile phase under the following conditions: flow rate, 0.9 ml/min; detection wavelength, 210 nm; column temperature, 30°C; sample injection volume, 10 μl. The sample values were determined based on a calibration curve developed using five standards (Asp, Glu, Leu, His, and Arg).

2.4.2. Sodium dodecyl sulfate-polyacrylamide gel electrophoresis

SDS-PAGE was performed following a previously reported method (21) to analyze the primary structure of the protein. PAGE was performed using 12% concentrated and 4% separated glues at a loading amount of 20 μl.

2.5. Determination of sugar and organic acid content during fermentation

2.5.1. Determination of sugar content

Changes in free oligosaccharide content were detected using ion chromatography. Briefly, 0.2 g soybean yogurt was dissolved in 10 ml water and diluted to 25 ml by water. The chromatographic separation was performed using a DIONEX ICS-3000 USA system fitted with a Carbo PacTMPA20 3*150 mm analytical column (Diane Corporation of the United States), a pulse ampere detector, and gold electrode under the following conditions: Eluent solution, 250 mM NaOH; flow rate, 0.5 ml/min; injection volume, 10 μl. The separation was carried out under gradient elution conditions using pure water (solvent A) and 250 mM NaOH (Solvent B) as follows: 0–20 min, 94% A, 6% B; 20–20.1 min, 20% A, 80% B; 20.1–30 min, 20% A, 80% B, 30.1–40 min, 94% A, 6% B.

2.5.2. Determination of organic acid content

The organic acid content was determined using HPLC. The chromatography was performed using a CAPCELL PAK C18 (150 mm × 4.6 mm × 3 μm) LC column and sodium dihydrogen phosphate solution (20 mmol/L) at a flow rate of 0.9 ml/min as the mobile phase. A sample volume of 10 μl was injected, and the signals were detected using a UV detector at 215 and 210 nm. Oxalic, tartaric, lactic, acetic, citric, succinic, malic, and ascorbic acids were used as standard solutions to develop the calibration curve. Briefly, One gram sample was dissolved in 15 ml buffer containing 0.5 ml potassium ferrocyanide (106 g/L) and 0.5 ml zinc sulfate (300 g/L) and allowed to stand for 1 h at room temperture. Afterward, the sample was centrifuged at 7104 × *g* and analyzed, individually.

2.6. Determination of the content of minerals, their speciation, and absorptive rate during fermentation

2.6.1. Determination of mineral (Ca, Zn, Mg, Fe, P) content of soy milk during fermentation

Soybean milk or YA samples (0.20 g) were weighed (accurate to 0.0001 g), placed in a Teflon (Polytetrafluoroethylene; PTFE) tank, combined with concentrated HNO_3 (3:1), and left to stand for 4 h. Then, the PTFE tank was placed into a stainless steel coat and heated for 4 h at 165°C. The Ca, Zn, Mg, Fe, and P contents of the samples were determined using inductively coupled atomic emission spectrometry (ICP-AES; Prodigy xp,GmbH). The experimental conditions, including the auxiliary and gas flow rates, cooling gas flow, and generator power, were 0.8 L/min, 0.8 L/min, 12 L/min, and 1.4 kW, respectively.

2.6.2. Mineral speciation analysis of soybean milk during fermentation

HPLC, in combination with inductively coupled plasma-mass spectrometry (ICP-MS), was used to detect mineral and trace element species in YA samples during fermentation. Samples were separated using an XBridge Protein BEH SEC 200 Å column (7.8 mm × 300 mm × 3.5 μm). Briefly, the samples (50 mg) were dissolved in 0.03 mol/L Tris–HCl buffer (pH 7.4) and filtered using a 0.45 m filter membrane. The sample (20 μl) was injected and separated using – mobile phase at a flow rate of 0.5 ml/min; the detection wavelength was 214 nm (UV detector). The analysis was performed with external calibration by developing the calibration curve derived from five standards: BSA (66.4 kDa), trypsin inhibitor (20.1 kDa), insulin (5.8 kDa), VB12 (1.35 kDa), and L-tyrosine (0.187 kDa). The molecular weight of the sample peaks was determined based on that of the standards.

2.6.3. Cell culture, transport assays, and calculation of apparent permeability

The human colon carcinoma cell line, Caco-2, was used as an intestinal barrier model. Transport assays were performed in Transwell systems using the method described by Wang et al. (22). Three transport sides were tested: apical, intermediate, and basal. The Transwell layer was rinsed twice with standard solutions of Hank's balanced salt solution (HBSS) without magnesium and calcium. Caco-2 cells were laid as the intermediate layer and washed twice using HBSS. Subsequently, 1.5 and 0.5 ml of HBSS were added on the basolateral and apical sides, respectively, and the cells were preincubated for 30 min at 37°C.The absorption assays were performed by adding 0.5 ml sample fractions (0.1 mg/ml) and replenishing the HBSS on the apical side. Afterward, the cells were cultured at 37°C for 2 h. The apical, intermediate, and basal fluids were collected according to the method described in Table 1. The mineral content was determined using ICP-AES (ICAP-6300, Thermo Electron Corporation, USA). The calcium absorption was calculated using the following formula:

$$\text{Absorption of mineral}(\%) = \left[\begin{array}{l}(C_{Basal} \times V_{Basal}) + \\ (C_{Intermediate} \times V_{Intermediate}) / \\ (C_{Apical} \times V_{Apical}) + \\ (C_{Basal} \times V_{Basal}) + \\ (C_{Intermediate} \times V_{Intermediate})\end{array}\right] \times 100\% \quad (1)$$

C_{Basal} indicates the calcium concentration at different time points on the basal interior side; V_{Basal} denotes the volume corresponding to the time points on the inner basal side; $C_{Intermediate}$ and C_{Apical} represent the mineral concentrations on the middle and apical sides, respectively; $V_{Intermediate}$ and V_{Apical} denote the corresponding volumes at the middle and apical sides, respectively.

TABLE 1 Changes of free oligosaccharide in soybean milk fermented by *Lactiplantibacillus plantarum* CICC21022 and *Enterococcus faecalis* ATCC19433.

Free oligosaccharide	Composition (%)		
	Soybean milk	Yogurt alternative$_{(LP)}$	Yogurt alternative$_{(EF)}$
Glucose	0.02	0.03	0.03
Sucrose	47.29	26.47	28.05
Fructose	0.03	0.04	0.04
Raffinose	0.09	0.14	0.21
Stachyose	23.00	19.80	15.53

2.6.4. Absorptivity clustering analysis of minerals in YA

We obtained the data on mineral absorptivity, Bacterial strain, and mineral type were collected and subjected to orthogonal transformation analysis using SPSS 16 software. A group of variables speculated to be correlated was converted into linearly unrelated variables to reduce the dimension while maintaining the characteristics to which the variance contributes the most. Then, we performed principal component analysis (PCA) using the 'vegan' package based on the Bray–Curtis distance on the R platform to analyze the correlations and trends of the data. The outputs were obtained in a grid, and the color-synthesis results of the first and second principal components were previewed.

2.7. Evaluation of fermentation broth against glucocorticoid-induced osteoporosis using Zebrafish larva

2.7.1. Zebrafish maintenance and fermentation broth treatment

All the procedures were performed in accordance with the National Institutes of Health Guidelines for the Care and Use of Laboratory Animals. Adult zebrafish AB strains were kept at 28.5°C under a normal light/dark cycle of 14 h/10 h at 28°C for natural maturation. Zebrafish embryos were cultured in 6-well plates. The collected embryos were placed in fish water containing 5.0 mM NaCl, 0.17 mM KCl, 0.33 mM $CaCl_2$, and 0.33 mM $MgSO_4$ and treated with 0.1% DMSO (vehicle), 25 μM prednisolone (model), or co-incubated 3.3–30 μM CBP, or 0.308 μM alendronate (positive control) after 3 pdf till 7 dpf. On pdf 7, larvae were collected for skeletal staining and behavioral analysis.

2.7.2. Vital skeletal staining and image acquisition

The fish at 7 dpf were vitally stained with 0.2% calcein solution (pH adjusted to 7.0–7.5) for 5 min in the dark. Next, fish were rinsed thrice for 5 min with the system water, anesthetized with 0.016% MS-222, and fixed in 3% methylcellulose. At the end of the treatment, the regenerated bone areas on the larvae were visualized using a fluorescence microscope (Leica DMi8, Wetzlar, Germany), and images were captured using digital cameras (10X objective, and Retiga 2000R). The relative fluorescence intensity (RFI) of skull bone mass per zebrafish was determined using ImageJ software (n = 6).

2.8. Statistical analyses

All tests were performed at least in triplicates in six independent experiments. The results were subjected to statistical analysis using one-way ANOVA with Duncan's posthoc test for comparison with the vehicle. All figures were drawn using GraphPad Prism 5.0 (GraphPad Software, San Diego, CA, USA) and Excel (Microsoft, San Francisco, CA, USA). Differences at a p-value of <0.05 were considered statistically significant.

3. Results

3.1. Acidity of YA, free oligosaccharide, and availability of lactic acid bacteria culture during fermentation

Changes in pH during fermentation with the two different strains are shown in Figure 1. The largest decrease in pH occurred at 3 h, and the pH range of 4.6–4.7 was obtained after 8 h of fermentation. This phenomenon might be due to the growth of *L. plantarum* and *E. faecalis*, which produce more lactic acid from sugar (23). Compared to *E. faecalis*, *L. plantarum* showed faster acid-producing characteristics. To improve the growth characteristics of lactic acid bacteria during the initial fermentation stage, sucrose was added to soybean milk. The total sugar content in the YA at 0 h was higher than that in soybean milk. However, the proportion of threose decreased, possibly due to the decomposition of raffinose and stachyose. As the pH decreased, *L. plantarum* and *E. faecalis* grew faster, and *L. plantarum* showed higher acid tolerance than *E. faecalis*. The lactic acid contents of soybean milk samples containing different strains after 12 h of fermentation are shown in Figure 2. Increasing the fermentation time significantly affected the formation of acetic acid in soybean milk. Furthermore, consistent with the changes in pH, the lactic acid content of *L. plantarum* was higher than that of *E. faecalis*.

3.2. Effect of fermentation on YA components

3.2.1. Effect of fermentation on protein composition

The analysis of the changes in soluble protein in YA fermented by *L. plantarum* revealed a sharp decrease in the amount of soluble protein from 20.3016 to 1.71 μg/ml at first 4 h, which reached 1.33 μg/ml at rock bottom. Furthermore, SDS-PAGE analysis to characterize the polypeptide composition of the globulin fractions identified 7S as the main fraction with α (67 kDa), α′(71 kDa), and β (45–50 kDa) subunits (Figure 3). In addition, 11S, with AS (32 kDa) and BS (28 kDa) subunits, was also identified as a minor fraction. The

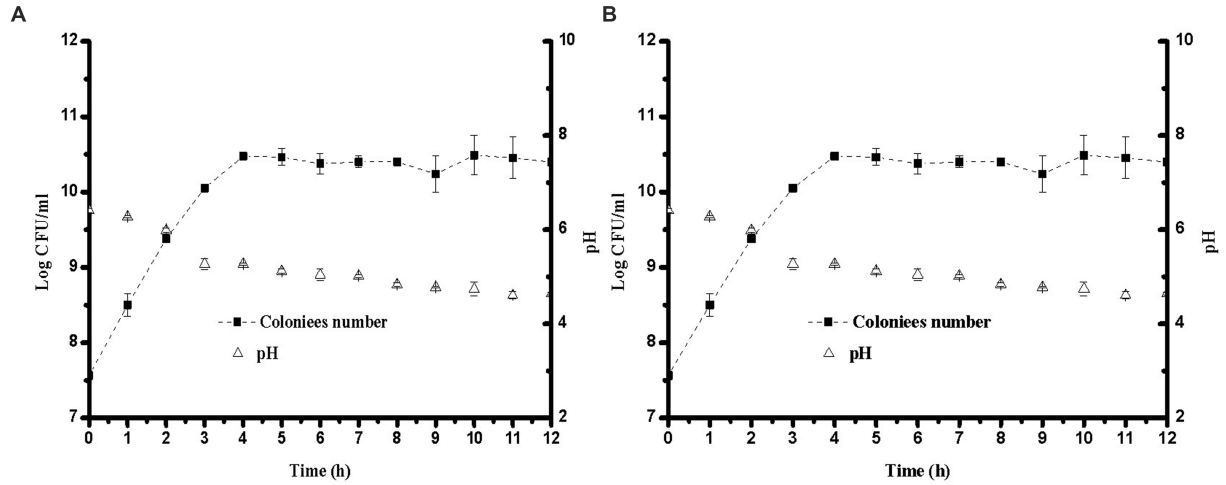

FIGURE 1
Growth curve and pH for different lactobacillus in soybean milk at 37°C over 12 h. **(A)** *Lactiplantibacillus plantarum* CICC 21022; **(B)** *Enterococcus faecalis* ATCC19433.

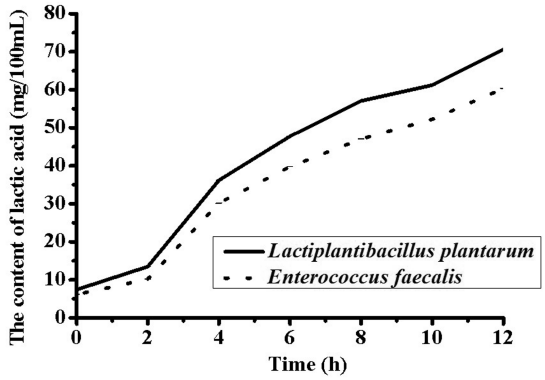

FIGURE 2
Changes of Organic acid in soy yogurt fermented by *Lactiplantibacillus plantarum* CICC 21022 and *Enterococcus faecalis* ATCC19433.

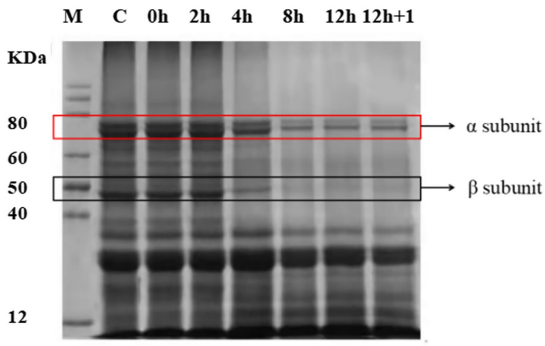

FIGURE 3
Sodium dodecyl sulfate-polyacrylamide gel electrophoresis (SDS-PAGE) analysis of the changes of soybean milk protein during fermentation by *Lactiplantibacillus plantarum* CICC 21022.

SDS-PAGE patterns did not change until 4 h of fermentation, indicating that the subunits remained intact within this time point. However, at 8 h, the band intensities of 7S and 11S globulins decreased slightly. After 12 h, the 7S globulin bands largely disappeared, and the basic subunit of 11S globulin was fainter than the initial one. These changes in protein content and structure observed in *L. plantarum*-fermented SYA were similar to those in *E. faecalis*-fermented SYA (Supplementary Figure S1).

3.2.2. Effect of fermentation on amino acid composition

The amino acid order and content determine the shape and functional activity of the protein (24). Changes in amino acid composition were analyzed to explore the relationship between the mineral components and bioactivity during fermentation. As shown in Table 2, the content of individual amino acids increased after fermentation, among which Glu was the most abundant, followed by Asp. The acidic amino acid contents of Glu and Asp in soybean milk and YA fermented with *L. plantarum* increased by 2.93 to 3.23 and 1.71 to 1.82, respectively. These changes were also observed in soybean milk and SYA fermented with *E. faecalis*.

3.3. Contribution of fermentation to mineral absorptivity

3.3.1. Analysis of total mineral absorption ratio

Changes in the total mineral absorption ratio during fermentation are shown in Figure 4. For *L. plantarum* and *E. faecalis* inoculations, the detection of total minerals was most evident in a time-dependent manner in all treatment groups. Both *L. plantarum* and *E. faecalis* significantly increased the absorption rate from 4 to 8 h and reached a maximum at 12 h, with a calcium absorption rate of 60%. At 4 h, the calcium absorption rate of *L. plantarum*-fermented YA was higher (25%) than that of *E. faecalis*-fermented YA (21%). A similar trend of increased absorption in *L. plantarum*-fermented YA compared to that

TABLE 2 The composition of amino acid in soybean milk and Yogurt alternatinve fermented by *Lactiplantibacillus plantarum* CICC21022 and *Enterococcus faecalis* ATCC19433 for 12h.

Amino acid	Composition (%)		
	Soybean milk	Yogurt alternative$_{(LP)}$	Yogurt alternative$_{(EF)}$
Asp	17.19	18.19	18.92
Thr	5.06	5.8	5.58
Ser	6.63	7.43	7.29
Glu	29.31	32.34	32.50
Gly	5.61	6.36	6.21
Ala	5.65	6.41	6.27
Cys	0.72	0.99	0.71
Val	6.43	7.23	7.16
Met	1.30	1.62	1.43
Ile	6.27	7.08	6.99
Leu	10.22	11.53	11.40
Tyr	3.66	4.59	3.34
Phe	7.10	7.93	7.88
Lys	8.54	9.53	9.49
His	3.56	3.98	3.93
Ar	12.72	11.13	11.86
Pro	6.96	7.84	8.05

A. Yogurt Alternative$_{(LP)}$: the yogurt alternative feremened by *Lactobacillus plantarum* for 12 h; B. Y ogurt Alternative$_{(EF)}$: the yogurt alternative feremened by *Enterococcus faecalis* for 12 h.

in *E. faecalis*-fermented YA was observed in absorption of ferrum, zinc, magnesium, and phosphorus, which declined up to 2 h, and increased thereafter.

3.3.2. Analysis of contribution to mineral absorption by different bacteria

Different stains Absorptivity clustering analysis of minerals in soy yogurt fermented by different strains is shown in Figure 5A. Figure 5B shows the distribution of the samples as a function of the two principal components extracted by PCA analysis, which accounted for 96.49%, presenting the preliminary information about the sample. Additionally, there were a few differences between calcium absorption and iron absorption according to the apparent overlap. The other elements were far apart, and the parallelism of each element was close, demonstrating a significant difference and comprehensive repetition. In the correlation analysis (Figure 5C), different degrees of correlation were observed among various attributes. The pH values were negatively correlated with other parameters. At the same time, the absorption rate of minerals was positively correlated with fermentation time, number of colonies, and organic acid content. These results agree with the absorption ratio data. In summary, the absorption profiles of YAs can be comprehensively evaluated by measuring these components.

3.3.3. Analysis of mineral speciation

The molecular weight distribution and morphology distribution of minerals in soybean milk during fermentation by *L. plantarum* are shown in Figure 6. Most molecules were isolated at 11.56 min with a total molecule weight of 170 kDa. The molecular weight of

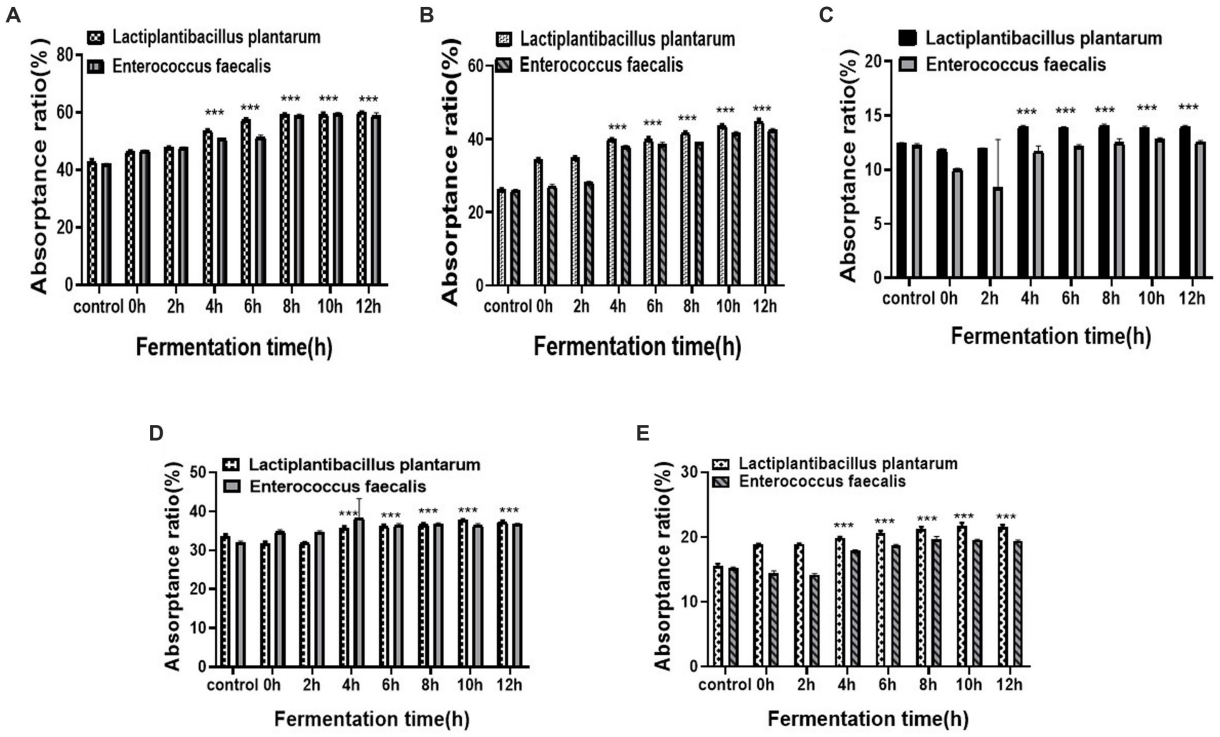

FIGURE 4
Total mineral absorptance ratio over different fermentation times **(A)** Calcium; **(B)** Ferrum; **(C)** Magnesium; **(D)** Zinc; **(E)** Phosphorus. Data are presented as means ± SEDs and analyzed by one-way ANOVA followed by Tukey's multiple comparison test $^{**}p < 0.01$, and $^{***}p < 0.001$ vs. control.

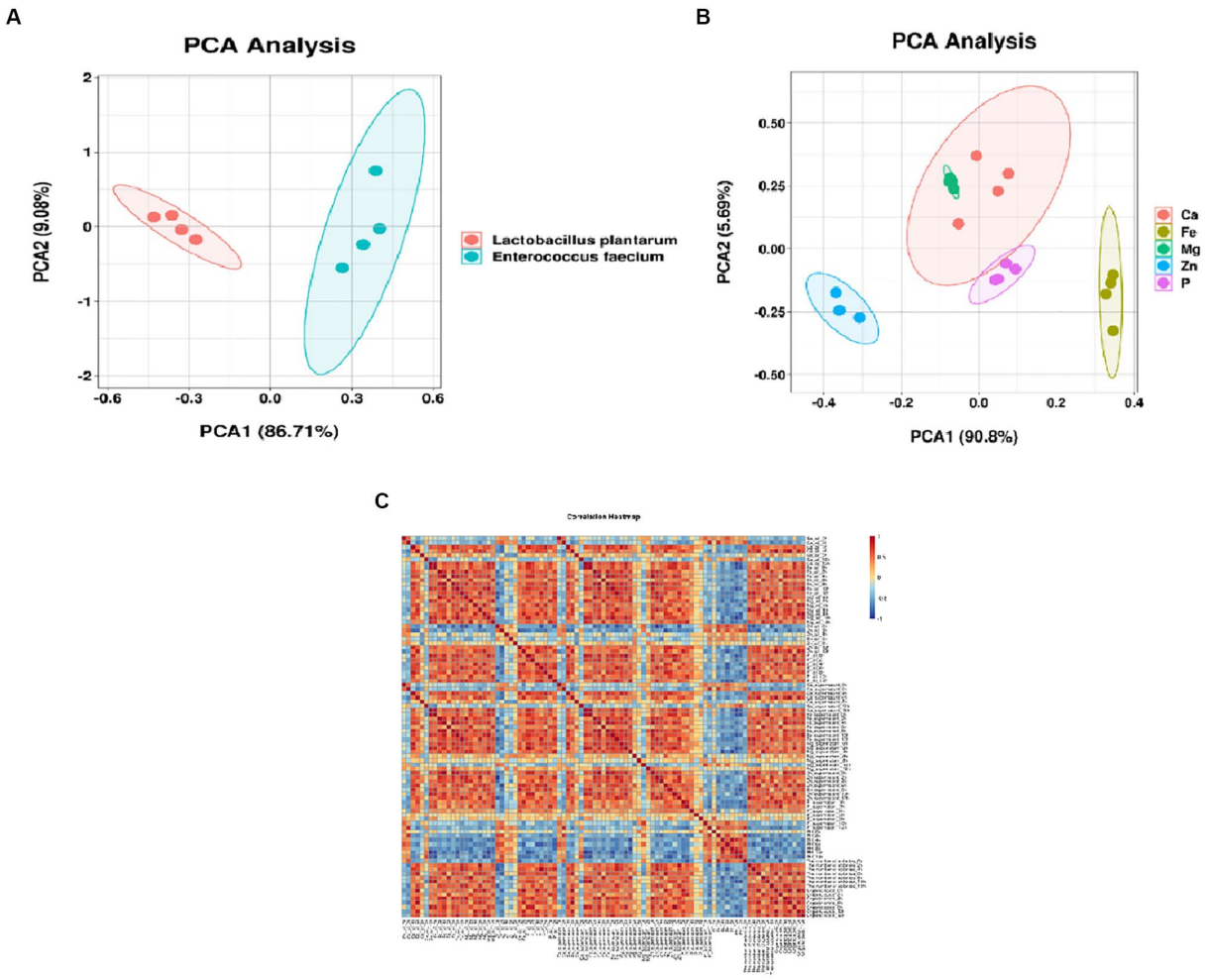

FIGURE 5
Absorptivity clustering analysis of minerals in soy yogurt **(A)** different strains; **(B)** different minerals; **(C)** correction analysis of strains, kinds and absorptivity of soy yogurt).

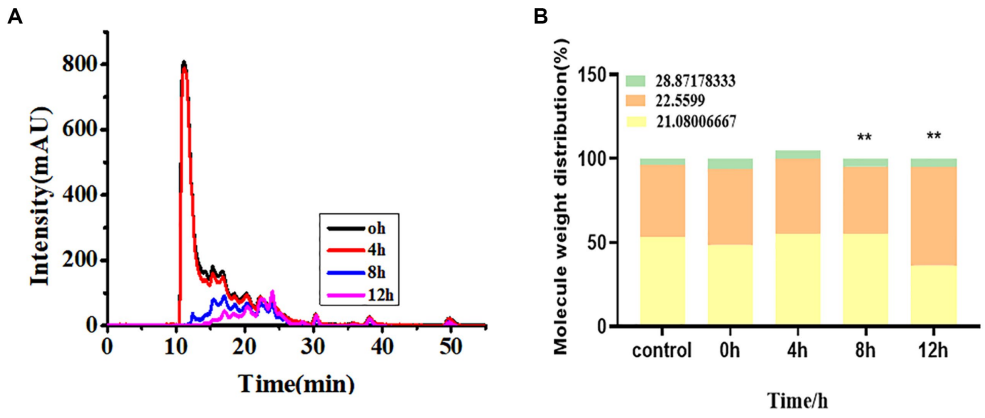

FIGURE 6
(A) Chemical form changes, **(B)** molecular weight distribution of hydrolysate over different fermentation times.

individual molecules ranged from 1 to 63 kDa. The inoculation of fermentation strains into soybean milk increased the abundance of low-molecular-weight minerals with a significant increase at 4 h; this was stabilized at 10 h because of protein flocculation and precipitation. Additionally, the lower molecular weight (1,500 Da) signal increased after 6 h, which suggests that more acidic amino

acids provide mineral binding sites, thus leading to high bioavailability.

Next, to understand the effect of the form of the mineral on bioavailability, we evaluated the possible mineral forms using HPLC-ICP-MS. As shown in Figure 6B, the elution of three calcium peaks was observed with retention times of 21.08, 22.56, and 28.87 min, corresponding to molecular weights of 2,866, 1,532, and 102.8 Da, respectively. A few peaks were observed at 0 h and 2 h 12 min, which disappeared after 4 h. Nevertheless, the signal of the lower molecule weight (1,500 Da) increased after 6 h, which suggests more hydrolyzed acidic amino acids provide a calcium-binding site, thus leading to high bioavailability. Morphological changes in iron, magnesium, zinc, and phosphorus during fermentation are shown in Supplementary Figure S2. Soybean milk fermented with *E. faecalis* exhibited a similar trend.

3.4. Effect of YA on bioavailability *in vivo*

Zebrafish have become an attractive animal model for studying mineral bioavailability because of their small size, short developmental cycle, and transparent embryos. Calcium is essential for the prevention of osteoporosis, and adequate intakes of zinc, magnesium, magnesium, and phosphorus are also presumed to play important roles in osteoporosis prevention (25). To investigate the preventive effects of yogurt on mineral bioavailability, we recapitulated prednisolone(PSL)-induced osteoporosis-like phenotypes. In addition, calcein, as a green fluorescent chromophore, specifically binds to calcium used for vital staining (26). Compared to the control group, prednisolone exposure caused a significant decrease in the stained mineralized larval tissue. In a well-established model, we observed a reduction in fluorescence intensity in Alendronate (ALN; 0.308 μM) and fermentation broth (*L. plantarum*) treatments, which reversed (Glucocorticoid Induced Osteoporosis)GIOP-induced bone loss, as shown in Figure 7. Quantitative analysis using the ImageJ software revealed that the RFI of zebrafish in the model group was lower than that in the control group. Moreover, in the fermentation treatment group, a significant increase was observed in the RFI of bone mass compared with that in the prednisolone treatment group, reaching 28% SYA treatment group at 100 μg/ml. These results indicate that the enhancement of the absorption rate of the YA can prevent bone loss symptoms in the skulls of zebrafish.

4. Discussion

Yogurt, a fermented milk product obtained by lactic acid bacteria-mediated acidification of milk, is consumed widely in developing and developed countries due to its functional activities (27). However, an increasing number of people expect to replace yogurt with plant-fermented beverages because of problems such as allergenicity and the desire for vegetarian alternatives (28). SYA, obtained by fermenting soybean milk using lactic acid bacteria, has gained increased interest because of its rich protein content, multiple mineral elements, and low price. Moreover, several studies have demonstrated its potential as an excellent alternative to cow's milk (29). However, the market share of YAs is relatively low because of limited deep processing. Therefore, understanding the influence of processing conditions on the composition and function of YAs is important for production and sales, as high mineral content in food does not necessarily guarantee high absorptivity.

In this study, the effect of different types of lactic acid bacteria on the absorption rate of minerals during fermentation was analyzed using a Caco-2 cell model *in vitro* and a zebrafish model *in vivo*. Consumer attitudes toward and acceptability of YAs were also investigated. We found that the content of soluble substances and the absorption rate of minerals increased with decreasing pH during fermentation. The heterolactic lactic acid bacteria performed better than the heterolactic lactic acid bacteria in terms of the absorptivity of the minerals in YA they produced.

The minimum intake of essential minerals is related to a lack of micronutrients, whereas their maximum intake is associated with an increased risk of developing chronic diseases (30). In this study, we determined the total calcium, iron, zinc, magnesium, and phosphorus contents in soybean milk. We found the content of Ca (476.01 μg/ml), Fe (724.32 μg/ml), Zn (19.88 μg/ml), Mg (840.15 μg/ml), and P (2259.37 μg/ml) and the other soluble contents in soybean milk were increased during the fermentation, which may be due to the following four reasons. First, phytase converts calcium and magnesium phytate into calcium, magnesium ions, inositol, and inorganic phosphorus, consequently increasing the soluble content in soybean milk (31). Second, *L. plantarum* uses the carbon source in soybean milk to produce organic acids during fermentation, which reduces the pH, leading to charge neutralization or a shielding effect on the protein surface. Most negatively charged proteins are converted to positively charged (32). Thus, calcium and magnesium ions bound to the proteins were released, leading to an increase in soluble content in soybean milk. Third, the pH in YA reached 4.2–4.5 after fermentation, which is lower than the pK value of calcium and magnesium. Some calcium and magnesium organic compounds bound by chemical bonds dissociate into their ionic forms. Fourth, the lactic acid bacteria adsorb metallic elements. However, as the pH decreases, the competitive binding effect of H^+ occurs at the position where lactic acid bacteria and calcium ions combine; thus, calcium ions are released by dissociation, and the content of water-soluble calcium ions increases. Consistent with these findings, the results of a previous study have shown that lactic acid bacteria starter cultures improved the calcium content in whole meal rye flour bread (33). Furthermore, the pre-fermentation organic phosphorus was significantly below the control levels, which rose above the control levels at the post-fermentation stage. This indicated that the production and consumption of phosphorus affect the fluctuations in water-soluble phosphorus during fermentation.

The speciation and absorptivity of the minerals determine their final bioavailability in foods (13). Here, to investigate the absorptivity, transformation, and speciation of minerals in soybean milk regulated by different types of bacterial strains, we constructed a Caco-2 cell-based intestinal barrier absorption model. The results showed that Calcium, Magnesium, Ferric, Zinc, and Phosphorus absorption rates increased during fermentation, especially at 4 h after fermentation when the pH of the protein was lower than its isoelectric point. The absorption rate reached a maximum at 8–12 h after fermentation and was stable when the microbial enzyme production activity was the highest. This is consistent with the change in the water-soluble mineral content. The increase in the calcium absorption rate may

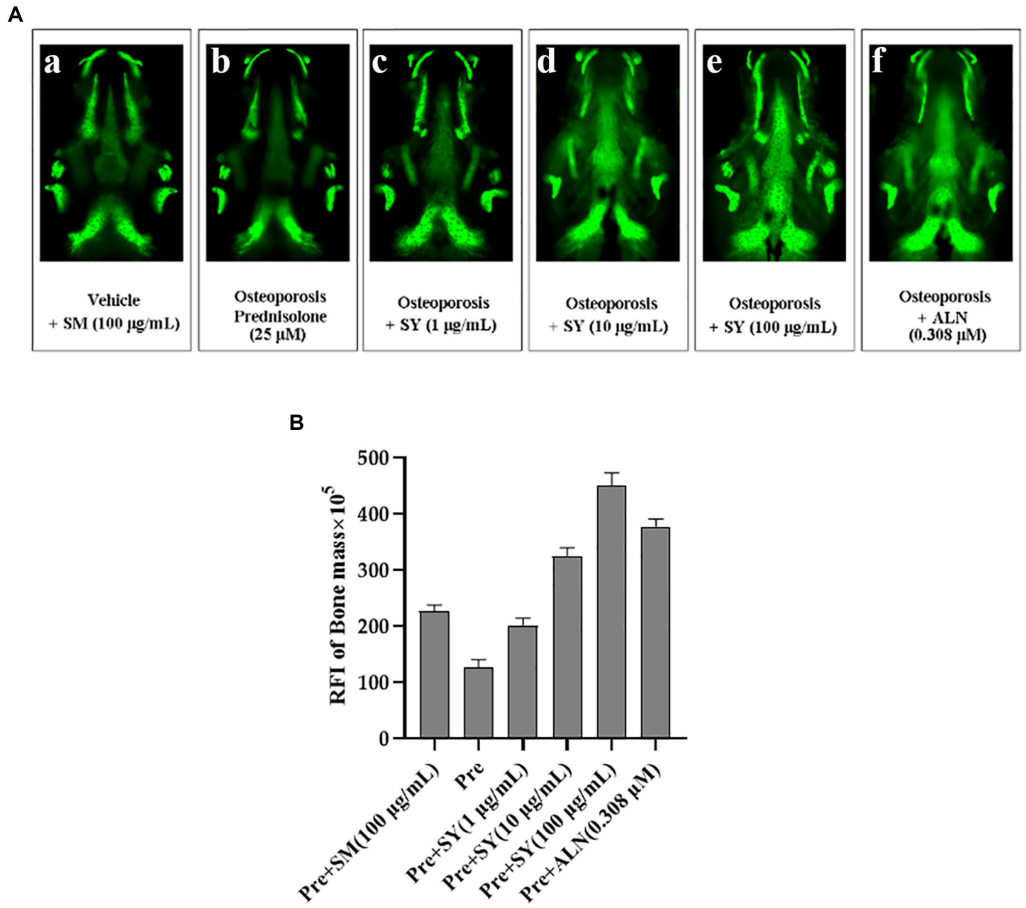

FIGURE 7
Effects of soy yogurt on anti-osteoporosis in the zebrafish model of GIOP. **(A)** Quantification of the relative fluorescence intensity (RFI) of the zebrafish skull at 7 dpf. **(B)** Representative fluorescence images of the zebrafish skull with different samples at 7 dpf (a) 0.1% DMSO (Vehicle), (b) 100 μg/ml prednisolone (Osteoporosis),or co-administered with soy yogurt (1 μg/ml, 10 μg/ml, 100 μg/ml; c–e), or 0.308 μM alendronate (positive control; f) for 96h. Data are expressed as mean±SEM. $^{\#\#}p<0.01$, $^{\#\#\#}p<0.001$ vs. Vehicle, $^{*}p<0.05$, $^{**}p<0.01$, and $^{***}p<0.001$ vs. Pre, ns, not significant (Pre, prednisolone; ALN, alendronate).

be caused by the change in quantity and the increase in soluble calcium content, on the one hand, and the change in the form of calcium, on the other hand. To better analyze the contribution of the content and mineral form to the mineral absorption rate, their speciation was found to be converted from giant molecules to small molecules along with the continuous decline of pH. This increment was time-dependent for bacterial strains cultured for 0–12 h, indicating that bacterial strains induced an increase in mineral and trace element absorptivity by converting their speciation. We speculated that this was due to the protein being broken down into peptides, which could improve the absorption of minerals through mineral–peptide complexes. Sun et al. (34) isolated a pentapeptide (DHTKE) from egg white hydrolysates and reported that the DHTKE–calcium complex improved calcium absorption by more than seven times. Sato discovered that casein phosphopeptides from cow milk resulted in more effective calcium absorption upon chelation with calcium through the phosphate groups of serine, forming soluble complexes (35). Compared to soybean milk, an unprecedented increase in absorption was observed, as stated above, which was influenced by its poor content in soybean milk. In addition, we deduced that the coordination force with minerals was weak in soybean milk.

Different metabolic types of lactic acid bacteria have different effects on the absorption rate. Homotypic lactic acid bacteria showed a higher conversion ratio during fermentation. During lactic acid fermentation, the protein was degraded through a complex proteolytic system (36). In general, the proteolytic system consists of serial chain reactions, which are produced from a serine proteinase that is proline-specific and linked to the cell wall, followed by the specific transport of dipeptides, tripeptides, and oligopeptides, and finally, by the action of a countless number of intracellular peptidases and aminopeptidases (37). In the present study, *L. plantarum* generated a higher level of calcium absorption than *E. faecalis*. This could be because *Lactobacillus* strains act with better adhesion ability, involved in the process of calcium absorption process (38). Furthermore, *Lactobacillus* strains induce the expression of calcium-absorbing host protein by promoting *MUC3* mRNA transcription and translation, improving calcium absorption (39). Additionally, these differences may have resulted from the differences in the metabolic pathways of the strains. Kleerebezem et al. (40) found that *L. plantarum* lacks genes encoding cell wall hydrolases but is abundant in peptide transport systems: oligopeptide permease transporter (pp) and dipeptide and tripeptide transporter (DtpT), which can transport extracellular peptides into cells; meanwhile, many peptidases in cells can further degrade

peptides (40). A study reporting the whole genome sequence of *L. plantarum* strain 5–2 isolated from fermented soybeans identified genes encoding transport systems and intracellular peptidases with different characteristics; however, the study could not identify genes encoding cell wall proteases (41).

Changes in the structure of the protein could affect its binding ability to minerals, which changes with pH. This study used SDS-PAGE, infrared spectroscopy, and fluorescence spectroscopy to analyze protein structure changes during fermentation. Differential chromatograms indicated that the intensity of the peaks corresponding to low-molecular-mass species increased with longer fermentation times, whereas the intensity of the peaks corresponding to high-molecular-mass species diminished. A peptide with a molecular weight between 1 and 3 kDa is generally considered a small peptide, whereas that with less than 1 kDa is considered an amino acid or small-molecule substance. The peptide Glu-Gly from whey protein hydrolysates was recently identified as a strong calcium binder (42). Similarly, Asp-Glu dipeptides have been found to bind calcium more strongly than predicted by these two amino acids. In addition, it has been proved that some amino acids are potential mineral-binding ligands, such as aspartic acid and glutamic acid (34). Based on the above morphological distribution, we concluded that the YAs contained many small peptides and amino acids that could chelate minerals.

In addition, the mineral nutrients in processed foods are not directly converted into an absorbable form for human needs. For example, several ligands like phytates, oxalates, and dietary fibers may bind with minerals and reduce the bioavailability of these nutrients (43). Changes in organic matter content have dual effects on the bioavailability of minerals in soybean milk. The binding state of hydrophilic organic acids is easily transformed into an applicable state, which is affected by physical and chemical properties (pH, redox potential (Eh), organic matter content), and other factors during the fermentation process. The high content of organic matter will combine with mineral elements to form a complex and then become soluble small-molecule organic matter, thus increasing absorptivity. Heterogeneous mixtures of soluble organic molecules (proteins and polysaccharides) and various functional groups (carboxyl, phenolic, and amino) have different affinities for mineral elements. Therefore, to determine the potential reason for the increased absorption, the organic acid content was determined. Generally, the organic acid content shows a significant decrease with decreasing pH, indicating that pH plays an essential role in transforming the valence states and forms of mineral elements.

Both the quality and demand of consumers affect product sales (44). To better understand market sales, the knowledge of consumers on YAs and yogurt and acceptance of beany flavors were observed. All consumers participating in the study indicated a link to fermented food, although the frequency of consumption varied. An increased frequency of yogurt consumption increases the acceptability scores for YAs. However, the beany smell would affect purchase desire, while more details about fungi in YAs would increase purchasing power.

The absorbed calcium ions can improve bone density after entering the body. To better understand mineral absorption *in vivo*, a zebrafish animal model was used to analyze bone density and neuroactivity. The results confirmed that 100 mg/L yogurt significantly promoted the formation of new bone ($p < 0.05$), which was much better than soybean milk. Similarly, mineral and trace elements significantly improve the nervous system, enhancing swimming distance in zebrafish.

5. Conclusion

In this study, the effects of homotypic (*Enterococcus faecalis*) and heterolactic (*Lactiplantibacillus plantarum* CICC 21022) lactic acid bacteria fermentation on the nutritional and mineral bioavailability of SYA was investigated. The Caco-2 cell model showed the potential of fermentation to improve the acidic amino acid and organic acid contents as well as mineral absorptivity in SYA. The fermentation altered the speciation of minerals from a large molecular type to a small one. Furthermore, the chemical composition changes revealed that peptide calcium might be the main mineral form resulting from fermentation. YA substantially increased the bone mass in a zebrafish osteoporosis model. The analyses in the zebrafish model showed that YA could effectively improve the bioavailability of minerals and trace elements, further highlighting the potential of lactic acid bacterial fermentation for mineral bioavailability. Overall, this study provides evidence that lactic acid bacteria regulates the form and bioavailability of minerals and trace elements in soybean milk during fermentation. The results provide a foundation for understanding the influence of processing conditions on the composition and function of YAs and can assist in the production and sales of SYA.

Data availability statement

The original contributions presented in the study are included in the article/Supplementary material, further inquiries can be directed to the corresponding authors.

Author contributions

JG were responsible for conceptualizing, designing this study, validation, data curation, and writing original draft preparation. XK, KW, YuC, MD, and JX played an important role in software and formal analysis. BX and ZW participated in investigation and visualization. YoC and TY contributed to resources, writing review and editing, supervision, project administration, and funding acquisition. All authors contributed to the article and approved the submitted version.

Funding

The work was supported by the National Science Foundation of China (31871450) and the Natural Science Foundation of Shandong (ZR2022MC217) granted its approval to conduct this research. In addition, the Center for Mitochondria and Healthy Aging, College of Life Sciences, Yantai University partly provided support.

Conflict of interest

The authors declare that the research was conducted in the absence of any commercial or financial relationships that could be construed as a potential conflict of interest.

Publisher's note

All claims expressed in this article are solely those of the authors and do not necessarily represent those of their affiliated organizations, or those of the publisher, the editors and the reviewers. Any product that may be evaluated in this article, or claim that may be made by its manufacturer, is not guaranteed or endorsed by the publisher.

Supplementary material

The Supplementary material for this article can be found online at: https://www.frontiersin.org/articles/10.3389/fnut.2023.1198456/full#supplementary-material

References

1. Takagi A, Kano M, Kaga C. Possibility of breast cancer prevention: use of soy isoflavones and fermented soy beverage produced using probiotics. *Int J Mol Sci*. (2015) 16:10907–20. doi: 10.3390/ijms160510907

2. Maleki Z, Jazayeri S, Eslami O, Shidfar F, Hosseini AF, Agah S, et al. Effect of soy milk consumption on glycemic status, blood pressure, fibrinogen and malondialdehyde in patients with non-alcoholic fatty liver disease: a randomized controlled trial. *Complement Ther Med*. (2019) 44:44–50. doi: 10.1016/j.ctim.2019.02.020

3. Rebholz CM, Reynolds K, Wofford MR, Chen J, Kelly TN, Mei H, et al. Effect of soybean protein on novel cardiovascular disease risk factors: a randomized controlled trial. *Eur J Clin Nutr*. (2013) 67:58–63. doi: 10.1038/ejcn.2012.186

4. Vanga SK, Raghavan V. How well do plant based alternatives fare nutritionally compared to cow's milk? *J Food Sci Technol*. (2018) 55:10–20. doi: 10.1007/s13197-017-2915-y

5. Aljewicz M, Cichosz G. The effect of probiotic *Lactobacillus rhamnosus* HN001 on the in vitro availability of minerals from cheeses and cheese-like products. *LWT Food Sci Technol*. (2015) 60:841–7. doi: 10.1016/j.lwt.2014.09.052

6. Bailey RL, West KP Jr, Black RE. The epidemiology of global micronutrient deficiencies. *Ann Nutr Metab*. (2015) 66:22–33. doi: 10.1159/000371618

7. Chaudhary V, Saraswathy KN, Sarwal R. Dietary diversity as a sustainable approach towards micronutrient deficiencies in India. *Indian J Med Res*. (2022) 156:31–45. doi: 10.4103/ijmr.ijmr_3314_21

8. Ciosek Z, Kot K, Kosik-Bogacka D, Lanocha-Arendarczyk N, Rotter I. The effects of calcium, magnesium, phosphorus, fluoride, and Lead on bone tissue. *Biomol Ther*. (2021) 11:506. doi: 10.3390/biom11040506

9. Grober U, Schmidt J, Kisters K. Magnesium in prevention and therapy. *Nutrients*. (2015) 7:8199–226. doi: 10.3390/nu7095388

10. Kumssa DB, Joy EJ, Ander EL, Watts MJ, Young SD, Walker S, et al. Dietary calcium and zinc deficiency risks are decreasing but remain prevalent. *Sci Rep*. (2015) 5:10974. doi: 10.1038/srep10974

11. Said HM. Intestinal absorption of water-soluble vitamins in health and disease. *Biochem J*. (2011) 437:357–72. doi: 10.1042/BJ20110326

12. Polzonetti V, Pucciarelli S, Vincenzetti S, Polidori P. Dietary intake of vitamin D from dairy products reduces the risk of osteoporosis. *Nutrients*. (2020) 12:1743. doi: 10.3390/nu12061743

13. Rzymski P, Pischel I, Conrad F, Zwingers T, Rzymski P, Opala T. The bioavailability of calcium in the form of pyruvate, carbonate, citrate–malate in healthy postmenopausal women. *Eur Food Res Technol*. (2015) 242:45–50. doi: 10.1007/s00217-015-2516-9

14. Badea M, Uivarosi V, Olar R. Improvement in the pharmacological profile of copper biological active complexes by their incorporation into organic or inorganic matrix. *Molecules*. (2020) 25:5830. doi: 10.3390/molecules25245830

15. Bingtong L, Yongliang Z, Liping S. Identification and characterization of the peptides with calcium-binding capacity from tilapia (*Oreochromis niloticus*) skin gelatin enzymatic hydrolysates. *J Food Sci*. (2020) 85:114–22. doi: 10.1111/1750-3841.14975

16. Rekha CR, Vijayalakshmi G. Bioconversion of isoflavone glycosides to aglycones, mineral bioavailability and vitamin B complex in fermented soymilk by probiotic bacteria and yeast. *J Appl Microbiol*. (2010) 109:1198–208. doi: 10.1111/j.1365-2672.2010.04745.x

17. O'Dell BL, and Sunde RA. Mineral-ion interaction as assessed by bioavailability and ion channel function In: . *Handbook of nutritionally Essential Mineral Elements* (1997).

18. Hill CH, Matrone G. Chemical parameters in the study of in vivo and in vitro interactions of transition elements. *Fed Proc*. (1970) 29:1747–81.

19. Salanta L. C., Uifalean A., Iuga C. A., Pop C. R., González CV. (2020). Valuable food molecules with potential benefits for human health.

20. Kong X, Xiao Z, Du M, Wang K, Yu W, Chen Y, et al. Physicochemical, textural, and sensorial properties of soy yogurt as affected by addition of low acyl Gellan gum. *Gels*. (2022) 8:453. doi: 10.3390/gels8070453

21. Laemmli UK. Cleavage of structural proteins during the assembly of the head of bacteriophage t4. *Nature*. (1970) 227:680–5. doi: 10.1038/227680a0

22. Wang XX, Liu GY, Yang YF, Wu XW, Xu W, Yang XW. Intestinal absorption of triterpenoids and flavonoids from Glycyrrhizae radix et rhizoma in the human Caco-2 monolayer cell model. *Molecules*. (2017) 22:1627. doi: 10.3390/molecules22101627

23. Su L, Walsh H, Gokavi S, Guo M. Interactions between *Lactobacillus acidophilus* strains and the starter cultures, Lactobacillus bulgaricus and *Streptococcus thermophilus* during fermentation of goats' milk. *Afr J Biotechnol*. (2012) 11, 11271–11279. doi: 10.5897/AJB12.496

24. Nemeth SP, Fox LG, Demarco M, Brugge JS. Deletions within the amino-terminal half of the c-src gene product that alter the functional activity of the protein. *Mol Cell Biol*. (1989) 9:1109–19. doi: 10.1128/mcb.9.3.1109-1119.1989

25. Morato-Martinez M, Lopez-Plaza B, Santurino C, Palma-Milla S, Gomez-Candela C. A dairy product to reconstitute enriched with bioactive nutrients stops bone loss in high-risk menopausal women without pharmacological treatment. *Nutrients*. (2020) 12:2203. doi: 10.3390/nu12082203

26. Chen JR, Lai YH, Tsai JJ, Hsiao CD. Live fluorescent staining platform for drug-screening and mechanism-analysis in zebrafish for bone mineralization. *Molecules*. (2017) 22:2068. doi: 10.3390/molecules22122068

27. Castellone V, Bancalari E, Rubert J, Gatti M, Neviani E, Bottari B. Eating fermented: health benefits of LAB-fermented foods. *Foods*. (2021) 10:2639. doi: 10.3390/foods10112639

28. Craig WJ, Brothers CJ. Nutritional content and health profile of non-dairy plant-based yogurt alternatives. *Nutrients*. (2021) 13:4069. doi: 10.3390/nu13114069

29. Almghawesh E, Slik S, Okkou H. Processing of functional yoghurt-like product from soymilk supplemented by probiotics. *Int J Food Sci*. (2022) 2022:1–7. doi: 10.1155/2022/5898537

30. Heffernan SM, Horner K, De Vito G, Conway GE. The role of mineral and trace element supplementation in exercise and athletic performance: a systematic review. *Nutrients*. (2019) 11:696. doi: 10.3390/nu11030696

31. Gupta RK, Gangoliya SS, Singh NK. Reduction of phytic acid and enhancement of bioavailable micronutrients in food grains. *J Food Sci Technol*. (2015) 52:676–84. doi: 10.1007/s13197-013-0978-y

32. Cabuk B, Stone AK, Korber DR, Tanaka T, Nickerson MT. Effect of Lactiplantibacillus plantarum fermentation on the surface and functional properties of pea protein-enriched flour. *Food Technol Biotechnol*. (2018) 56:411–20. doi: 10.17113/ftb.56.03.18.5449

33. Litwinek D, Boreczek J, Gambus H, Buksa K, Berski W, Kowalczyk M. Developing lactic acid bacteria starter cultures for wholemeal rye flour bread with improved functionality, nutritional value, taste, appearance and safety. *PLoS One*. (2022) 17:e0261677. doi: 10.1371/journal.pone.0261677

34. Sun N, Jin Z, Li D, Yin H, Lin S. An exploration of the calcium-binding mode of egg white peptide, asp-his-Thr-Lys-Glu, and in vitro calcium absorption studies of peptide-calcium complex. *J Agric Food Chem*. (2017) 65:9782–9. doi: 10.1021/acs.jafc.7b03705

35. Ryuichiro S, Tadashi N, Casein HN. Casein phosphopeptide (CPP) enhances calcium absorption from the ligated segment of rat small intestine. (1986). doi: 10.3177/jnsv.32.67

36. Hebert EM, Villegas JM, Saavedra L, Mozzi F, Verapingitore E, Brown L. Lactic acid bacteria as cell factories for the generation of bioactive peptides. *Protein Pept Lett*. (2017) 24:146–155. doi: 10.2174/0929866524666161123111333

37. Chen. YS, Steele JL. Genetic characterization and physiological role of endopeptidase O from *Lactobacillus helveticus* CNRZ32. *AEM*. (1998) 64:3411–5. doi: 10.1128/AEM.64.9.3411-3415.1998

38. Collins Kevin J, Dunne C, Murphy L, Morrissey D, O'Mahony L. A randomised controlled trial of a probiotic Lactobacillus strain in healthy adults: assessment of its delivery, transit and influence on microbial Flora and Enteric immunity. *Microb Ecol Health Dis*. (2002) 14:81–9. doi: 10.1080/08910600260081720

39. Mack DR, Ahrne S, Hyde L, Wei S, Hollingsorth MA. Extracellular MUC3 mucin secretion follows adherence of Lactobacillus strains to intestinal epithelial cells in vitro. *Small Intestine*. (2003) 52:827–33. doi: 10.1136/gut.52.6.827

40. Kleerebezem M, Boekhorst J, Van KR, Molenaar D, Kuipers OP, Leer R, et al. Complete genome sequence of Lactiplantibacillus plantarum WCFS1. *Proc Natl Acad Sci U S A*. (2003) 100:1990–5. doi: 10.1073/pnas.0337704100

41. Liu CJ, Wang R, Gong FM, Liu XF, Zheng HJ, Luo YY, et al. Complete genome sequences and comparative genome analysis of Lactiplantibacillus plantarum strain 5-2 isolated from fermented soybean. *Genomics*. (2015) 106:404–11. doi: 10.1016/j.ygeno.2015.07.007

42. Zhao L, Huang Q, Huang S, Lin J, Wang S, Huang Y, et al. Novel peptide with a specific calcium-binding capacity from whey protein hydrolysate and the possible chelating mode. *J Agric Food Chem*. (2014) 62:10274–82. doi: 10.1021/jf502412f

43. Singh A, Karjagi C, Rakshit S. Minimally altering a critical kinase for low-phytate maize. *Sci Rep*. (2020) 10:6324. doi: 10.1038/s41598-020-63016-5

44. Fiorentini M, Kinchla AJ, Nolden AA. Role of sensory evaluation in consumer acceptance of plant-based meat analogs and meat extenders: a scoping review. *Foods*. (2020) 9:1334. doi: 10.3390/foods9091334

frontiers | Frontiers in Nutrition

TYPE Review
PUBLISHED 30 June 2023
DOI 10.3389/fnut.2023.1196816

OPEN ACCESS

EDITED BY
Yu-Chung Chang,
Washington State University, United States

REVIEWED BY
Yong-Quan Xu,
Chinese Academy of Agricultural Sciences, China
Zuobing Xiao,
Shanghai Jiao Tong University, China
Shuang Chen,
Jiangnan University, China

*CORRESPONDENCE
Hehe Li
✉ xyzhehe@126.com

RECEIVED 30 March 2023
ACCEPTED 25 May 2023
PUBLISHED 30 June 2023

CITATION
Zhang G, Xiao P, Yuan M, Li Y, Xu Y, Li H, Sun J and Sun B (2023) Roles of sulfur-containing compounds in fermented beverages with 2-furfurylthiol as a case example. *Front. Nutr.* 10:1196816. doi: 10.3389/fnut.2023.1196816

Roles of sulfur-containing compounds in fermented beverages with 2-furfurylthiol as a case example

Guihu Zhang[1,2], Peng Xiao[1,2], Mengmeng Yuan[1,2], Youming Li[3], Youqiang Xu[1,2], Hehe Li[1,2,4]*, Jinyuan Sun[1,2,4] and Baoguo Sun[1,2,4]

[1]China Food Flavor and Nutrition Health Innovation Center, Beijing Technology and Business University, Beijing, China, [2]Key Laboratory of Geriatric Nutrition and Health (Beijing Technology and Business University), Ministry of Education, Beijing, China, [3]Inner Mongolia Taibus Banner Grassland Brewing Co., Ltd., Xilin Gol League, China, [4]Beijing Key Laboratory of Quality and Safety, Beijing Technology and Business University, Beijing, China

Aroma is a critical component of the flavor and quality of beverages. Among the volatile chemicals responsible for fragrance perception, sulfur compounds are unique odorants due to their extremely low odor threshold. Although trace amounts of sulfur compounds can enhance the flavor profile of beverages, they can lead to off-odors. Sulfur compounds can be formed via Maillard reaction and microbial metabolism, imparting coffee aroma and altering the flavor of beverages. In order to increase the understanding of sulfur compounds in the field of food flavor, 2-furfurylthiol (FFT) was chosen as a representative to discuss the current status of their generation, sensory impact, enrichment, analytical methods, formation mechanisms, aroma deterioration, and aroma regulation. FFT is comprehensively reviewed, and the main beverages of interest are typically baijiu, beer, wine, and coffee. Challenges and recommendations for FFT are also discussed, including analytical methods and mechanisms of formation, interactions between FFT and other compounds, and the development of specific materials to extend the duration of aroma after release.

KEYWORDS

2-furfurylthiol, flavor chemical interaction, Maillard reaction, microorganism, enzyme catalysis

1. Introduction

Aroma is a crucial factor in the flavor and quality of beverages, and it has a profound impact on the acceptability of consumers. In addition to taste, olfaction plays a vital role in the perception of flavor. During consumption, aroma compounds are released from the foods matrix and transported to the olfactory receptor in the nose, leading to orthonasal and/or retronasal perception, which may affect the experience of consumers (1, 2). A vast number of volatile odorants are released, detected, and discriminated by odorant receptors expressed in the olfactory sensory neurons of the nose (3). This processing is highly accurate, and combined with aroma and other sensor inputs helps to produce complex taste perceptions (4, 5). Previous studies have shown that sulfur-containing compounds can enhance the aroma profiles of beverages with relatively low content (6–11). Among these compounds, FFT is a unique aroma molecule found in many beverages such as coffee (9), grape wine (12), and baijiu (13, 14) (Figure 1), usually formed

FIGURE 1
Main liquid matrices enriched with FFT.

during fermentation and/or Maillard reaction, and impart aromas of toasted sesame or coffee to the final product.

The significance of FFT lies in its widespread presence in beverages and its potential to influence overall quality including color, flavor, and texture (8, 15–17). Generally, the positive aspects of FFT in beverages can be summarized into the following three points. First, FFT serves as an aroma enhancer at very low thresholds of aroma perception. FFT plays a vital role in the aroma perception of several foodstuffs as a kind of compound with a slight fragrance. For example, fermented soybean paste miso, a traditional Japanese seasoning, actively contributes to the aroma characteristics of miso as a diary element at concentrations ranging from 25 to 409 ng/kg (18). Similarly, baijiu is one of the most popular alcoholic beverages in China. According to previously published data, FFT was found in sauce-flavored, light-flavored, strong-flavored, and sesame-flavored baijiu. Despite its low levels, typically at μg/L, it is also considered to be one of the key aroma compounds that distinguish sesame-flavored baijiu from other odorants substances, as confirmed by aroma recombination and omission analyses (10, 11, 14, 19–21). Moreover, the flavor contribution of FFT to foodstuffs has been demonstrated in other fermented or heat-treated products such as wine (22), sake (23), roasted goose/duck (8, 24), sesame oil (25), Hazelnuts (26), and coffee (9).

Second, FFT can be utilized as a vital compound for classifying different types of characteristic markers in authenticity. Additionally, 2-methyl-3-furanethiol, which has a meaty flavor, and FFT are characteristic aromas of sauce-flavored baijiu and can be used to distinguish sauce-flavored baijiu from light and strong baijiu (14). Similarly, as a characteristic aroma compound in coffee, FFT serves as a quality marker for coffee quality level identification and to distinguish yeast extracts produced at different temperatures, respectively (27, 28). This applies to grading, authenticity, and quality regulation, which are vital in protecting the interests of manufacturers and consumers. Third, perceived interactions between FFT and other compounds in food were identified. Although chlorogenic acid may have a masking effect on the aroma release of FFT in coffee, the interactions between FFT and other molecules are still under-researched (29). The presence of FFT as a flavor factor also influences aroma perception, making it crucial to explore the appropriate content of FFT in beverages.

In addition to boosting the flavor of products, FFT is a double-edged sword, and FFT can enhance the overall flavor of baijiu at low concentrations, but a pickle-like taste is an off-odor in sauce-flavor baijiu that can be degraded by FFT and other volatile sulfur-containing compounds at high concentrations, which are associated with strong odor intensity (30). Nevertheless, to the best

of our knowledge, few studies have been conducted on the effect of FFT on the aroma composition of beverages. To better provide researchers with a direction for their research, this study presents the contribution of aroma, discusses the main analytical methods, highlights their advantages and disadvantages, and elucidates the mechanisms of FFT formation in beverages. Our review is expected to increase the understanding of FFT by readers and provide guidance for further research on FFT.

2. Occurrence and sensory contribution of 2-furfurylthiol

A literature review of the Web of Science database showed that 145 articles were published under the keyword "2-furfurylthiol" between 2000 and 2022 (Figure 2). FFT is a sort of compound that contains a sulfhydryl group whose boiling point is always lower than that of the corresponding alcohol and is characterized by a strong odor with a trace odor threshold (31, 32). Typically, FFT is present in diverse fermented or thermally processed beverages (13, 22, 23, 33, 34), as well as in other related foods such as Iberian Ham (35) and squid broth (36). It provides consumers with an enticing and distinctive aroma of roasted coffee or toasted sesame seeds.

FFT, reminiscent of roast meat aroma and roasted coffee aroma or roasted sesame seeds (10, 37), is usually present in baijiu at concentrations below 118 μg/L (38), with a perception threshold equal to 0.1 μg/L in hydroalcoholic solution (10). In addition, FFT always occurs in coffee at a high content level of exceeding 1,000 μg/kg, except for Arabica and Robusta coffee at a concentration close to 0.06∼0.18 μg/kg (39–41). However, comprehensively and deeply study of the contribution of aroma compounds to food matrices cannot be achieved by considering the concentration and threshold values alone.

Gas chromatography-olfactometry (GC-O) constitutes the best method for screening odor-active molecules, using the mimic human nose as a detector to identify compounds eluting from the GC column (42). A study of GC-O analysis on baijiu revealed a distinctive odor zone on the column reminiscent of roasted sesame seeds, which was later identified as a contribution from FFT (37). However, olfactometry does not take into account the antagonist and synergic effects between volatiles in a complex matrix such as wine, coffee, as well as aroma enhancers or depressors.

In parallel to olfactometry measurements, the ratio between the concentration of specific volatiles and their perception threshold

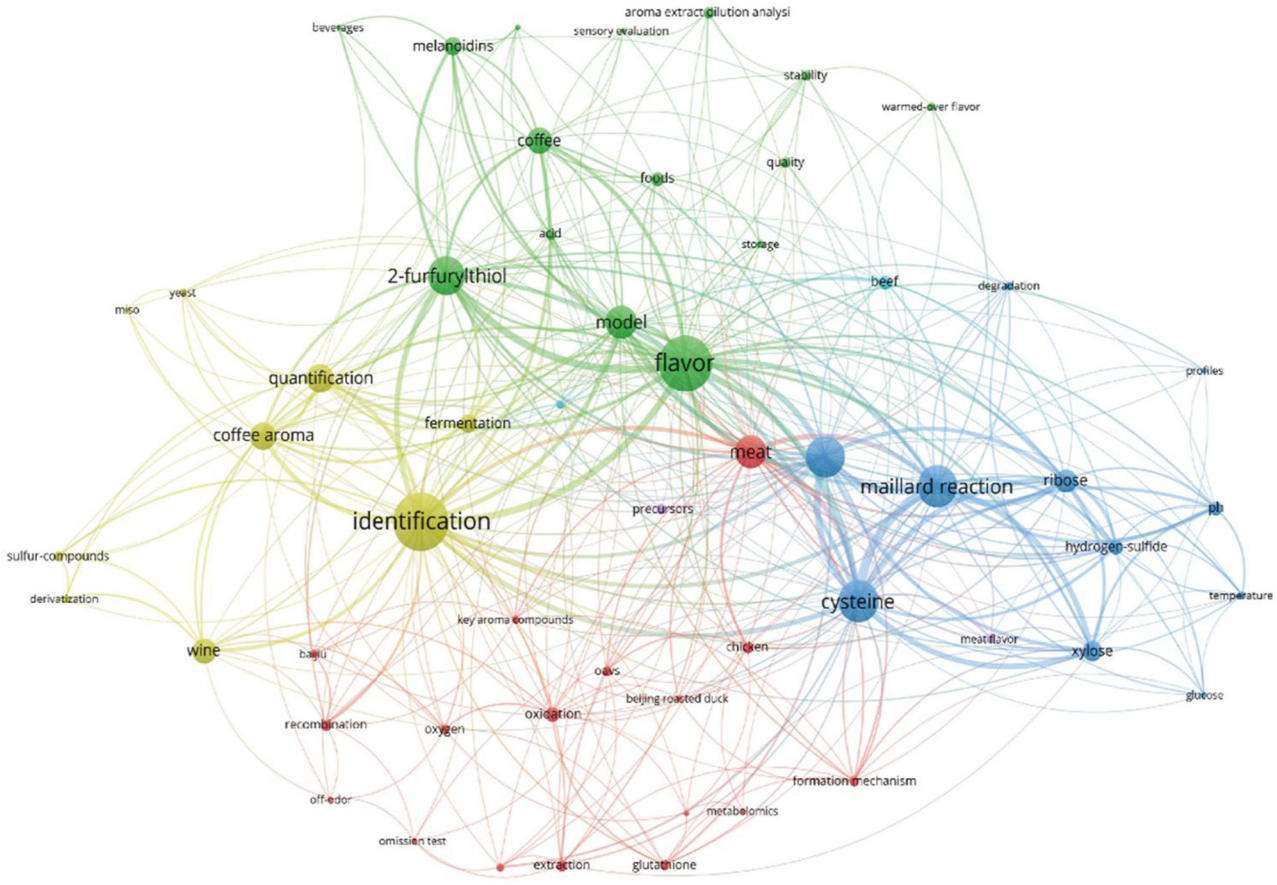

FIGURE 2
Keyword co-occurrence network diagram in FFT studies in food and beverages, bibliometric diagram of FFT studies visualized in 145 articles retrieved from the Web of Science database published from 2000 to 2022.

helps to identify the most active odorants in foodstuffs. Based on a previous study (43), using aroma extract dilution analysis (AEDA), FFT was identified as the main olfactory contributor in roasted white sesame seeds. Thirty common compounds, including FFT, and other 29 chemicals contributed significantly to the aroma profile of coffee brew through the same approach (9). Similarly, a study of Chinese roasted sesame-flavored baijiu revealed the importance of FFT on the flavor of such baijiu (10). To support the qualitative determination, quantitative aspects [e.g., the calculation of odor activity values (OAVs, defined as the ratio of concentration to perception threshold)] have been applied to the identification of influential odors in roasted sesame-flavored baijiu (10, 26).

Finally, odor reconstitution represents the optimal approach to quantitatively measure the contribution of the matrix to the aroma of beverages. A global strategy consisting of qualitative and quantitative determinations of impact odorants followed by omission tests with synthetic aroma models has demonstrated that FFT is the most important odorant in many matrices such as coffee (8, 44, 45). Sensory and quantitative chemical analyses are often carried out in parallel to comprehensively and in-depth characterize odoriferous molecules in foods and beverage matrices.

3. Analytical determination of 2-furfurylthiol

The analytical assay of FFT in beverages is mainly hindered by their low concentrations, complexity of the matrices, and susceptibility to oxidative degradation reactions, which result in the rapid conversion of FFT to disulfides through autoxidation or degradation at high-temperature auto-oxidation or degradation at high temperatures (31, 46). In recent years, various methods have been employed to determine FFT in diverse food products, including non-specific techniques applicable to a wide range of volatile compounds, and methods that are selective for FFT. In the following section, common analytical methods for the characterization of FFT in the flavor research area will be discussed, and both the advantages and drawbacks will be highlighted.

3.1. Pre-treatment approaches

The concentration, solubility, volatility, and chemical properties of all molecules in food matrices vary widely, resulting in no fixed method for the simultaneous analysis of all substances. Thus, solid phase microextraction (SPME), liquid–liquid extraction (LLE), stir bar sorptive extraction (SBSE), solid phase extraction (SPE), dispersive liquid–liquid microextraction (DLLME), agitator adsorption, supercritical carbon dioxide extraction, and others have been extensively used for the studies in the field of flavor analysis (Table 1). Considering the extremely low content of FFT in matrices, it is difficult to achieve efficient isolation by using conventional extraction/enrichment techniques to analyze FFT due to its instability and possible interactions between FFT and other compounds (54). Therefore, it is of great significance to develop and apply efficient enrichment methods before analysis. SPME is a common, solvent-free technology developed based on SPE and can effectively solve the problems of blocking and channeling existing in SPE and other traditional pre-treatment technologies and requires less samples to handle shorter processing time (47, 59). Generally, SPME can be categorized into headspace solid phase microextraction (HS-SPME) and direct immersion solid phase microextraction (DI-SPME), in which the former is widely used in comparison to DI-SPME (51). HS-SPME has been widely used in various matrices to enrich target odor substances with relatively good results, for instance, HS-SPME has been introduced in wine (12, 48) and coffee (60). Furthermore, it is necessary to select the appropriate extraction fiber due to the discrepancy in extraction efficiency and capacity of the various types of analyte extraction fibers (13). Moreover, it is worth noting that temperature is a non-negligible factor that cannot be ignored due to the tendency of FFT to oxidize or degrade at high temperatures (61, 62).

Moreover, LLE can extract the analyte and squash the matrix through the analyte solubility divergence between an aqueous sample and water-immiscible organic solvent; ether and dichloromethane are commonly used as extraction solvents. In addition, sensitivity is improved by blowing nitrogen and injecting the final sample for analysis during extraction (51, 63). Pre-concentration FFT of brewed coffee prior to LLE analysis was reported by Casas et.al. Notably, this operation is laborious, tedious, and time-consuming. Especially, the operator will be exposed to hazardous chemicals and, despite the advantage of the small sample size required, some compounds with similar properties may be removed at the same time (64). In addition, the addition of large amounts of organic solvents and inorganic salts to improve the recovery of target compounds may interfere with subsequent chromatographic analysis (52). Fortunately, implantation of liquid–liquid microextraction (LLME) can reduce the volume of solvent required. The choice of solvent depends on the compounds to be extracted and must be safe for the operator and the environment.

Similar to LLE, solvent-assisted flavor evaporation (SAFE) involves the use of organic matter and long extraction times. In contrast to the former, it is a gentle but comprehensive method for extracting volatiles from complex food matrices devised by Engel et al. (58). The SAFE system is a compatible combination of a distillation unit and a high vacuum pump to reduce the loss of heat-sensitive substrates from the sample and to maximize the preservation of the original flavor of the analytes and is particularly suitable for the separation and analysis of volatile molecules in complex matrices (42, 65). SAFE is a highly time-intensive and laborious practice in flavor analysis. The flavor profiles of wine were concentrated before further analysis, despite this method requires significant time and may reduce the loss of target analytes with highly volatile (i.e., FFT) characteristics from the sample (44, 66–68). In addition, unlike SPME, which is commonly used for sample preparation and combined with GC-O analysis, SAFE requires the preparation of a large number of samples (42).

Recently introduced for FFT analysis in wine (56), stir bar sorptive extraction (SBSE) is a novel method for SPME sample pre-treatment. In parallel to SPME, it has a large volume of stationary phase and extraction capacity, allowing for the simultaneous extraction and enrichment of a greater number of trace components without the need for additional stirrers. However, the selection of the type and thickness of the

TABLE 1 Several common pre-treatment methods in flavor analysis.

Methods	Advantages	Drawbacks	References
SPME	Solvent-free volatile molecule extraction method, rapid, brief, and low extraction temperature	Extraction of fibers is costly and stability needs to be improved	(47–50)
LLE	Wide range of appropriate substrates, a broad range of extraction solvents, high concentration multiplier, and simple operation	To facilitate the extraction of certain compounds, some of the low boiling point chemicals may be lost during the extraction and concentration process Large amounts of solvent are required and contain environmentally harmful contaminants. Extracted samples will contain small amounts of non-volatile components, contaminating analytical instruments	(51–53)
SPE	High efficiency, wide pH scope, mild operation conditions; enhances sample recovery and handles little volume specimens, effectively separates analytes from interferents, can eliminate matrix effects caused by ethanol, access great reproducibility in quantitative analysis	Complex and costly operation, extraction effect depends on sample matrix and analyte properties, time-consuming	(20, 54, 55)
SBSE	High sensitivity, selectivity, and excellent reproducibility	Poor efficiency, high-budget, sparse and selective coated extraction materials, and stirrers can cause the disproportionation of polar compounds; time-consuming, tedious operation process	(56, 57)
SAFE	Mild extraction conditions and good retention for aromatic substances	Time-consuming and cumbersome to manipulate	(9, 44, 58)
Derivatization reaction	Improved thermal stability of compounds that are difficult to detect and transform for GC detection and also for LC detection; improved extraction recovery, higher detection precision, and lower detection limits	Derivatives make chromatographic separation difficult and can easily introduce impurities or interfering peaks, increasing analytical costs	(31)

coating on the extraction head is equivalent to the selection of the column in chromatographic analysis (59). Furthermore, in SBSE, only two coatings of polydimethylsiloxane (PDMS) and ethylene glycol silicone (EG silicone) are commercially available (59, 69). In addition, there is a balance between coating thickness and equilibrium extraction time as the adsorption capacity of the analyte is determined. Furthermore, the detection limits are positively correlated with coating thickness and vice versa for the equilibrium extraction time (49, 59). The limited available adsorbents may become a bottleneck for the SBSE technique in FFT analysis, while the availability of new materials (e.g., carbon, metal-organic frameworks, polymers) with high concentration capacity for some specific analytes offers great opportunities for the development of efficient SBSE coatings (51, 70).

In addition to the pre-treatment methods mentioned above, other extraction methods have been used to extract FFT in foodstuffs such as solid phase extraction (SPE) (71, 72), derivatization (64, 73), and simultaneous distillation extraction (SDE) (74). Each method has advantages and disadvantages when used. Therefore, it is necessary to consider the physical–chemical properties of the target compound and the variability of the matrix in order to select the appropriate extraction method to achieve a comprehensive and accurate analysis of FFT in different matrices.

3.2. Non-specific technology

Sample preparation is followed by instrumental separation and analysis. With advances in theory and technology, there have been significant improvements in instrumentation for the detection of trace components in the field of flavor analysis. Generally, FFT in various matrices can be separated from the mixture by diverse columns in gas chromatography (GC) or liquid chromatography (LC) and further analyzed by high-sensitivity detectors such as mass spectrometry (MS) and flame ionization detector (FID).

Sulfur compounds are a kind of pivotal trace component in foodstuffs, often produced from sulfur-containing amino acids, and as such, many advanced analytical instruments are used to analyze various sulfur-containing compounds (e.g., FFT). GC-MS technology has become the most widely used technology in flavor component analysis due to its highly commercialized, powerful separation, and qualitative ability (75). Moreover, the qualification and quantification of aroma odorants in GC-MS are based on the divergence of different compounds and the concentration of molecules being related to peak intensity. GC-MS was used to identify FFT from roasted duck and it was regarded as a key aroma molecule (8). However, the detection limit for trace amounts of material is not sufficient, although it is fast, simple, and has fewer solvents. Other instruments are also suitable for the analysis of FFT in complex matrices, such as the gas chromatography pulsed flame photometric detector (GC-PFD), a detector with good selectivity and sensitivity for the analysis of sulfur-containing compounds such as FFT, at low cost. Recently, GC-PFPD was used to qualify and quantify the FFT in baijiu (10). Similar to GC-PFPD, GC-FID and gas chromatography-flame photometric detector (GC-FPD) have been also employed to analyze FFT in diverse matrices. For instance, Zhang et al. (37) applied GC-MS and GC-FPD coupled with GC-O to analyze sesame-flavored volatile compounds in baijiu and detected seven sulfur-containing compounds, including FFT and six other sulfur-containing chemicals (37). In a recent study, volatile thiols,

FFT, benzenemethanethiol, and three compounds of ethyl 2-mercaptopropionate were quantified by GC-MS and GC-FPD in four types of heat-treated soy sauce and raw soy sauce (76). Gas chromatography-sulfur chemiluminescence detector (GC-SCD) is the most efficient detector for sulfur-containing compounds with features of high sensitivity, selectivity, and equimolar concentration compared to other detectors such as FPD and PFPD. This stems from the chemiluminescent detection mechanism that sulfur-containing compounds are burned into SO at high temperature and then react with O_3 to generate an excited state SO_2^*, and when it degrades to the ground state, the excited state SO2* emits a characteristic spectrum (77–79). Due to the complexity of the actual sample composition, samples need to be pretreated for separation before SCD testing. In most applications, researchers combine SCD with GC to improve the purity and sensitivity of the analytes (80). Additionally, gas chromatography-time-of-flight mass spectrometry (GC-TOF/MS) is a versatile detector that is of increasing interest to analysts and industry investors for its fast response, high sensitivity, high accuracy, and high upper limits of mass for the determination of macromolecules (81).

Recently, GC-SCD and GC-TOF/MS were utilized to analyze FFT in wine (67, 74). To overcome the complexity of matrices, and improve peak capacity and separation of aroma compounds, GC × GC systems offer the advantages of increased peak capacity and high resolving power, which are essential for analyzing complex samples (82). For instance, comprehensive two-dimensional gas chromatography/time-of-flight mass spectrometry (GC × GC-TOFMS) and comprehensive two-dimensional gas chromatography-sulfur chemiluminescence detector (GC × GC-SCD) were utilized to characterize the FFT of baijiu and wine (11, 67, 83), respectively. Despite the extremely high sensitivity and response values of SCD detectors for sulfur-containing compounds, their maintenance costs need to be reduced and detection stability needs to be further improved in future studies. Furthermore, their application in practical research less popular since these apparatus (for example, SCD detector) are quite expensive and sensitive to external environmental changes, as well as the high maintenance costs. Additionally, the content of FFT may also experience loss caused by high-temperature GC inlet (generally 250°C) due to the instability when exposed to high temperatures.

3.3. Selective methods

The development of analytical approaches and the adaptation of derivatization to achieve more selective, efficient, complex and simplified thiol separation procedures, and/or thiol stabilization have been major developments in thiol separation and resolution. On the one hand, derivatization tempts to hide the sulfhydryl group (or shield a carbonyl group, take 4-mercapto-4-methylpentan-2-one as an example), and the thiol derivatives formed are chemically settled for isolation, as well as thermally stable for GC analysis (84–86). On the other hand, the introduction of substitutions implies that thiol derivatives indicate greater hydrophobicity, lower polarity, or higher proton affinity and may lead to better liquid chromatography (LC) separations and signal enhancement for mass spectrometry (MS)-based detection (54, 85).

In order to retard thiol degradation during analytical procedures, selective derivatization stabilizes the free thiol group. Similarly, for a more selective, efficient, and simplified study of FFTs in flavor analysis, derivatization and/or selective extraction in combination with chromatographic analysis is widely used, as derivatization is more easily extracted, chromatographed, and detected. For this reason, the analysis of FFT frequently implies the use of thiol-specific derivatization agents, such as p-hydroxymercury benzoate (p-HMB) (18) and 4,4′-dithiodipyridine (DTDP) (71).

2,3,4,5,6-pentafluorobenzyl bromide (PFBBr) is a derivative reagent for thiol compounds and is commonly used in the study of thiol compounds. This can be attributed to that the bromine atom is particularly susceptible to nucleophilic substitution by thiols in the presence of a base, thus obtaining PFBBr thiol derivatives desirable for not only stabilizing thiols but also providing electron capture capability and MS detection (87). The derivatization reaction between volatile thiols, such as FFT in wine, and PFBBr has been evaluated in several formats: automated headspace on-fiber derivatization (87), derivatization in organic reagent system (88), and derivatization in SPE column (89). SPME for fiber derivatization is fast, automated, and solvent-free. A polydimethylsiloxane/divinylbenzene (PDMS/DVB) SPME fiber is exposed successively to the vapors of tributylamine (5 min), PFBBr solution (5 min), subsequent, and pre-incubated wine sample (containing ethylenediaminetetraacetic acid, salt, and internal standard) to extraction for 10 min at 55°C (87). This approach provides convenience and less potential interference by using an autosampler and HS-SPME fiber, whereas the linear range of the studied thiols is not very wide and only two thiols (FFT and 3-mercaptohexyl acetate) can be analyzed by this method (87).

Furthermore, several sample preparations may require pH adjustment prior to injection. The p-hydroxymercuribenzoate (p-HMB) selective extraction process is tedious, laborious intensive, and hazardous as it is quite time-consuming due to the need to adjust pH and the use of organic reagents. More importantly, FFT is prone to oxidation during the laborious phase of sample preparation, which may further affect its quantification (23, 90). The FFT of misos were extracted by p-HMB and percolated on a basic anion-exchange column, then washed with high-purity water, released from the FFT-p-HMB complex in the column by using a cysteamine solution (500 mg/50 mL, pH 7), and concentrated and dried in a final step (18). Although this operation can be completed by GC-MS, there is instead room for future modifications of the method due to a large amount of solvent used, time-consuming, and labor-intensive.

Fortuitously, there is a derivatization reagent that can react with FFT in a wide pH range (55, 91). Thiol derivatization with DTDP has also been devised for wine analysis owing to the excellent derivatization ability of sulfhydryl groups at acidic pH, whereby DTDP selectively and rapidly directly reacts with thiols in the natural wine pH range (71). It has been reported that DTDP was used to react with FFT in baijiu (20) and wine (71), followed by SPE coupled with high-performance liquid chromatography-mass spectrometry (HPLC-MS/MS), resulting in excellent result with a limit of detection of 0.7∼1.5 ng/L. In coffee, the derivatization of FFT with ebselen has been reported (41). After extraction and derivatization, the concentration of FFT in coffee powder was

quantified by applying high-performance liquid chromatography-high resolution mass spectrometry (HPLC-HRMS). Notably, the presence of some important sulfur-containing molecules in coffee powder, such as 4-mercapto-1-butanol and 4-methoxy-2-methyl-2-buthiol, was also determined by the above method (41). Moreover, HRMS provides information on the molecular structure and composition of the molecule, which is crucial in food analysis and contributes to accuracy and reliability (75). The procedure is based on a selective and efficient reaction between thiols and ebselen (selenium-containing reagents), which enables the derivatization and separation of thiols in a time-saving and reduced sample manipulation manner. In summary, a number of key factors need to be considered when selecting the available derivatization reagents, namely reaction specificity and efficiency, matrix complexity and compatibility, sample manipulation required, introduction of interferences, and whether the interferences occur before or after the extraction of the analyte.

Moreover, to mitigate the loss of FFT caused by isolation procedures and decrease quantification errors, solvent extraction and concentration combined with stable isotope dilution assay (SIDA) was utilized (14, 24, 76), another approach is SPME (92, 93). This technique allows for the precise quantification of FFT in samples by using internal standards labeled with stable isotopes, which are often synthesized or purchased using expensive reagents. Recommendations are provided for analytical chemists interested in developing better methods for quantifying FFT in various matrices such as wine, baijiu, and other related matrices. Table 2 provides an overview of general published strategies with sample preparation, types of analysis, and major advantages and drawbacks.

4. Formation mechanism and manipulation of 2-furfurylthiol

The formation mechanism of FFT is highly complex, as it is influenced by variations in beverage production techniques. Previous studies have identified two key factors for its formation: thermochemical reactions and microbial metabolism (98–100). Hence in this section, relevant studies on the mechanisms of FFT formation in chemical reactions and microbial metabolism are summarized.

4.1. Chemical formation mechanism

The formation mechanism of FFT is not fully understood. It is generally accepted that sulfur-containing amino acids are key precursors and sources of sulfur for reactions with sugars and other minor compounds during manufacture (101–103). As early as 20 years ago, a theory was put forward that Maillard-type reactions play an indispensable role in FFT formation (104, 105). In accordance with previous literature, pentoses or hexoses and L-cysteine could produce FFT by producing furfural and H_2S in a model system (105–107), as demonstrated experimentally by bionic beans (102). In addition, the disturbance factors associated with their production, i.e., the yield of FFT, were also investigated in relation to the factors mentioned above. Temperature is one of the most significant factors in thermal treatment and/or fermentation and dominates manufacturing (108, 109). By adding L-cysteine and ribose to yeast extracts and heating them at high temperatures (100°C and 160°C, respectively), a model of the Maillard reaction was developed, showing that the yield of FFT increased with increasing temperature (27). Model experiments performed by L-cysteine and various carbohydrates at 145°C and 180°C, respectively, confirmed similar results (110). Moreover, pH is an essential factor in deciding the production of FFT. Generally, the amount of FFT is negatively correlated with the change in pH and its production generally increases with decreasing pH. This could also explain, to some extent, the fact that most FFT-rich beverages are acidic matrices (110, 111). Subsequently, the Maillard reaction between L-cysteine and xylose at different pH values from 4.0 to 7.0 confirmed this conclusion and clarified that the yield of FFT increased significantly when the pH was reduced from 7 to 4 (112). Similarly, the yield of FFT, the product of the Maillard reaction, varied depending on the type of carbohydrate. The effect of sugar type on FFT yields has been previously investigated and, in general, the Maillard reaction occurs following high-temperature treatment of L-cysteine and sugar, and the order of concentration of FFT obtained is ribose > xylose > fructose > glucose > rhamnose (107, 110). This phenomenon may be explained by the fact that L-cysteine mainly provides a sulfur source, carbohydrates produce furfural by dehydration, and the structure of pentose seems to have a higher yield/yield of furfural through reaction compared with hexose in terms of structure and composition (113–116). However, it is regrettable that these studies failed to fully investigate the pathways/reactions of furfural and L-cysteine for FFT production at the molecular level. The carbon module labeling (CAMOLA) technical approach is a powerful method to enucleate the formation mechanism of flavor molecules by labeling experiments and isotopomeric quantitation (117).

Based on the aforementioned studies, a comprehensive, appropriate, and in-depth study was performed on the model reaction system and real sample system (99). The main pathway for FFT formation involves the Maillard reaction, via dehydration of sugars, as presented in Figure 3 (113, 114). During high-temperature heating, glucose and L-cysteine undergo Amadori rearrangement and 1,2-enolisation to form 3-deoxyglucosone. Further hydroxyl-aldol condensation reactions are carried out, removing one molecule of alcohol and two molecules of water in turn, gradually producing 3-deoxypentosone and the final product furfural. The furfural undergoes a reduction reaction to generate 2-furfuryl alcohol. Finally, H_2S from the pyrolysis of L-cysteine reacts with 2-furfuryl alcohol to remove one molecule of water, which in turn produces FFT. In addition, previous investigations have suggested that furfural can form FFT by reacting with H_2S in significantly higher yields than the reaction between L-cysteine and furfural (110). This may be related to the fact that H_2S is a hydrolysis product of L-cysteine, omitting the hydrolysis reaction step. In addition to thermochemical reactions under thermal treatment conditions, microbial metabolism or enzyme catalysis is essential in the production of FFT. Therefore, the contribution of related microorganisms or enzymes during fermentation will be discussed in the following section.

TABLE 2 Analytical methods developed for the analysis of FFT in various matrices.

Sample preparation	Analysis	Quantification	LOD (μg/L)	Advantages (+)/ drawbacks (-)	Matrices	References
Non-specific techniques						
SPME	GC-MS	External calibration	na	(+) less solvents	Fermentation broth	Zha et al. (94)
HS-SPME	GC-PFPD	Internal calibration ISTD:(4-methylthio-1-butanol)	6.0	(+) less solvents	Baijiu	Sha et al., (10)
HS-SPME	GC×GC-TOFMS	na	na	(+) less solvents	Baijiu	Cheng and Xu (83)
HS-SPME	GC-MS	Internal calibration ISTD:(2-methyl-3 Heptanone)	na	(+) less solvents	Beijing roasted duck	Liu et al. (8)
HS-SPME	GC-MS	ISTD:(2-octanol)	na	(+) less solvents	Fermented fish	Gao et al., (92)
HS-SPME	GC-IMS	ISTD:(2-methyl-3-heptanone)	na	(+) less solvents	Yeast extract	Raza et al., (27)
HS-SPME	GC-MS	Internal calibration ISTD:(1,2-dichlorobenzene)	na	(+) less solvents (+) extremely low limit of quantification	Coffee	Sun et al., (34)
SPME	GC-MS	ISTD:(2-octanol)	na	(+) less solvents	Seasoning product	Li and Liu (15)
LLE	GC×GC-SCD	ISTD:(4-(methylthio)-1-butanol)	0.83×10^{-3}	(-) organic solvent (+) sensitive to sulfur-containing compounds	Baijiu	Song et al. (14)
LLE	GC-FPD	na	na	(-) organic solvent (-) Time-consuming	Baijiu	Zhang et al. (37)
LLE	GC-MS	Internal calibration ISTD: (4-methoxy-2-methyl-2-mercaptobutane)	na	(-) organic solvents	Soy sauce	Meng et al. (76)
SAFE	GC-MS	Internal calibration ISTD:(1,2-dichlorobenzene)	na	(-) Time-consuming (-) laborious (-) organic solvent	Youtiao	Du et al. (44)
SAFE	GC-MS	Standard addition ISTD:(1-octanol-d18)	na	(-) long extraction time (-) large sample volume (-) hazardous dichloromethane	Roasted goose	Gasior et al. (24)
SAFE	GC-MS	Internal calibration ISTD:(1,2-dichlorobenzene)	na	(-) long extraction time (-) large sample volume (-) hazardous dichloromethane	Pig pork broth	Zhao et al. (68)
SBSE	GC-MS	Internal calibration ISTD: (6MH)	0.36	(-) pH adjustment	Wine	Elpa et al. (56)
Target methods						
Extraction with p-HMB and ETP, followed by rinsing on ion exchange resin	GC-MS	Internal calibration ISTD:(ETP derivatives (2FM))	na	(-) Time-consuming (-) organic solvent	Japanese sake	Osafune et al. (23)
Derivatization with DTDP followed by SPE extraction	HPLC-MS/MS	External calibration	$0.7 \sim 1.5 \times 10^{-3}$	(-) organic solvent (+) Moderate amounts of sample required (+) non-hazardous chemical	Wine	Capone et al. (71)
Extraction with p-HMB, followed by rinsing on SPE and adjusting pH	GC-MS	ISTD:(3-methoxymethylbutanethiol, 3MMB)	na	(-) Time-consuming (-) pH adjustment	Wine	Picard et al. (95)

(Continued)

TABLE 2 (Continued)

Sample preparation	Analysis	Quantification	LOD (μg/L)	Advantages (+)/ drawbacks (-)	Matrices	References
SPE extraction followed by derivatization with DBU and PFBBr	GC-MS	Internal calibration ISTD:(4-methoxy-R-toluenethiol)	4×10^{-3}	(-) Time-consuming (-) organic solvent (-) Large sample volume needed	Wine	Mateo-Vivaracho et al. (96)
Derivatization with ebselen followed by LLE extraction	HPLC-MS	Internal calibration ISTD:(4-methoxy-α-toluenethiol)	na	(-) organic solvent (+) extremely low LOQ(0.01ng/L)	Beer and wine	Vichi et al. (97)
Extraction with p-HMB, followed by release from the thiol-p-HMB complex by using cysteamine solution	GC-MS	Internal calibration ISTD:(4-methoxy-2-methyl-2-mercaptobutane)	na	(-) organic solvent (-) pH adjustment (-) Time-consuming (-) laborious	Fermented soybean paste miso	Ohata et al. (18)
HS-SPME	GC-MS	SIDA ISTD:(2-[$2H_2$]-furfurylthiol)	na	(+) Simple and fast extraction (+) less solvents (-) expensive reagent	Coffee	Kulapichitr et al. (93)
Derivatization with ebselen followed by extraction with dichloromethane	HPLC-HRMS	Internal calibration ISTD:(4-methoxy-α-toluenethiol)	na	(+) extremely low LOQ (0.1ng/L) (-) hazardous reagent	Coffee	Quintanilla-Casas et al. (64)
Extraction with hexane and derivatization with ebselen	HPLC-HRMS	Internal calibration ISTD:(4-methoxy-α-toluenethiol)	na	(-) organic solvent	Coffee powder	Vichi et al. (41)
SAFE	GC×GC-TOF-MS	SIDA ISTD:(2-[$2H_2$]-furfurylthiol)	na	(-) organic solvent (-) Large reagent volume needed (-) time-consuming	Hazelnuts	Kiefl and Schieberle (6)
Derivatization with DTDP and SPE extraction	HPLC-MS/MS	SIDA ISTD: (d_5-2-furfurylthiol)	na	(-) organic solvent (+) moderate amounts of sample required	Wine	Siebert et al. (12)
Derivatization with DTDP and SPE extraction	UPLC-MS/MS	ISTD:(2-phenylethanethiol) internal calibration	0.001	(+) moderate amounts of sample required (+) low LOD (-) cumbersome operation (-) organic solvent	Baijiu	Yan et al. (20)

na, not available; SIDA, stable isotope dilution assay; DTDP, 4,4-dithiodipyridine; ISTD, internal stand; 6MH, 6-mercaptohexanol; SBSE, stir bar sorptive extraction; DBU, 1,8-diazabicyclo [5.4.0] undec-7-ene; PFBBr, 2,3,4,5,6-pentafluorobenzylbromide; SAFE, solvent-assisted flavor evaporation; Ebselen, 2-phenyl-1,2-benzisoselenazol-3(2H)-one; LOQ, limit of quantification; ETP derivatives (2FM), derivatization of 2FM using ETP; 2FM, 2-furfurylthiol.

4.2. Microbial metabolism or enzyme catalysis

Microorganisms constitute the complicated micro-ecological environment of the fermentation system, and flavor metabolites generated in the presence of these microflora are closely related to the quality and flavor of fermented beverages (21, 119–121). Yeast, molds, and bacteria are the main microorganisms in the fermentation process. Generally, these members can offer the impetus for the development of fermentation and flavor components. For instance, *Pichia*, *Saccharomyces*, *Aspergillus*, *Rhizomucor*, and *Rhizopus* in jiuqu (a sort of starter in Chinese baijiu), molds in soy sauce, and *Bacillus subtilis* in natto would secrete enzymes to hydrolyze starches and proteins of raw materials (38, 122, 123), respectively, and leads to hydrolysates undergoing Maillard reactions under appropriate conditions. Additionally, microorganisms also consume carbohydrates to produce corresponding metabolites, such as yeast and lactic acid bacteria, which could convert glucose into alcohol and lactic acid (124–126). Consequently, the formation of FFT during fermentation can be a dynamic transversion motivated by the action of microorganisms and enzymes. Conversely, there is still a lack of systematic and comprehensive knowledge regarding the exact role of microbes in the formation of FFT although several studies have been conducted on the formation mechanism of FFT, and some achievements have been obtained.

Based on the preliminary literature research, the biotransformation mechanism of 2-furfurylthiol was summarized and a metabolic production pathway was mapped as follows (Figure 4). In previous reports, furfural and L-cysteine could be used as precursors and produce FFT through yeast metabolism (127). *Pichia*, *Schizosaccharomyces*, *Saccharomyces*, and *Zygosaccharomyces* are dominant yeast species in baijiu

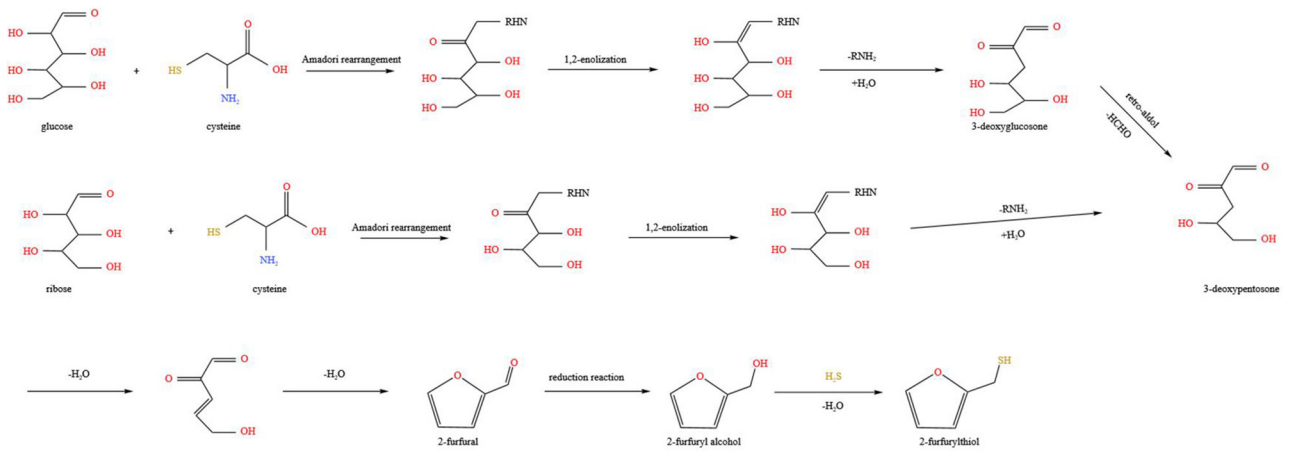

FIGURE 3
Hypothetical reaction schemes of the formation of FFT from glucose and ribose via Maillard reaction, respectively. Adapted from Liu et al. (99), Zhao et al. (118).

fermentation, which are essential for the formation of flavor compounds (128). An isolated *S. cerevisiae strain* G20 showed the highest production capacity of FFT with a yield of 3.03 mg/L, and the genes STR3 and CYS3 (encoded cystathionine β-lyase, and cystathionine γ-lyase, respectively) were found to be closely related to FFT synthesis by gene knockout and overexpression verification (94, 129). In addition to flavor compound-producing strain, microbial interactions were found to be an alternative strategy to regulate the formation of flavor compounds during fermentation. *Bacillus subtilis* is an indispensable strain in the fermentation process of baijiu. Amino acids are mainly converted from proteins via the hydrolysis of protease, and *Bacillus subtilis* was one of the major microorganisms producing protease (130). There are synergistic effects between *Bacillus subtilis* and other functional microorganisms. For example, in the fermentation of baijiu inoculated with *Bacillus subtilis* LBM 10019 and *Bacillus vallismortis* LBM 10020, the FFT content in baijiu increased from 1.29 μg/L to 2.44 μg/L after inoculation compared to the non-inoculated group (33). This phenomenon can be explained by the inoculation of *Bacillus*. *Bacillus* inoculation provides a constant supply of L-cysteine and more sulfur sources to the associated FFT-producing strains, thus increasing the FFT content of the final baijiu (131, 132).

In general, there are two main pathways to generate FFT. (1) In the process of alcohol fermentation, mercaptan compounds are released from their non-aromatic precursors through the function of yeast. Although the exact mechanisms by which yeast convert cysteinylated and glutathionylated precursors into the corresponding volatile thiols are still not fully understood, some consensus exists regarding these mechanisms. Previous studies have reported that the uptake of cysteine-3-mercaptohexan-1-ol (3MH) adduct precursors is structurally similar to L-cysteine and is induced by amino acid transport proteins; therefore, it is suggested that furfuryl-cysteine adducts, precursors of FFT, are also induced by amino acid transporters (133, 134). Thus, L-cysteine reacts with furfural to produce furfural-cysteine conjugates (129), which are subsequently transported into the cell by amino acid permeases encoded by genes MUP1, Bap2, Bap3, Gnp1, and OPT1 (encoding Mup1p, branched-chain amino acid permease, amino acid transporter, glutamine permease, oligopeptide transporter, respectively) (134–138). The furfuryl-cysteine adduct is cleaved *in vitro* or after transport into the cell by the C-S lyase encoded by the genes CYS3 and STR3 to produce FFT, pyruvate, and ammonia (129). (2) L-cysteine is transferred into cells under the action of amino acid transporters and then produced as hydrogen sulfide under the guidance of α- and β-elimination reactions or cystathionine β-synthase and cystathionine γ-cleavage enzymes encoded by genes CYS4 and CYS3, respectively (139, 140). Meanwhile, it is worth noting that although L-cysteine is an essential sulfur source of FFT, a high concentration of L-cysteine will restrain the growth of yeast (141). In most cases, the dehydration of carbohydrates produces furfuryl alcohol correspondingly produced by reduction reactions, and the hydroxyl group is replaced by the HS^- ion in hydrogen sulfide, ultimately producing FFT, which is secreted extracellularly by the action of carrier proteins (113, 142, 143). It also has been reported that hydrogen sulfide can be used as a precursor to produce FFT from furfural in yeast (100, 142, 144). Many enzymes secreted by microbes in the fermentation environment can catalyze the substrate of materials to generate consequential flavor compounds during growth and metabolism. Lipase from *Candida albicans* served as a biocatalyst to react with S-2-furfuryl thioacetate, and obtained the corresponding product, FFT (145). This finding provides an alternative, environmentally friendly approach to producing natural thiol species and offers theoretical support and technical guidance for generating characteristic flavors in fermented beverages. Future research can focus on the metabolic mechanisms and driving factors of microorganisms and enzymes during catalysis to better regulate the production of FFT during fermentation.

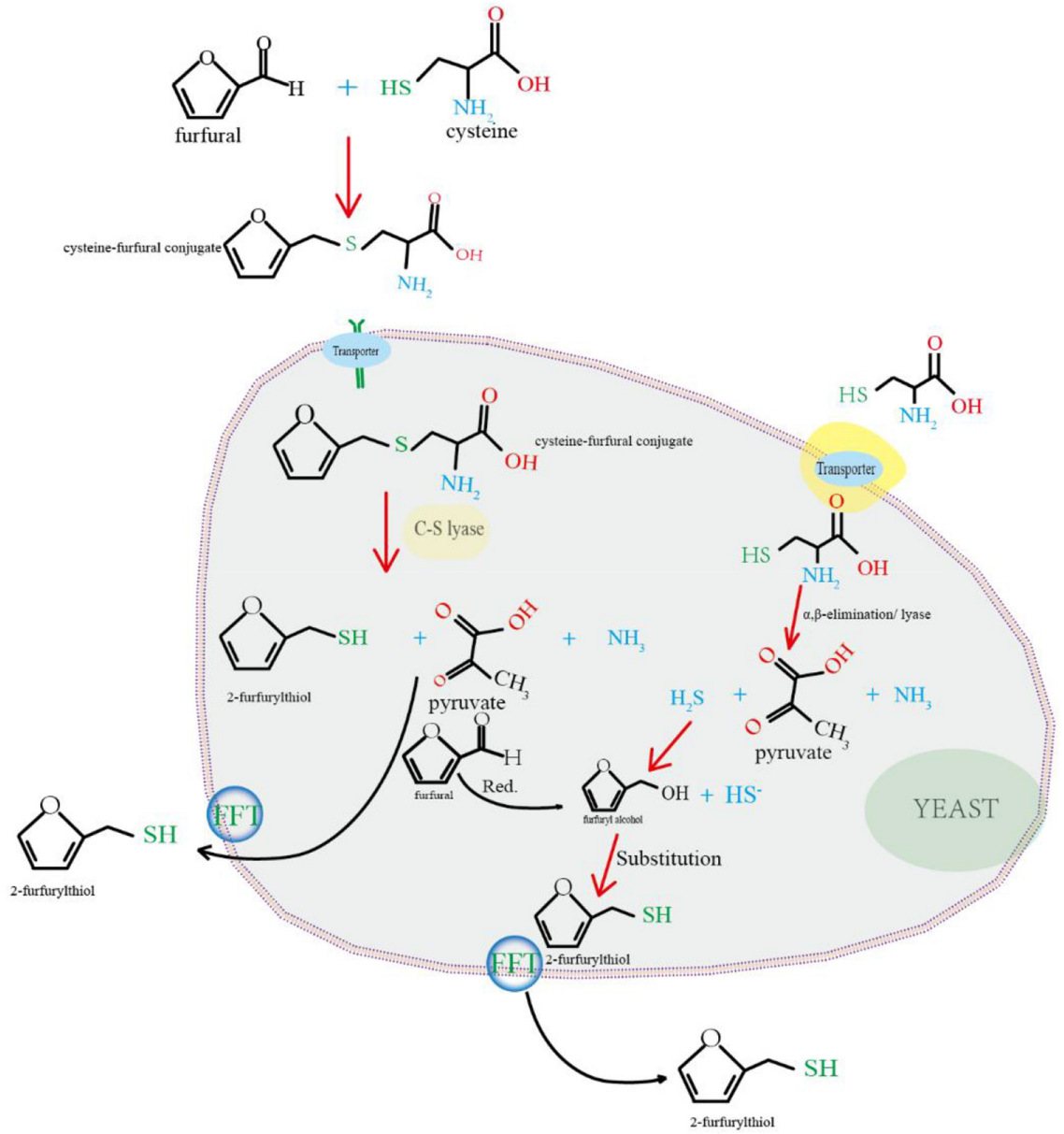

FIGURE 4
Schematic diagram of the hypothesized biotransformation of FFT.

4.3. Staling mechanism and regulation of FFT

Aroma plays a crucial role in determining the quality and flavor of a product, as well as influencing individual preferences. However, various external and internal factors lead to the degradation or loss of aroma components in beverages during processing, storage, and transportation. These factors can significantly affect the homogeneity of flavor and quality of the product, ultimately affecting the sensory experience of the consumer and the economic interests of the manufacturer. Correspondingly, we propose to investigate the mechanisms and regulation of aroma deterioration associated with FFT in the following paragraphs.

4.3.1. Staling pathway of FFT

Previous studies have reported that the content of FFT may present unstable/loss problems during production or storage owing to its highly volatile and reactive properties (29, 31, 146). To better understand the degradation mechanism of FFT, the research status on the dissipation mechanism of FFT is discussed.

The fading mechanism of FFT can be categorized into physical and chemical factors. The physical factor involves the irreversible physical diffusion of FFT in coffee, as it is highly volatile and readily evaporates into the headspace in free form, ultimately leading to the loss of sulfur/roast aroma. Nevertheless, chemically induced FFT fading is the result of a combination of reaction mechanisms: ionic and free radical reaction pathways (147).

1 Ionic reaction. Ionic reaction involves electron transfer between the electron donor (nucleophile) and electron acceptor (electrophile) (17). From the perspective of structure, FFT is a strong nucleophilic reagent owing to the existence of sulfhydryl groups of FFT and is easy to participate in the nucleophilic reaction because it is unstable in nature and prone to be oxidized (148). There are several electrophilic addition sites in the coffee matrix, and some of these electrophilic reagents are formed by oxidation. For instance, polyphenols will generate semiquinones and quinones under oxidation conditions (149), while quinones have the potential to add to nucleophiles such as thiols (150, 151). Melanoids, a common macromolecular compound in coffee, contain the 1,4-bis (5-amino-5-carboxy-1-pentyl) pyrazine radical cation (CROSSPY), which can covalently bind to FFT to form conjugates, leading to the degradation of FFT in model systems and in freshly brewed coffee (152, 153). In addition, chlorogenic acid is the main organic acid in coffee, although it does not reduce FFT in studies of model systems (153, 154). Nevertheless, degradation products of chlorogenic hydroxyquinolines can act as aroma-binding precursors for FFT in a semi-simulated reaction system prepared with raw coffee beans, leading to a depletion of FFT (154, 155). Findings similar to the above results were repeated in subsequent studies (156, 157).

2 Free radical reaction. Free radicals can also react with non-volatile components from aroma components or coffee matrices (156). Blank et al. (148) found that the hydroxyl radical generated by hydrogen peroxide and transition metal during brewing coffee could induce FFT to form the corresponding dimer. In addition, the degradation rate of FFT was positively correlated with the activity of hydroxyl radical by investigating the influence of Fenton reaction model conditions on FFT. Subsequently, the model test further proved that furfuryl disulfide is the main oxidation product of free radical reaction (148, 156). Apart from the storage phase, FFT may change significantly during coffee consumption (158). Buettner et al. revealed through model tests that enzymes in saliva can alter the physicochemical properties and sensory characteristics of FFT (158, 159). Initial progress has been made in the study of the rapid decay of FFT caused by non-volatile components in the coffee matrix. In general, it is mainly caused by free radical reaction and ionic reaction (46), and some potential aroma-binding substances have been proposed. Nevertheless, the study of each degradation reaction pathway remains relatively isolated, and the integration and comparative evaluation between each pathway are still insufficient. The main reasons and key components of the rapid degradation of FFT need to be further investigated in future.

4.3.2. Stabilization of FFT

To enhance the stability of holistic aroma during processing and storage, several methods have been proposed to stabilize aroma odor substances. For instance, cyclodextrins are often used as fragrance stabilizers to embed flavor substances to form inclusion complexes, thereby improving the storage stability of volatile flavor substances (160, 161).

Since the staling of FFT in coffee is divided into reversible or irreversible, some studies on the reversible release of FFT have been carried out based on reversible binding studies, and some initial progress has been made on this research topic. Early studies have found that L-cysteine releases FFT bound by the coffee matrix (162), and high concentration of L-cysteine prevents the formation of FFT dimer for quantification in aroma analysis (34). As a hydroxyl radical scavenger, ascorbic acid can be used to mitigate the degradation of FFT caused by free radicals. Furthermore, appropriate anaerobic conditions favor the persistence of aroma compounds. An interesting phenomenon is that FFT exhibits better stability under anaerobic conditions than aerobic conditions (156). Recently, a protective effect provided by ascorbic acid, H_2S, and wine flavanols has been observed (163). More recently, Sun et al. selected different additives (L-cysteine, ascorbic acid, methionine, sodium sulfite, and glutathione) as aroma-releasing agents; it was finally determined that the addition of 0.045 g/L of L-cysteine and 0.05 g/L of ascorbic acid improved the aroma of fresh coffee and could increase the content of sulfur-containing compounds (17). However, there are relatively few studies investigating the extended aroma duration of FFT. In future, additional studies on aroma modulation by FFT in different matrices could be considered, e.g., the development of food-grade aroma retardants packaged in specialized capsules to prolong the release of beverage aroma.

5. Perspectives and conclusion

Aroma is a key factor in the flavor and quality of food products, and the perception of aroma plays an important role during consumption. Challenges in FFT investigation are the need to modify analytical methods, including specific extraction and detection due to trace concentrations, non-uniform distribution in the same/similar species, and interactions between FFT and other species in the matrix. Extraction processes often need to be fast, solvent less, efficient, and simple, while detection often requires low detection limits and high stability due to low FFT concentrations. In terms of specific extraction, currently, available approaches can be coupled with the popular MS detection for sensitive analysis of FFT. Appropriate analytical methods can provide more accurate and comprehensive information, as this is a primary prerequisite for flavor studies. FFT has a pivotal effect on the flavor and quality of beverages. Beverages have long been consumed as an integral part of the daily human diet. Nevertheless, much less attention has been paid to FFT in fermentation matrices than in thermal treatments and model systems. This review provides the first systematic review of FFT. The presence of FFT is the result of diverse factors that affect the precursor concentrations. This occurs at all levels: (i) in raw materials, (ii) released during heat treatment and/or fermentation, and (iii) stored under convenient conditions until the final product is consumed.

The presence of precursors in crude materials depends on several factors, such as the type and content of amino acid and sugar, vine management, and maturity. These aspects are currently well-known, even if the mechanisms implicated are not fully elucidated. The conversion of these precursors into FFT during

heating and/or fermentation remains the key step and the subject of most research in this field. Studies carried out by research groups worldwide have been able to identify many precursors and determine their conversion mechanisms, depending on the composition of the substance (i.e., the type of sugars and amino acids and the location of the precursors in the matrix), as well as yeast genetic information and process conditions. In most of these studies, organic chemistry is necessary for the identification and quantification of FFT and its precursors and for the better comprehension of yeast contributions and physiology. As the discovery of some precursors is new, many aspects in this field have not been comprehensively investigated. After final products are obtained, all of the technology employed must focus on preventing oxidation and binding upon the release of the FFT. Consequently, chemistry and biochemistry offer the only tool to understand the various mechanisms (oxidation or nucleophilic substitution) and therefore propose ways to avoid the loss of aroma due to the disappearance of these compounds. Our review helps the academic community to grasp the current state of research and informs further studies on FFT in beverages.

Author contributions

GZ investigation, methodology, writing—original draft, and writing—review and editing. PX, MY, and BS: writing—review and editing. YX: data curation, formal analysis, writing—original draft, and writing—review and editing. HL: supervision, validation, and writing—review and editing. YL: project administration and resources. JS: supervision. All authors contributed to the article and approved the submitted version.

Funding

This study was supported by the National Natural Science Foundation of China (32172340 and 31972193) and the Young Elite Scientists Sponsorship Program by CAST (2022QNRC001).

Conflict of interest

GZ and HL were employed by Beijing Technology and Business University. YL was employed by Inner Mongolia Taibus Banner Grassland Brewing Co., Ltd.

The remaining authors declare that the research was conducted in the absence of any commercial or financial relationships that could be construed as a potential conflict of interest.

Publisher's note

References

1. Lyu J, Chen S, Nie Y, Xu Y, Tang K. Aroma release during wine consumption: factors and analytical approaches. *Food Chem.* (2021) 346:128957. doi: 10.1016/j.foodchem.2020.128957

2. Pu D, Shan Y, Wang J, Sun B, Xu Y, Zhang W, et al. Recent trends in aroma release and perception during food oral processing: a review. *Crit Rev Food Sci Nutr.* (2022) 21:1–17. doi: 10.1080/10408398.2022.2132209

3. Armelin-Correa LM, Malnic B. Combining in vivo and in vitro approaches to identify human odorant receptors responsive to food odorants. *J Agric Food Chem.* (2018) 66:2214–8. doi: 10.1021/acs.jafc.6b04998

4. Shepherd GM. The human sense of smell: are we better than we think? *PLoS Biol.* (2004) 2:e146. doi: 10.1371/journal.pbio.0020146

5. Shepherd GM. Outline of a theory of olfactory processing and its relevance to humans. *Chem Senses.* (2005) 30:i3–i5. doi: 10.1093/chemse/bjh085

6. Kiefl J, Schieberle P. Evaluation of process parameters governing the aroma generation in three hazelnut cultivars (corylus avellana l.) by correlating quantitative key odorant profiling with sensory evaluation. *J Agric Food Chem.* (2013) 61:5236–5244. doi: 10.1021/jf4008086

7. Li H, Qin D, Wu Z, Sun B, Sun X, Huang M, et al. Characterization of key aroma compounds in Chinese Guojing sesame-flavor Baijiu by means of molecular sensory science. *Food Chem.* (2019) 284:100–7. doi: 10.1016/j.foodchem.2019.01.102

8. Liu H, Wang Z, Zhang D, Shen Q, Pan T, Hui T, et al. Characterization of key aroma compounds in Beijing Roasted Duck by gas chromatography–olfactometry–mass spectrometry, odor-activity values, and aroma-recombination experiments. *J Agric Food Chem.* (2019) 67:5847–56. doi: 10.1021/acs.jafc.9b01564

9. Majcher MA, Klensporf-Pawlik D, Dziadas M, Jelen HH. Identification of aroma active compounds of cereal coffee brew and its roasted ingredients. *J Agric Food Chem.* (2013) 61:2648–2654. doi: 10.1021/jf304651b

10. Sha S, Chen S, Qian M, Wang C, Xu Y. Characterization of the typical potent odorants in Chinese roasted sesame-like flavor type liquor by headspace solid phase microextraction–aroma extract dilution analysis, with special emphasis on sulfur-containing odorants. *J Agric Food Chem.* (2017) 65:123–31. doi: 10.1021/acs.jafc.6b04242

11. Song X, Zhu L, Wang X, Zheng F, Zhao M, Liu Y, et al. Characterization of key aroma-active sulfur-containing compounds in Chinese laobaigan Baijiu by gas chromatography-olfactometry and comprehensive two-dimensional gas chromatography coupled with sulfur chemiluminescence detection. *Food Chem.* (2019) 297:124959. doi: 10.1016/j.foodchem.2019.124959

12. Siebert TE, Barker A, Pearson W, Barter SR, de Barros Lopes MA, Darriet P, et al. Volatile compounds related to 'stone fruit' aroma attributes in viognier and chardonnay wines. *J Agric Food Chem.* (2018) 66:2838–50. doi: 10.1021/acs.jafc.7b05343

13. Chen S, Sha S, Qian M, Xu Y. Characterization of volatile sulfur compounds in Moutai liquors by headspace solid-phase microextraction gas chromatography-pulsed flame photometric detection and odor activity value. *J of Food Sci.* (2017) 82:2816–22. doi: 10.1111/1750-3841.13969

14. Song X, Zhu L, Jing S, Li Q, Ji J, Zheng F, et al. Insights into the role of 2-methyl-3-furanthiol and 2-furfurylthiol as markers for the differentiation of Chinese light, strong, and soy sauce aroma types of Baijiu. *J Agric Food Chem.* (2020) 68:7946–54. doi: 10.1021/acs.jafc.0c04170

15. Li X, Liu SQ. Effect of thermal treatment on aroma compound formation in yeast fermented pork hydrolysate supplemented with xylose and cysteine. *J Sci Food Agric.* (2022) 102:1457–65. doi: 10.1002/jsfa.11480

16. Sun J, Wang Z, Sun B. Low quantity but critical contribution to flavor: review of the current understanding of volatile sulfur-containing compounds in Baijiu. *J Food Compos Anal.* (2021) 103:104079. doi: 10.1016/j.jfca.2021.104079

17. Sun Z, Cui H, Yang N, Ayed C, Zhang X, Fisk ID. Enhancement of coffee brew aroma through control of the aroma staling pathway of 2-furfurylthiol. *Food Chem.* (2020) 322:126754. doi: 10.1016/j.foodchem.2020.126754

18. Ohata M, Tominaga T, Dubourdieu D, Kubota K, Sugawara E. Quantification and odor contribution of 2-furanmethanethiol in different types of fermented soybean paste miso. *J Agric Food Chem.* (2009) 57:2481–5. doi: 10.1021/jf803258c

19. Xu Y, Zhao J, Liu X, Zhang C, Zhao Z, Li X, et al. Flavor mystery of Chinese traditional fermented baijiu: The great contribution of ester compounds. *Food Chem.* (2022) 369:130920. doi: 10.1016/j.foodchem.2021.130920

20. Yan Y, Lu J, Nie Y, Li C, Chen S, Xu Y. Characterization of volatile thiols in Chinese liquor (Baijiu) by ultraperformance liquid chromatography–mass spectrometry and ultraperformance liquid chromatography–quadrupole-time-of-flight mass spectrometry. *Front Nutr.* (2022) 9:1022600. doi: 10.3389/fnut.2022.1022600

21. Yang L, Fan W, Xu Y. Metaproteomics insights into traditional fermented foods and beverages. *Compr Rev Food Sci Food Saf.* (2020) 19:2506–29. doi: 10.1111/1541-4337.12601

22. Pérez D, Denat M, Minebois R, Heras JM, Guillamón JM, Ferreira V, et al. Modulation of aroma and chemical composition of albariño semi-synthetic wines by non-wine *Saccharomyces* yeasts and bottle aging. *Food Microbiol.* (2022) 104:103981. doi: 10.1016/j.fm.2022.103981

23. Osafune Y, Toshida K, Han J, Kishimoto T, Iizuka-Furukawa S, Isogai A, et al. Identification of 2-furanmethanethiol contributing to roast aroma in honkaku shochu and awamori. *J Biosci Bioeng.* (2022) 133:555–9. doi: 10.1016/j.jbiosc.2022.03.003

24. Gasior R, Wojtycza K, Majcher MA, Bielińska H, Odrzywolska A, Baczkowicz M, et al. Key aroma compounds in roasted white kołuda goose. *J Agric Food Chem.* (2021) 69:5986–96. doi: 10.1021/acs.jafc.1c01475

25. Jia X, Zhou Q, Wang J, Liu C, Huang F, Huang Y. Identification of key aroma-active compounds in sesame oil from microwaved seeds using e-nose and hs-spme-gc×gc-tof/ms. *J Food Biochem.* (2019) 43:e12786. doi: 10.1111/jfbc.12786

26. Burdack-Freitag A, Schieberle P. Characterization of the key odorants in raw italian hazelnuts (corylus avellana l. var tonda romana) and roasted hazelnut paste by means of molecular sensory science. *J Agric Food Chem.* (2012) 60:5057–64. doi: 10.1021/jf300908d

27. Raza A, Song H, Begum N, Raza J, Iftikhar M, Li P, et al. Direct classification of volatile organic compounds in heat-treated glutathione-enriched yeast extract by headspace-gas chromatography-ion mobility spectrometry (hs-gc-ims). *Food Anal Methods.* (2020) 13:2279–89. doi: 10.1007/s12161-020-01847-8

28. Rocchetti G, Braceschi GP, Odello L, Bertuzzi T, Trevisan M, Lucini L. Identification of markers of sensory quality in ground coffee: an untargeted metabolomics approach. *Metabolomics.* (2020) 16:1–12. doi: 10.1007/s11306-020-01751-6

29. Sun Z, Yang N, Liu C, Linforth RST, Zhang X, Fisk ID. Aroma binding and stability in brewed coffee: a case study of 2-furfurylthiol. *Food Chem.* (2019) 295:449–55. doi: 10.1016/j.foodchem.2019.05.175

30. Wang L, Fan S, Yan Y, Yang L, Chen S, Xu Y. Characterization of potent odorants causing a pickle-like off-odor in Moutai-aroma type Baijiu by comparative aroma extract dilution analysis, quantitative measurements, aroma addition, and omission studies. *J Agric Food Chem.* (2020) 68:1666–77. doi: 10.1021/acs.jafc.9b07238

31. Dulsat-Serra N, Quintanilla-Casas B, Vichi S. Volatile thiols in coffee: a review on their formation, degradation, assessment and influence on coffee sensory quality. *Food Res Int.* (2016) 89:982–8. doi: 10.1016/j.foodres.2016.02.008

32. Roland A, Schneider R, Razungles A, Cavelier F. Varietal thiols in wine: discovery, analysis and applications. *Chem Rev.* (2011) 111:7355–76. doi: 10.1021/cr100205b

33. Shen T, Liu J, Wu Q, Xu Y. Increasing 2-furfurylthiol content in Chinese sesame-flavored Baijiu via inoculating the producer of precursor l-cysteine in Baijiu fermentation. *Food Res Int.* (2020) 138:109757. doi: 10.1016/j.foodres.2020.109757

34. Sun Z, Hayat K, Yu J, Karangwa E, Duhoranimana E, Zhang X, et al. Quantification of free 2-furfurylthiol in coffee brew using a prefabricated coffee model. *Food Anal Methods.* (2018) 11:654–62. doi: 10.1007/s12161-017-1034-8

35. Carrapiso AI, Ventanas J, García C. Characterization of the most odor-active compounds of iberian ham headspace. *J Agric Food Chem.* (2002) 50:1996–2000. doi: 10.1021/jf011094e

36. Carrascon V, Escudero A, Ferreira V, Lopez R. Characterisation of the key odorants in a squid broth (illex argentinus). *LWT - Food Sci Technol.* (2014) 57:656–62. doi: 10.1016/j.lwt.2014.02.010

37. Zhang Y, Sun J, Zhang F, Huang M, Liu Y, Sun B. Analysis of sulfur compounds in sesame flavor liquor. *J Chinese Institute Food Sci Technol.* (2014) 14:218–25.

38. Wang B, Wu Q, Xu Y, Sun B. Synergistic effect of multiple saccharifying enzymes on alcoholic fermentation for Chinese Baijiu production. *Appl Environ Microbiol.* (2020) 86:e00013–20. doi: 10.1128/AEM.00013-20

39. Baggenstoss J, Poisson L, Kaegi R, Perren R, Escher F. Coffee roasting and aroma formation: application of different time–temperature conditions. *J Agric Food Chem.* (2008) 56:5836–46. doi: 10.1021/jf800327j

40. Cheong MW, Tong KH, Ong JJM, Liu SQ, Curran P, Yu B. Volatile composition and antioxidant capacity of Arabica coffee. *Food Res Int.* (2013) 51:388–96. doi: 10.1016/j.foodres.2012.12.058

41. Vichi S, Jeri Y, Cortes-Francisco N, Palacios O, Caixach J. Determination of volatile thiols in roasted coffee by derivatization and liquid chromatography-high resolution mass spectrometric analysis. *Food Res Int.* (2014) 64:610–7. doi: 10.1016/j.foodres.2014.07.044

42. Song H, Liu J. GC-O-MS technique and its applications in food flavor analysis. *Food Res Int.* (2018) 114:187–98. doi: 10.1016/j.foodres.2018.07.037

43. Tamura H, Fujita A, Steinhaus M, Takahisa E, Watanabe H, Schieberle P. Identification of novel aroma-active thiols in pan-roasted white sesame seeds. *J Agric Food Chem.* (2010) 58:7368–75. doi: 10.1021/jf100623a

44. Du W, Zhao M, Zhen D, Tan J, Wang T, Xie J. Key aroma compounds in Chinese fried food of youtiao. *Flavour Frag J.* (2019) 35:88–98. doi: 10.1002/ffj.3539

45. Mayer F, Czerny M, Grosch WE. Sensory study of the character impact aroma compounds of a coffee beverage. *Eur Food Res Technol.* (2000) 211:272–6. doi: 10.1007/s002170000169

46. Weerawatanakorn M, Wu J, Pan M, Ho C. Reactivity and stability of selected flavor compounds. *J Food Drug Anal.* (2015) 23:176–90. doi: 10.1016/j.jfda.2015.02.001

47. Xu CH, Chen GS, Xiong ZH, Fan YX, Wang XC, Liu Y. Applications of solid-phase microextraction in food analysis. *Trac-Trends Anal Chem.* (2016) 80:12–29. doi: 10.1016/j.trac.2016.02.022

48. Domínguez ANA, Agosin E. Gas chromatography coupled with mass spectrometry detection for the volatile profiling of vitis vinifera cv. carménère wines. *J Chil Chem Soc.* (2010) 55:385–91. doi: 10.4067/S0717-97072010000300025

49. Zheng J, Huang J, Yang Q, Ni C, Xie X, Shi Y, et al. Fabrications of novel solid phase microextraction fiber coatings based on new materials for high enrichment capability. *TrAC Trends Analyt Chem.* (2018) 108:135–53. doi: 10.1016/j.trac.2018.08.021

50. Li X, Liu S. Impacts of thermal treatment, xylose and cysteine addition on aroma compounds profile in lactic acid bacterium fermented pork hydrolysates. *Lwt-Food Sci Technol.* (2021) 152:112368. doi: 10.1016/j.lwt.2021.112368

51. Marín-San Román S, Rubio-Bretón P, Pérez-Álvarez EP, Garde-Cerdán T. Advancement in analytical techniques for the extraction of grape and wine volatile compounds. *Food Res Int.* (2020) 137:109712. doi: 10.1016/j.foodres.2020.109712

52. Dong W, Lin W, Chen X, Lian X, Shen C, Liu M, et al. Reducing the background interference of liquid–liquid extraction method during Baijiu aroma analysis. *Food Chem.* (2023) 404:134557. doi: 10.1016/j.foodchem.2022.134557

53. Fan W, Xu Y. Methodology for aroma compounds in Baijiu. *J Food Sci Techno.* (2018) 36:1–10. doi: 10.3969/j.issn.2095-6002.2018.03.001

54. Chen L, Capone DL, Jeffery DW. Analysis of potent odour-active volatile thiols in foods and beverages with a focus on wine. *Molecules.* (2019) 24:2472. doi: 10.3390/molecules24132472

55. Wu Z, Qin D, Duan J, Li H, Sun J, Huang M, et al. Characterization of benzenemethanethiol in sesame-flavour baijiu by high-performance liquid chromatography-mass spectrometry and sensory science. *Food Chem.* (2021) 364:130345. doi: 10.1016/j.foodchem.2021.130345

56. Elpa D, Duran-Guerrero E, Castro R, Natera R, Barroso CG. Development of a new stir bar sorptive extraction method for the determination of medium-level volatile thiols in wine. *J Sep Sci.* (2014) 37:1867–72. doi: 10.1002/jssc.201400308

57. Tang P, Shan Q, Wang L, Wang F, Li C, Lu J. A review of research methods in Baijiu flavor chemistry and recent progress in the flavor chemistry of maotai-flavored Baijiu. *J Food Sci.* (2020) 41:315–324. doi: 10.7506/spkx1002-6630-20190822-228

58. Engel W, Bahr W, Schieberle P. Solvent assisted flavour evaporation – a new and versatile technique for the careful and direct isolation of aroma compounds from complex food matrices. *Eur Food Res Technol.* (1999) 209:237–41. doi: 10.1007/s002170050486

59. Jia W, Fan Z, Du A, Li Y, Zhang R, Shi Q, et al. Recent advances in Baijiu analysis by chromatography based technology–a review. *Food Chem.* (2020) 324:126899. doi: 10.1016/j.foodchem.2020.126899

60. Kalschne DL, Viegas MC, De Conti AJ, Corso MP, Benassi MDT. Steam pressure treatment of defective coffea canephora beans improves the volatile profile and sensory acceptance of roasted coffee blends. *Food Res Int.* (2018) 105:393–402. doi: 10.1016/j.foodres.2017.11.017

61. Kumazawa K, Masuda H. Investigation of the change in the flavor of a coffee drink during heat processing. *J Agric Food Chem.* (2003) 51:2674–8. doi: 10.1021/jf021025f

62. van Seeventer PB, Weenen H, Winkel C, Kerler J. Stability of thiols in an aqueous process flavoring. *J Agric Food Chem.* (2001) 49:4292–5. doi: 10.1021/jf010348t

63. Francisco Pena-Pereira ILCB. Miniaturized preconcentration methods based on liquid–liquid extraction and their application in inorganic ultratrace analysis and speciation: a review. *Spectrochimica Acta Part B.* (2009) 64:1–15. doi: 10.1016/j.sab.2008.10.042

64. Quintanilla-Casas B, Dulsat-Serra N, Cortés-Francisco N, Caixach J, Vichi S. Thiols in brewed coffee: assessment by fast derivatization and liquid chromatography–high resolution mass spectrometry. *LWT - Food Sci Technol.* (2015) 64:1085–90. doi: 10.1016/j.lwt.2015.07.010

65. Schlumpberger P, Stübner CA, Steinhaus M. Development and evaluation of an automated solvent-assisted flavour evaporation (asafe). *Eur Food Res Technol.* (2022) 248:2591–602. doi: 10.1007/s00217-022-04072-1

66. Zellner BD, Dugo P, Dugo G, Mondello L. Gas chromatography–olfactometry in food flavour analysis. *J Chromatogr A.* (2008) 1186:123–143. doi: 10.1016/j.chroma.2007.09.006

67. Schoenauer S, Schieberle P. Screening for novel mercaptans in 26 fruits and 20 wines using a thiol-selective isolation procedure in combination with three detection methods. *J Agric Food Chem.* (2019) 67:4553–9. doi: 10.1021/acs.jafc.9b01242

68. Zhao J, Wang M, Xie J, Zhao M, Hou L, Liang J, et al. Volatile flavor constituents in the pork broth of black-pig. *Food Chem.* (2017) 226:51–60. doi: 10.1016/j.foodchem.2017.01.011

69. Kortes Serrano De La Hoz MRS, Ferrandino A. Different coatings for the hs sbse grape volatile analysis in model solution: preliminary results. *Food Chem.* (2016) 212:814–20. doi: 10.1016/j.foodchem.2016.06.047

70. Godage NH, Gionfriddo E. A critical outlook on recent developments and applications of matrix compatible coatings for solid phase microextraction. *TrAC Trends Analyt Chem.* (2019) 111:220–8. doi: 10.1016/j.trac.2018.12.019

71. Capone DL, Ristic R, Pardon KH, Jeffery DW. Simple quantitative determination of potent thiols at ultratrace levels in wine by derivatization and high-performance liquid chromatography–tandem mass spectrometry (hplc-ms/ms) analysis. *Anal Chem.* (2015) 87:1226–31. doi: 10.1021/ac503883s

72. Geffroy O, Lopez R, Serrano E, Dufourcq T, Gracia-Moreno E, Cacho J, et al. Changes in analytical and volatile compositions of red wines induced by pre-fermentation heat treatment of grapes. *Food Chem.* (2015) 187:243–53. doi: 10.1016/j.foodchem.2015.04.105

73. Mafata M, Stander M, Thomachot B, Buica A. Measuring thiols in single cultivar south African red wines using 4,4-dithiodipyridine (DTDP) derivatization and ultraperformance convergence chromatography-tandem mass spectrometry. *Foods.* (2018) 7:138. doi: 10.3390/foods7090138

74. Lee SM, Kwon GY, Kim K, Kim Y. Metabolomic approach for determination of key volatile compounds related to beef flavor in glutathione-maillard reaction products. *Anal Chim Acta.* (2011) 703:204–11. doi: 10.1016/j.aca.2011.07.028

75. Kaufmann A. The current role of high-resolution mass spectrometry in food analysis. *Anal Bioanal Chem.* (2012) 403:1233–49. doi: 10.1007/s00216-011-5629-4

76. Meng Q, Kakuta T, Sugawara E. Quantification and odor contribution of volatile thiols in Japanese soy sauce. *Food Sci Technol Res.* (2012) 18:429–36. doi: 10.3136/fstr.18.429

77. Luong J, Gras R, Hawryluk M, Shearer R. A brief history and recent advances in ozone induced chemiluminescence detection for the determination of sulfur compounds by gas chromatography. *Anal Methods.* (2016) 8:7014–24. doi: 10.1039/C6AY01887D

78. Pan Y, Li Z, Zhou X, Wang W, Wang X, Fang Z, et al. A system consisted of flame ionization detector and sulfur chemiluminescence detector for interference free determination of total sulfur in natural gas. *Chin Chem Lett.* (2017) 28:1670–4. doi: 10.1016/j.cclet.2017.04.014

79. Pu S, Pan Y, Zhang L, Lv Y. Recent advances in chemiluminescence and cataluminescence for the detection of volatile sulfur compounds. *Appl Spectrosc Rev.* (2021) 2021:1–27. doi: 10.1080/05704928.2021.2016792

80. Siebert TE, Solomon MR, Pollnitz AP, Jeffery DW. Selective determination of volatile sulfur compounds in wine by gas chromatography with sulfur chemiluminescence detection. *J Agric Food Chem.* (2010) 58:9454–62. doi: 10.1021/jf102008r

81. Lacorte S, Fernandez-Alba AR. Time of flight mass spectrometry applied to the liquid chromatographic analysis of pesticides in water and food. *Mass Spectrom Rev.* (2006) 25:866–80. doi: 10.1002/mas.20094

82. Yan Y, Chen S, Nie Y, Xu Y. Characterization of volatile sulfur compounds in soy sauce aroma type Baijiu and changes during fermentation by gc × gc-tofms, organoleptic impact evaluation, and multivariate data analysis. *Food Res Int.* (2020) 131:109043. doi: 10.1016/j.foodres.2020.109043

83. Chen S, Xu Y. Characterization of volatile compounds in Chinese roasted sesame-like flavor type liquor by comprehensive two-dimensional gas chromatography/time-of-flight mass spectrometry. *Food Ferment Ind.* (2017) 43:207–13.

84. Dagan L, Reillon F, Roland A, Schneider R. Development of a routine analysis of 4-mercapto-4-methylpentan-2-one in wine by stable isotope dilution assay and mass tandem spectrometry. *Anal Chim Acta.* (2014) 821:48–53. doi: 10.1016/j.aca.2014.03.004

85. Huang T, Armbruster MR, Coulton JB, Edwards JL. Chemical tagging in mass spectrometry for systems biology. *Anal Chem.* (2019) 91:109–25. doi: 10.1021/acs.analchem.8b04951

86. Ochiai N, Sasamoto K, Kishimoto T. Development of a method for the quantitation of three thiols in beer, hop, and wort samples by stir bar sorptive extraction within situ derivatization and thermal desorption–gas chromatography–tandem mass spectrometry. *J Agric Food Chem.* (2015) 63:6698–706. doi: 10.1021/acs.jafc.5b02298

87. Mateo-Vivaracho L, Ferreira V, Cacho J. Automated analysis of 2-methyl-3-furanthiol and 3-mercaptohexyl acetate at ng L^{-1} level by headspace solid-phase microextracion with on-fibre derivatisation and gas chromatography–negative chemical ionization mass spectrometric determination. *J Chromatogr A.* (2006) 1121:1–9. doi: 10.1016/j.chroma.2006.04.029

88. Mateo-Vivaracho L, Cacho J, Ferreira V. Quantitative determination of wine polyfunctional mercaptans at nanogram per liter level by gas chromatography–negative ion mass spectrometric analysis of their pentafluorobenzyl derivatives. *J Chromatogr A.* (2007) 1146:242–50. doi: 10.1016/j.chroma.2007.02.003

89. Mateo-Vivaracho L, Cacho J, Ferreira V. Improved solid-phase extraction procedure for the isolation and in-sorbent pentafluorobenzyl alkylation of polyfunctional mercaptans. *J Chromatogr A.* (2008) 1185:9–18. doi: 10.1016/j.chroma.2008.01.037

90. Mateo-Vivaracho L, Cacho J, Ferreira V. Selective preconcentration of volatile mercaptans in small spe cartridges: quantitative determination of trace odor-active polyfunctional mercaptans in wine. *J Sep Sci.* (2009) 32:3845–53. doi: 10.1002/jssc.200900296

91. Grassetti DR, Murray JF. Determination of sulfhydryl groups with 2,2′- or 4,4′-dithiodipyridine. *Arch Biochem Biophys.* (1967) 119:41–9. doi: 10.1016/0003-9861(67)90426-2

92. Gao P, Xia W, Li X, Liu S. Optimization of the maillard reaction of xylose with cysteine for modulating aroma compound formation in fermented tilapia fish head hydrolysate using response surface methodology. *Food Chem.* (2020) 331:127353. doi: 10.1016/j.foodchem.2020.127353

93. Kulapichitr F, Borompichaichartkul C, Suppavorasatit I, Cadwallader KR. Impact of drying process on chemical composition and key aroma components of arabica coffee. *Food Chem.* (2019) 291:49–58. doi: 10.1016/j.foodchem.2019.03.152

94. Zha M, Yin S, Sun B, Wang X, Wang C. STR3 and cys3 contribute to 2-furfurylthiol biosynthesis in Chinese sesame-flavored Baijiu yeast. *J Agric Food Chem.* (2017) 65:5503–11. doi: 10.1021/acs.jafc.7b01359

95. Picard M, Thibon C, Redon P, Darriet P, de Revel G, Marchand S. Involvement of dimethyl sulfide and several polyfunctional thiols in the aromatic expression of the aging bouquet of red bordeaux wines. *J Agric Food Chem.* (2015) 63:8879–89. doi: 10.1021/acs.jafc.5b03977

96. Mateo-Vivaracho L, Zapata J, Cacho J, Ferreira V. Analysis, occurrence, and potential sensory significance of five polyfunctional mercaptans in white wines. *J Agric Food Chem.* (2010) 58:10184–94. doi: 10.1021/jf101095a

97. Vichi S, Cortés-Francisco N, Caixach J. Analysis of volatile thiols in alcoholic beverages by simultaneous derivatization/extraction and liquid chromatography-high resolution mass spectrometry. *Food Chem.* (2015) 175:401–8. doi: 10.1016/j.foodchem.2014.11.095

98. Belda I, Ruiz J, Esteban-Fernández A, Navascués E, Marquina D, Santos A, et al. Microbial contribution to wine aroma and its intended use for wine quality improvement. *Molecules.* (2017) 22:189. doi: 10.3390/molecules22020189

99. Liu H, Wang Z, Hui T, Fang F, Zhang D. New insight into the formation mechanism of 2-furfurylthiol in the glucose-cysteine reaction with ribose. *Food Res Int.* (2021) 143:110295. doi: 10.1016/j.foodres.2021.110295

100. Ugliano M. Oxygen contribution to wine aroma evolution during bottle aging. *J Agric Food Chem.* (2013) 61:6125–36. doi: 10.1021/jf400810v

101. Cerny C. The aroma side of the maillard reaction. *Ann NY Acad Sci.* (2008) 1126:66–71. doi: 10.1196/annals.1433.011

102. Poisson L, Schmalzried F, Davidek T, Blank I, Kerler J. Study on the role of precursors in coffee flavor formation using in-bean experiments. *J Agric Food Chem.* (2009) 57:9923–31. doi: 10.1021/jf901683v

103. Zhang Z, Zang M, Zhang K, Wang S, Li D, Li X. Effects of phospholipids and reheating treatment on volatile compounds in phospholipid-xylose-cysteine reaction systems. *Food Res Int.* (2021) 139:109918. doi: 10.1016/j.foodres.2020.109918

104. Hofmann T, Schieberle P. Evaluation of the key odorants in a thermally treated solution of ribose and cysteine by aroma extract dilution techniques. *J Agric Food Chem.* (1995) 43:2187–94. doi: 10.1021/jf00056a042

105. Hofmann T, Schieberle P. Identification of key aroma compounds generated from cysteine and carbohydrates under roasting conditions. *Zeitschrift fuer Lebensmittel-Untersuchung und-Forschung A.* (1998) 207:229–36. doi: 10.1007/s002170050324

106. Cerny C, Davidek T. Formation of aroma compounds from ribose and cysteine during the maillard reaction. *J Agric Food Chem.* (2003) 51:2714–21. doi: 10.1021/jf026123f

107. Hofmann T, Schieberle P. Identification of potent aroma compounds in thermally treated mixtures of glucose/cysteine and rhamnose/cysteine using aroma extract dilution techniques. *J Agric Food Chem.* (1997) 45:898–906. doi: 10.1021/jf960456t

108. Chen X, Lu ZM, Zhang XJ, Wang ST, Ao L, Sheng CH, et al. Bio-heat is a key environmental driver shaping the microbial community of medium-temperature Daqu. *Appl Environ Microbiol.* (2017) 83:e1517–50. doi: 10.1128/AEM.01550-17

109. Martins FCOL, Alcantara GMRN, Silva AFS, Melchert WR, Rocha FRP. The role of 5-hydroxymethylfurfural in food and recent advances in analytical methods. *Food Chem.* (2022) 395:133539. doi: 10.1016/j.foodchem.2022.133539

110. Hofmann T, Schieberle P. Quantitative model studies on the effectiveness of different precursor systems in the formation of the intense food odorants 2-furfurylthiol and 2-methyl-3-furanthiol. *J Agric Food Chem.* (1998) 46:235–41. doi: 10.1021/jf9705983

111. Meynier A, Mottram DS. The effect of pH on the formation of volatile compounds in meat-related model systems. *Food Chem.* (1995) 52:361–6. doi: 10.1016/0308-8146(95)93282-V

112. Cerny C, Briffod M. Effect of pH on the maillard reaction of [13 c5] xylose, cysteine, and thiamin. *J Agric Food Chem.* (2007) 55:1552–6. doi: 10.1021/jf062874w

113. Cocchi M, Durante C, Lambertini P, Manzini S, Marchetti A, Sighinolfi S, et al. Evolution of 5-(hydroxymethyl)furfural and furfural in the production chain of the aged vinegar aceto balsamico tradizionale di modena. *Food Chem.* (2011) 124:822–32. doi: 10.1016/j.foodchem.2010.06.101

114. Gong M, Zhou Z, Liu S, Zhu S, Li G, Zhong F, et al. Formation pathways and precursors of furfural during Zhenjiang aromatic vinegar production. *Food Chem.* (2021) 354:129503. doi: 10.1016/j.foodchem.2021.129503

115. Pereira V, Albuquerque FM, Ferreira AC, Cacho J, Marques JC. Evolution of 5-hydroxymethylfurfural (hmf) and furfural (f) in fortified wines submitted to overheating conditions. *Food Res Int.* (2011) 44:71–6. doi: 10.1016/j.foodres.2010.11.011

116. Yaylayan VA, Huyghues-Despointes A, Feather MS. Chemistry of amadori rearrangement products: analysis, synthesis, kinetics, reactions, and spectroscopic properties. *Crit Rev Food Sci Nutr.* (1994) 34:321–69. doi: 10.1080/10408399409527667

117. Schieberle P. The carbon module labeling (camola) technique: a useful tool for identifying transient intermediates in the formation of Maillard-type target molecules. *Ann NY Acad Sci.* (2005) 1043:236–48. doi: 10.1196/annals.1333.029

118. Zhao J, Wang T, Xie J, Xiao Q, Cheng J, Chen F, et al. Formation mechanism of aroma compounds in a glutathione-glucose reaction with fat or oxidized fat. *Food Chem.* (2019) 270:436–44. doi: 10.1016/j.foodchem.2018.07.106

119. Wu Q, Zhu Y, Fang C, Wijffels RH, Xu Y. Can we control microbiota in spontaneous food fermentation? – Chinese liquor as a case example. *Trends Food Sci Technol.* (2021) 110:321–31. doi: 10.1016/j.tifs.2021.02.011

120. Xu Y, Huang H, Lu H, Wu M, Lin M, Zhang C, et al. Characterization of an *Aspergillus niger* for efficient fatty acid ethyl ester synthesis in aqueous phase and the molecular mechanism. *Front Microbiol.* (2022) 12:820380. doi: 10.3389/fmicb.2021.820380

121. Xu Y, Wang X, Liu X, Li X, Zhang C, Li W, et al. Discovery and development of a novel short-chain fatty acid ester synthetic biocatalyst under aqueous phase from *Monascus purpureus* isolated from Baijiu. *Food Chem.* (2021) 338:128025. doi: 10.1016/j.foodchem.2020.128025

122. Tamang JP, Shin D, Jung S, Chae S. Functional properties of microorganisms in fermented foods. *Front Microbiol.* (2016) 7:578. doi: 10.3389/fmicb.2016.00578

123. Wang B, Wu Q, Xu Y, Sun B. Specific volumetric weight-driven shift in microbiota compositions with saccharifying activity change in starter for Chinese Baijiu fermentation. *Front Microbiol.* (2018) 9:2349. doi: 10.3389/fmicb.2018.02349

124. De Vuyst L, Leroy F. Functional role of yeasts, lactic acid bacteria and acetic acid bacteria in cocoa fermentation processes. *Fems Microbiol Rev.* (2020) 44:432–53. doi: 10.1093/femsre/fuaa014

125. Yang S, Fan W, Xu Y. Melanoidins present in traditional fermented foods and beverages. *Compr Rev Food Sci Food Saf.* (2022) 21:4164–88. doi: 10.1111/1541-4337.13022

126. Xu Y, Wu M, Zhao D, Zheng J, Dai M, Li X, et al. Simulated fermentation of strong-flavor baijiu through functional microbial combination to realize the stable synthesis of important flavor chemicals. *Foods.* (2023) 12:644. doi: 10.3390/foods12030644

127. Huynh-Ba T, Matthey-Doret W, Fay LB, Bel Rhlid R. Generation of thiols by biotransformation of cysteine–aldehyde conjugates with baker's yeast. *J Agric Food Chem.* (2003) 51:3629–35. doi: 10.1021/jf026198j

128. Song Z, Du H, Zhang Y, Xu Y. Unraveling core functional microbiota in traditional solid-state fermentation by high-throughput amplicons and metatranscriptomics sequencing. *Front Microbiol.* (2017) 8. doi: 10.3389/fmicb.2017.01294

129. Zha M, Sun B, Yin S, Mehmood A, Cheng L, Wang C. Generation of 2-furfurylthiol by carbon-sulfur lyase from the Baijiu yeast *Saccharomyces cerevisiae* g20. *J Agric Food Chem.* (2018) 66:2114–20. doi: 10.1021/acs.jafc.7b06125

130. Yu Z, Yang Z. Understanding different regulatory mechanisms of proteinaceous and non-proteinaceous amino acid formation in tea (camellia sinensis) provides new insights into the safe and effective alteration of tea flavor and function. *Crit Rev Food Sci Nutr.* (2020) 60:844–58. doi: 10.1080/10408398.2018.1552245

131. Du R, Liu J, Jiang J, Wang Y, Ji X, Yang N, et al. Construction of a synthetic microbial community for the biosynthesis of volatile sulfur compound by multi-module division of labor. *Food Chem.* (2021) 347:129036. doi: 10.1016/j.foodchem.2021.129036

132. Liu J, Wu Q, Wang P, Lin J, Huang L, Xu Y. Synergistic effect in core microbiota associated with sulfur metabolism in spontaneous Chinese liquor fermentation. *Appl Environ Microbiol.* (2017) 83:e1417–75. doi: 10.1128/AEM.01475-17

133. Coetzee C, du Toit WJ. A comprehensive review on sauvignon blanc aroma with a focus on certain positive volatile thiols. *Food Res Int.* (2012) 45:287–98. doi: 10.1016/j.foodres.2011.09.017

134. Subileau M, Schneider R, Salmon J, Degryse E. New insights on 3-mercaptohexanol (3mh) biogenesis in sauvignon Blanc wines: cys-3mh and (e)-hexen-2-al are not the major precursors. *J Agric Food Chem.* (2008) 56:9230–5. doi: 10.1021/jf801626f

135. During-Olsen L, Regenberg B, Gjermansen C, Kielland-Brandt MC, Hansen J. Cysteine uptake by *Saccharomyces cerevisiae* is accomplished by multiple permeases. *Curr Genet.* (1999) 35:609–17. doi: 10.1007/s002940050459

136. Kaur J, Bachhawat AK. Yct1p, a novel, high-affinity, cysteine-specific transporter from the yeast *Saccharomyces cerevisiae*. *Genetics.* (2007) 176:877–90. doi: 10.1534/genetics.107.070342

137. Kosugi A, Koizumi Y, Yanagida F, Udaka S. Mup1, high affinity methionine permease, is involved in cysteine uptake by *Saccharomyces cerevisiae*. *Biosci Biotechnol Biochem.* (2001) 65:728–31. doi: 10.1271/bbb.65.728

138. Winter G, Van Der Westhuizen T, Higgins VJ, Curtin C, Ugliano M. Contribution of cysteine and glutathione conjugates to the formation of the volatile thiols 3-mercaptohexan-1-ol (3mh) and 3-mercaptohexyl acetate (3mha) during fermentation by *Saccharomyces cerevisiae*. *Aust J Grape Wine Res.* (2011) 17:285–290. doi: 10.1111/j.1755-0238.2011.00127.x

139. Yoshida Y, Negishi M, Amano A, Oho T, Nakano Y. Differences in the beta c-s lyase activities of viridans group streptococci. *Biochem Biophys Res Commun.* (2003) 300:55–60. doi: 10.1016/S0006-291X(02)02803-6

140. Chen, Z. *Metabolism of Sulfur in Saccharomyces cerevisiae.* [dissertation]. [Shan dong (Ji nan)]: Shandong University. (In Chinese). China-national-knowledge-internet (CNKI) (2018). Available online at: https://kns.cnki.net/KCMS/detail/detail.aspx?dbname=CDFDLAST2019&filename=1019007218.nh

141. Deshpande AA, Bhatia M, Laxman S, Bachhawat AK. Thiol trapping and metabolic redistribution of sulfur metabolites enable cells to overcome cysteine overload. *Microb Cell.* (2017) 4:112–26. doi: 10.15698/mic2017.04.567

142. Blanchard L, Tominaga T, Dubourdieu D. Formation of furfurylthiol exhibiting a strong coffee aroma during oak barrel fermentation from furfural released by toasted staves. *J Agric Food Chem.* (2001) 49:4833–5. doi: 10.1021/jf010539w

143. Swiegers JH, Pretorius IS. Modulation of volatile sulfur compounds by wine yeast. *Appl Microbiol Biotechnol.* (2007) 74:954–60. doi: 10.1007/s00253-006-0828-1

144. Geffroy O, Morère M, Lopez R, Pasquier G, Condoret J. Investigating the aroma of syrah wines from the northern rhone valley using supercritical CO_2-dearomatized wine as a matrix for reconstitution studies. *J Agric Food Chem.* (2020) 68:11512–23. doi: 10.1021/acs.jafc.0c04328

145. Bel Rhlid R, Matthey-Doret W, Blank I, Fay LB, Juillerat MA. Lipase-assisted generation of 2-methyl-3-furanthiol and 2-furfurylthiol from thioacetates. *J Agric Food Chem.* (2002) 50:4087–90. doi: 10.1021/jf0202335

146. Nikolantonaki M, Chichuc I, Teissedre P, Darriet P. Reactivity of volatile thiols with polyphenols in a wine-model medium: impact of oxygen, iron, and sulfur dioxide. *Anal Chim Acta.* (2010) 660:102–9. doi: 10.1016/j.aca.2009.11.016

147. Charles-Bernard M, Kraehenbuehl K, Rytz A, Roberts DD. Interactions between volatile and nonvolatile coffee components. 1 screening of nonvolatile components. *J Agric Food Chem.* (2005) 53:4417–25. doi: 10.1021/jf048021q

148. Blank I, Pascual EC, Devaud S, Fay LB, Stadler RH, Yeretzian C, et al. Degradation of the coffee flavor compound furfuryl mercaptan in model fenton-type reaction systems. *J Agric Food Chem.* (2002) 50:2356–64. doi: 10.1021/jf011329m

149. Cilliers JJL, Singleton VL. Nonenzymic autoxidative phenolic browning reactions in a caffeic acid model system. *J Agric Food Chem.* (1989) 37:890–6. doi: 10.1021/jf00088a013

150. Cilliers JJL, Singleton VL. Caffeic acid autoxidation and the effects of thiols. *J Agric Food Chem.* (1990) 38:1789–96. doi: 10.1021/jf00099a002

151. Negishi O, Negishi Y, Ozawa T. Effects of food materials on removal of allium -specific volatile sulfur compounds. *J Agric Food Chem.* (2002) 50:3856–61. doi: 10.1021/jf020038q

152. Hofmann T, Czerny M, Calligaris S, Schieberle P. Model studies on the influence of coffee melanoidins on flavor volatiles of coffee beverages. *J Agric Food Chem.* (2001) 49:2382–6. doi: 10.1021/jf0012042

153. Hofmann T, Schieberle P. Chemical interactions between odor-active thiols and melanoidins involved in the aroma staling of coffee beverages. *J Agric Food Chem.* (2002) 50:319–26. doi: 10.1021/jf010823n

154. Müller C, Hemmersbach S, van't Slo G, Hofmann T. Synthesis and structure determination of covalent conjugates formed from the sulfury–roasty-smelling 2-furfurylthiol and di- or trihydroxybenzenes and their identification in coffee brew. *J Agric Food Chem*. (2006) 54:10076–10085. doi: 10.1021/jf062728q

155. Lang R, Mueller C, Hofmann T. Development of a stable isotope dilution analysis with liquid chromatography–tandem mass spectrometry detection for the quantitative analysis of di- and trihydroxybenzenes in foods and model systems. *J Agric Food Chem.* (2006) 54:5755–62. doi: 10.1021/jf061118n

156. Charles-Bernard M, Roberts DD, Kraehenbuehl K. Interactions between volatile and nonvolatile coffee components. 2 mechanistic study focused on volatile thiols. *J Agric Food Chem.* (2005) 53:4426–33. doi: 10.1021/jf048020y

157. Müller C, Hofmann T. Quantitative studies on the formation of phenol/2-furfurylthiol conjugates in coffee beverages toward the understanding of the molecular mechanisms of coffee aroma staling. *J Agric Food Chem.* (2007) 55:4095–102. doi: 10.1021/jf070095p

158. Itobe T, Kumazawa K, Nishimura O. New factor characterizing the in-mouth release of odorants (volatile thiols): compositional changes in odorants exhaled from the human nose during drinking. *J Agric Food Chem*. (2009) 57:11297–301. doi: 10.1021/jf902239g

159. Buettner A. Influence of human salivary enzymes on odorant concentration changes occurring in vivo. 1 esters and thiols. *J Agric Food Chem.* (2002) 50:3283–9. doi: 10.1021/jf011586r

160. Szente L, Szejtli J. Cyclodextrins as food ingredients. *Trends Food Sci Technol.* (2004) 15:137–42. doi: 10.1016/j.tifs.2003.09.019

161. Zhu G, Xiao Z, Yu G, Zhu G, Niu Y, Liu J. Formation and characterization of furfuryl mercaptan-β-cyclodextrin inclusion complex and its thermal release characteristics. *Pol J Chem Technol.* (2021) 23:35–40. doi: 10.2478/pjct-2021-0035

162. Mestdagh F, Davidek T, Chaumonteuil M, Folmer B, Blank I. The kinetics of coffee aroma extraction. *Food Res Int.* (2014) 63:271–4. doi: 10.1016/j.foodres.2014.03.011

163. Nikolantonaki M, Waterhouse AL. A method to quantify quinone reaction rates with wine relevant nucleophiles: a key to the understanding of oxidative loss of varietal thiols. *J Agric Food Chem.* (2012) 60:8484–91. doi: 10.1021/jf302017j

frontiers | Frontiers in Nutrition

TYPE Original Research
PUBLISHED 31 July 2023
DOI 10.3389/fnut.2023.1222988

OPEN ACCESS

EDITED BY
Dandan Pu,
Beijing Technology and Business University, China

REVIEWED BY
Jingjing Liu,
Northeast Electric Power University, China
Ren Likun,
Harbin University of Commerce, China

*CORRESPONDENCE
Wenshen Jia
✉ jiawenshen@163.com

RECEIVED 15 May 2023
ACCEPTED 03 July 2023
PUBLISHED 31 July 2023

CITATION
Qin Y, Jia W, Sun X and LV H (2023) Development of electronic nose for detection of micro-mechanical damages in strawberries. *Front. Nutr.* 10:1222988. doi: 10.3389/fnut.2023.1222988

Development of electronic nose for detection of micro-mechanical damages in strawberries

Yingdong Qin[1,2], Wenshen Jia[1,3,4,5]*, Xu Sun[6] and Haolin LV[7]

[1]Institute of Quality Standard and Testing Technology, Beijing Academy of Agriculture and Forestry Sciences, Beijing, China, [2]College of Computer and Information Engineering, Beijing University of Agriculture, Beijing, China, [3]Department of Risk Assessment Lab for Agro-products (Beijing), Ministry of Agriculture and Rural Affairs, Beijing, China, [4]Key Laboratory of Urban Agriculture (North China), Ministry of Agriculture and Rural Affairs, Beijing, China, [5]Lu'an Branch, Anhui Institute of Innovation for Industrial Technology, Lu'an, China, [6]School of Mechanical Engineering and Automation, Liaoning University of Technology, Jinzhou, Liaoning, China, [7]College of Computer and Information, China Three Gorges University, Yichang, China

A self-developed portable electronic nose and its classification model were designed to detect and differentiate minor mechanical damage to strawberries. The electronic nose utilises four metal oxide sensors and four electrochemical sensors specifically calibrated for strawberry detection. The selected strawberries were subjected to simulated damage using an H2Q-C air bath oscillator at varying speeds and then stored at 4°C to mimic real-life mechanical damage scenarios. Multiple feature extraction methods have been proposed and combined with Principal Component Analysis (PCA) dimensionality reduction for comparative modelling. Following validation with various models such as SVM, KNN, LDA, naive Bayes, and subspace ensemble, the Grid Search-optimised SVM (GS-SVM) method achieved the highest classification accuracy of 0.84 for assessing the degree of strawberry damage. Additionally, the Feature Extraction ensemble classifier achieved the highest classification accuracy (0.89 in determining the time interval of strawberry damage). This experiment demonstrated the feasibility of the self-developed electronic nose for detecting minor mechanical damage in strawberries.

KEYWORDS

electronic nose, strawberry, mechanical damage, non-destructive testing, food inspection, embedded systems, classification model

1. Introduction

1.1. Background

Strawberries are popular small fruits that are well-suited for their delicious taste and rich nutritional value (1). Phenolic compounds in strawberries are known for their antioxidant and anti-inflammatory actions (2). They are abundant in vitamin C, anthocyanins, phenolic compounds, and other antioxidants (3), which promote antioxidation in the human body and reduce the risk of cardiovascular diseases and cancer (4). Strawberries also possess direct and indirect antimicrobial, anti-allergic, and antihypertensive properties (5). Although dried strawberries undergo dehydration, they retain high pro-health potential and maintain acceptable sensory qualities (6). Consequently, strawberries have become an indispensable part of their daily diet. Strawberries have various shapes and sizes, bright colours, smooth skin, tender and jurious flesh, and a rich taste. Conversely, strawberries have delicate exteriors, making them

prone to mechanical damage during processes such as harvesting, transportation, and packaging (7). This minor damage may have accelerated the oxidation and deterioration of the strawberries. Moreover, strawberries are susceptible to fungal infections (8), and damaged areas can facilitate infection, leading to a decline in quality and waste from multiple perspectives. To avoid this situation, non-destructive detection and screening of strawberries with minor damage have become an important issue (9).

Electronic nose technology is an embodiment of the biomimetic olfaction concept that aims to mimic animal olfaction for fuzzy odour judgment without the need for precise chemical analysis. With the application of the e-nose technology, fruits can be tested in large quantities without damage. Detecting minor fruit damage, particularly during the early stages, can be challenging. In addition, image recognition methods may prove ineffective when fruits are stacked and obstruct each other. Traditional chemical analysis equipment typically requires sample extraction, which damages the external appearance of the fruit. This not only results in incomplete detection but also risks harming the packaging or fruit itself. In contrast, the electronic nose technology allows for rapid, non-destructive, and bulk assessments.

1.2. Research purpose and method

To ensure that the appearance and experience of strawberries are not negatively affected during sales, it is crucial to determine the timing of the damage and infer the cause in order to improve logistics and other pre-sales processes. Precise identification of damaged strawberry samples is needed so that they can be assessed and removed, providing a rapid, convenient, and non-destructive solution for the early detection of minor strawberry damage. We need to develop an electronic nose specifically designed to detect volatile gases emitted by strawberries using a sensor array that primarily meets the requirements for strawberry detection.

2. Literature review

2.1. Development of electronic nose for fruit and vegetable food inspection

In the 1960s, researchers designed microelectrodes to mimic the olfactory mechanism of animals by comparing it with that of olfactory hair. In 1963, Wilkens from Cornell University proposed that a differential response sensitivity to various volatiles could be obtained under any given microelectrode condition. By comparing the reactions to several odours under different electrode conditions, a differential response specificity similar to that of the different human olfactory receptor sites was discovered (10). In 1982, Persaud compared the olfactory system to an electronic nose. A comparison of electrical signals from sheep olfactory mucosa and semiconductor sensors showed some similarities. By adjusting these parameters, highly specific receptors can be replaced with a single sensor (11).

Electronic noses are widely used for the detection of diseases in fruits and vegetables. Gómez et al. used a portable PEN2 electronic nose device with ten different metal oxide sensors to evaluate the ability of electronic noses to monitor changes in volatile production during tomato ripening. Principal Component Analysis (PCA) and Linear Discriminant Analysis (LDA) were used to determine whether the electronic nose could distinguish different ripening stages (unripe, half-ripe, fully ripe, and overripe) (12). Chen et al. developed an electronic nose system for fruit ripeness and quality detection with an identification accuracy of up to 100% (13). Qian et al. detected Chinese noodles using an Electronic Nose (e-nose). The e-nose results indicated that the primary flavour differences in noodles were primarily attributed to inorganic sulphides, alcohols, aldehydes, and ketones (14). Zhao et al. proposed a rapid electronic nose method to detect whether apples were infected with fungi, and the recognition accuracy of the SSA-BPNN model reached 98.40% (15).

Commercial electronic noses commonly used for agriproduct detection include Germany's AIRSENSE PEN 3 and France's Alpha MOS Fox 4,000. In a study on the TVB-N content of eggs, Liu et al. used a Pen 3 electronic nose. Using the array response of the electronic nose, they established a content model capable of describing the egg storage period (16). Labreche et al. used a Fox 4,000 electronic nose to determine the shelf life of milk. An electronic nose was used to analyse milk samples stored at different temperatures and times (17).

2.2. The electronic nose as a common device for food detection

The electronic nose has always been a research hotspot for food detection. Elizabeth reviewed the applications of modern electronic noses and tongues in the food and pharmaceutical industries. The review covers various types of electronic nose sensors based on different principles, including organic polymers, metal oxides, quartz crystal microbalances, and the combination of gas chromatography (GC) and mass spectrometry (MS) (18). Shi et al. reviewed the development of electronic noses in science and technology, and their applications in fresh food. This review focuses on the sensing and recognition systems of electronic noses as well as their applications in fresh food classification, flavour detection, and spoilage evaluation (19). Sanaeifar et al. reviewed the applications of electronic noses in the food industry and discussed future development trends, prospects, and challenges (20). Jia summarised the research on agriproduct detection. This review discusses the applications of electronic noses in agriproduct analysis (such as fruits, vegetables, tea, grains, livestock meat, and fish), including freshness evaluation, quality classification, authenticity assessment, variety identification, geographical origin identification, and disease detection (21). Hotel reviewed algorithms for volatile compound recognition in electronic noses based on surface acoustic wave (SAW) sensors. This review describes several machine learning algorithms and compares their performance on different features used in state-of-the-art electronic nose systems (22). Zheng et al. reviewed electronic noses based on metal oxide sensors for crop pest detection. When crops are attacked by pests, they release (VOCs) to alert their natural enemies, which can then be captured using metal oxide semiconductor gas sensors. This review introduces the principles, techniques, and progress of crop pest detection (23). Baietto et al. summarised the applications of electronic noses in fruit identification, ripeness, and quality grading. This study reviews the chemical properties of fruit volatiles during fruit production, describes some more important applications provided by electronic nose

(e-nose) technology for fruit aroma characterisation, and summarises recent research on e-nose data (24).

2.3. Study on strawberry-related gases, damage, and electronic nose detection

In 2006, Iannetta et al. investigated the relationship between ethylene (C2H4) and carbon dioxide (CO2) to represent strawberry ripening. Their experiments showed that the C2H4 level increased linearly (without diurnal fluctuations) to approximately 1 nL fruit-1 h-1 as the strawberries reached the red-ripe stage. 24 hours after the red fruits began to produce C2H4 again, the CO2 levels increased approximately threefold, indicating a climacteric respiration period (25). In 2012, Hu et al. studied the effects of hydrogen sulphide (H2S) on the post-harvest shelf life and antioxidant metabolism of strawberries. Fumigation with H2S gas released from the H2S donor NaHS prolonged the postharvest shelf life of strawberry fruit in a dose-dependent manner (26). Positive effects of hydrogen gas on the nutrition, texture, and sensory freshness of strawberries have been observed (27).

Zhang J and colleagues used an electronic nose (e-nose), headspace solid-phase microextraction-gas chromatography–mass spectrometry (HS-SPME-GC–MS), and gas chromatography-ion mobility spectrometry (GC-IMS) to study the aroma of freshly squeezed strawberry juice during storage at 4 ± 1°C. By analysing the volatile organic compound (VOC) content, they enhanced our understanding of VOCs and provided a basis for studying the aromatic characteristics of freshly squeezed strawberry juice (28). Granitto et al. employed PTR-MS technology to analyse volatile compounds and applied various data mining techniques to achieve rapid and non-destructive detection of individual strawberries (29). Lu developed a mobile electronic nose to detect strawberry decay using gas sensors. Six metal oxide sensors were selected, and the sensor array was combined with a mobile unit and computer to construct a mobile electronic nose device (30). Pan L and colleagues employed an electronic nose and gas chromatography–mass spectrometry (GC–MS) to detect and classify early post-harvest fruit pathogen infections. In the experiment, strawberries inoculated with grey mould, blue mould, and root mould fungi decayed within 2 d at 5°C. A multilayer perceptron neural network model accurately discriminated between four groups of strawberries with fungal infections with an accuracy rate of 96.6% (8). Xing M and colleagues developed a custom electronic nose system called "Red Face" for detecting the freshness of strawberries during different storage periods. The system consists of six metal oxide semiconductor sensors connected to a data acquisition system and a computer equipped with pattern recognition software (31).

Electronic noses often demonstrate good performance in detecting berry fruits such as white berries and blackberries (32). In 2020, Rao Jingshan, Zhang Yuchen, and colleagues investigated the use of (e-nose) technology to predict the volatile organic compounds (VOCs) in vibration-damaged strawberry fruits during storage on all four sampling days. The best models for the residual prediction deviation values were 2.984 and 5.478. The discrimination model for damaged strawberries also achieved good classification results, with an average correct response rate of 99.24% for both calibration and prediction (33). In 2022, Cao Yang, Zhang Yuchen, and others improved upon previous research. By studying the detection of damaged strawberries through VOCs and establishing and predicting models for the degree of damage and impact time, they demonstrated that mechanical impact caused changes in the VOCs in strawberries and that using electronic nose technology to detect impact-damaged strawberries was feasible (34). In 2022, Al-Dairi Mai et al. conducted research on the postharvest transportation of fresh agriproducts and introduced an experimental method for measuring vibration levels during the transportation process. Factors affecting vibration levels include surface conditions, vehicle speed, vibration duration, vibration direction, and packaging units (35).

3. Experiment and equipment

3.1. E-nose used in the experiment

As an independent detection device, we must consider the ease of use for operators in addition to the sensor array. We developed a complete set of equipment based on a microcontroller incorporating a 10-inch capacitive touchscreen that integrates the device's functions for operation and control, including sampling and cleaning switches, experimental data grouping, baseline zeroing, data combination display, column display, and time display. Furthermore, our electronic nose features a multilevel data saving function to ensure data security (36). In an electronic nose system, data stored on a TF card can also be uploaded to a server for backup storage via Wi-Fi. Figure 1 shows the electronic nose used in the experiment.

Figure 2 depicts the working and structural principles of the electronic nose used in the experiment. The electronic nose was equipped with a 12 W vacuum pump, which, after pulse width modulation (PWM) speed regulation, provided suction to the gas chamber as per demand, thereby drawing the sample gas into the chamber through a hose. The gas chamber contained embedded sensors that transmitted signals to the MCU. The data were calculated and displayed on a 10-inch touchscreen. In addition to the gas information, temperature, humidity, time, and group information were stored in the TF card.

FIGURE 1
The independently developed e-nose.

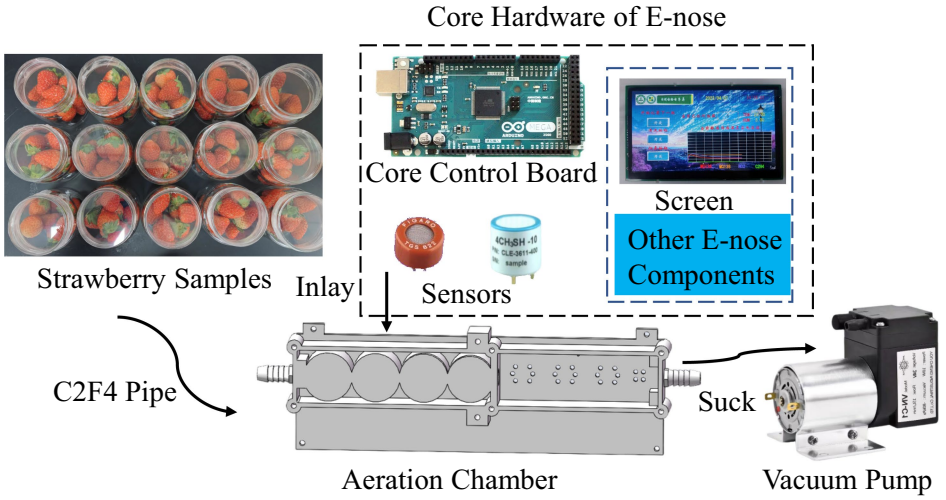

FIGURE 2
Schematic diagram of the e-nose operation.

TABLE 1 Group and oscillation frequency.

Group	Oscillation frequency(r/min)	Time(min)
a	0	0
b	120	60
c	160	60
d	200	60
e	240	60

3.2. Strawberry sample preparation

To obtain strawberries with minor damage, we simulated the damage to freshly harvested strawberries. To simulate the mechanical damage in strawberries, two commonly used methods are freefall (34) and oscillation (33). However, in this particular study, the variety of strawberries investigated (double winter strawberries) was characterised by its small size and abundant fruit quantity, making oscillation the preferred method for simulating mechanical damage to strawberries. To facilitate gas detection, we selected Shuangliu winter strawberries with an average weight of 8.5 g, that were in good and fresh condition. Nine strawberries were placed in a 250 mL wide-mouth bottle and sealed with sealing film. Sealed strawberries were divided into groups to induce varying degrees of minor damage. An H2Q-C air-bath shaker was used to simulate the shaking process. The groups were divided according to the shaking intensity, as shown in Table 1, with 10 parallel samples in each group. After shaking, the samples are placed in a 4.5°C refrigerator for detection (Figure 3).

It is noteworthy that we tested different shakers, and the results varied under different devices, owing to factors such as the degree of fixation of the shaker and equipment resonance. If strawberries continually shift their positions within the bottle, severe damage may occur. However, if strawberries are packed tightly or subjected to high centrifugal force due to rapid rotation, there may be little displacement, resulting in damage caused by compression only. In this experiment, the shaker used at a rotation speed of 240 r/min still led to relatively intense collisions among the strawberries, but did not result in direct damage or loss of the fruit flesh.

3.3. Difficulty in sample detection

This experiment was challenging for several reasons. First, the damage to strawberries after shaking was minimal and did not directly damage the flesh. Even when observing with the naked eye, we needed to be close to the samples. After shaking, strawberries may exhibit swelling and darkening of colour, both of which are indicators of damage. Second, unlike previous studies, our experiment involved storing all samples in cold storage. Under refrigeration, strawberries are difficult to oxidise and rot.

These two factors account for the fact that, in the current strawberry harvesting and transportation processes, single-fruit packaging is often employed, road transportation conditions have improved, and the hardness and quality of the fruit have increased, making direct damage less common. Moreover, owing to the short shelf life of strawberries, refrigeration is commonly used for daily storage.

3.4. Detection method

Electronic nose collection experiments were conducted on the prepared samples after 24 h, 48 h, 72 h, 96 h, and 120 h of refrigeration. Before starting the experiment, the custom-built electronic nose needs to be preheated for 2–4 h. Once the electrochemical sensors are unbiased and the metal-oxide sensors operate stably, data collection can begin. The collection phase can be divided into ventilation calibration, sampling, and cleaning phases.

3.4.1. Calibration

After basic ventilation calibration, our self-developed electronic nose can respond to sensors in air, perform zero calibration on electrochemical sensors, and output G/G0 for metal oxide sensors.

FIGURE 3
Strawberry pre-processing: **(A)** using H2Q-C air bath shaker for oscillation, **(B)** the distribution of strawberries in the shaker and **(C)** refrigerate at 4°C Celsius.

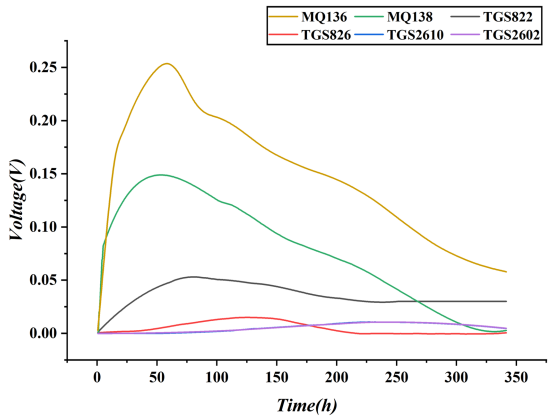

FIGURE 4
Comparison of experimental results for metal oxide sensors.

3.4.2. Sampling

A rigid plastic sampling head was used to quickly puncture the sealing film, and a 12 W vacuum pump gradually pumped the detected gas into the gas chamber.

3.4.3. Cleaning

In comparison to the zeroing method mentioned in Reference (24), we still opt to sacrifice efficiency in favour of sensor accuracy by using a 40 W high-power vacuum pump and waiting for natural zeroing as much as possible. If natural calibration is not possible, wait 10 min after cleaning before recalibration.

After experimental data collection, the obtained sample data had two labels: time and damage groups. The goal was to ensure that the e-nose model built at a later stage could accurately judge strawberry damage under various conditions.

3.5. Sensor array selection

Compared to existing electronic noses in the market, we chose to develop our own, tailored to the specific characteristics of the fruit being detected. Pen-3 is a mature commercial electronic nose widely favoured by researchers and is primarily fabricated using ten metal oxide sensors. These metal oxide sensors have broad applicability, a relatively long lifespan, and strong detection sensitivity owing to their cross-sensitivity, although they cannot accurately determine the specific composition of the reacted substances.

The method of selecting metal oxide sensors to detect the corresponding substances was in accordance with Reference (31); however, the models of the selected sensors were not the same. Preliminary tests were conducted on other batches of strawberries under the same experimental conditions. We applied the Savitzky–Golay method to denoise the data and plotted the response curves of the sensor modules over time (Figure 4) to select relatively sensitive metal-oxide sensors. It can be observed that the curves of TGS2602 and TGS2610 overlap; therefore, only one curve needs to be retained. The response of TGS826 was not obvious, whereas MQ136, MQ138, and MQ822 had relatively higher contributions. To ensure sufficient gas chamber space and increase the contact area between the unit gas and the sensor, TGS826 and TGS2602 were removed, leaving only MQ136, MQ138, TGS826, and TGS2602.

Electrochemical sensors have a more precise range and can accurately determine the chemical changes between the sensor and the reacted substances using millivolt-level voltages, thus obtaining precise reaction changes. However, electrochemical sensors mainly measure specific inorganic substances with a relatively high specificity. In existing strawberry research, the detection of substances, such as ethylene, sulphides, and alcohols, is often required. Therefore, we prioritised the selection of electrochemical sensors that can detect these types of substances.

As a result, we chose the metal oxide sensors TGS822, TGS2602, MQ136, and MQ138 and the electrochemical sensors $4CH_3SH$-10, $4NO_2$-20, $4NH_3$-100, and $4H_2$-1,000. Based on the voltage change characteristics of the two types of sensor modules, we plotted Figure 5, which shows their sensitivity to various substances under known conditions. A value of 0 indicated no reaction or an unclear reaction. The sensitivity of these sensors to various substances was sufficient to detect the changes caused by strawberry volatiles.

Electrochemical sensors are more precise in their measurement range, and by utilising their millivolt-level voltage, they can accurately determine the chemical changes between the sensor and the substances being reacted, thereby obtaining precise reaction changes. However, electrochemical sensors are mainly used to measure a few inorganic substances and have a relatively high specificity for detection. In existing strawberry research, the detection of substances,

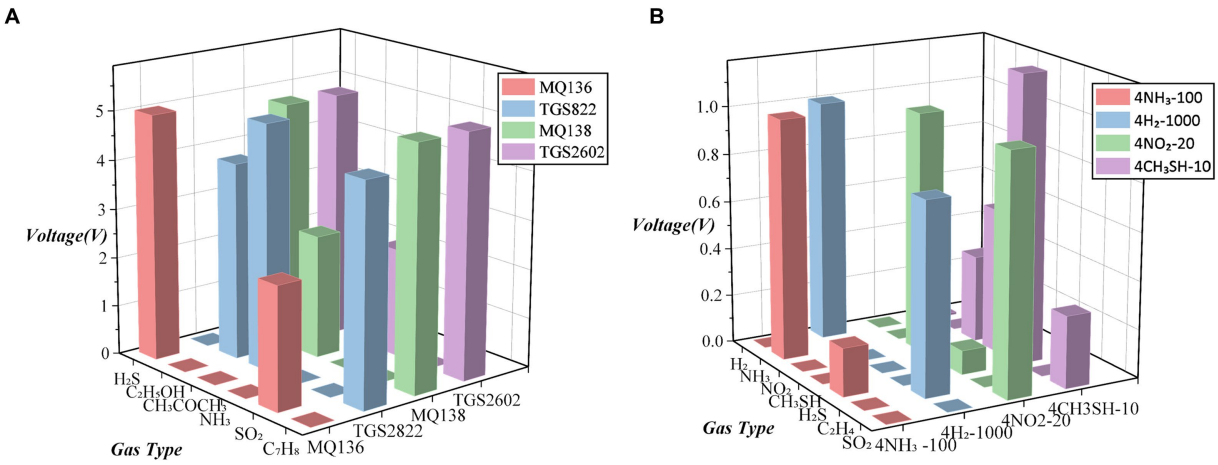

FIGURE 5
Sensitive response characteristic substances of 8 types of sensors: **(A)** sensitive substances for metal oxide sensors and **(B)** sensitive substances for electrochemical sensors.

such as ethylene, sulphides, and alcohols, is often required. Therefore, we prioritised the selection of electrochemical sensors that can detect these types of substances. Metal-oxide sensors have high repeatability and stability, allowing them to operate stably over long periods of time. In addition, they exhibit different characteristics in response to different gases, which enables them to distinguish and identify different gases.

3.6. Experimental phenomenon

Strawberries exhibited varying levels of damage depending on the applied oscillation frequency. Group A represented undamaged strawberries, whereas group B consisted of samples obtained at a rotation speed of 120 rpm. The rotation speed increased progressively throughout the groups, with group E containing samples obtained at 240 rpm (Table 1). To ensure a proportional relationship between the rotation speed and the degree of damage, it is crucial that strawberries collide and move, even at the highest rotation speed. Strawberries with abnormal oscillations were removed by visual inspection. The visual distinctions among different groups can be discerned by examining the captured images of strawberries (Figure 6).

Group A contained undamaged strawberries. They are fresh, glossy, vibrant, and well formed, with a faintly sweet fragrance. Even after cold storage, they remained intact, although some of their gloss was lost.

In group B, strawberries exhibited slight surface wrinkling due to mild oscillation. Their scent was similar to that of group A. After a few days of cold storage, some strawberries in Group B showed a slight darkening of colour, but those with uneven collisions maintained their freshness.

Group C strawberries experienced an increase in wrinkle depth, and their edges became less defined. Their scent was similar to that of Group A, but slightly stronger. After several days of cold storage, the fruit loses moisture and the dark red colour becomes more pronounced.

In group D, the collision frequency reached a high-intensity rotation speed of 200 rpm, resulting in several strawberries with large areas of wrinkling and a dark red colour. They appeared soft and mushy, with a sweeter scent. After cold storage, the collision areas darken further, and dehydration issues arise, accompanied by a stimulating sweet aroma.

Finally, group E strawberries could not maintain their original angular shape after oscillation and gradually became smooth and round. Generally, they are soft and mushy. After a few days of storage, they developed a rich sweet scent that grew increasingly intense.

4. Results and analysis

4.1. Electronic nose detection data

To clearly show the changes in the sample gas, we provide an example from the experimental data (Figure 7). As the degree of damage changed over time, the sensor signals exhibited different variations. One noticeable observation was that the required detection time varied. On average, group E samples took longer to detect than group A and C samples. This may be because, when gas exchange occurs, the gas diffuses and intermingles. When the gas concentration is high, it takes longer for the gas to fully diffuse in the gas chamber; consequently, the rise and fall of the gas concentration also require more time. Different sensors exhibit varying sensitivities at different response stages. To further analyse this, we calculated all data.

Based on the experimental results, the response ratios of the sensors were visualised using eight 3D stacked bar charts of the voltage ratios of the metal oxide sensors (Figure 8). Calculations were performed on all the raw data from the experiments. The charts depict the voltage values (V) of each sensor during the entire response phase for different groups (groups) and times (h). These visualisations demonstrate the proportion of each sensor response under various experimental conditions. First, because the voltage range of metal oxide sensors differs from that of electrochemical sensors, we scaled the electrochemical sensor data to match the voltage range of the

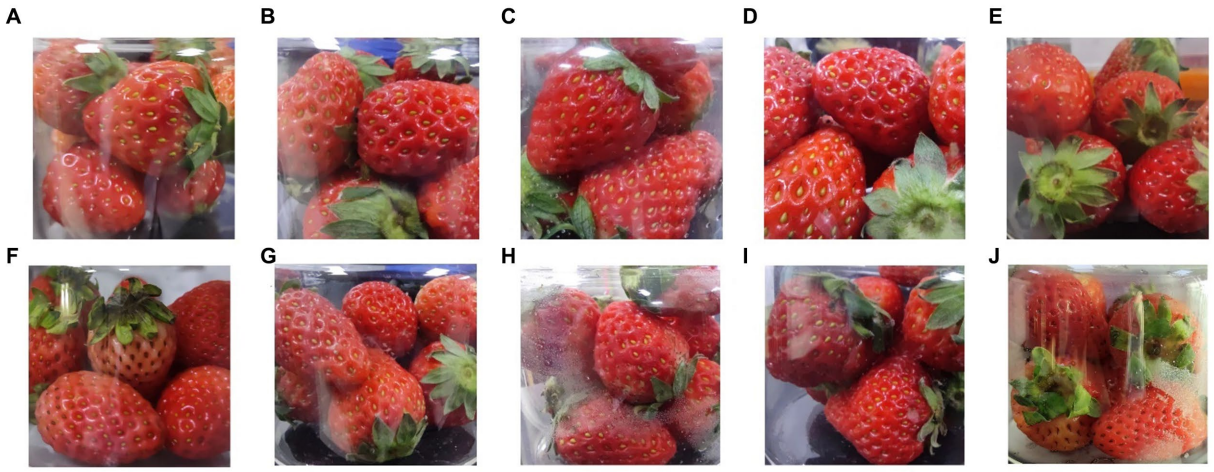

FIGURE 6
The visual observations of strawberries from the different groups. Photographs **(A–E)** were taken immediately after oscillation, when the strawberries were fresh, and photographs **(F–J)** were taken after 72 h of cold storage. Photographs **(A–E)** and **(F–J)** both correspond to the groups **(A–E)** described in Table 1.

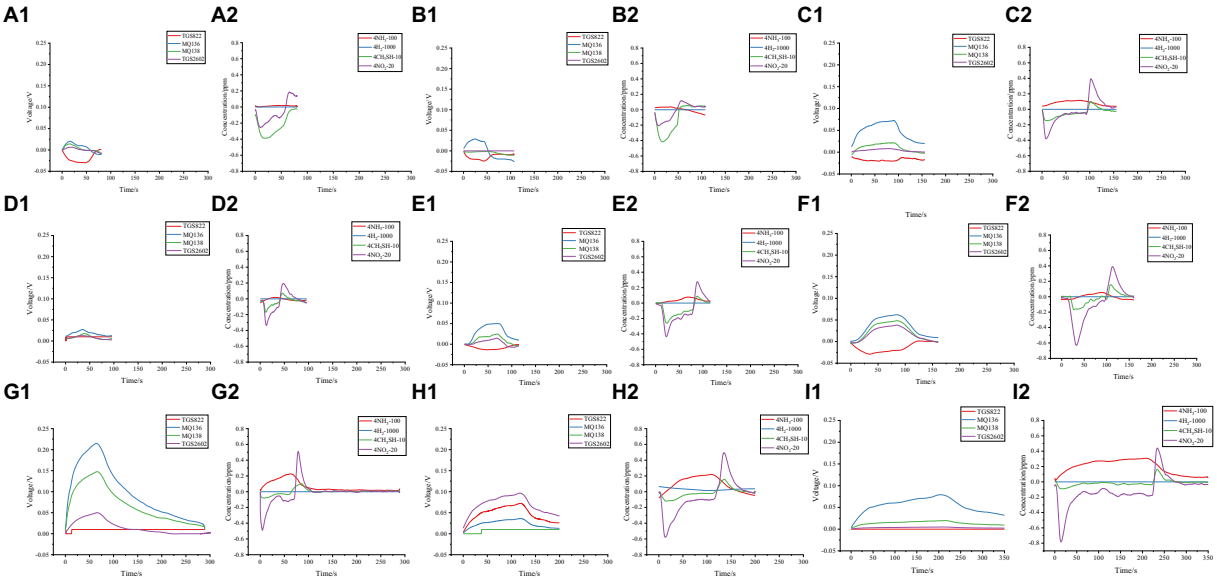

FIGURE 7
Comparison of electronic nose responses for individual samples at different experimental stages: **(A1)**, **(B1)**, and **(C1)** represent the voltage changes of the metal oxide sensor module for group A samples at 24 h, 72 h, and 120 h, respectively. **(A2)**, **(B2)**, and **(C2)** represent the changes in gas concentration detected by the electrochemical sensor module for group A samples at 24 h, 72 h, and 120 h, respectively. Similarly, **(D1)**, **(E1)**, and **(F1)** represent the voltage changes of the metal oxide sensor module for group C samples at 24 h, 72 h, and 120 h, while **(D2)**, **(E2)**, and **(F2)** represent the changes in gas concentration detected by the electrochemical sensor module for group C samples at 24 h, 72 h, and 120 h. **(G1)**, **(H1)**, and **(I1)** represent the voltage changes of the metal oxide sensor module for group E samples at 24 h, 72 h, and 120 h, while **(G2)**, **(H2)**, and **(I2)** represent the changes in gas concentration detected by the electrochemical sensor module for group E samples at 24 h, 72 h, and 120 h.

metal oxide sensors for comparison. Next, we calculated the mean values for each sensor during the entire reaction cycle (sampling, rising, peaking, and cleaning). This approach, which incorporates all the data, offers greater stability and versatility than the use of maximum or minimum absolute values. It can offset fluctuating electrical signals near 0, and conversely, it can include stable values throughout the entire reaction process. The following information can be obtained from the chart.

1. The chart displays only the activity of the sensors and does not reflect their contributions to the results. The higher the proportion of the sensor, the higher is its activity, which may also be influenced by noise. However, for different orders of magnitude, a sensor with a larger proportion is more likely to be sensitive to the reactants.
2. The mean voltage represented by the y-axis does not reveal the voltage pattern, because the data used were from the entire

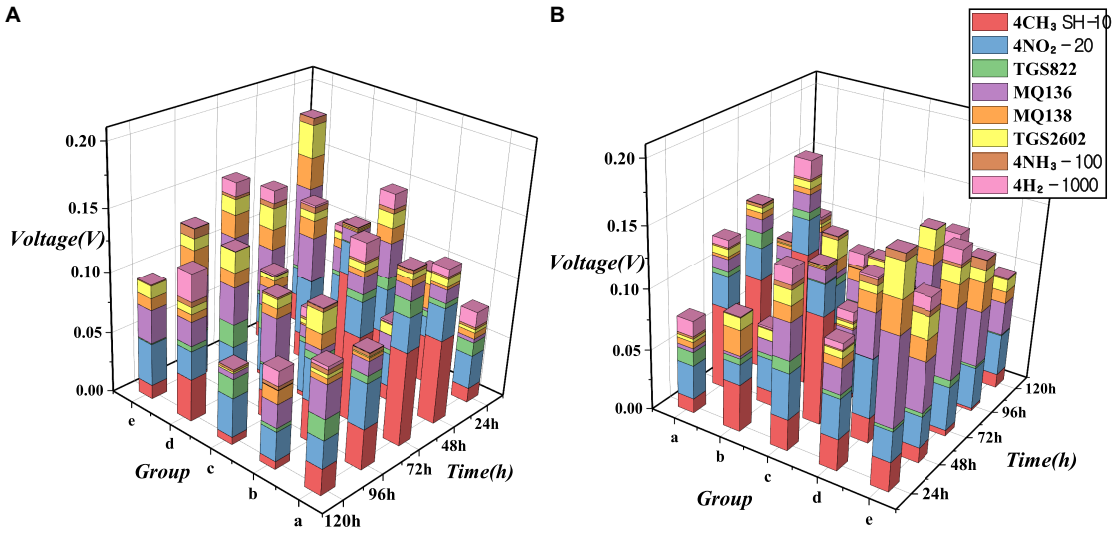

FIGURE 8
Voltage proportion of the 8 sensors under various experimental conditions: **(A)** viewpoint 1st and **(B)** viewpoint 2nd.

detection process. The peak and cleaning times varied under different experimental conditions (e.g. the detection time for group E was several times that for group A). The time required to reach the peak and the time required to complete the cleaning process differed for the samples under different conditions. A low voltage might indicate a small reaction; however, in most cases, this is due to prolonged cleaning times, which lowers the average voltage value after taking the mean. Therefore, only the proportions of various sensors can be compared.

3. The sensors with the lowest proportions were $4H_2$-1000 and $4NH_3$-100. Possible reasons for their low responses are either an overly large measurement range or a small amount of reactive gases.
4. Sensors TGS2602 and MQ138 have a slightly smaller proportion than MQ136, which is consistent with experimental expectations.
5. The sensors with the highest proportions were $4CH_3SH$-10, $4NO_2$-20, MQ136, and TGS822. For electrochemical sensors $4CH_3SH$-10 and $4NO_2$-20, their small measurement range allow them to capture reaction states more sensitively within their range. For MQ136 and TGS822, this was because of the presence of sensitive reactants corresponding to them.
6. The response level (also known as the activity level) of each sensor may vary under different conditions. For example, the red $4CH_3SH$-10 sensor may become less active than the other sensors as the damage level increases. The MQ136 sensor's activity level may also increase as the time interval and damage level increase. However, some sensors do not exhibit a clear pattern, and may require other statistical or processing methods for analysis.

4.2. Use PCA to perform feature extraction on the raw data

Dimensionality reduction of the collected full-process data using PCA: The sample data obtained from the electronic nose is a time series, which is continuous data that change over time. Different sensor data were generated at each time point, and the data for each period constituted a sample. By employing principal component analysis (PCA) for dimensionality reduction, the original eigenvalues became matrices. In time series data, each sample typically contains data from multiple time points. We consider each time point as a feature and each sample as a vector, allowing us to convert the time-series data into a matrix. Subsequently, we can perform PCA on this matrix to obtain low-dimensional data features.

4.2.1. Data for different damage groups

This set of data simultaneously shows the electronic nose response data for different damage groups A–E at the same time. PCA dimensionality reduction is applied to address the issue of determining the degree of damage. PCA1 and PCA2 account for more than 81% of the total, and the first three principal components account for 91%. As shown in Figure 9, the first two principal components accounted for 81% of the explainable variance, and points within the same group were clustered together. However, the boundaries were blurred and there was some overlap between groups A and B. This could be due to the low level of damage in Group B, which was not significantly different from the undamaged state, making it difficult to distinguish.

4.2.2. Data for different detection times

Subsequently, calculations were carried out for determining time periods, using strawberry samples with the same degree of damage, comparing their electronic nose voltage responses between 24 h and 120 h of storage at 4°C. PCA1 and PCA2 account for more than 70% of the total, with the first four principal components exceeding 91%. Figure 10 shows that the confidence ellipses have multiple orientations, indicating different trends in different principal component directions and large variances in these directions. The confidence ellipse shapes and sizes vary. Although the data points are relatively concentrated, possibly owing to the small mean differences between multiple groups, the variances can be clearly distinguished, and there is a clustering trend for points of the same type.

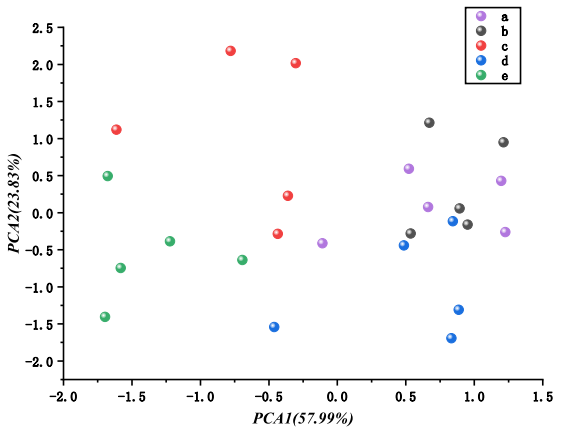

FIGURE 9
Comparison of images before and after cold storage for different groups.

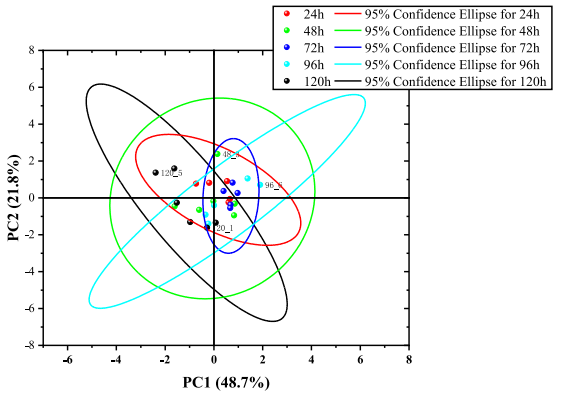

FIGURE 10
Comparison of images before and after cold storage for different groups.

Because the damage changes among the five groups of strawberries were not significant and the storage over time was at a low temperature, it was difficult to distinguish the obtained data. The introduction of data collection throughout the entire process (zero baseline, response emergence, peak, stability, and cleaning) may result in various situations that are difficult to interpret and classify, particularly the uncertainty of the cleaning time. In addition, the lack of designed weight values causes less important times and critical judgment points to have the same weight, thereby reducing their characteristic representations.

Although the PCA chart does not directly distinguish between groups, the size, direction, and aggregation of confidence ellipses and scatter points display a rich range of possibilities, indicating potential value for classification.

4.3. Use eigenvalue extraction methods to perform feature extraction on the raw data

Using eigenvalue extraction methods: The advantage of the electronic nose feature extraction is its flexibility in choosing different eigenvalues according to the requirements of the application scenario. It can be combined with domain knowledge and experience for selection and is convenient for interpreting practical meanings. In EN data processing of the electronic nose, it is necessary to extract effective eigenvalues from raw data for pattern recognition and classification. In this study, we propose nine effective eigenvalues: the maximum value, minimum value, mean value, Variance, Differential mean, integral mean, start-up differential value, average slope near the extreme value, and count of data points greater than the absolute mean value (abbreviated as count). Owing to the uncertainty in the detection time, the differential and integral means are more practically meaningful. The integral mean was calculated using a trapezoidal formula. The average slope near the extreme value has a peak shape. The larger the value, the sharper the peak, and the smaller the value, the smaller the peak. Moreover, because a stronger odour can result in a longer cleaning time, which can lower the mean value, the count is a good indicator of samples with strong volatility.

4.4. Prediction model

The experimental data come from two sources: one is the PCA values obtained through dimensionality reduction of the time-series PCA, where their sum is greater than 95%, and the other is the dimensionality reduction using eigenvalues. The calculation method for the eigenvalues was introduced in the previous section, and nine eigenvalues were selected. MQ138 and TGS2602, which exhibited response curves similar to those of MQ136, were removed to reduce the probability of overfitting. Among the remaining six sensors, 4H2-1,000 and 4NH3-100 had minimal impact owing to their larger measurement ranges compared to the measured gas content. In clean air, the voltage fluctuations are of the same order of magnitude as those in the sensitive gas; therefore, most eigenvalues are not applicable. Only the means and variances of the two sensors were retained to avoid adverse effects. Finally, four of the six sensors retained nine eigenvalues and two sensors retained two eigenvalues, resulting in a total of 40 eigenvalues per sample. A comparison of the two methods is presented in Table 2.

The dimensionality-reduced experimental data from both methods were imported into classifiers for classification. The classifiers mainly employ the LDA (37), SVM (38), KNN (39), naïve Bayes (40), and Subspace Discriminant (41) methods, among which the Subspace Discriminant is an ensemble classifier. The accuracy of the directed extraction method using eigenvalues was significantly higher than that of the PCA method applied to all the data in the time series. Moreover, performing PCA on the extracted 40 eigenvalues did not improve the accuracy.

For the damage problem, the ensemble classifier Subspace Discriminant performed the best, reaching an accuracy of 0.89, whereas the model for the timing problem achieved an accuracy of 0.81. This enabled a relatively clear classification of the five data categories. Table 3 presents the effects of the other classifiers, with SVM, KNN, and Linear Discriminant Analysis having relatively good classification results.

4.5. Model optimization

At the current stage of research, there are still some limitations. The sensor selection can be further optimised. By

TABLE 2 Comparison of classification accuracy between the two dimensionality reduction methods.

Problem classification	Dimensionality reduction method	Classification methods	Cross-validation	Accuracy
Time classification	Feature extraction	Subspace ensemble	5	0.88
Time classification	PCA	Subspace ensemble	5	0.6
Damage classification	Feature extraction	Subspace ensemble	5	0.81
Damage classification	PCA	SVM	5	0.38

TABLE 3 The accuracy of the first four models for the two classification problems.

Problem classification	Classification methods	Accuracy
Time classification	Subspace discriminant	0.89
Time classification	SVM	0.81
Time classification	Fine KNN	0.77
Time classification	Naive Bayes	0.77
Damage classification	Subspace discriminant	0.82
Damage classification	LDA	0.78
Damage classification	Medium Gaussian SVM	0.78
Damage classification	Weighted KNN	0.74

TABLE 4 Comparison of classification accuracy results for the time-based problem.

Dimensionality reduction method	Optimization method	Accuracy	Cross-validation
Feature extraction	None	0.80	5
PCA	None	0.38	5
Feature extraction	Grid search	0.84	5
Feature extraction	Random search	0.84	5
PCA	Grid search	0.46	5
PCA	Random search	0.34	5

comparing and verifying a greater variety of sensor models, the best sensor types can be selected, thereby enhancing the recognition capabilities of the electronic nose from a hardware perspective. There is also room for improvement in data extraction. One possible approach is to process the data only prior to the peak, thus avoiding the negative impact caused by the uncertainty of stabilisation and cleaning times. The selection of feature values should also involve comparing a wider range of extraction methods to further improve accuracy.

From Table 4, it can be concluded that by using Grid Search optimization, the accuracy of SVM was improved from the original 0.80 to 0.84 using Grid Search SVM (GS-SVM), and the PCA-reduced data increased from the original 0.38 to 0.46. As shown in Table 5, using the GS-SVM method, the accuracy increased from 0.71 to 0.84%; however, it was not as high as that of the subspace discriminant model, which was 0.89. For the original PCA-processed data, the accuracy increased from 0.40 to 0.58. The performance of the random search-optimised SVM

TABLE 5 Comparison of classification accuracy results for the damage-based problem.

Dimensionality reduction method	Optimization method	Accuracy	Cross-validation
Feature extraction	None	0.71	5
PCA	None	0.40	5
Feature extraction	Grid search	0.84	5
Feature extraction	Random search	0.84	5
PCA	Grid search	0.58	5
PCA	Random search	0.42	5

(RS-SVM) was not as good as that of the GS-SVM. The final experimental results for damage and time discrimination accuracy are shown in Table 6, where the subspace discriminant model achieved 0.89 for a time classification problem and 0.84 for a damage degree classification problem.

5. Discussion

5.1. Limitations and future improvements

At the current stage of research, there are still some limitations. The sensor selection can be further optimised. By comparing and verifying a greater variety of sensor models, the best sensor types can be selected, thereby enhancing the recognition capabilities of the electronic nose from a hardware perspective. There is also room for improvement in data extraction. One possible approach is to process the data only prior to the peak, thus avoiding the negative impact caused by the uncertainty of stabilisation and cleaning times. The selection of feature values should also involve comparing a wider range of extraction methods to further improve accuracy.

Moreover, it is essential to further optimise the sample space, acquire more valid data, and enhance the robustness of detection. As research progresses, these areas of improvement can be addressed, leading to a more refined and effective non-destructive electronic nose technology for strawberries.

5.2. Applications and significance

The development prospects for non-destructive strawberry detection technologies are broad. Food safety regulatory agencies can use this technology to spot-check strawberries to ensure consumer food safety and health. Non-destructive electronic

TABLE 6 Final accuracy.

Problem classification	Dimensionality reduction method	Accuracy	Classification methods	Cross-validation
Time classification	Feature extraction	0.89	Subspace ensemble	5
Time classification	PCA	0.6	Subspace ensemble	5
Damage classification	Feature extraction	0.84	GS-SVM	5
Damage classification	PCA	0.58	GS-SVM	5

nose technology can be applied during the production and processing of strawberries to monitor and control their quality and freshness. Production and processing companies can use this technology to screen raw strawberries and ensure product quality and safety.

Non-destructive electronic nose technology for strawberries will continue to be developed and improved, and its application scope will become more extensive. Simultaneously, electronic nose technology will continue to innovate, thereby improving its detection accuracy and sensitivity, and better serving people's lives and health.

6. Conclusion

In this study, an electronic nose was developed to detect minor mechanical damage to strawberries. A shaker with a range of 120–240 r/min was used to simulate minor mechanical damage in strawberries, which were stored at 4°C for 120 h under low-temperature refrigeration. An array of sensors specifically designed to detect volatile gases emitted by strawberries was employed in the experiments. Among the electrochemical sensors, 4CH_3SH-10 and 4NO_2-20 exhibit the best detection responses. Among the metal oxide sensors, MQ136 and TGS822 demonstrated the highest responsiveness. Various feature extraction methods were applied to effectively capture the characteristics of strawberry data, and the electronic nose achieved an accuracy rate of over 0.8 for the detection of minor mechanical damage in strawberries. The multiclassification accuracy for determining the timing of strawberry damage was 0.84, and that for determining the degree of strawberry damage was 0.89. The experimental results indicated that the device could effectively differentiate the degree of mechanical damage in grouped strawberries and roughly estimate the time at which the damage occurred.

Data availability statement

The original contributions presented in the study are included in the article/Supplementary material, further inquiries can be directed to the corresponding author.

Author contributions

YQ: equipment design and manufacturing, formal analysis, experiment, data processing and analysis, designing and creating charts and graphs, writing – original draft, and writing – review and editing. WJ: conceptualization, methodology, formal analysis, supervision, and writing – review and editing. XS: equipment design and manufacturing, and experiment. HL: experiment, and writing – review and editing. All authors contributed to the article and approved the submitted version.

Funding

This study was funded by the Key Research and Development Projects of Hebei Province (21375501D), Innovation and Capacity Building Project of Beijing Academy of Agriculture and Forestry Sciences (KJCX20200213) and Innovative Entrepreneurial Team Project of Anhui Institute of Innovation for Industrial Technology (LAY-2022-CXGB-006) and National Natural Science Foundation of China (No. 31872094) and Capacity Building Project of Beijing Academy of Agriculture and Forestry Sciences (KJCX20230309).

Conflict of interest

The authors declare that the research was conducted in the absence of any commercial or financial relationships that could be construed as a potential conflict of interest.

Publisher's note

References

1. El-Sharabasy S, Issa F, Hammad G, El DM. Effect of different amino acids at different concentrations on multiplication and rooting stage of in vitro propagation of strawberries (*Fragaria X Ananassa* Duch cv. Chandler). *Egypt J Genet Cytol.* (2015) 44.

2. Giampieri F, Tulipani S, Alvarez-Suarez JM, Quiles JL, Mezzetti B, Battino M. The strawberry: composition, nutritional quality, and impact on human health. *Nutrition.* (2012) 28:9–19. doi: 10.1016/j.nut.2011.08.009

3. Wang SY, Lin HS. Antioxidant activity in fruits and leaves of blackberry, raspberry, and strawberry varies with cultivar and developmental stage. *J Agric Food Chem.* (2000) 48:140–6. doi: 10.1021/jf9908345

4. Sun J, Chu YF, Wu X, Liu RH. Antioxidant and antiproliferative activities of common fruits. *J Agric Food Chem.* (2002) 50:7449–54. doi: 10.1021/jf0207530

5. Giampieri F, Alvarez-Suarez JM, Mazzoni L, Romandini S, Bompadre S, Diamanti J, et al. The potential impact of strawberry on human health. *Nat Prod Res*. (2013) 27:448–55. doi: 10.1080/14786419.2012.706294

6. Kowalska J, Kowalska H, Marzec A, Brzeziński T, Samborska K, Lenart A. Dried strawberries as a high nutritional value fruit snack. *Food Sci Biotechnol*. (2018) 27:799–807. doi: 10.1007/s10068-018-0304-6

7. Yang Z, Wu Q, Jiang F, Zheng D, Wu D, Chen K. Indirect treatment of plasma-processed air to decrease decay and microbiota of strawberry fruit caused by mechanical damage. *Food Chem*. (2023) 408:135225. doi: 10.1016/j.foodchem.2022.135225

8. Pan L, Zhang W, Zhu N, Mao S, Tu K. Early detection and classification of pathogenic fungal disease in post-harvest strawberry fruit by electronic nose and gas chromatography–mass spectrometry. *Food Res Int*. (2014) 62:162–8. doi: 10.1016/j.foodres.2014.02.020

9. Sánchez M-T, De la Haba MJ, Benítez-López M, Fernández-Novales J, Garrido-Varo A, Pérez-Marín D. Non-destructive characterization and quality control of intact strawberries based on NIR spectral data. *J Food Eng*. (2012) 110:102–8. doi: 10.1016/j.jfoodeng.2011.12.003

10. Wilkens WF, Hartman JD. An electronic analog for the olfactory processes a. *J Food Sci*. (1964) 29:372–8. doi: 10.1111/j.1365-2621.1964.tb01746.x

11. Persaud K, Dodd G. Analysis of discrimination mechanisms in the mammalian olfactory system using a model nose. *Nature*. (1982) 299:352–5. doi: 10.1038/299352a0

12. Gómez AH, Hu G, Wang J, Pereira AG. Evaluation of tomato maturity by electronic nose. *Comput Electron Agric*. (2006) 54:44–52. doi: 10.1016/j.compag.2006.07.002

13. Chen L-Y, Wong D-M, Fang C-Y, Chiu C-I, Chou T-I, Wu C-Cet al. editors. (2018). Development of an electronic-nose system for fruit maturity and quality monitoring IEEE international conference on applied system invention (ICASI). 2018 IEEE.

14. Lin Q, Ren A, Liu R, Xing Y, Yu X, Jiang H. Flavor properties of Chinese noodles processed by dielectric drying. *Front Nutr*. (2022) 9:1007997. doi: 10.3389/fnut.2022.1007997

15. Zhao C, Ma J, Jia W, Wang H, Tian H, Wang J, et al. An apple fungal infection detection model based on BPNN optimized by sparrow search algorithm. *Biosensors*. (2022) 12:692. doi: 10.3390/bios12090692

16. Liu P, Tu K. Prediction of TVB-N content in eggs based on electronic nose. *Food Control*. (2012) 23:177–83. doi: 10.1016/j.foodcont.2011.07.006

17. Labreche S, Bazzo S, Cade S, Chanie E. Shelf life determination by electronic nose: application to milk. *Sensors Actuators B Chem*. (2005) 106:199–206. doi: 10.1016/j.snb.2004.06.027

18. Baldwin EA, Bai J, Plotto A, Dea S. Electronic noses and tongues: applications for the food and pharmaceutical industries. *Sensors*. (2011) 11:4744–66. doi: 10.3390/s110504744

19. Shi H, Zhang M, Adhikari B. Advances of electronic nose and its application in fresh foods: a review. *Crit Rev Food Sci Nutr*. (2018) 58:2700–10. doi: 10.1080/10408398.2017.1327419

20. Sanaeifar A, ZakiDizaji H, Jafari A, de la Guardia M. Early detection of contamination and defect in foodstuffs by electronic nose: a review. *TrAC Trends Anal Chem*. (2017) 97:257–71. doi: 10.1016/j.trac.2017.09.014

21. Jia W, Liang G, Jiang Z, Wang J. Advances in electronic nose development for application to agricultural products. *Food Anal Methods*. (2019) 12:2226–40. doi: 10.1007/s12161-019-01552-1

22. Hotel O, Poli J-P, Mer-Calfati C, Scorsone E, Saada S. A review of algorithms for SAW sensors e-nose based volatile compound identification. *Sensors Actuators B Chem*. (2018) 255:2472–82. doi: 10.1016/j.snb.2017.09.040

23. Zheng Z, Zhang C. Electronic noses based on metal oxide semiconductor sensors for detecting crop diseases and insect pests. *Comput Electron Agric*. (2022) 197:106988. doi: 10.1016/j.compag.2022.106988

24. Baietto M, Wilson AD. Electronic-nose applications for fruit identification, ripeness and quality grading. *Sensors*. (2015) 15:899–931. doi: 10.3390/s150100899

25. Iannetta PP, Laarhoven LJ, Medina-Escobar N, James EK, McManus MT, Davies HV, et al. Ethylene and carbon dioxide production by developing strawberries show a correlative pattern that is indicative of ripening climacteric fruit. *Physiol Plant*. (2006) 127:247–59. doi: 10.1111/j.1399-3054.2006.00656.x

26. Hu L-Y, Hu S-L, Wu J, Li Y-H, Zheng J-L, Wei Z-J, et al. Hydrogen sulfide prolongs postharvest shelf life of strawberry and plays an antioxidative role in fruits. *J Agric Food Chem*. (2012) 60:8684–93. doi: 10.1021/jf300728h

27. Alwazeer D, Özkan N. Incorporation of hydrogen into the packaging atmosphere protects the nutritional, textural and sensorial freshness notes of strawberries and extends shelf life. *J Food Sci Technol*. (2022) 59:3951–64. doi: 10.1007/s13197-022-05427-y

28. Jingwen G., Leiqing PAN, Kang TU. Aroma determination of three freshly squeezed strawberry juice based on E-nose, HS-SPME-GC-MS and GC-IMS. *Science and Technology of Food Industry*. (2023) 44:286–96. doi: 10.13386/j.issn1002-0306.2022040207

29. Granitto P, Biasioli F, Aprea E, Mott D, Furlanello C, Mark T, et al. Rapid and non-destructive identification of strawberry cultivars by direct PTR-MS headspace analysis and data mining techniques. *Sensors Actuators B Chem*. (2007) 121:379–85. doi: 10.1016/j.snb.2006.03.047

30. Han L, Xing M, Chen J, Tu K. Development of electronic nose equipment based on gas sensor for mobile detection of strawberry rot. *J Food Saf Qual*. (2019) 10:2502–8.

31. Xing M, Sun K, Liu Q, Pan L, Tu K. Development of novel electronic nose applied for strawberry freshness detection during storage. *Int J Food Eng*. (2018) 14:20180111. doi: 10.1515/ijfe-2018-0111

32. Aghilinategh N, Dalvand MJ, Anvar A. Detection of ripeness grades of berries using an electronic nose. *Food Sci Nutr*. (2020) 8:4919–28. doi: 10.1002/fsn3.1788

33. Rao J, Zhang Y, Yang Z, Li S, Wu D, Sun C, et al. Application of electronic nose and GC–MS for detection of strawberries with vibrational damage. *Food Qual Saf*. (2020) 4:181–92. doi: 10.1093/fqsafe/fyaa025

34. Cao Y, Zhang Y, Lin M, Wu D, Chen K. Non-destructive detection of damaged strawberries after impact based on analyzing volatile organic compounds. *Sensors*. (2022) 22:427. doi: 10.3390/s22020427

35. Al-Dairi M, Pathare PB, Al-Yahyai R, Opara UL. Mechanical damage of fresh produce in postharvest transportation: current status and future prospects. *Trends Food Sci Technol*. (2022) 124:195–207. doi: 10.1016/j.tifs.2022.04.018

36. Yingdong Q, Wenshen J. Real-time monitoring system for rabbit house environment based on NB-IoT network. *Smart Agric*. (2023) 5:155–65. doi: 10.12133/j.smartag.SA202211008

37. Fisher RA. The use of multiple measurements in taxonomic problems. *Ann Eugenics*. (1936) 7:179–88. doi: 10.1111/j.1469-1809.1936.tb02137.x

38. Cortes C, Vapnik V. Support-vector networks. *Mach Learn*. (1995) 20:273–97. doi: 10.1007/BF00994018

39. Altman NS. An introduction to kernel and nearest-neighbor nonparametric regression. *Am Stat*. (1992) 46:175–85. doi: 10.1080/00031305.1992.10475879

40. Mosteller F, Wallace DL. Inference in an authorship problem: a comparative study of discrimination methods applied to the authorship of the disputed federalist papers. *J Am Stat Assoc*. (1963) 58:275–309. doi: 10.1080/01621459.1963.10500849

41. Ho TK. The random subspace method for constructing decision forests. *IEEE Trans Pattern Anal Mach Intell*. (1998) 20:832–44. doi: 10.1109/34.709601

frontiers | Frontiers in Nutrition

TYPE Original Research
PUBLISHED 14 August 2023
DOI 10.3389/fnut.2023.1234807

OPEN ACCESS

EDITED BY
Dandan Pu,
Beijing Technology and Business University, China

REVIEWED BY
Hasim Kelebek,
Adana Science and Technology University, Türkiye
Lishuang Lv,
Nanjing Normal University, China

*CORRESPONDENCE
Ying Gao
✉ yinggao@tricaas.com
Yong-Quan Xu
✉ yqx33@126.com

†These authors have contributed equally to this work

RECEIVED 05 June 2023
ACCEPTED 18 July 2023
PUBLISHED 14 August 2023

CITATION
Tang P, Wang J-Q, Wang Y-F, Jin J-C, Meng X, Zhu Y, Gao Y and Xu Y-Q (2023) Comparison analysis of full-spectrum metabolomics revealed on the variation of potential metabolites of unscented, *Chloranthus spicatus* scented, and *Osmanthus fragrans (Thunb.)* Lour. scented *Congou* black teas. *Front. Nutr.* 10:1234807. doi: 10.3389/fnut.2023.1234807

Comparison analysis of full-spectrum metabolomics revealed on the variation of potential metabolites of unscented, *Chloranthus spicatus* scented, and *Osmanthus fragrans (Thunb.)* Lour. scented *Congou* black teas

Ping Tang[1†], Jie-Qiong Wang[2,3†], Yong-Feng Wang[4], Jian-Chang Jin[5], Xin Meng[6], Yan Zhu[6], Ying Gao[2*] and Yong-Quan Xu[2*]

[1]Hangzhou Vocational & Technical College, Hangzhou, China, [2]Key Laboratory of Biology, Genetics and Breeding of Special Economic Animals and Plants, Ministry of Agriculture and Rural Affairs, Tea Research Institute Chinese Academy of Agricultural Sciences, Hangzhou, China, [3]College of Food Science, Southwest University, Chongqing, China, [4]Jingdezhen Jin Gui Yuan Agricultural Development Co Ltd, Jingdezhen, China, [5]College of Biological and Environmental Engneering, Zhejiang Shuren University, Hangzhou, China, [6]College of Food and Health, Zhejiang A&F University, Hangzhou, China

Introduction: In recent years, scented black tea has attracted much attention due to its pleasant floral aroma and mellow flavor, but little research has been carried out on its flavor metabolic profile.

Methods: In this study, the flavor metabolic profiles of unscented, Chloranthus spicatus scented, and Osmanthus fragrans (Thunb.) Lour. scented Congou black teas were investigated using full-spectrum metabolomics analysis method, the first time that the flavor profiles of scented black tea were characterized in detail.

Results and Discussion: The results revealed that a total of 3,128 metabolites were detected in the three teas. Based on the criteria of variable importance in the project >1 and fold change ≥2 or≤ 0.5, 761 non-volatile metabolites and 509 volatile metabolites were filtered as differential metabolites. Many differential non-volatile metabolites belonged to flavonoids, phenolic acids, and terpenoids. Floral, fruity and herbaceous volatile metabolites were significantly up-regulated in Chloranthus spicatus scented Congou black tea while sweet and fruity volatile metabolites were significantly down-regulated in Osmanthus fragrans (Thunb.) Lour. scented Congou black tea. The results contribute to a better understanding of the scenting techniques on the flavor quality of scented black teas and provide some information on the flavor chemistry theory of scented black teas.

KEYWORDS

scented black teas, *Osmanthus fragrans (Thunb.)* Lour., *Chloranthus spicatus*, non-volatile metabolites, volatile metabolites

1. Introduction

Black tea, a fully fermented tea, is loved by consumers around the world for its health benefits (1–4) and mellow taste. Black tea is widely produced in countries such as China, India, Sri Lanka, Kenya and Indonesia (5, 6). It is popular and ranks first in the world in terms of production and consumption. The world black tea production accounted for around 65% of total tea production in 2017 (7). The *Congou* black tea (CK), a unique Chinese black tea variety, are with tightly striped shape, sweet and mellow taste, and floral and fruity aroma (8). The aroma of CK can be classified as sweet, floral or fruity, based on sensory characteristics (9). The general processes of producing CK are divided into two phases. The enzymatic phase includes the withering, rolling and fermentation processes, while the non-enzymatic phase include the drying process (10). The flavour quality is mainly formed in the enzymatic phase by the conversion of non-volatile metabolites, such as flavonoids, amino acids, fatty acids, and volatile metabolites derived from fatty acids, amino acids, terpenoids, carotenoids, and glycosidically bound volatiles (11).

In recent years, scented teas have been gaining attention for their pleasant floral aroma and mellow flavour. As a material with both ornamental and health benefits, such as protecting stomach and liver, dispersing phlegm, and antioxidant activity, *Osmanthus fragrans (Thunb.)* Lour. is ideal to be the raw material for the production of scented tea (12). Linalool, ionone and ocimene are aroma-contributing substances in it (13). Chloranthus spicatus is well-known for its elegance and is one of the "*The Four Famous Chinese Camellias*," along with jasmine, *Michelia alba DC.* and *Citrus aurantium*. As one of the traditional Chinese scented teas, Chloranthus spicatus was also ideal for the production of scented tea.

The changes in various volatile metabolites during the scenting process are crucial to the formation of scented tea aroma. The scenting process decreased alcohols but increased ketones and esters in *Osmanthus* scented black tea (14). Nonyl aldehyde, γ-decalactone, 1-octene-3-ol, trans-2-hexenyl pentanoate, and phenethyl butyrate were key odorants contributing to its *Osmanthus* aroma. Currently, the changes of volatile metabolites during the scenting process of producing *Chloranthus spicatus* scented black tea is less studied. The changes of non-volatiles metabolites during the scenting process should have an effect on the formation of scented tea quality, but still largely remain unveiled.

Based on these facts, the present study characterized the flavor metabolites of CK, *Osmanthus* scented *Congou* black tea (OF), and *Chloranthus spicatus* scented *Congou* black tea (CH) by ultra-performance liquid chromatography tandem mass spectrometry (UPLC-MS/MS) and gas chromatography–mass spectrometry (GC–MS). The results aim to understand the effect of the scenting process on the metabolic profile of black tea and help broaden the ideas for the study of flavor quality of scented black tea.

2. Materials and methods

2.1. Chemicals

Methanol, acetonitrile and hexane (all chromatography grade) for the tests were obtained from Merck (Darmstadt, Germany). Formic acid was purchased from Aladdin (Shanghai, China). Sodium chloride was produced from Sinopharm (Shanghai, China). Authentic standards used in the full-spectrum metabolomics analysis were obtained from MetWare (Wuhan, China).

2.2. Preparation of tea samples

The CK used in the experiment was purchased from Jingdezhen Jin Gui Yuan Agricultural Development Co (Jiangxi, China). The black tea was made according to the traditional *Congou* black teas process, which consisted mainly of indoor withering, rolling, fermentation and drying. The CH and OF were scented with CK as the raw material, and the specific scenting process was as follows (15):

1. Flower spreading: Pick *Chloranthus* spicatus and *Osmanthus* buds, ensure their integrity during the picking process, remove impurities such as flower tips, stalks and leaves and then stall them indoors. Indoor environment: ventilation, humidity of 65–75%, temperature of 20–24°C, thickness of 15 cm, spreading time of 30 min.
2. Mixing and resting of tea flowers: 1/3 of the CK was used to produce CH and the other 1/3 was used to produce OF. For CH, the flowers are mixed with CK in a ratio of 3:100 (flowers: dried tea, w:w) for 100 d. For OF, the flowers are mixed with CK in a ratio of 3:10 (flowers: dried tea, w: w) for 2 days, with 1 renewal, the process lasts about 4 days in total.
3. Drying: The scented teas were baked at 85°C (6CTH-30, Zhejiang Chunjiang Tea Machinery Co., Ltd.) for 412 min, cooled for 40 min, baked at 75°C for 90 min and cooled for 120 min before removing the petals and debris, resulting in scented *Congou* black teas. Three replicates were set for each treatment. The samples from three treatments were stored in a refrigerator at −80°C until assayed. The three samples were mixed and sampled three times for subsequent testing to ensure homogeneity and traceability.

2.3. UPLC-MS/MS based analysis of non-volatile metabolites

2.3.1. Sample pretreatment

The three samples were vacuum freeze-dried in a lyophilizer (Scientz-100F) before being ground (30 Hz, 1.5 min) into powder by a grinder (MM 400, Retsch). Afterwards, 50 mg of sample powder was accurately weighed and 1.2 mL of 70% methanolic aqueous internal standard extraction solution pre-chilled at −20°C was added. The sample was vortexed once every 30 min for 30 s, for a total of 6 times. Then centrifuged (12,000 rpm, 3 min), the supernatant was aspirated and filtered through 0.22 μm microporous membrane for determination.

2.3.2. UPLC-MS/MS conditions

An UPLC system equipped with a tandem mass spectrometer was used to analyze the non-volatile metabolites in the samples. (1) Liquid phase conditions: An Agilent SB-C18 1.8 μm, 2.1 mm * 100 mm column was equipped with a flow rate of 0.35 mL/min, a column temperature of 40°C, and an injection volume of 2 μL. The mobile phase A was 0.1%

formic acid/ultrapure water and mobile phase B was 0.1% formic acid/acetonitrile. The gradient elution method was as follows: mobile phase B was 5% at 0 min; increased linearly to 95% at 9 min, maintained for 1 min; decreased to 5% at 10–11.10 min and equilibrated at that ratio until 14 min. (2) Mass spectrometry conditions: electrospray ionization temperature (ESI) of 500°C, ion spray (IS) voltage of 5,500 V (positive ion mode) and −4,500 V (negative ion mode); ion source gases I (GSI), gases II (GS II), and curtain gas (CUR) of 50, 60 and 25 psi, respectively; collision-induced ionization parameters of high. The multiple reaction monitoring (MRM) mode was used for triple quadrupole (QQQ) scanning, and the collision gas (nitrogen) was medium. The declustering potential (DP) and collision energy (CE) of individual MRM ion pairs were evaluated by further DP and CE optimization. A specific set of MRM ion pairs was monitored in each period depending on the metabolites eluted during the period (16).

2.3.3. Identification of non-volatile metabolites

Based on the MWDB (metware database), the substance characterization was performed based on the secondary spectrum information of the substance, and the analysis removed the isotopic signals, the duplicate signals containing K^+, Na^+, NH_4^+, and the duplicate signals of fragment ions that were themselves other larger molecular weight substances. After obtaining the metabolite spectral analysis data of different samples, the peaks of all substances were integrated by peak area using MultiQuant software, and the mass spectra of the same metabolite in different samples among them were corrected for the integration of the peaks.

2.4. GC–MS based analysis of volatile metabolites

2.4.1. Sample pretreatment

The sample was removed from the refrigerator at −80°C and firstly ground by liquid nitrogen, followed by vortexing to make a homogeneous mixture. The 500 mg of the sample was accurately weighed in a headspace vial, subsequently 2 mL of saturated sodium chloride solution were added, the vial was sealed, and then the sample was extracted by fully automated headspace solid phase microextraction (HS-SPME) for GC–MS analysis.

2.4.2. GC–MS conditions

The headspace vial containing the tea samples was shaken and equilibrated at 60°C for 5 min, followed by insertion of a 120 μm divinylbenzene/carboxen/polydimethylsiloxane (DVB/CWR/PDMS) extraction head into the vial for 15 min (stirring while extracting was used in the extraction process with a stirring rate of 1,000 rpm, thus stability and homogeneity of the extraction process and reducing human error), followed by desorption at the inlet end at 250°C for 5 min for subsequent GC–MS separation and identification. It should be noted that the extraction head should be heated at the inlet end at 250°C for 5 min before sampling. (1) Chromatographic conditions: DB-5MS capillary column (30 m × 0.25 mm × 0.25 μm, Agilent J&W Scientific, Folsom, CA, United States) supplemented with high purity helium (purity not less than 99.999%) as carrier gas. The program temperature was set as follows: 40°C for 3.5 min, then 10°C/min to 100°C, then 7°C/min to 180°C, and finally 25°C/min to 280°C for 5 min. (2) Mass spectrometry conditions: electron bombardment ion source (EI); ion source, quadrupole and mass spectrometry interface temperatures of 230°C, 150°C and 280°C, respectively; electron energy of 70 eV, scanning mode of selected ion detection mode (SIM), qualitative and quantitative ion precision scanning (GB 23200.8–2016).

2.4.3. Identification of volatile metabolites

Based on multi-species, literatures, authentic standards, and retention index (RI), the database was established independently, containing the identified retention time (RT) as well as qualitative and quantitative ions for the selected ion detection mode for precise scanning, with one quantitative ion and two to three qualitative ions selected for each compound, respectively. All ions to be detected in each group were detected separately in the order of of their peaks, in separate time periods. If the retention time of the detected peaks was consistent with the authentic standard and the selected ions all appeared in the mass spectra of the samples after background deduction, the substance would be ascertained. The odor descriptions for the qualitative aroma substances were taken from websites such as http://www.thegoodscentscompany.com, http://perflavory.com/, http://www.odour.org.uk, http://foodflavorlab.cn. The quantitative ions were selected by MassHunter software for the integration and calibration of the peaks in order to enhance the accuracy of quantification.

2.5. Statistical analysis

All samples were set up with three biological replicates and statistical analysis was performed using IBM SPSS statistics (version 25.0, SPSS Inc., Chicago, IL). The principal component analysis (PCA), partial least squares-discriminant analysis (PLS-DA), clustering heat map, K-Means plot, and key metabolite kyoto encyclopedia of genes and genomes (KEGG) enrichment pathway maps were done by R software.[1] The identified metabolites were first annotated through the KEGG compound database,[2] and subsequently the annotated completed metabolites were mapped to the KEGG pathway database.[3] The pathways mapped to metabolites with significant regulation were subsequently sent to metabolite set enrichment analysis (MSEA), whose significance was determined by *p*-values of hypergeometric tests.

3. Results and discussion

3.1. Overall profile of metabolites in the three black teas

Metabolomics allows the detection and screening of significant differential metabolites from different biological samples, which can be used as a basis to further elucidate the metabolic processes and mechanisms of change in biological samples. In this study, a full-spectrum metabolomics analysis based on dual platforms of UPLC-MS/MS and GC–MS was carried out. A total of 3,128 metabolites, including 2,396 non-volatile metabolites and 732 volatile metabolites, were detected in three black tea samples.

1 www.r-project.org/
2 http://www.kegg.jp/kegg/compound/
3 http://www.kegg.jp/kegg/pathway.html

As shown in Figures 1A, a total of 26 categories of metabolites were detected in black teas. Flavonoids, phenolic acids, terpenoids, others, alkaloids, lipids, amino acids and derivatives together occupied 68.76% of all metabolites. Lignans and coumarins (4.03%), organic acids (4.19%), esters (3.8%), heterocyclic compounds (3.64%), nucleotides and derivatives (2.65%), tannins (2.05%), hydrocarbons (1.92%), ketones (1.85%), alcohols (1.76%), aldehydes (1.44%), aromatics (1.37%) were minor metabolites. Acids, quinones, amines, sulfur compounds, nitrogen compounds, phenols, ethers, and halogenated hydrocarbons accounted for less than 1%. A previous study also pointed out that flavonoids played an important role in the quality and flavour of black tea during black tea processing (17), which was similar to the above results.

The heatmap distribution in Figure 1B indicated that the metabolite contents in the three black tea samples were significantly different. To further validate the above results, PCA, as an unsupervised pattern recognition method for multidimensional data statistical analysis, was introduced to analyze the differences of overall metabolites (Figure 1C), non-volatile metabolites (Figure 1D), and volatile metabolites (Figure 1E) among the three black tea samples. The results revealed that the three samples achieved good separation in each PCA model, and the sum of the first and second principal components of the above three data sets explained more than 50% of the whole data set, reaching 63.81, 50.41 and 79.91%, respectively, indicating that the three black tea metabolites reached significant

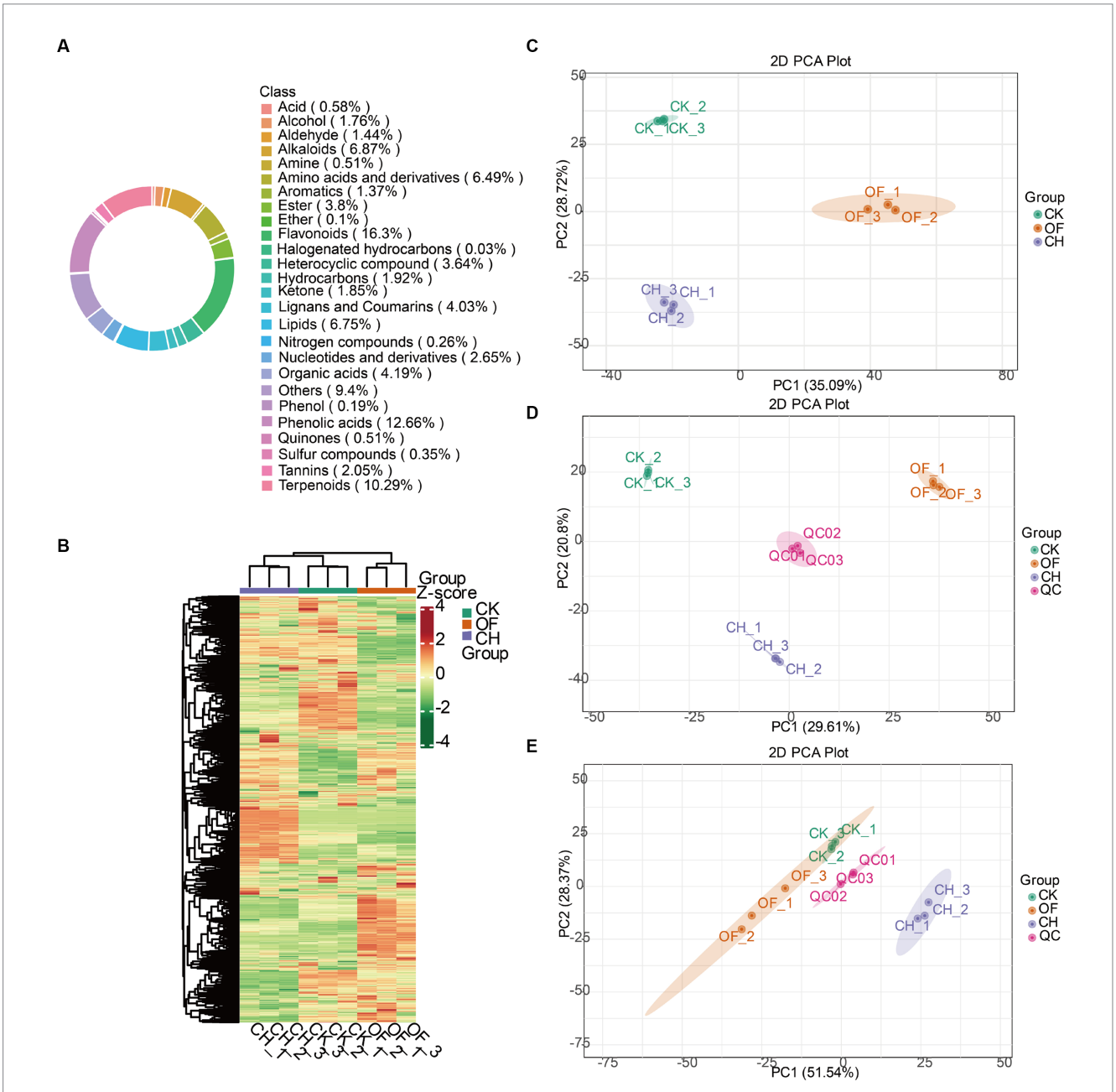

FIGURE 1
Analysis of all metabolites in three types of black tea (CK, CH and OF). **(A)** Ring diagram of total metabolite class composition; **(B)** Heat map of total metabolite content clustering (processed by Z-score); **(C)** PCA analysis of total metabolites; **(D)** PCA analysis of non-volatile metabolites; **(E)** PCA analysis of volatile metabolites. CK, Congou black tea; OF, Osmanthus black tea; CH, Chloranthus spicatus black tea. Same below.

differences among them. The results provided some data support for further screening the important differential metabolites.

3.2. Important differential metabolites among the three black teas

1,270 differential metabolites were initially identified based on the screening criteria of variable importance in the project (VIP)>1 and fold change (FC) ≥2 or ≤0.5, among which 761 non-volatile metabolites (Supplementary Table S1) and 509 volatile metabolites (Supplementary Table S2) were identified.

The Venn plot indicated the relationships of differential metabolites between different black tea samples. The results showed that there were 59 differential metabolites between the three comparison groups (CK vs. OF, CK vs. CH, OF vs. CH) and 82, 50, 96 differential metabolites were unique to each group (Figure 2A). To further verify whether the differential metabolites among the three black tea samples reached significant differences, an unsupervised model statistical method, i.e., PCA (Figure 2B), and a supervised model statistical method, i.e., PLS-DA (Figure 2C), were used simultaneously to screen for differential metabolites. It was found that both models could achieve good separation. In 200 permutations of validation of the PLS-DA model (Figure 2D), R2X = 0.733, R2Y = 1 ($p < 0.005$), Q2 = 0.979 ($p < 0.005$), indicating a good model fit.

The Volcano plot was mainly used to show the relative abundances of metabolites between two samples. Each dot in the plot indicated a differential metabolite. Green dots indicated down-regulated substances, red dots indicated up-regulated substances, and gray indicated substances with insignificant differences. The results showed that compared to CK, 197 substances were up-regulated and 85 substances were down-regulated in CH (Figure 2E), while 92 substances were up-regulated and 193 substances were down-regulated in OF (Figure 2F), which might be related to the different flowers used in the scenting process.

The K-means plot focused on classifying the trends of relative abundances of important differential metabolites under different comparison groups to facilitate subsequent targeted analysis. According to Figure 2G, three different trends in the levels of these important differential metabolites were detected in CK, CH and OF. Among them, 342 metabolites were lower in OF than in CK and 371 metabolites were higher in CH than in CK. It was obvious that more substances were up-regulated in CH and down-regulated in OF after CK was scented, suggesting that the type of flower had a great influence on the metabolites of CK.

Subsequently, the top 20 KEGG metabolic pathways in the three samples were screened based on differential abundance (DA) scores and *p*-values sizes (Figures 2H,I). The sesquiterpenoid and triterpenoid biosynthesis, limonene and pinene degradation, and tyrosine metabolism reached significant levels in the metabolite expression of CH (compared to CK), with the first two pathways being significantly up-regulated and the last one remaining basically stable. Sesquiterpenoids and triterpenoids were generally biosynthesized *via* the cytoplasmic mevalonate (MVA) pathway in plants (18–20). Triterpenoids usually had a variety of stereoisomers and positional isomers, but the main compounds were the madecassic acid isomer and asiatic acid isomer (21). In OF, the expression of metabolic pathways such as terpenoid backbone biosynthesis, flavone and flavonol biosynthesis, and tyrosine metabolism were significantly down-regulated overall. Terpenoids were derived from the same C5 isoprene backbone produced from isopentenyl pyrophosphates (IPP) and dimethyl allyl pyrophosphates (DMAPP) and were used in the synthesis of terpene backbones by rearrangement and cyclisation reactions (22), where linalool, nerol and alpha-terpineol could be produced by further reactions in the biosynthesis of terpene backbones (23). The results revealed differences in flavor quality between different scented black teas (CH and OF) from a metabolomics perspective. However, the most critical contributors to this difference were still unknown, both in terms of non-volatile and volatile substances.

3.3. Analysis of key differential non-volatile metabolites among the three black teas

3.3.1. Analysis of key differential categories

Based on the percentage of metabolite categories, all non-volatile metabolites were further screened and a total of 173 metabolites were selected (Table 1). In terms of categories, the metabolites in the three black teas mainly consisted of amino acids and derivatives, phenolic acids, flavonoids, lipids, accounting for 7.69, 20.12, 52.66 and 19.53%, respectively. In terms of peak area, flavonoids accounted for a relatively large proportion of all key metabolites, reaching 96.30% in CK, and compared with CK, the percentage of peak area of flavonoids increased by 0.39 and 6.72% in CH and OF, respectively. The variation of flavonoids was determined by the thermal stability during the drying stage (17). Compared with CK, the peak area of lipids in CH was reduced by 0.43%. The lipids were important precursors of volatile metabolites in tea leaves (24). It was reported that lipids were degraded by enzymatic hydrolysis or oxidation of glycolipids and phospholipids to produce flavor volatiles during black tea processing (25), which was in accordance with our experimental results. The total peak area of amino acids and derivatives in OF was reduced by 5.18% compared to CK (Supplementary Table S1), which indicated that the Maillard reaction, deamidation polymerization and caramelization might occur during the scenting process (26).

Overall, there was a downward trend in the non-volatile metabolites of black tea after scenting. Compared to CK, phenolic acids were significantly up-regulated in CH (Log2FC = 31.66) whilst flavonoids were significantly down-regulated (Log2FC = −39.00). Amino acids and derivatives were significantly up-regulated in OF (Log2FC = 17.60) whilst flavonoids were significantly down-regulated (Log2FC = −30.43).

3.3.2. Analysis of key differential compounds

Based on the values of magnitude of the difference multiplier (Log2FC) in each comparison group (CK vs. CH, CK vs. OF), the substances ranked the top 20 of the key non-volatile differential metabolites were prioritized for further discussion. As illustrated in Figures 3A,B, the Log2FC of the selected metabolites ranged from −22.58 to 18.83 in CK vs. CH and − 14.62 to 18.03 in CK vs. OF. Based on |Log2FC| > 15, 7 and 4 substances were screened as key differential compounds in CH (Figure 3D) and OF (Figure 3C), respectively.

The results revealed that the 11 substances were divided into two main groups, which were flavonoids and phenolic acids. Combined with the relevant information in Table 1, it was concluded that compared to CK, forsythoside H, alpha-asarone,

10.3389/fnut.2023.1234807

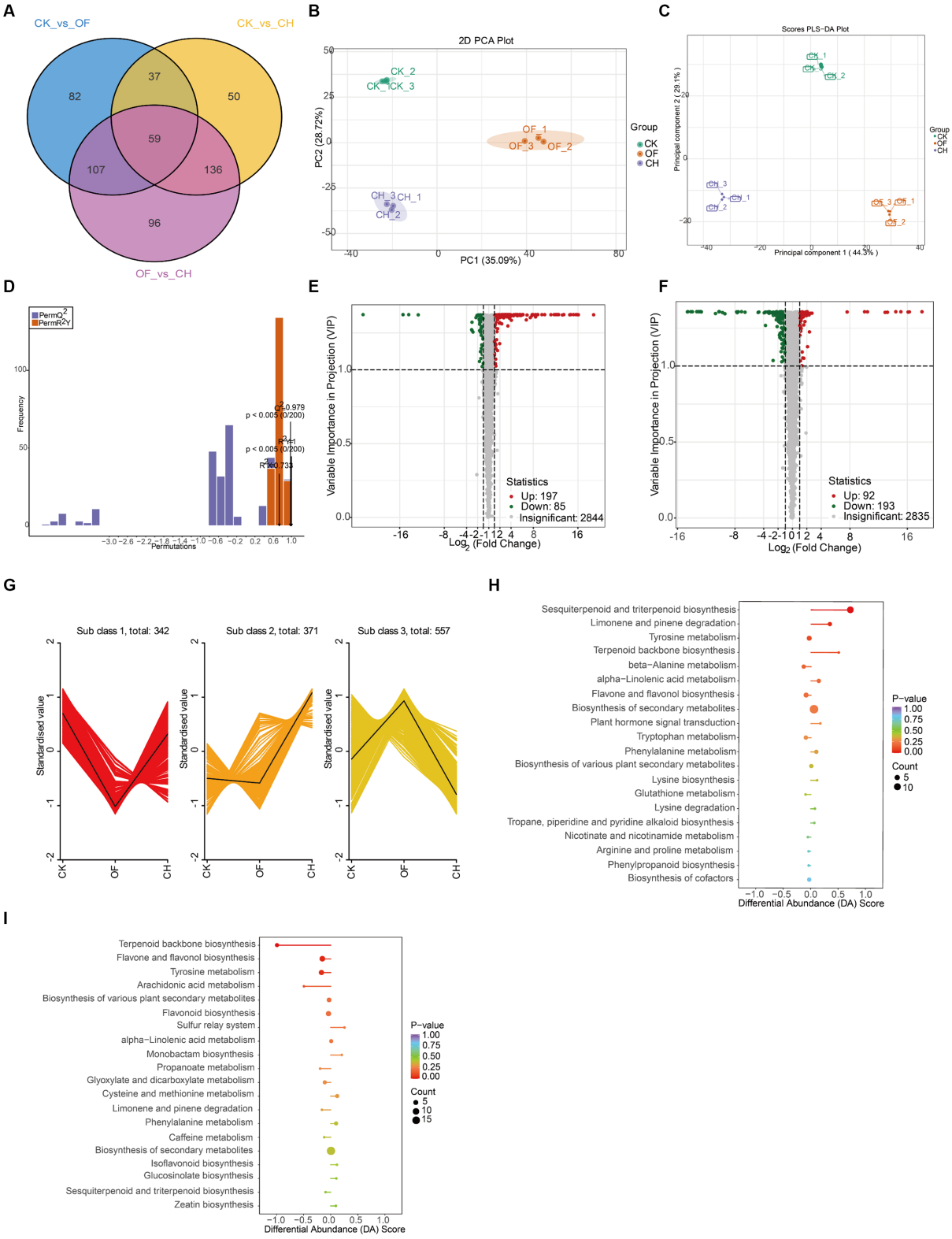

FIGURE 2
Analysis of important differential metabolites in three types of black tea (CK, CH and OF). **(A)** Venn plot; **(B)** PCA plot; **(C)** PLS-DA plot; **(D)** PLS-DA 200-permutation plot; **(E,F)** Volcano plot (E. CK vs. CH; F. CK vs. OF); **(G)** K-means plot; **(H,I)** KEGG differential abundance score plot (H. CK vs. CH; I. CK vs. OF; where the color and size of the dots indicated the size of the *p*-values and number of metabolites, respectively; DA score indicated the overall change of all metabolites in the metabolic pathway, 1: up-regulation, –1: down-regulation, and the length of the line segment indicated the DA score).

TABLE 1 Key differential non-volatile metabolites changes among the three black teas.

No.	Molecular weight (Da)	Q1 (Da)[a]	Q3 (Da)[b]	Formula	Ionization model[c]	Compounds[d]	Level[e]	CH_FC[f]	CH_ Log_2FC[g]	CH_ Type[h]	OF_FC[f]	OF_ Log_2FC[g]	OF_ Type[h]
Amino acids and derivatives (13)													
1	145.0739	144.07	126.06	$C_6H_{11}NO_3$	$[M-H]^-$	Allysine	3	2.19	1.13	Up			
2	149.0510	150.06	61.01	$C_5H_{11}NO_2S$	$[M+H]^+$	DL-Methionine	3				4.18	2.06	Up
3	163.0667	164.07	56.05	$C_6H_{13}NO_2S$	$[M+H]^+$	L-Homomethionine	3				2.63	1.39	Up
4	188.1273	189.13	144.10	$C_7H_{16}N_4O_2$	$[M+H]^+$	Homoarginine	3				3.16	1.66	Up
5	191.0616	192.07	56.05	$C_7H_{13}NO_3S$	$[M+H]^+$	N-Acetyl-L-Methionine	3				5.16	2.37	Up
6	215.0946	214.09	153.07	$C_{13}H_{13}NO_2$	[M-H]-	3-(2-Naphthyl)-L-alanine	3				2.98	1.57	Up
7	222.1004	223.11	120.09	$C_{11}H_{14}N_2O_3$	$[M+H]^+$	L-Glycyl-L-phenylalanine*	2				2.04	1.03	Up
8	246.1004	245.09	203.08	$C_{13}H_{14}N_2O_3$	[M-H]-	N-acetyl-tryptophan	1	0.47	−1.09	Down			
9	294.1216	295.13	120.08	$C_{14}H_{18}N_2O_5$	$[M+H]^+$	γ-Glutamylphenylalanine	2				2.07	1.05	Up
10	321.0995	322.11	130.05	$C_{11}H_{19}N_3O_6S$	$[M+H]^+$	S-(Methyl)glutathione	1				2.07	1.05	Up
11	384.1216	385.13	250.00	$C_{14}H_{20}N_6O_5S$	$[M+H]^+$	S-(5′-Adenosy)-L-homocysteine	3				2.64	1.40	Up
12	398.1372	399.14	250.09	$C_{15}H_{22}N_6O_5S$	$[M+H]^+$	S-(5′-Adenosyl)-L-methionine	3				4.01	2.00	Up
13	399.1445	399.14	250.09	$C_{15}H_{23}N_6O_5S^+$	[M]+	S-Adenosylmethionine	3				4.01	2.00	Up
Phenolic acids (34)													
14	110.0368	109.03	81.03	$C_6H_6O_2$	[M-H]-	Hydroquinone	3				0.35	−1.52	Down
15	120.0575	121.06	77.04	C_8H_8O	$[M+H]^+$	Phenylacetaldehyde	3	9503.89	13.21	Up	1052.15	10.04	Up
16	126.0317	125.02	79.02	$C_6H_6O_3$	[M-H]-	Pyrogallol	2				0.50	−1.01	Down
17	150.0681	149.06	131.05	$C_9H_{10}O_2$	[M-H]-	p-Coumaryl alcohol	3				2.19	1.13	Up
18	152.0473	153.05	123.04	$C_8H_8O_3$	$[M+H]^+$	Methyl salicylate	3	0.49	−1.03	Down			
19	153.0426	152.04	108.05	$C_7H_7NO_3$	$[M-H]^-$	3-Aminosalicylic acid	3	0.29	−1.80	Down	0.30	−1.73	Down
20	153.0426	152.03	108.05	$C_7H_7NO_3$	$[M-H]^-$	4-Aminosalicylic acid	3	0.39	−1.36	Down	0.31	−1.69	Down
21	154.0266	153.02	109.03	$C_7H_6O_4$	$[M-H]^-$	Gentisic Acid*	1				0.34	−1.58	Down
22	154.0266	153.02	109.03	$C_7H_6O_4$	$[M-H]^-$	Protocatechuic acid*	1				0.34	−1.57	Down
23	154.0266	153.02	109.03	$C_7H_6O_4$	$[M-H]^-$	Methyl cumalate	1				0.34	−1.57	Down
24	168.0423	167.03	123.05	$C_8H_8O_4$	$[M-H]^-$	3,4-Dihydroxybenzeneacetic acid	3	0.48	−1.05	Down			
25	180.0786	179.07	92.03	$C_{10}H_{12}O_3$	$[M-H]^-$	Propyl 4-hydroxybenzoate	3	2.63	1.39	Up			
26	208.1099	209.12	179.07	$C_{12}H_{16}O_3$	$[M+H]^+$	alpha-Asarone	2	69747.14	16.09	Up	79115.94	16.27	Up
27	212.0685	213.07	195.07	$C_{10}H_{12}O_5$	$[M+H]^+$	2,4,5-Trimethoxybenzoic acid	3				0.30	−1.74	Down

(Continued)

10.3389/fnut.2023.1234807

TABLE 1 (Continued)

No.	Molecular weight (Da)	Q1 (Da)[a]	Q3 (Da)[b]	Formula	Ionization model[c]	Compounds[d]	Level[e]	CH_FC[f]	CH_ Log_2FC[g]	CH_ Type[h]	OF_FC [f]	OF_ Log_2FC[g]	OF_ Type[h]
28	238.0841	237.08	163.04	$C_{12}H_{14}O_5$	$[M-H]^-$	1-*O*-p-Cumaroylglycerol	3	2.26	1.18	Up			
29	268.0947	269.10	177.05	$C_{13}H_{16}O_6$	$[M+H]^+$	2-Feruloyl-sn-glycerol	3				0.45	−1.15	Down
30	286.0325	285.03	133.02	$C_{11}H_{10}O_9$	$[M-H]^-$	L-Malic acid-2-*O*-gallate	3	2.05	1.04	Up	2.17	1.12	Up
31	308.0896	309.10	147.04	$C_{15}H_{16}O_7$	$[M+H]^+$	1-*O*-(p-coumaroyl) 3-Hydroxy-3-methylglutaric acid	1	0.45	−1.17	Down			
32	308.0896	309.10	147.04	$C_{15}H_{18}O_{10}$	$[M+H]^+$	5-*O*-Galloyl-methyl quinine ester	1	0.37	−1.43	Down			
33	326.1002	325.09	145.03	$C_{15}H_{18}O_8$	$[M-H]^-$	1-*O*-p-Coumaroyl-β-D-glucose*	2	0.45	−1.15	Down			
34	338.1002	337.09	163.04	$C_{16}H_{18}O_8$	$[M-H]^-$	1-*O*-p-Coumaroylquinic acid	1				0.47	−1.08	Down
35	346.0900	345.08	139.04	$C_{14}H_{18}O_{10}$	$[M-H]^-$	1-*O*-(3,4-Dihydroxy-5-methoxy-benzoyl)-glucoside	3	0.32	−1.63	Down			
36	356.1107	355.10	121.03	$C_{16}H_{20}O_9$	$[M-H]^-$	Homovanilloylquinic acid	3				0.36	−1.47	Down
37	360.0845	359.08	161.02	$C_{18}H_{16}O_8$	$[M-H]^-$	Rosmarinic acid	2	0.12	−3.01	Down	0.00	−9.73	Down
38	360.0851	359.08	197.05	$C_{18}H_{16}O_8$	$[M-H]^-$	Salvianic acid B	2	0.12	−3.08	Down	0.00	−7.68	Down
39	360.0851	359.08	197.05	$C_{29}H_{36}O_{15}$	$[M-H]^-$	Magnoloside D	2	345.65	8.43	Up			
40	418.1839	477.20	181.09	$C_{19}H_{30}O_{10}$	$[M+CH3COO]^-$	2-[4-(3-Hydroxypropyl)-2-methoxyphenoxy]-1,3-propanediol 1-glucoside	3				267109.16	18.03	Up
41	466.1264	467.13	147.04	$C_{25}H_{22}O_9$	$[M+H]^+$	3,4-*O*-Di-p-Coumaroylshikimic acid	3				0.48	−1.07	Down
42	474.0434	473.04	169.01	$C_{21}H_{14}O_{13}$	$[M-H]^-$	Trigallic acid	2				0.37	−1.45	Down
43	481.0600	481.06	275.00	$C_{20}H_{18}O_{14}$	$[M-H]^-$	4,6-(S)-Hexahydroxydiphenoyl-D-glucose	2				2.20	1.14	Up
44	624.2054	623.20	461.17	$C_{29}H_{36}O_{15}$	$[M-H]^-$	Acteoside	2	13.27	3.73	Up			
45	624.2054	623.20	161.02	$C_{29}H_{36}O_{15}$	$[M-H]^-$	Forsythoside H*	3	465047.40	18.83	Up	1396.47	10.45	Up
46	624.2054	623.20	161.03	$C_{29}H_{36}O_{15}$	$[M-H]^-$	Forsythoside I*	3	337.38	8.40	Up			
47	798.1491	797.14	645.10	$C_{33}H_{34}O_{23}$	$[M-H]^-$	2-*O*-Trigalloyl-glucose–glucose	3				0.00	−14.62	Down
Flavonoids (89)													
48	254.0579	255.07	137.02	$C_{15}H_{10}O_4$	$[M+H]^+$	6,7-Dihydroxyflavone	3	3.85	1.95	Up			
49	270.0528	271.06	215.07	$C_{15}H_{10}O_5$	$[M+H]^+$	4′,6,7-Trihydroxyisoflavone	3				2.07	1.05	Up
50	274.0841	275.09	107.05	$C_{15}H_{14}O_5$	$[M+H]^+$	Epiafzelechin	1				2.06	1.05	Up
51	288.0634	287.06	125.03	$C_{15}H_{12}O_6$	$[M-H]^-$	2-hydroxynaringenin	2	2.15	1.10	Up	2.29	1.19	Up

(Continued)

10.3389/fnut.2023.1234807

TABLE 1 (Continued)

No.	Molecular weight (Da)	Q1 (Da)[a]	Q3 (Da)[b]	Formula	Ionization model[c]	Compounds[d]	Level[e]	CH_FC[f]	CH_ Log_2FC[g]	CH_ Type[h]	OF_FC [f]	OF_ Log_2FC[g]	OF_ Type[h]
52	302.0427	301.04	151.00	$C_{15}H_{10}O_7$	$[M-H]^-$	Tricetin	2				0.44	−1.20	Down
53	306.0740	305.07	125.02	$C_{15}H_{14}O_7$	$[M-H]^-$	Leucocyanidin	1	0.45	−1.16	Down	0.41	−1.30	Down
54	306.0740	307.08	139.04	$C_{15}H_{14}O_7$	$[M+H]^+$	Gallocatechin	2	0.47	−1.09	Down	0.49	−1.04	Down
55	314.1154	315.12	181.05	$C_{18}H_{18}O_5$	$[M+H]^+$	Flavokawain A	1	35.05	5.13	Up	0.07	−3.93	Down
56	328.0947	329.10	299.05	$C_{18}H_{16}O_6$	$[M+H]^+$	5-Hydroxy-7,3′,4′-trimethoxyflavone	3				0.32	−1.62	Down
57	344.0896	345.10	284.07	$C_{18}H_{16}O_7$	$[M+H]^+$	5,7-Dihydroxy-3′,4′,5′-trimethoxyflavone	3				0.33	−1.58	Down
58	360.0845	359.08	161.02	$C_{18}H_{16}O_8$	$[M-H]^-$	Myricetin-3,7,3′-trimethyl ether	2	0.14	−2.84	Down	0.00	−9.39	Down
59	366.0046	365.00	285.04	$C_{15}H_{10}O_9S$	$[M-H]^-$	Kaempferol-3-*O*-sulfonate	3	0.43	−1.23	Down			
60	381.9995	380.99	301.04	$C_{15}H_{10}O_{10}S$	$[M-H]^-$	Quercetin-3-*O*-Sulfonate	3	0.33	−1.59	Down			
61	397.9944	396.99	317.03	$C_{15}H_{10}O_{11}S$	$[M-H]^-$	Myricetin-3-*O*-sulfonate	3	0.40	−1.33	Down			
62	402.0951	403.10	367.08	$C_{20}H_{18}O_9$	$[M+H]^+$	Apigenin-6-C-arabinoside*	2				0.30	−1.71	Down
63	402.0951	403.10	367.08	$C_{20}H_{18}O_9$	$[M+H]^+$	Apigenin-8-C-Arabinoside*	2				0.34	−1.54	Down
64	402.1315	403.14	373.09	$C_{21}H_{22}O_8$	$[M+H]^+$	3,5,6,7,8,4'-Hexamethoxyflavone	3	0.45	−1.14	Down			
65	418.0900	419.10	383.07	$C_{20}H_{18}O_{10}$	$[M+H]^+$	Luteolin-8-C-arabinoside	3				0.47	−1.09	Down
66	418.1264	419.13	383.10	$C_{21}H_{22}O_9$	$[M+H]^+$	*O*-MethylNaringenin-8-C-arabinoside	3				0.50	−1.00	Down
67	432.1056	431.10	311.05	$C_{21}H_{20}O_{10}$	$[M-H]^-$	Isovitexin	1				0.37	−1.43	Down
68	432.1056	433.11	313.07	$C_{21}H_{20}O_{10}$	$[M+H]^+$	Vitexin	1				0.46	−1.13	Down
69	432.1056	433.11	283.06	$C_{21}H_{20}O_{10}$	$[M+H]^+$	Genistein-8-C-glucoside	3	0.49	−1.04	Down	0.32	−1.63	Down
70	432.1420	433.15	403.11	$C_{22}H_{24}O_9$	$[M+H]^+$	3,5,6,7,8,3′,4'-Heptamethoxyflavone	3	0.32	−1.65	Down			
71	434.0849	435.09	303.05	$C_{20}H_{18}O_{11}$	$[M+H]^+$	Morin-3-*O*-xyloside	3				0.35	−1.50	Down
72	434.1213	433.11	271.06	$C_{21}H_{22}O_{10}$	$[M-H]^-$	Choerospondin	2	0.46	−1.12	Down			
73	436.1369	435.13	315.09	$C_{21}H_{24}O_{10}$	$[M-H]^-$	Trilobatin	3	0.48	−1.05	Down			
74	448.1006	449.11	303.05	$C_{21}H_{20}O_{11}$	$[M+H]^+$	Quercitrin	3	0.20	−2.31	Down	0.33	−1.59	Down
75	450.1162	449.11	287.06	$C_{21}H_{22}O_{11}$	$[M-H]^-$	Dihydrokaempferol-7-*O*-glucoside	3	59587.87	15.86	Up	69886.92	16.09	Up
76	452.1319	451.12	289.07	$C_{21}H_{24}O_{11}$	$[M-H]^-$	Catechin-5-*O*-glucoside	3	2.99	1.58	Up	2.86	1.52	Up
77	456.1056	455.10	289.07	$C_{23}H_{20}O_{10}$	$[M-H]^-$	Epicatechin-3-(3"-*O*-methyl) gallate	2				0.35	−1.52	Down
78	458.0849	459.09	139.04	$C_{22}H_{18}O_{11}$	$[M+H]^+$	Gallocatechin gallate*	1				0.48	−1.07	Down

(Continued)

10.3389/fnut.2023.1234807

TABLE 1 (Continued)

No.	Molecular weight (Da)	Q1 (Da)[a]	Q3 (Da)[b]	Formula	Ionization model[c]	Compounds[d]	Level[e]	CH_FC[f]	CH_ Log_2FC[g]	CH_ Type[h]	OF_FC [f]	OF_ Log_2FC[g]	OF_ Type[h]
79	464.0955	465.10	303.05	$C_{21}H_{20}O_{12}$	$[M+H]^+$	Rhodiolgin	1	0.43	−1.23	Down			
80	464.0955	465.10	303.05	$C_{21}H_{20}O_{12}$	$[M+H]^+$	Quercetin-5-*O*-β-D-glucoside*	1	0.48	−1.06	Down			
81	464.0955	465.10	333.07	$C_{21}H_{20}O_{12}$	$[M+H]^+$	6-Methoxyquercetin-3-*O*-Xyloside	3	0.31	−1.68	Down	0.21	−2.26	Down
82	472.1006	471.10	183.03	$C_{23}H_{20}O_{11}$	$[M-H]^-$	Epigallocatechin 3-*O*-(3-*O*-Methyl) Gallate	3				0.43	−1.21	Down
83	474.1162	475.12	271.06	$C_{23}H_{22}O_{11}$	$[M+H]^+$	Apigenin-7-*O*-(6″-acetyl) glucoside	3	10.78	3.43	Up			
84	478.1475	477.14	315.09	$C_{23}H_{26}O_{11}$	$[M-H]^-$	Persicoside	3				0.38	−1.41	Down
85	480.0904	481.10	319.05	$C_{21}H_{20}O_{13}$	$[M+H]^+$	Gossypetin-3-*O*-glucoside	2	0.40	−1.34	Down			
86	480.1268	481.13	319.05	$C_{22}H_{24}O_{12}$	$[M+H]^+$	3′,5′,5,7-Tetrahydroxy-4′-methoxyflavanone-3'-*O*-glucoside	1	0.42	−1.25	Down			
87	492.1268	493.13	331.08	$C_{23}H_{24}O_{12}$	$[M+H]^+$	Flavoyadorinin A	3				0.50	−1.01	Down
88	492.1268	493.13	331.08	$C_{23}H_{24}O_{12}$	$[M+H]^+$	Tricin-4'-*O*-glucoside	3				0.43	−1.23	Down
89	492.1268	493.13	331.08	$C_{23}H_{24}O_{12}$	$[M+H]^+$	Iristectorin A	3				0.42	−1.24	Down
90	494.0697	495.08	319.04	$C_{21}H_{18}O_{14}$	$[M+H]^+$	Myricetin-3-*O*-glucuronide	3	3.82	1.93	Up	4.92	2.30	Up
91	494.1060	495.11	333.07	$C_{22}H_{22}O_{13}$	$[M+H]^+$	Laricitrin-3-*O*-glucoside	2	0.40	−1.32	Down	0.49	−1.02	Down
92	494.1060	493.10	331.05	$C_{22}H_{22}O_{13}$	$[M-H]^-$	Mearnsetin-3-*O*-glucoside	2				0.50	−1.01	Down
93	506.1060	505.10	300.03	$C_{23}H_{22}O_{13}$	$[M-H]^-$	Quercetin-3-*O*-(6"-*O*-acetyl) galactoside	3	0.43	−1.23	Down			
94	506.1060	507.12	303.05	$C_{23}H_{22}O_{13}$	$[M+H]^+$	Quercetin-3-*O*-(6"-*O*-acetyl) glucoside	3	0.35	−1.51	Down	0.31	−1.68	Down
95	508.1217	509.13	347.08	$C_{23}H_{24}O_{13}$	$[M+H]^+$	5,6,3′,4'-Tetrahydroxy-3,7-dimethoxyflavone-6-*O*-glucoside	3	0.00	−15.40	Down			
96	508.1217	509.13	347.08	$C_{23}H_{24}O_{13}$	$[M+H]^+$	Limocitrin 3-Glucoside	3	0.00	−15.40	Down			
97	534.1010	535.11	287.05	$C_{24}H_{22}O_{14}$	$[M+H]^+$	Kaempferol-3-*O*-(6″-malonyl) glucoside*	1	0.38	−1.41	Down			
98	536.1166	535.11	287.05	$C_{24}H_{24}O_{14}$	$[M-H]^-$	Eriodictyol-7-*O*-(6″-malonyl) glucoside	2				2.24	1.16	Up
99	550.1323	551.14	497.10	$C_{25}H_{26}O_{14}$	$[M+H]^+$	Luteolin-6,8-di-C-arabinoside	3				0.41	−1.30	Down
100	564.1115	565.12	317.08	$C_{25}H_{24}O_{15}$	$[M+H]^+$	Isorhamnetin-3-*O*-(6″-malonyl) glucoside	3				7621.45	12.90	Up

(Continued)

10.3389/fnut.2023.1234807

TABLE 1 (Continued)

No.	Molecular weight (Da)	Q1 (Da)[a]	Q3 (Da)[b]	Formula	Ionization model[c]	Compounds[d]	Level[e]	CH_FC[f]	CH_ Log_2FC[g]	CH_ Type[h]	OF_FC [f]	OF_ Log_2FC[g]	OF_ Type[h]
101	564.1479	565.16	433.10	$C_{26}H_{28}O_{14}$	$[M+H]^+$	Genistein-8-C-apiosyl (1 → 6) glucoside	3				0.36	−1.47	Down
102	564.1479	565.16	433.11	$C_{26}H_{28}O_{14}$	$[M+H]^+$	Apigenin-6-C-(2″-xylosyl) glucoside	3				0.45	−1.15	Down
103	564.1479	565.15	433.11	$C_{26}H_{28}O_{14}$	$[M+H]^+$	Isovitexin-2”-*O*-xyloside*	3				0.44	−1.17	Down
104	566.1272	567.13	303.05	$C_{25}H_{26}O_{15}$	$[M+H]^+$	Quercetin-3-*O*-xylosyl (1 → 2) arabinoside	3	2280.49	11.16	Up			
105	578.1424	579.15	271.06	$C_{30}H_{26}O_{12}$	$[M+H]^+$	Apigenin-7-*O*-(6″-p-Coumaryl) glucoside	3	0.43	−1.21	Down			
106	578.1636	579.17	433.11	$C_{27}H_{30}O_{14}$	$[M+H]^+$	Vitexin-2”-*O*-rhamnoside	1				0.38	−1.40	Down
107	580.1428	581.15	287.06	$C_{26}H_{28}O_{15}$	$[M+H]^+$	Kaempferol-3-*O*-sambubioside	3	0.47	−1.08	Down			
108	592.1792	593.18	447.13	$C_{28}H_{32}O_{14}$	$[M+H]^+$	Chrysoeriol-6-C-rhamnoside-7-*O*-rhamnoside	3				0.44	−1.20	Down
109	594.1585	593.15	285.04	$C_{27}H_{30}O_{15}$	$[M-H]^-$	Nicotiflorin*	1	0.47	−1.08	Down			
110	594.1585	595.17	287.06	$C_{27}H_{30}O_{15}$	$[M+H]^+$	Kaempferol-3-*O*-glucorhamnoside*	1	0.00	−22.58	Down	0.40	−1.33	Down
111	594.1585	595.16	313.07	$C_{27}H_{30}O_{15}$	$[M+H]^+$	Vitexin-2”-*O*-glucoside	1				0.41	−1.29	Down
112	594.1585	595.17	313.07	$C_{27}H_{30}O_{15}$	$[M+H]^+$	Isosaponarin	1				0.48	−1.05	Down
113	594.1585	595.17	433.11	$C_{27}H_{30}O_{15}$	$[M+H]^+$	Saponarin*	1				0.46	−1.13	Down
114	594.1585	595.17	433.12	$C_{27}H_{30}O_{15}$	$[M+H]^+$	Vitexin-2”-*O*-galactoside*	1				0.40	−1.33	Down
115	594.1585	595.17	271.06	$C_{27}H_{30}O_{15}$	$[M+H]^+$	Apigenin-7-*O*-Gentiobioside	3				0.44	−1.20	Down
116	594.1585	595.17	433.12	$C_{27}H_{30}O_{15}$	$[M+H]^+$	4’-*O*-Glucosylvitexin	3				0.47	−1.09	Down
117	594.1585	595.16	449.11	$C_{27}H_{30}O_{15}$	$[M+H]^+$	Orientin-2”-*O*-rhamnoside	2				0.46	−1.13	Down
118	594.1585	595.17	449.11	$C_{27}H_{30}O_{15}$	$[M+H]^+$	Luteolin-6-C-glucoside-7-*O*-rhamnoside	3				0.43	−1.22	Down
119	598.1898	599.20	431.13	$C_{27}H_{34}O_{15}$	$[M+H]^+$	Phloretin 3′,5’-Di-C-Glucoside	1	2.27	1.18	Up			
120	600.1115	601.12	287.06	$C_{28}H_{24}O_{15}$	$[M+H]^+$	Kaempferol-3-*O*-(2″-galloyl) galactoside*	1	3.73	1.90	Up			
121	600.1115	601.12	287.06	$C_{28}H_{24}O_{15}$	$[M+H]^+$	Kaempferol-3-*O*-(6″-galloyl) galactoside*	1	3.73	1.90	Up			
122	610.1528	611.16	449.11	$C_{27}H_{30}O_{16}$	$[M+H]^+$	Orientin-2”-*O*-galactoside	3				0.48	−1.07	Down

(Continued)

10.3389/fnut.2023.1234807

TABLE 1 (Continued)

No.	Molecular weight (Da)	Q1 (Da)[a]	Q3 (Da)[b]	Formula	Ionization model[c]	Compounds[d]	Level[e]	CH_FC[f]	CH_ Log_2FC[g]	CH_ Type[h]	OF_FC [f]	OF_ Log_2FC[g]	OF_ Type[h]
123	614.0908	615.10	153.02	$C_{28}H_{22}O_{16}$	$[M+H]^+$	Kaempferol-3-*O*-(2”-*O*-galloyl) glucuronide	3	2.65	1.41	Up	2.33	1.22	Up
124	624.1690	625.18	317.06	$C_{28}H_{32}O_{16}$	$[M+H]^+$	6-C-Methylquercetin-3-*O*-rutinoside	3	0.50	−1.00	Down	0.49	−1.02	Down
125	624.1690	625.17	301.07	$C_{28}H_{32}O_{16}$	$[M+H]^+$	Chrysoeriol-5,7-di-*O*-glucoside	3				0.42	−1.24	Down
126	624.1690	625.18	317.07	$C_{28}H_{32}O_{16}$	$[M+H]^+$	Isorhamnetin-3-*O*-glucoside-7-*O*-rhamnoside	3				0.46	−1.12	Down
127	624.1690	625.18	487.12	$C_{28}H_{32}O_{16}$	$[M+H]^+$	Chrysoeriol-6,8-di-C-glucoside	3				0.00	−14.14	Down
128	626.1483	627.16	303.05	$C_{27}H_{30}O_{17}$	$[M+H]^+$	6-Hydroxykaempferol-6,7-*O*-Diglucoside*	2	2.43	1.28	Up			
129	626.1847	627.19	465.10	$C_{28}H_{34}O_{16}$	$[M+H]^+$	Hesperetin-8-C-glucoside-3’-*O*-glucoside	3	37838.48	15.21	Up	34878.58	15.09	Up
130	626.1847	627.19	465.20	$C_{28}H_{34}O_{16}$	$[M+H]^+$	Hesperetin-6-C-glucoside-7-*O*-glucoside	3	2.26	1.17	Up			
131	740.2164	741.22	287.06	$C_{33}H_{40}O_{19}$	$[M+H]^+$	Kaempferol-3-*O*-rutinoside-7-*O*-rhamnoside	2	0.00	−14.38	Down			
132	756.2113	757.22	577.20	$C_{33}H_{40}O_{20}$	$[M+H]^+$	Apigenin-6,8-di-C-glucoside-4’-*O*-glucoside	3	0.50	−1.01	Down			
133	772.2062	773.21	303.05	$C_{33}H_{40}O_{21}$	$[M+H]^+$	Quercetin-3-*O*-sophoroside-7-*O*-rhamnoside	3	0.44	−1.20	Down			
134	786.2007	787.21	339.11	$C_{37}H_{38}O_{19}$	$[M+H]^+$	Kaempferol-3-*O*-(6”-Feruloyl) glucosyl-(1 → 4)-galactoside	3	0.35	−1.50	Down	0.30	−1.73	Down
135	802.1956	803.20	339.11	$C_{37}H_{38}O_{20}$	$[M+H]^+$	Quercetin-3-*O*-(2‴-*O*-feruloyl) sophoroside	3	0.39	−1.36	Down			
136	902.2481	903.26	147.04	$C_{42}H_{46}O_{22}$	$[M+H]^+$	Vitexin-2”-*O*-(6‴-p-coumaroyl) glucoside-4’-*O*-glucoside	2	2.95	1.56	Up	4.29	2.10	Up
Lipids (33)													
137	276.2089	277.22	93.07	$C_{18}H_{28}O_2$	$[M+H]^+$	14,15-Dehydrocrepenynic acid	3				2.56	1.36	Up
138	336.2664	337.27	263.24	$C_{21}H_{36}O_3$	$[M+H]^+$	(Oxiran-2-yl) methyl octadeca-9,12-dienoate	1				0.34	−1.57	Down
139	338.2457	339.25	121.10	$C_{20}H_{34}O_4$	$[M+H]^+$	5,6-DiHETrE [(±)5,6-dihydroxy-8Z,11Z,14Z-eicosatrienoic acid]	3				0.48	−1.05	Down

(Continued)

10.3389/fnut.2023.1234807

TABLE 1 (Continued)

No.	Molecular weight (Da)	Q1 (Da)[a]	Q3 (Da)[b]	Formula	Ionization model[c]	Compounds[d]	Level[e]	CH_FC[f]	CH_ Log_2FC[g]	CH_ Type[h]	OF_FC [f]	OF_ Log_2FC[g]	OF_ Type[h]
140	356.2927	357.30	265.25	$C_{21}H_{40}O_4$	$[M+H]^+$	1-Oleoyl-Sn-Glycerol	1				0.41	−1.28	Down
141	447.2386	448.25	307.23	$C_{21}H_{38}NO_7P$	$[M+H]^+$	LysoPE 16:3	3				0.39	−1.37	Down
142	465.2855	466.29	325.27	$C_{22}H_{44}NO_7P$	$[M+H]^+$	LysoPE 17:1*	3				0.39	−1.36	Down
143	475.2699	476.28	335.26	$C_{23}H_{42}NO_7P$	$[M+H]^+$	LysoPE 18:3	1				0.43	−1.22	Down
144	475.2699	476.28	335.26	$C_{23}H_{42}NO_7P$	$[M+H]^+$	LysoPE 18:3(2n isomer)	1				0.37	−1.44	Down
145	477.2855	478.29	337.27	$C_{23}H_{44}NO_7P$	$[M+H]^+$	LysoPE 18:2	2				0.35	−1.52	Down
146	477.2855	478.29	337.27	$C_{23}H_{44}NO_7P$	$[M+H]^+$	LysoPE 18:2(2n isomer)	2				0.36	−1.48	Down
147	479.3012	480.31	339.29	$C_{23}H_{46}NO_7P$	$[M+H]^+$	LysoPE 18:1*	3				0.46	−1.13	Down
148	479.3012	480.31	339.29	$C_{23}H_{46}NO_7P$	$[M+H]^+$	LysoPE 18:1(2n isomer) *	3				0.46	−1.11	Down
149	481.3168	482.32	341.31	$C_{23}H_{48}NO_7P$	$[M+H]^+$	LysoPE 18:0(2n isomer)	3				0.43	−1.22	Down
150	482.2624	481.26	253.22	$C_{22}H_{43}O_9P$	$[M-H]^-$	LysoPG 16:1	3				0.19	−2.39	Down
151	493.3168	494.32	184.07	$C_{24}H_{48}NO_7P$	$[M+H]^+$	LysoPC 16:1(2n isomer) *	1				0.50	−1.01	Down
152	505.3168	504.31	279.23	$C_{25}H_{48}NO_7P$	$[M-H]^-$	1-Linoleoyl-2-Lysophosphatidic Acid Monobutylamine Ester	1				0.41	−1.28	Down
153	516.3298	515.32	279.23	$C_{27}H_{48}O_9$	$[M-H]^-$	1-*O*-Linoleoyl-3-*O*-galactopyranosyl-L-glycerol	1				0.23	−2.13	Down
154	517.3168	518.32	184.07	$C_{26}H_{48}NO_7P$	$[M+H]^+$	LysoPC 18:3	2				0.41	−1.27	Down
155	519.3325	520.34	184.07	$C_{26}H_{50}NO_7P$	$[M+H]^+$	LysoPC 18:2(2n isomer)	2				0.39	−1.37	Down
156	521.3481	522.36	184.07	$C_{26}H_{52}NO_7P$	$[M+H]^+$	LysoPC 18:1*	1				0.38	−1.39	Down
157	521.3481	522.36	184.07	$C_{26}H_{52}NO_7P$	$[M+H]^+$	LysoPC 18:1(2n isomer) *	1				0.40	−1.33	Down
158	533.3481	534.36	184.07	$C_{27}H_{52}NO_7P$	$[M+H]^+$	LysoPC 19:2(2n isomer)	2				0.15	−2.69	Down
159	553.3380	552.33	253.22	$C_{26}H_{52}NO_9P$	$[M-H]^-$	2-(2,3-dihydroxypropoxy)-3-(((2-(dimethylamino) ethoxy) (hydroxy) phosphoryl)oxy)propan-2-yl (E)-hexadec-9-enoate	2				0.48	−1.05	Down
160	577.3380	576.33	277.22	$C_{28}H_{52}NO_9P$	$[M-H]^-$	2-(2,3-dihydroxypropoxy)-3-(((2-(dimethylamino) ethoxy) (hydroxy) phosphoryl) oxy) propyl (8E,11Z,14Z)-octadeca-8,11,14-trienoate	1				0.41	−1.30	Down

(Continued)

10.3389/fnut.2023.1234807

TABLE 1 (Continued)

No.	Molecular weight (Da)	Q1 (Da)[a]	Q3 (Da)[b]	Formula	Ionization model[c]	Compounds[d]	Level[e]	CH_FC[f]	CH_ Log_2FC[g]	CH_ Type[h]	OF_FC [f]	OF_ Log_2FC[g]	OF_ Type[h]
161	581.3693	580.36	281.25	$C_{28}H_{56}NO_9P$	$[M-H]^-$	1-(2,3-dihydroxypropoxy)-3-(((2-(dimethylamino) ethoxy) (hydroxy) phosphoryl) oxy) propan-2-yl (Z)-14-Octadecenoic Acid	1				0.48	−1.06	Down
162	581.3693	580.36	281.25	$C_{28}H_{56}NO_9P$	$[M-H]^-$	2-(2,3-dihydroxypropoxy)-3-(((2-(dimethylamino) ethoxy) (hydroxy) phosphoryl) oxy) propan-2-yl (Z)-14-Octadecenoic Acid	1				0.47	−1.10	Down
163	654.3827	653.38	397.14	$C_{31}H_{58}O_{14}$	$[M-H]^-$	1-Palmitoyl-Sn-Glycerol 3-*O*-Diglucoside	2				0.46	−1.12	Down
164	654.3827	653.38	397.14	$C_{31}H_{58}O_{14}$	$[M-H]^-$	2-Palmitoyl-Sn-Glycerol 3-*O*-Diglucoside	2				0.42	−1.26	Down
165	676.3670	677.37	261.22	$C_{33}H_{56}O_{14}$	$[M+H]^+$	1-α-Linolenoyl-glycerol-2,3-di-*O*-glucoside	2				0.29	−1.77	Down
166	676.3670	677.37	261.22	$C_{33}H_{56}O_{14}$	$[M+H]^+$	2-α-Linolenoyl-glycerol-1,3-di-*O*-glucoside	1				0.26	−1.95	Down
167	676.3670	675.36	397.14	$C_{33}H_{56}O_{14}$	$[M-H]^-$	Gingerglycolipid A	3				0.29	−1.81	Down
168	678.3827	677.38	397.13	$C_{33}H_{58}O_{14}$	$[M-H]^-$	Gingerglycolipid B	3				0.18	−2.48	Down
169	680.3983	679.39	397.13	$C_{33}H_{60}O_{14}$	$[M-H]^-$	Gingerglycolipid C	3	2.40	1.27	Up			

[a]Molecular weight of the parent ion of the substance after ionization by the electrospray ion source.
[b]Characteristic fragment ions.
[c]Ionization mode (M + H is positively charged, M-H is negatively charged).
[d]An * indicates the possible presence of isomers.
[e]Metabolite identification criteriawhere 1 indicates a score of 0.7 or higher for the sample substance secondary mass spectrum (all fragment daughter ions of the substance), RT and database substance match; 2indicates a score of 0.5–0.7 for the sample substance secondary mass spectrum (all fragment daughter ions of the substance), RT and database substance match; 3: sample substance Q1, Q3, RT, DP, CE and database substance match.
[f]CH_FC and OF_FC indicate the fold change of CK vs FC and CK vs OF metabolites, respectively.
[g]Fold change were logarithmic with a base of 2.
[h]Metabolite up-and down-regulation type.

10.3389/fnut.2023.1234807

dihydrokaempferol-7-*O*-glucoside, and hesperetin-8-C-glucoside-3'-*O*-glucoside in CH were increased, with FC levels of 465047.40, 69747.14, 59587.87, and 37838.48, respectively. Forsythoside H, a caffeoyl phenylethanoid glycoside (CPG) isolated from Forsythia suspense (Thunb.) Vahl, was a type of forsythoside and might possess anti-inflammatory activity. Alpha-asarone was a polyphenol with anti-bacterial and anti-inflammatory activities. It was worth noting that the level of dihydrokaempferol-7-*O*-glucoside was reported to reduce during the withering process of CK (17), which was inconsistent with our results. It suggested that reactions during different stages of black tea processing were not the same. On the contrary, the relative abundances of three substances, including kaempferol-3-*O*-glucorhamnoside, 5,6,3′,4′-tetrahydroxy-3,7-dimethoxyflavone-6-*O*-glucoside, and limocitrin 3-glucoside, decreased significantly and the metabolites were significantly down-regulated compared to CK. Limocitrin 3-glucoside, as a flavonoid, which was previously detected in hickory seeds (27). In OF, the relative abundances of 2-[4-(3-Hydroxypropyl)-2-methoxyphenoxy]-1,3-propanediol 1-glucoside, alpha-asarone, dihydrokaempferol-7-*O*-glucoside, and hesperetin-8-C-glucoside-3'-*O*-glucoside were significantly increased compared to CK and the FC values ranged from 34878.58 to 267109.16. Among them, the latter three substances were common to both scented teas.

In summary, flavonoids and phenolic acids were key differential non-volatile metabolites between unscented and scented black teas. The relative abundances of dihydrokaempferol-7-*O*-glucoside, hesperetin-8-C-glucoside-3'-*O*-glucoside, and alpha-asarone significantly increased in scented teas (CH & OF). There was a significant decrease in kaempferol-3-*O*-glucorhamnoside, 5,6,3′,4′-tetrahydroxy-3,7-dimethoxyflavone-6-*O*-glucoside, and limocitrin 3-glucoside in CH, while the relative abundance of 2-[4-(3-Hydroxypropyl)-2-methoxyphenoxy]-1,3-propanediol 1-glucoside was significantly increased in OF. This result was in general concordance with the results of KEGG metabolic pathways analysis (Figures 2H,I).

3.4. Analysis of key differential volatile metabolites among the three black teas

3.4.1. Analysis of key differential categories

Based on the percentage of metabolite categories, all volatile metabolites were further screened and 110 metabolites with aroma contribution were selected, including 11 alcohols, 9 ketones, 29 esters, 31 terpenoids, 14 heterocyclic compounds, 4 aldehydes, 5 aromatics, 3 acids, 3 nitrogen compounds, and 1 phenol (Table 2). It was consistent with a previous study which revealed that terpenoids were the most important aroma components in CK (28). The sum of relative abundances of esters, terpenoids, heterocyclic compounds, alcohols, ketones and aromatics was 97.08% in CK. Compared to CK, the relative abundances of heterocyclic compounds and alcohols in CH decreased by 19.62 and 11.49%, respectively, while aromatics increased by 21.23%. In OF, the relative abundances of heterocyclic compounds and esters increased by 17.21 and 13.59%, respectively, while the relative abundances of terpenoids and ketones showed a decreasing trend, reaching 14.87 and 10.31%, respectively (Supplementary Table S2). A previous study found a significant increase in both ketones and esters during the scenting of *Osmanthus* black tea (14), which was not consistent with the results of this study and may be influenced by the variety of tea leaves, tea processing parameters and scenting process.

Overall, compared to CK, the sum of key volatile metabolites was significantly up-regulated (Log2FC = 187.05) in CH and down-regulated (Log2FC = −77.28) in OF. In particular, esters, terpenoids, heterocyclic compounds, aldehydes, acids, nitrogen compounds were down-regulated, while alcohols, ketones, aromatics and phenols were up-regulated.

3.4.2. Analysis of key differential compounds

Based on the magnitude of Log2FC in each comparison group (CK vs. CH, CK vs. OF), the top 20 substances in the key volatile differential metabolites were selected preferentially and their FCs were shown in Figures 4A,B. It was found that the selected metabolites were significantly up-regulated in CH compared to CK, while those in OF were significantly down-regulated. Based on |Log2FC| > 6, six and five substances were screened as key differential compounds in CH (Figure 4C) and OF (Figure 4D), respectively.

Among them, the terpenoids and ester accounted for a greater number, with six and three varieties, respectively. Acids and heterocyclic compounds each accounted for one. Combined with the relevant information in Table 2, the relative abundances of cis-beta-farnesene, bornyl butyrate, gamma-decalactone, d-nerolidol, gamma-selinene, and trans-alpha-bergamotene were significantly increased in CH (compared to CK) and FC values reached 51533.83, 4183.31, 400.92, 116.77, 64.68, 64.57, respectively. The cis-beta-farnesene and trans-alpha-bergamotene were significantly associated with floral aroma (28, 29). Trans-alpha-bergamotene was a citrus odorant which was considered to be the most important sesquiterpene in the characteristic odour of *Polygonum minus* (30). Bornyl butyrate, which presented an herbaceous aroma (31), usually presented in the *Aloysia triphylla* and *Aloysia citrodora*.[4] Gamma-decalactone, which delivered a pleasant peachy aroma, was regarded as one of the characteristic components contributing to the *Osmanthus* aroma of *Osmanthus* black tea (14). Nerolidol was considered to be one of the skeleton aroma components of CK (32). The decrease of nerolidol after scenting might be related to the drying process, as it was previously reported that there was a significant positive correlation between the content of nerolidol and the degree of roasting (33). Gamma-selinene, as a sesquiterpene with floral aroma, was detected in the essential oils from *Chloranthus spicatus* flowers (34).

Nevertheless, in OF, sabinene, neryl isobutyrate, 2-methyl-2-pentenoic acid, beta-ionone epoxide, and coumarin were significantly down-regulated (FC ≤ 0.01). Sabinene, a representative of the bicyclic monoterpenes, conveyed a typical citrus note (35). Beta-ionone epoxide (sweet berry aroma), an apo carotenoid monoterpenoid, was found decreased in summer green tea (*Camellia sinensis L.*) after

4 https://lotus.naturalproducts.net/

10.3389/fnut.2023.1234807

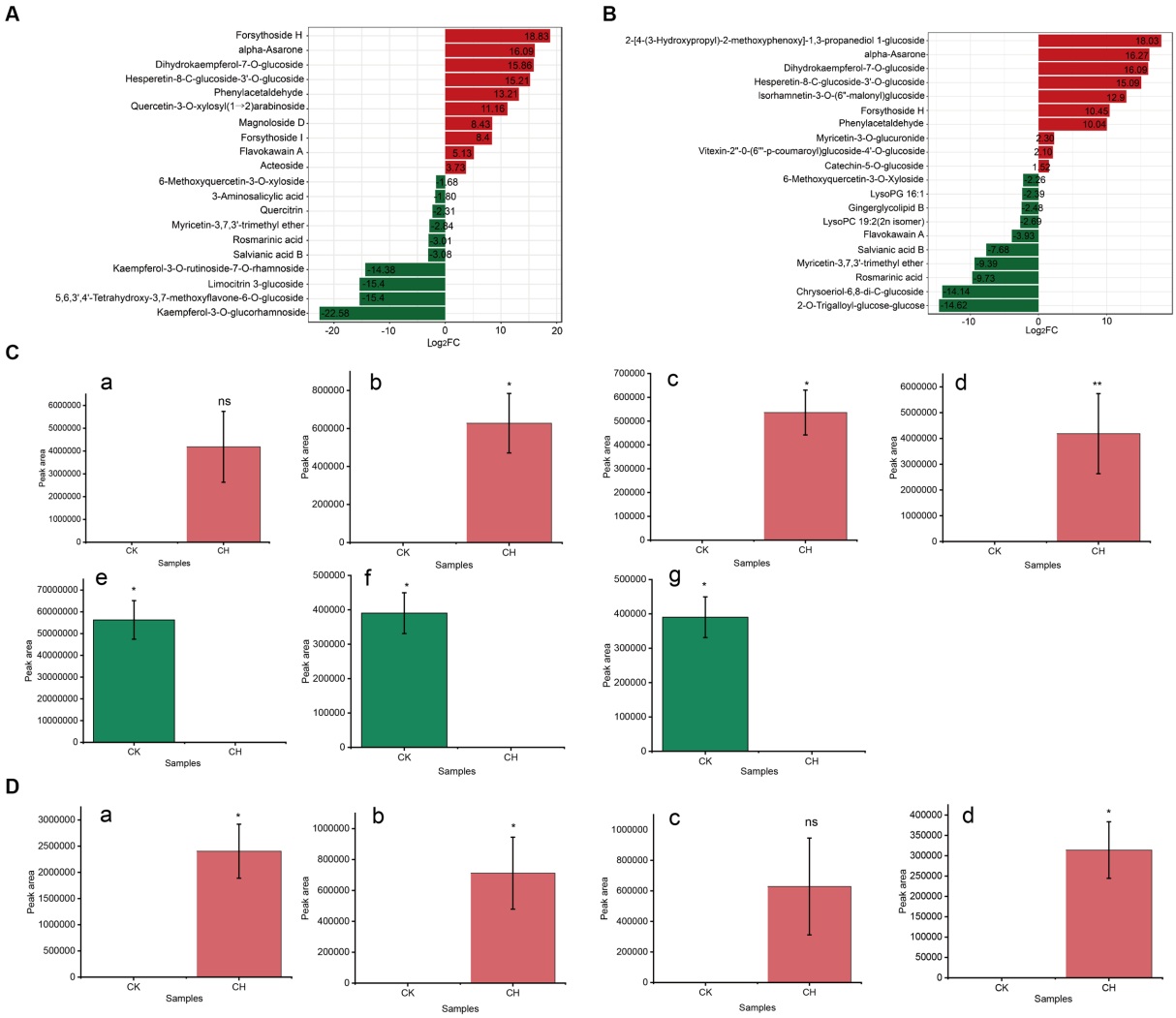

FIGURE 3
Analysis of key differential non-volatile metabolites in three types of black tea (CK, CH and OF). **(A,B)** Bar charts of the multiplicity of differences between different comparison groups (A. CK vs. CH, B. CK vs. OF); **(C,D)** Abundance histograms of key metabolites (|Log2FC| > 15, C. CK vs. CH; D. CK vs. OF). C-a, Forsythoside H; C-b, alpha-Asarone; C-c, Dihydrokaempferol-7-O-glucoside; C-d, Hes-peretin-8-C-glucoside-3'-O-glucoside; C-e, Kaempferol-3-O-glucorhamnoside; C-f, 5,6,3',4'-Tetrahydroxy-3,7-dimethoxyflavone-6-O-glucoside; C-g, Limocitrin 3-Glucoside; D-a, 2-[4-(3-Hydroxypropyl)-2-methoxyphenoxy]-1,3-propanediol 1-glucoside; D-b, alpha-Asarone; D-c, Dihydrokaempferol-7-O-glucoside; D-d, Hesperetin-8-C-glucoside-3'-O-glucoside. * Indicated a significant difference between treated samples at the 0.05 level; ** indicated a significant difference at the 0.01 level and 'ns' indicated a non-significant difference.

yellowing (36) and steamed green tea after baking (37), which was consistent with the results of this study. Neryl isobutyrate rendered a sweet rose scent and 2-methyl-2-pentenoic acid offered a fruity note (31). Chen (38) and Su et al. (32) both revealed that coumarin was one of the key substances in the formation of the typical aroma of special grade *Keemun* black tea. The coumarin was described as a sweet grass and cherry blossom-like aroma, which was formed by intramolecular esterification of hydroxycinnamic acid following hydrolysis of 2-coumaric acid primeveroside (18). The reduction of coumarin in OF might be related to the drying process (39).

In conclusion, terpenes, including monoterpenes and sesquiterpenes, were the main differential category. The increase of cis-beta-farnesene and bornyl butyrate might contribute to an increased in floral, fruity and herbaceous aromas in CH. The decrease of sabinene and neryl isobutyrate might be related to the insignificant sweet fruity aroma in OF. The result was generally consistent with the results of KEGG metabolic pathways analysis (Figures 2H,I). As such, potential differential metabolites between the CK vs. CH and CK vs. OF comparator groups were characterized in scented teas with CK as the tea raw material.

4. Conclusion

The full-spectrum metabolomics (UPLC-MS/MS and GC–MS) adopted in this study permits a more comprehensive and objective characterization of the differences in non-volatile and volatile flavor metabolites among unscented and scented Congou

TABLE 2 Key differential volatile metabolites changes among the three black teas.

RI[a]	Quan. Ion[b]	Qual. Ion[c]	Compounds	Odor[d]	CH_FC[e]	CH_ Log_2FC[f]	CH_ Type[g]	OF_ FC[e]	OF_ Log_2FC[f]	OF_ Type[g]
Alcohols (11)										
766	42	55	1-Pentanol	Plastic, moderately strong, green, fusel oil-like	0.32	−1.66	Down			
851	98	41	Furfuryl alcohol	Alcoholic, chemical, musty, sweet, caramel, bread, coffee				2.10	1.07	Up
862	57	41	(E)-2-Hexen-1-ol	Fresh, green, leafy, fruity, unripe banana				2.01	1.01	Up
970	70	56	1-Heptanol	Grassy	0.26	−1.97	Down			
1,004	79	77	(E, E)-2,4-Heptadien-1-ol	Green, fruity, nutty, cheese				2.06	1.04	Up
1,030	57	41	2-Ethyl-1-hexanol	Citrus, fresh, floral, oily, sweet	2.49	1.32	Up			
1,143	55	41	(E)-3-Nonen-1-ol	Green, waxy, melon, cucumber	2.11	1.08	Up			
1,371	55	69	1-Undecanol	Fresh, waxy, rose, soapy, clean, clothes, floral, citrus				2.20	1.14	Up
1,378	41	55	2-Butyl-2-octenal	Aldehydic, green, watery, fruity, metallic, oily, tropical, fatty, sweaty, goaty	0.42	−1.27	Down			
1,382	91	73	3-Methyl-1-phenyl-3-pentanol	Sweet, fresh, cayloxol, lilac, anisic, earthy, narcissus, peony	6.04	2.59	Up			
1,474	55	69	1-Dodecanol	Earthy, soapy, waxy, fatty, honey, coconut	3.91	1.97	Up	0.16	−2.65	Down
Ketones (9)										
745	100	71	2-Methyl-3-pentanone	Mint	0.28	−1.84	Down			
798	83	55	4-Methyl-3-penten-2-one	Pungent, earthy, vegetable, acrylic	0.43	−1.22	Down			
881	55	70	1-Hepten-3-one	Metallic				3.16	1.66	Up

(Continued)

TABLE 2 (Continued)

RI[a]	Quan. Ion[b]	Qual. Ion[c]	Compounds	Odor[d]	CH_FC[e]	CH_ Log_2FC[f]	CH_ Type[g]	OF_ FC[e]	OF_ Log_2FC[f]	OF_ Type[g]
895	58	71	2-Heptanone	Fruity, spicy, sweet, herbal, coconut, woody	0.34	−1.55	Down			
972	69	41	5-Methyl-(E)-2-hepten-4-one	Hazelnut, nutty	0.24	−2.04	Down			
1,035	111	55	(E)-3-Octen-2-one	Herbaceous, mushroom	0.46	−1.13	Down			
1,374	105	77	1-Phenyl-1-pentanone	Balsam, valerian				0.46	−1.13	Down
1,433	121	161	Dihydro-beta-ionone	Earthy, woody, mahogany, orris, dry, amber	45.10	5.50	Up			
1,513	135	77	1-(4-methoxyphenyl)-1-propanone	Musty, anisic	7.17	2.84	Up			
Esters (29)										
876	70	55	3-Methyl-1-butanol acetate	Sweet, fruity, banana, green, ripe				2.60	1.38	Up
910	70	61	Acetic acid pentyl ester	Fruity, ba	0.37	−1.44	Down	2.18	1.12	Up
925	74	87	Hexanoic acid methyl ester	Ethereal, fruity, pineapple, apricot, strawberry, tropical, fruit, banana, bacon	0.30	−1.73	Down			
1,009	82	67	(Z)-acetate 3-Hexen-1-ol	Fresh, green, sweet, fruity, banana, apple, grassy				2.04	1.03	Up
1,107	70	85	3-Methyl-butanoic acid 2-methylbutyl ester	Herbal, fruity, earthy, cheese, apple, green	7.50	2.91	Up			
1,129	70	43	Acetic acid 2-ethylhexyl ester	Earthy, herbal, humus, undergrowth				2.92	1.55	Up
1,136	83	55	Cyclohexanecarboxylic acid ethyl ester	Fruity, cheese, winey	2.02	1.01	Up			
1,236	103	57	2-Methyl-butanoic acid hexyl ester	Green, waxy, fruity, apple, spicy, tropical				2.02	1.01	Up
1,299	91	108	2-Methyl-propanoic acid phenylmethyl ester	Jasmin, oily, fruity, sweet, rose, tropical	2.01	1.01	Up	2.08	1.06	Up
1,301	69	41	Geranyl formate	Fresh, rose, neroli, tea, rose, green				2.40	1.27	Up

(Continued)

TABLE 2 (Continued)

RI[a]	Quan. Ion[b]	Qual. Ion[c]	Compounds	Odor[d]	CH_FC[e]	CH_ Log_2FC[f]	CH_ Type[g]	OF_ FC[e]	OF_ Log_2FC[f]	OF_ Type[g]
1,347	108	91	Butanoic acid phenylmethyl ester	Fresh, fruity, jasmin, apricot, loganberry	3.40	1.77	Up			
1,379	131	103	(E)-3-Phenyl-2-propenoic acid methyl ester	Sweet, balsam, strawberry, cherry				0.12	−3.07	Down
1,393	91	136	Benzeneacetic acid 2-methylpropyl ester	Sweet, floral, honey, chocolate, amber	5.95	2.57	Up			
1,404	164	132	2-(Dimethylamino)-benzoic acid methyl ester	Fruity, orange, leaf, petitgrain				2.25	1.17	Up
1,408	165	105	2-(Methylamino)-Benzoic acid methyl ester	Fruity, musty, sweet, neroli, powdery, phenolic, wine				2.05	1.03	Up
1,435	95	55	Cyclohexanepropanoic acid 2-propenyl ester	Sweet, pineapple, tropical, fruity, candy, waxy	30.783	4.944	Up			
1,444	104	105	beta-Phenylethyl butyrate	Musty, sweet, floral, yeast, strawberry	2.005	1.004	Up			
1,463	131	103	(E)-3-Phenyl-2-propenoic acid ethyl ester	Floral, honey, balsamic				0.34	−1.55	Down
1,464	129	100	Diisopropyl adipate	Mild, estery, fatty, sour				0.42	−1.26	Down
1,466	91	119	Myrtenyl isobutyrate	Fruity, woody, pine	0.336	−1.572	Down	0.09	−3.46	Down
1,471	85	29	gamma-Decalactone	Fresh, oily, waxy, peach, coconut, buttery, sweet	400.922	8.647	Up			
1,475	69	93	Neryl isobutyrate	Sweet, fresh, fruity, raspberry, strawberry, green				0.00	−13.07	Down
1,476	71	95	Bornyl butyrate	Herbal, woody	4183.310	12.030	Up			
1,488	115	71	2-Phenoxyethyl isobutyrate	Green, fruity, waxy, apple, nuances	10.170	3.346	Up			
1,491	191	131	4-(1,1-dimethylethyl)-benzeneacetic acid methyl ester	Dairy, buttermilk, leafy, creamy, green, waxy, fatty, hyacinth, melon, rind, rubbery	47.075	5.557	Up			

(Continued)

TABLE 2 (Continued)

RI[a]	Quan. Ion[b]	Qual. Ion[c]	Compounds	Odor[d]	CH_FC[e]	CH_ Log_2FC[f]	CH_ Type[g]	OF_ FC[e]	OF_ Log_2FC[f]	OF_ Type[g]
1,514	69	68	Geranyl isobutyrate	Sweet, floral, fruity, green, peach, apricot, rose	10.971	3.456	Up	0.41	−1.30	Down
1,546	56	57	n-Capric acid isobutyl ester	Oily, sweet, brandy, apricot, fermented, cognac	35.991	5.170	Up			
1,656	83	82	Methyl dihydrojasmonate	Floral, oily, jasmin, green, lactonic, tropical, natural	7.996	2.999	Up	0.09	−3.41	Down
1926	74	87	Hexadecanoic acid methyl ester	Oily, waxy, fatty, orris				0.46	−1.12	Down
Terpenoids (31)										
937	93	91	alpha-Pinene	Fresh, camphor, sweet, pine, earthy, woody	5.137	2.361	Up	0.22	−2.19	Down
972	93	91	Sabinene	Woody, terpene, citrus, pine, spice	8.945	3.161	Up	0.00	−14.55	Down
1,138	108	67	trans-Limonene oxide	Fresh, citrus				0.46	−1.11	Down
1,212	81	67	Pulegone	Minty	21.364	4.417	Up			
1,285	95	93	Bornyl acetate	Woody, pine, herbal, cedar, spice				2.21	1.14	Up
1,306	136	121	Dihydrocarvyl acetate	Floral, rose, cuminseed, sweet, minty				2.29	1.19	Up
1,355	69	41	Geranic acid	Green	2.757	1.463	Up			
1,376	161	119	Copaene	Woody, spicy, honey	6.841	2.774	Up			
1,384	81	80	(−)-beta-Bourbonene	Herbal, woody, floral, balsamic	2.407	1.267	Up			
1,406	41	93	Isocaryophyllene	Woody, spicy				2.36	1.24	Up
1,422	121	93	Ionone	Violet, sweet, floral, woody	11.222	3.488	Up	3.33	1.74	Up
1,435	119	93	trans-alpha-Bergamotene	Woody, warm, tea	64.573	6.013	Up			
1,444	41	69	cis-beta-Farnesene	CItrus, green	51533.833	15.653	Up			
1,457	41	69	(E)-beta-Famesene	Woody, citrus, herbal, sweet	2.462	1.300	Up			
1,473	161	81	(+)-gamma-Gurjunene	Musty	0.302	−1.729	Down	0.04	−4.78	Down

(Continued)

TABLE 2 (Continued)

RI[a]	Quan. Ion[b]	Qual. Ion[c]	Compounds	Odor[d]	CH_FC[e]	CH_ Log_2FC[f]	CH_ Type[g]	OF_ FC[e]	OF_ Log_2FC[f]	OF_ Type[g]
1,473	123	41	beta-Ionone epoxide	Fruity, sweet, berry, woody, violet, orris, powdery	2.719	1.443	Up	0.00	−10.16	Down
1,479	189	133	gamma-Selinene	Woody	64.683	6.015	Up			
1,483	119	132	alpha-curcumene	Herbal	8.013	3.002	Up			
1,486	41	105	β-selinene	Herbal	8.151	3.027	Up			
1,490	161	105	beta-Guaiene	Sweet, woody, dry, guaiacwood, spicy, powdery	9.407	3.234	Up			
1,495	119	93	Zingiberene	Spice, fresh, sharp	5.804	2.537	Up	0.31	−1.69	Down
1,495	121	93	(+)-Bicyclogermacrene	Green, woody, weedy	7.295	2.867	Up	0.15	−2.71	Down
1,508	41	93	alpha-Farnesene	Citrus, herbal, lavender, bergamot, myrrh, neroli, green	15.290	3.935	Up			
1,513	161	105	gamma-Cadinene	Herbal, woody	14.136	3.821	Up	0.44	−1.17	Down
1,542	157	142	alpha-Calacorene	Woody	2.161	1.112	Up			
1,544	69	41	d-Nerolidol	Mild, floral	116.773	6.868	Up			
1,600	95	150	Cedrol	Cedarwood, woody, dry, sweet, soft	54.332	5.764	Up			
1,656	69	41	Farnesal	Floral, minty	4.910	2.296	Up	0.48	−1.06	Down
1,658	81	83	Citronellyl tiglate	Rose, fruity, floral, geranium, leafy, tea	6.324	2.661	Up	0.32	−1.62	Down
1,671	82	93	beta-Bisabolol	Citrus, floral, tangy, lemon, fresh, sweet, herbal	7.603	2.927	Up	0.11	−3.15	Down
1,695	93	55	beta-Sinensal	Orange, sweet, fresh, waxy, juicy	9.257	3.211	Up			
Heterocyclic compounds (14)										
816	93	66	2-Methyl-pyridine	Sweat				0.43	−1.23	Down
829	94	67	Methyl pyrazine	Nutty, cocoa, roasted, chocolate, peanut, green				0.49	−1.03	Down
904	110	40	Methoxy pyrazine	Sweet, nutty, cocoa	0.422	−1.245	Down	0.40	−1.31	Down
910	95	110	1-(2-Furanyl)-ethanone	Nut-like, sweet, roast	0.422	−1.245	Down			

(Continued)

TABLE 2 (Continued)

RI[a]	Quan. Ion[b]	Qual. Ion[c]	Compounds	Odor[d]	CH_FC[e]	CH_ Log_2FC[f]	CH_ Type[g]	OF_ FC[e]	OF_ Log_2FC[f]	OF_ Type[g]
966	83	55	5-Ethyl-2(5H)-furanone	Spice	0.485	−1.043	Down			
976	107	51	4-Pyridinecarboxaldehyde	Fruity	6.444	2.688	Up	0.37	−1.42	Down
1,065	81	82	2-Ethoxy-3-methylpyrazine	Hazelnut, roasted, almonds, pineapple, earthy				2.43	1.28	Up
1,081	135	136	3-Ethyl-2,5-dimethyl-pyrazine	Potato, cocoa, roasted, nutty				0.43	−1.20	Down
1,084	135	136	2-Ethyl-3,5-dimethyl-pyrazine	Burnt, almonds, roasted, nuts, coffee				0.38	−1.38	Down
1,277	97	98	2-Hexyl-thiophene	Floral, fruity, gassy, green, meaty				2.30	1.20	Up
1,282	125	168	2-Butyl-5-ethyl-thiophene	Fruity, berry, earthy				2.28	1.19	Up
1,317	122	135	2,5-Dimethyl-3-(3-methylbutyl)-pyrazine	Fruity				0.36	−1.48	Down
1,440	146	118	Coumarin	Sweet, hay, tonka, new mown hay	21.458	4.423	Up	0.01	−6.60	Down
1,501	97	68	Massoia lactone	Coconut, driedfigs	5.658	2.500	Up			
Aldehydes (4)										
1,283	79	107	alpha-Terpinen-7-al	Fatty, spicy				2.53	1.34	Up
1,430	81	41	(E, E)-2,4-Undecadienal	Oily, caramellic, spicy, citrus, buttery, baked	48.858	5.611	Up			
1,449	69	70	2,6-Dodecadien-1-al	Citrus, mandarin, orange, melon	4.100	2.036	Up			
1,468	41	70	(E)-2 Dodecenal	Citrus, metallic, mandarin, orange, waxy, aldehydic	2.016	1.012	Up	0.11	−3.25	Down
Aromatics (5)										
763	91	92	Toluene	Sweet	0.343	−1.544	Down			
1,148	138	95	1,2-Dimethoxy-benzene	Sweet, creamy, vanilla, phenolic, musty	2.385	1.254	Up	3.41	1.77	Up
1,430	112	41	Geosmin	Fresh, musty, earthy, soil	26.482	4.727	Up			

(Continued)

TABLE 2 (Continued)

RI[a]	Quan. Ion[b]	Qual. Ion[c]	Compounds	Odor[d]	CH_FC[e]	CH_ Log_2FC[f]	CH_ Type[g]	OF_ FC[e]	OF_ Log_2FC[f]	OF_ Type[g]
1,492	178	163	(E)-Methyl isoeugenol	Spicy, clove, blossom, cartion, woody	26.994	4.755	Up			
1,513	205	57	Butylated hydroxytoluene	Mild, phenolic, camphor	6.030	2.592	Up			
Acids (3)										
974	41	69	2-Methyl-2-pentenoic acid	Dry, acid, sweaty, strawberry, woody, fruity, jam	22.103	4.466	Up	0.00	−10.24	Down
1,356	91	104	Hydrocinnamic acid	Sweet, fatty, rose, musk, cinnamon	2.268	1.182	Up			
1,446	115	134	Acetic acid cinnamyl ester	Sweet, floral, spicy, balsam, cinnamon	45.323	5.502	Up			
Nitrogen compounds (3)										
1,283	121	136	p-Menthene-8-thiol	Sulfury, aromatic, grapefruit, naphthyl, resinous, woody	0.458	−1.127	Down			
1,328	182	75	Dipropyltrisulfane	Sulfurous, green, onion, garlic, tropical	0.410	−1.285	Down	0.43	−1.22	Down
1,490	97	41	Dodecanenitrile	Dry, citrus, orange, peel, metallic, spicy	5.906	2.562	Up			
Phenols (1)										
1,282	137	152	4-Ethyl-2-methoxy-phenol	Clove, candy	3.531	1.820	Up	3.84	1.94	Up

[a]Retention index of metabolites on a non-polar column.
[b]Quantitative ions.
[c]Qualitative ions.
[d]Aroma description of the substance (http://www.thegoodscentscompany.com, http://perflavory.com/, http://www.odour.org.uk, http://foodflavorlab.cn).
[e]CH_FC and OF_FC indicate the fold change of CK vs FC and CK vs OF metabolites, respectively.
[f]Fold change were logarithmic with a base of 2.
[g]Metabolite up-and down-regulation type.

black teas. The results indicated that the scenting process and the types of flowers had a significant effect on the flavor quality of Congou black tea. Flavonoids, phenolic acids and terpenoids were screened as key differential categories by PCA and PLS-DA, with most significant changes in terpenoids in different scented teas. Floral, fruity and herbaceous volatiles were significantly up-regulated in CH, whilst the sweet fruity volatiles were significantly down-regulated. This study is the first to characterize the flavor profiles of CH and OF in some detail, the results enrich the research on flavor metabolisms of scented black tea and has certain implications for the processing and quality control of scented black tea. Future research needs to broaden the range of other types of flowers and to extend this study to the other five major tea categories, so as to find the most suitable flowers for each tea category to better guide the production of scented teas.

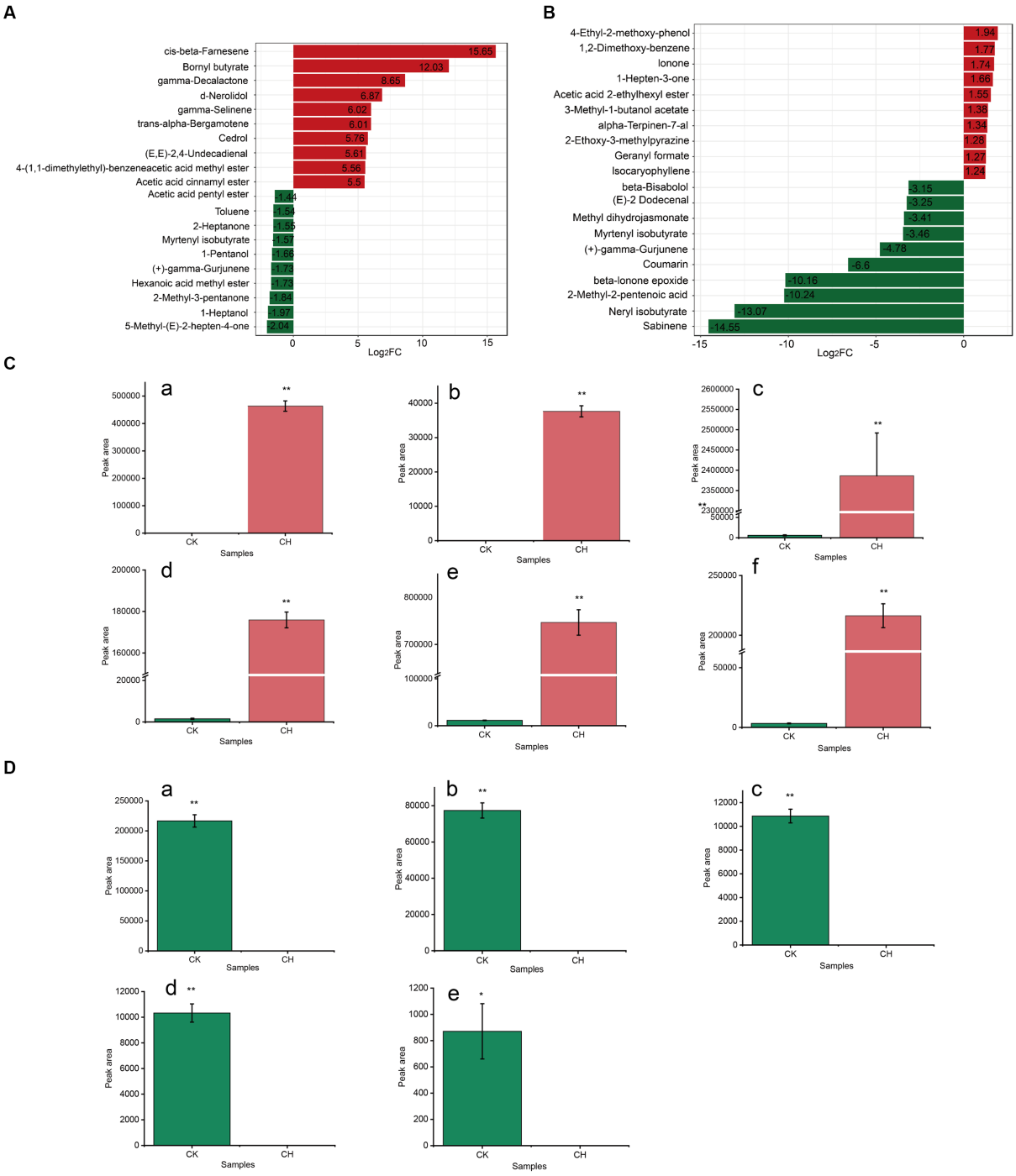

FIGURE 4
Analysis of key differential volatile metabolites in three types of black tea (CK, CH and OF). **(A,B)** Bar charts of the multiplicity of differences between different comparison groups (A. CK vs. CH, B. CK vs. OF); **(C,D)** Abundance histograms of key metabolites (|Log2FC| > 6, C. CK vs. CH; D. CK vs. OF). C-a, cis-beta-Farnesene; C-b, Bornyl butyrate; C-c, gamma-Decalactone; C-d, d-Nerolidol; C-e, gamma-Selinene; C-f, trans-alpha-Bergamotene; D-a, Sabinene; D-b, Neryl isobutyrate; D-c, 2-Methyl-2-pentenoic acid; D-d, beta-Ionone epoxide; D-e, Coumarin. * Indicated a significant difference between treated samples at the 0.05 level; ** indicated a significant difference at the 0.01 level.

Data availability statement

The original contributions presented in the study are included in the article/Supplementary material, further inquiries can be directed to the corresponding authors.

Author contributions

PT, J-QW, YG, and Y-QX: conceptualization. PT and J-QW: data curation and formal analysis and writing—review and editing. PT and Y-QX: funding acquisition. Y-FW, J-CJ, XM, and YZ: investigation. PT,

J-QW, YG, and Y-QX: methodology. Y-QX: project administration and validation. YG and Y-QX: supervision. All authors have read and agreed to the published version of the manuscript.

Funding

This work was supported by the Agricultural and Social Development General Program of Hangzhou (20201203B100), the Key Research and Development Program of Zhejiang (2022C02033), the Central Public-interest Scientific Institution Basal Research Fund (Y2023XK11), and the China Agriculture Research System of MOF and MARA (CARS-19).

Conflict of interest

Y-FW was employed by Jingdezhen Jin Gui Yuan Agricultural Development Co Ltd.

The remaining authors declare that the research was conducted in the absence of any commercial or financial relationships that could be construed as a potential conflict of interest.

Publisher's note

Supplementary material

The Supplementary material for this article can be found online at: https://www.frontiersin.org/articles/10.3389/fnut.2023.1234807/full#supplementary-material

References

1. Yi MS, Wu XT, Zhuang W, Xia L, Chen Y, Zhao R, et al. Tea consumption and health outcomes: umbrella review of meta-analyses of observational studies in humans. *Mol Nutr Food Res*. (2019) 63:e1900389. doi: 10.1002/mnfr.201900389

2. Persson IAL, Josefsson M, Persson K, Andersson RGG. Tea flavanols inhibit angiotensin-converting enzyme activity and increase nitric oxide production in human endothelial cells. *J Pharm Pharmacol*. (2010) 58:1139–44. doi: 10.1211/jpp.58.8.0016

3. Hindmarch I, Quinlan PT, Moore KL, Parkin C. The effects of black tea and other beverages on aspects of cognition and psychomotor performance. *Psychopharmacology*. (1998) 139:230–8. doi: 10.1007/s002130050709

4. Duffy SJ, Keaney Jr JF, Holbrook M, Gokce N, Swerdloff PL, Frei B, et al. Short- and long-term black tea consumption reverses endothelial dysfunction in patients with coronary artery disease. *Monograph (American Heart Association)*. (2001) 104:151–6. doi: 10.1161/01.CIR.104.2.151

5. Jiang H, Xu WD, Chen QS. Evaluating aroma quality of black tea by an olfactory visualization system: selection of feature sensor using particle swarm optimization. *Food Res Int*. (2019) 126:108605. doi: 10.1016/j.foodres.2019.108605

6. Mao SH, Lu CQ, Li MF, Ye Y, Wei X, Tong H. Identification of key aromatic compounds in congou black tea by partial least-square regression with variable importance of projection scores and gas chromatography–mass spectrometry/gas chromatography–olfactometry. *J Sci Food Agric*. (2018) 98:5278–86. doi: 10.1002/jsfa.9066

7. Liu PP, Zheng PC, Gong ZM, Ye F, Feng L, Gao SW, et al. Quality analysis and comprehensive evaluation of Chinese congou black tea. *Food Sci*. (2021) 42:195–205. doi: 10.7506/spkx1002-6630-20200611-150

8. Liu Y, Chen QC, Liu DC, Yang L, Hu W, Kuang L, et al. Multi-omics and enzyme activity analysis of flavour substances formation: major metabolic pathways alteration during congou black tea processing. *Food Chem*. (2023) 403:134263. doi: 10.1016/j.foodchem.2022.134263

9. Kang SY, Yan H, Zhu Y, Liu X, Lv HP, Zhang Y, et al. Identification and quantification of key odorants in the world's four most famous black teas. *Food Res Int*. (2023) 121:73–83. doi: 10.1016/j.foodres.2019.03.009

10. Zhang L, Ho CT, Zhou J, Santos JS, Armstrong L, Granato D. Chemistry and biological activities of processed *Camellia sinensis* teas: a comprehensive review. *Compr Rev Food Sci Food Saf*. (2019) 18:1474–95. doi: 10.1111/1541-4337.12479

11. Dai WD, Tan JF, Lu ML, Zhu Y, Li P, Peng Q, et al. Metabolomics investigation reveals that 8-C N-Ethyl-2-pyrrolidinone-substituted Flavan-3-ols are potential marker compounds of stored white teas. *J Agric Food Chem*. (2018) 66:7209–18. doi: 10.1021/acs.jafc.8b02038

12. Li HL, Chai Z, Shen GX, Li CY. Polyphenol profiles and antioxidant properties of ethanol extracts from *Osmanthus fragrans (Thunb.)* Lour Flowers. *Pol J Food Nutr Sci*. (2017) 67:317–25. doi: 10.1515/pjfns-2017-0008

13. Cai X, Mai RZ, Zou JJ, Zhang HY, Zeng XL, Zheng RR, et al. Analysis of aroma-active compounds in three sweet Osmanthus (*Osmanthus fragrans*) cultivars by GC-olfactometry and GC-MS. *J Zhejiang Univ-Sc B*. (2014) 15:638–48. doi: 10.1631/jzus.B1400058

14. Chen HM, Shi ZG, Di TM, Hu JH, Zhang ZQ, Zhang XF. The scenting technology and aroma analysis by HS-SPME/GC-O-MS for Osmanthus black tea. *Modern Food Sci Technol*. (2018) 34:243–54. doi: 10.13982/j.mfst.1673-9078.2018.11.036

15. Xia T. *Tea Science*. Beijing: China Agriculture Press (2016).

16. Chen W, Wang WS, Peng M, Gong L, Gao Y, Wan J, et al. Comparative and parallel genome-wide association studies for metabolic and agronomic traits in cereals. *Nat Commun*. (2016) 7:12767. doi: 10.1038/ncomms12767

17. Liu F, Wang Y, Corke H, Zhu H. Dynamic changes in flavonoids content during congou black tea processing. *LWT*. (2022) 170:114073. doi: 10.1016/j.lwt.2022.114073

18. Yang ZY, Baldermann S, Watanabe N. Recent studies of the volatile compounds in tea. *Food Res Int*. (2013) 53:585–99. doi: 10.1016/j.foodres.2013.02.011

19. Liao P, Hemmerlin A, Bach TJ, Chye ML. The potential of the mevalonate pathway for enhanced isoprenoid production. *Biotechnol Adv*. (2016) 34:697–713. doi: 10.1016/j.biotechadv.2016.03.005

20. Hemmerlin A, Harwood JL, Bach TJ. A raison d'être for two distinct pathways in the early steps of plant isoprenoid biosynthesis? *Prog Lipid Res*. (2012) 51:95–148. doi: 10.1016/j.plipres.2011.12.001

21. Gao Y, Wang JQ, Fu YQ, Yin JF, Shi J, Xu YQ. Chemical composition, sensory properties and bioactivities of Castanopsis lamontii buds and mature leaves. *Food Chem*. (2020) 316:126370. doi: 10.1016/j.foodchem.2020.126370

22. Fei XT, Qi YC, Lei Y, Wang S, Hu H, Wei A. Transcriptome and metabolome dynamics explain aroma differences between green and red prickly ash fruit. *Foods*. (2021) 10:391. doi: 10.3390/foods10020391

23. Deng XJ, Huang GH, Tu Q, Zhou H, Li Y, Shi H, et al. Evolution analysis of flavor-active compounds during artificial fermentation of Pu-erh tea. *Food Chem*. (2021) 357:129783. doi: 10.1016/j.foodchem.2021.129783

24. Zheng XQ, Li QS, Xiang LP, Liang YR. Recent advances in volatiles of teas. *Molecules*. (2016) 21:338. doi: 10.3390/molecules21030338

25. Bhuyan LP, Mahanta PK. Studies on fatty acid composition in tea *Camellia sinensis*. *J Sci of Food Agric*. (1989) 46:325–30. doi: 10.1002/jsfa.2740460310

26. Wan XC. *Biochemistry of tea*. Beijing: China Agricultural Press (2003).

27. Li Y, Wang JH, Wang KT, Lyu S, Ren L, Huang C, et al. Comparison analysis of widely-targeted metabolomics revealed the variation of potential astringent ingredients and their dynamic accumulation in the seed coats of both Carya cathayensis and *Carya illinoinensis*. *Food Chem*. (2022) 374:131688. doi: 10.1016/j.foodchem.2021.131688

28. Xue JJ, Guo GY, Liu PP, Chen L, Wang W, Zhang J, et al. Identification of aroma-active compounds responsible for the floral and sweet odors of congou black teas using gas chromatography-mass spectrometry/olfactometry, odor activity value, and chemometrics. *J Sci of Food Agric*. (2022) 102:5399–410. doi: 10.1002/jsfa.11893

29. Chen MJ, Guo L, Zhou HW, Guo Y, Zhang Y, Lin Z, et al. Absolute quantitative volatile measurement from fresh tea leaves and the derived teas revealed contributions of postharvest synthesis of endogenous volatiles for the aroma quality of made teas. *Appl Sci-Basel*. (2021) 11:613. doi: 10.3390/app11020613

30. Rusdi NA, Goh HH, Baharum SN. GC-MS/Olfactometric characterisation and aroma extraction dilution analysis of aroma active compounds in *Polygonum minus* essential oil. *Plant Omics*. (2016) 9:289–91. doi: 10.21475/poj.16.09.04.p7901

31. Burdock GA. *Fenarolis handbook of flavor ingredients*. 6th ed (2010).

32. Su D, He JJ, Zhou YZ, Li YL, Zhou HJ. Aroma effects of key volatile compounds in Keemun black tea at different grades: HS-SPME-GC-MS, sensory evaluation, and chemometrics. *Food Chem*. (2022) 373:131587. doi: 10.1002/ffj.3725

33. Yue CA, Li WJ, Li C, Wang Z, Peng H, Yang P. Differential characterization of volatile components and aroma sensory properties of different types of Hehong tea (congou black tea). *Flavour Frag J*. (2023) 38:61–72. doi: 10.1016/j.foodchem.2021.131587

34. Chang-heng ZHAO, Yong-xiang WU, Zhi-bing WAN, Meng-xue WU, Ya-li WANG, Tian-zhong CAO, et al. Effect of different drying methods on composition and biological activities of essential oils from Chloranthus spicatus flowers. *Nat Prod Res Dev*. (2020) 32:1030–7. doi: 10.16333/j.1001-6880.2020.6.017

35. Bordiga M. *Food aroma evolution during food processing, cooking, and aging* (2020).

36. Wei YM, Yin XC, Wu HT, Zhao M, Huang J, Zhang J, et al. Improving the flavor of summer green tea (*Camellia sinensis* L.) using the yellowing process. *Food Chem*. (2022) 388:132982. doi: 10.1016/j.foodchem.2022.132982

37. Wang JQ, Fu YQ, Chen JX, Wang F, Feng ZH, Yin JF, et al. Effects of baking treatment on the sensory quality and physicochemical properties of green tea with different processing methods. *Food Chem*. (2022) 380:132217. doi: 10.1016/j.foodchem.2022.132217

38. Chen D. *The study of flavor characteristic of premium Keemum black tea* China Agricultural University (2017). doi: 10.27628/d.cnki.gzndu.2017.000114

39. Ho CT, Zheng X, Li SM. Tea aroma formation. *Food Sci Hum Well*. (2015) 4:9–27. doi: 10.1016/j.fshw.2015.04.001

10.3389/fnut.2023.1234807

Glossary

CK	*Congou* black tea
CH	*Chloranthus spicatus* black tea
OF	*Osmanthus* black tea
UPLC-MS/MS	ultra-performance liquid chromatography tandem mass spectrometry
GC–MS	gas chromatography–mass spectrometry
ESI	electrospray ionization temperature
IS	ion spray
GSI I (II)	ion source gases I (II)
CUR	curtain gas
MRM	multiple reaction monitoring
QQQ	triple quadrupole
DP	declustering potential
CE	collision energy
MWDB	metware database
HS-SPME	headspace solid phase microextraction
DVB/CWR/PDMS	divinylbenzene/carboxen/ polydimethylsiloxane
EI	electron bombardment ion source
SIM	selected ion detection mode
RI	retention index
RT	retention time
PCA	principal component analysis
PLS-DA	partial least squares-discriminant analysis
KEGG	kyoto encyclopedia of genes and genomes
MSEA	metabolite set enrichment analysis
VIP	variable importance in the project
FC	fold change
DA	differential abundance
MVA	cytoplasmic mevalonate
IPP	isopentenyl pyrophosphates
DMAPP	dimethyl allyl pyrophosphates
CPG	caffeoyl phenylethanoid glycoside

frontiers | Frontiers in Nutrition

TYPE Original Research
PUBLISHED 24 August 2023
DOI 10.3389/fnut.2023.1232251

OPEN ACCESS

EDITED BY
Dandan Pu,
Beijing Technology and Business University, China

REVIEWED BY
Kai Wang,
South China Agricultural University, China
Malgorzata Ziarno,
Warsaw University of Life Sciences, Poland

*CORRESPONDENCE
Yong Sui
✉ suiyong0429@foxmail.com
Xin Mei
✉ liangshijiagong@126.com

RECEIVED 31 May 2023
ACCEPTED 10 August 2023
PUBLISHED 24 August 2023

CITATION
Zhou L, Sui Y, Zhu Z, Li S, Xu R, Wen J, Shi J, Cai S, Xiong T, Cai F and Mei X (2023) Effects of degree of milling on nutritional quality, functional characteristics and volatile compounds of brown rice tea.
Front. Nutr. 10:1232251.
doi: 10.3389/fnut.2023.1232251

Effects of degree of milling on nutritional quality, functional characteristics and volatile compounds of brown rice tea

Lei Zhou[1,2], Yong Sui[1]*, Zhenzhou Zhu[2], Shuyi Li[2], Rui Xu[1,2], Junren Wen[1], Jianbin Shi[1], Sha Cai[1], Tian Xiong[1], Fang Cai[1] and Xin Mei[1]*

[1]Key Laboratory of Agro-Products Cold Chain Logistics, Ministry of Agriculture and Rural Affairs, Institute of Agro-Products Processing and Nuclear-Agricultural Technology, Hubei Academy of Agricultural Science, Wuhan, China, [2]School of Modern Industry for Selenium Science and Engineering, Wuhan Polytechnic University, National R&D Center for Se-Rich Agricultural Products Processing, Hubei Engineering Research Center for Deep Processing of Green Se-rich Agricultural Products, Wuhan, China

This study investigated the effects of rice preparation using different degrees of milling (DOM) from 0% to 13% on the nutritional composition, functional properties, major volatile compounds and safety of brown rice tea (BRT). We found that 2% DOM reduced 52.33% of acrylamide and 31.88% of fluorescent AGEs. When DOM was increased from 0% to 13%, the total phenolic content (TPC) of brown rice tea decreased by 48.12%, and the total flavonoid content (TFC) and condensed tannin content (CTC) also decreased significantly, with the smallest decrease at 2% DOM. In addition, the inhibitory activities of α-amylase, α-glucosidase and pancreatic lipase as well as the antioxidant activity also decreased gradually. Analysis by electronic nose and gas chromatography-mass spectrometry (GC-MS) showed that alkanes, furans, aldehydes, pyrazines and alcohols were the major volatiles in BRT, with 2% DOM having the greatest retention of aroma compounds. An orthogonal partial least squares discriminant analysis (OPLS-DA) and VIP score (VIP > 1 and $p < 0.05$) analysis were used to screen 25 flavor substances that contributed to the differences in BRT aroma of different DOMs. These results suggest that 2% milled BRT can improve safety and palatability while maximizing the retention of flavor compounds and nutrients. The findings of this study contribute to an enhanced understanding of the dynamics of changes and preservation of aroma compounds and nutrients present during the processing of BRT.

KEYWORDS

brown rice tea, degree of milling, nutrients, aroma compounds, OPLS-DA

1. Introduction

Rice can be eaten on its own as a staple food or processed into products including cereal teas, noodles, wine, cookies, bread and condiments (1, 2). Among them, brown rice tea (BRT) is popular in East Asia because of its rich roasted flavor and probiotic effects (1). However, the edible quality of BRT made from brown rice is poor and hard in texture, which seriously affects the market value (3). DOM is a critical parameter that influences the physicochemical and organoleptic properties of rice. Previous studies have shown that higher DOM improves sensory

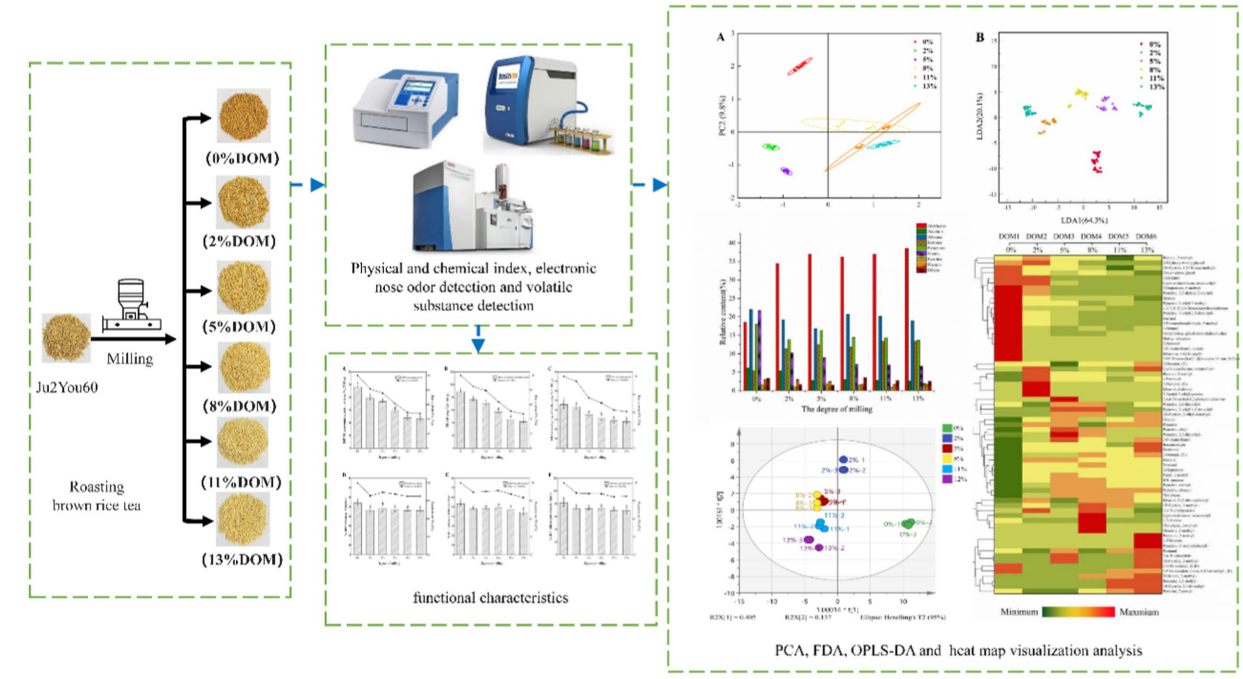

GRAPHICAL ABSTRACT

quality and consumer acceptability, but leads to a decrease in the content of key nutrients, TPC and cellular antioxidant activity values in rice (4). Current studies have concentrated on the effects of DOM on phenolic compounds, physicochemical properties and functional properties of rice, but there are no relevant studies on BRT. Also, the effect of the DOM on acrylamide (AA) and advanced glycation end products (AGEs) in BRT has not been studied.

Furthermore, different DOMs can significantly affect the volatile compounds of rice due to the different concentrations of volatile compounds produced during the milling process (5). Previous studies have shown that the total volatiles of both rice and black rice were significantly lower after milling, but moderate milling resulted in better aroma characteristics and acceptability (5, 6). However, to date, few reports have investigated the effect of processing on the dynamics and small differences in the key aroma volatiles of BRT. Therefore, further research on proper BRT milling conditions is necessary to better understand the causes of flavor substance changes in BRT. This could provide theoretical support to improve the current BRT production technology and retain the aroma compounds in BRT.

Taking into account above factors, the security, physicochemical properties, phenolic compounds content and functional characteristics of BRT with different DOMs were investigated. Additionally, the effect of milling on BRT aroma compounds was analyzed by using a combination of electronic nose and GC–MS. Finally, the OPLS-DA model was used to gain insight into the correlation between the aroma volatility spectrum and the DOM. The conclusions will help to optimize the grinding conditions for BRT processing and provide a scientific basis for balancing the flavor quality and nutritional composition of BRT during the grinding process.

2. Materials and methods

2.1. Preparation of BRT

Rice of the indica cultivar Juliangyou-60 was supplied by the Food Crops Institute, Hubei Academy of Agricultural Sciences (Hubei Province, China). The brown rice was milled for 0 s, 1 s, 3 s, 6 s, 9 s and 12 s using the SXJMJ-858 rice milling machine (Zhejiang Taizhou Huachen Grain and Oil Machinery Co. Ltd., Zhejiang, China). Six different DOMs of rice (0, 2, 5, 8, 11 and 13% DOM) were obtained by the ratio of the weight of milled rice bran to the weight of unmilled brown rice. DOM is calculated according to Eq. (1) According to Nie et al. (7), BRT is produced by three sequential steps of soaking, drying, and roasting. Brown rice was soaked in water (1,10 w/v) for 10 min at room temperature. Approximately 100 g of drained brown rice was roasted at 200°C for 35 min, cooled, and collected and stored.

$$DOM = 1 - \frac{\text{weight of milled rice}}{\text{weight of brown rice}} \times 100\% \quad (1)$$

2.2. Physicochemical characteristics

The atmospheric pressure drying method was used to determine the moisture content. AACC method 08–01 and method 86–80 were used to determine the content of ash, protein, lipid, and dietary fiber (DF) (8). The total starch content was established according to the procedure reported by Hongyan et al. (9). The content of reducing

sugars (glucose) was determined by Zhiming et al. (8), with minor modifications. The color characteristics of BRT were measured with a CS-580B spectrophotometer (CHN Spec, LTD, China). The browning index (BI) and color difference (ΔE) were calculated by the literature equations (1, 10).

2.3. Determination of acrylamide and fluorescent AGEs

Acrylamide was analyzed in triplicate according to the method of Champrasert et al. (11), with slight modifications. An HPLC system equipped with an autosampler and UV detector (Waters e2695) was used. Two micro-open samples were injected with the autosampler and separated with an Iintersustain AQ-C18 analytical column (4.6 mm x 250 mm, 5 μm). The mobile phase was 0.8 mL/min of methanol (Sigma-Aldrich) (95% water). There was a run time of 10 min and a retention time of 6.73 min for acrylamide. A range of concentrations (0.1–2 μg/mL) of acrylamide solutions were prepared using acrylamide (Sigma-Aldrich. A9099). Using Milli-Q water, test samples were diluted, filtered through Nizhny Tsuji filters (0.45 μm) (Sigma-Aldrich), and then analyzed for acrylamide.

Fluorescent AGEs were obtained using a method described by Wang et al. (12), with slight modifications. A fluorescence spectrophotometer was used to measure the fluorescence intensity of AGEs by taking 2.0 g of rice tea powder (passed through 100 mesh sieve), adding it to 50 mL of neutral phosphate buffer solution and shaking it at 37°C for 4 h to dissolve the fluorescence substance as completely as possible, then centrifuging it at 4000 r/min for 10 min, taking the supernatant and fixing it to 50 mL, then taking 3 mL of the solution and a 370 nm excitation wavelength, a 440 nm emission wavelength, and a 5 nm slit are used. A measurement of the fluorescence of phosphate buffer solution was used as 1 custom unit (AUF), and the fluorescence intensity of the sample was (AU/g).

2.4. Determination of TPC, TFC, and CTC

The extraction of bound and free polyphenols from BRT was made according to the method described by Li et al. (13). Based on these reports, to determine the phenolic content, flavonoids and condensed tannins (14, 15).

2.5. Estimation of antioxidant capacity of BRT

2.5.1. DPPH radical scavenging activity

The method for the DPPH assay was adapted from Fukui et al. (16). Briefly, 1.0 mL of rice tea extract and 2.0 mL of DPPH free radical ethanol solution (0.1 mM) were mixed well. A control was prepared by substituting 1.0 mL of aqueous methanol solution (40 mL/100 mL) for the extract. After mixing well, the mixture was left in the dark for 30 min and 517 nm absorbance measurement was conducted. Eq. (2) was used to calculate the radical scavenging activity of DPPH:

$$\text{DPPH radical scavenging activity}(\%) = (A_c - A_s) / A_c \times 100 \quad (2)$$

where, Ac = Absorbance of control at 517 nm, As = Absorbance of the sample at 517 nm.

2.5.2. Ferric reducing antioxidant power (FRAP) assay

Zhang et al. (17) reported a method for performing the FRAP assay.

2.5.3. Assay for the scavenging effect on hydroxyl (OH) radicals

The method for the OH assay was adapted from Yongxu et al. (18). Briefly, the reaction mixture contained 1.0 mL of 9 mM salicylic acid-methanol solution, 1.0 mL of 9 mM FeSO4, 1.0 mL of 8.8 mM H2O2, and 1 mL of extract for the reaction. Fill to 10 mL with vial. Distilled water. After standing for 20 min, the absorbance of the mixture was determined at 510 nm. Eq. (3) was used to calculate the OH assay:

$$\text{OH radical scavenging activity}(\%) = (A_c - A_s) / A_c \times 100 \quad (3)$$

where, Ac = Absorbance of control at 624 nm, As = Absorbance of the sample at 624 nm.

2.6. Inhibitory properties against α-amylase, α-glucosidase and pancreatic lipase

2.6.1. α-Amylase inhibition assay

The α-amylase inhibition assay was analyzed according to the method of Fatemeh et al. (19). Briefly, 0.3 mL of extract, 0.1 M sodium phosphate buffer (pH 6.8) in and 0.3 mL of α-amylase solution (1.0 U/mL) were mixed and set at 37°C for 10 min. After adding 0.3 mL of 1.0% (w/v) starch solution, it was again left to stand for 15 min., 0.5 mL of DNS was added and boiled for 8 min. After cooling, 517 nm absorbance measurement was conducted.

2.6.2. α-Glucosidase inhibition assay

The α-glucosidase inhibition assay was analyzed according to the method of Zhang et al. (17), with some modifications. Briefly, 110 μL of PBS, 20 μL of extract and 20 μL of α-glucosidase (2.5 U/mL) were mixed and allowed to stand for 10 min at 37°C. Then, 20 μL of 1.25 mM pNPG was added and allowed to stand at 37°C for 20 min. 80 μL of 0.1 M Na_2CO_3 was added, followed by determination of absorbance at 405 nm.

2.6.3. Pancreatic lipase inhibition assay

The pancreatic lipase inhibition assay was analyzed according to the method of Ruimin et al. (20). Briefly, 50 μL of extract and 50 μL of 25 U/mL pancreatic lipase were mixed and allowed to stand at 37°C for 10 min. Add 50 μL of 1.0 mg/mL of pNPB and leave at 37°C for 20 min, followed by determination of absorbance at 405 nm.

2.7. Electronic nose analysis

Using a slightly modified version of Yi et al.'s (21) method, we performed e-nose analysis, with slight modifications. About 2 g of

BRT, 10 mL of boiling water and 1.2 g of NaCl were added to a 20 mL headspace vial. After heating at 85°C for 30 min, an E-nose system (PEN3, AIRSENSE, Germany) was used. Acquisition at 50°C, 150 mL/min flow rate for 120 s and cleaning time for 120 s.

2.8. Volatile composition

With slight modifications, headspace solid-phase microextraction (HS-SPME) of the volatile components was conducted according to Yi et al. (21). Briefly, add 1 g BRT, 5 mL boiling water and 0.5 g NaCl to a 20 mL headspace vial. Stir in a water bath at 60°C for 20 min. The aged SPME fibers (DVB/CAR/PDMS fibers, Supelco Co., Bellefonte, PA, United States) were placed in the headspace of the sample vial for 30 min. The analysis of volatile aroma components was performed on an Agilent 7,890 gas chromatograph operated in combination with a 5975C triple quadrupole mass spectrometer (7890A/5975C, Agilent Technologies, Santa Clara, CA, United States). A DB-WAX capillary column (60 m × 250 μm × 0.25 μm) was used. See attached Supplementary data for parameter information.

2.9. Sensory evaluation of tea infusion

The sensory evaluation of rice tea was referenced from Hyun-Jin et al. (1) with slight modifications. Briefly, 25 g of complete BRT was boiled in 250 mL of boiling tap water for 3 min at a ratio of 1:10. The insulated tea infusion and rice grains were then separated and sensory evaluated. The sensory panel consisted of six male and six female members who were familiar with the principles and concepts of descriptive tea analysis. The evaluation included 5 aspects of aroma, flavor, color and overall acceptability/taste and was scored using a 9-point scale.

2.10. Statistical analysis

All data are averages obtained after repeating the experiment three times. Statistical analysis and graphical production of the data were performed by SPSS 26.0, Origin 2021, SIMCA-P version 14.1; and others the software was completed.

3. Results and discussion

3.1. Chromatic aberration

Color can greatly affect the quality of food and consumer acceptance (1). The color of BRT with different DOMs was presented in Table 1. There is a significant difference in the color, browning index and total color difference of BRT of different DOMs ($p < 0.05$). With the DOM of BRT increasing, the L* value increased, the a* and b* value decreased. These changes resulted in a decrease in the browning index (BI) of the BRT samples, indicating that grinding minimizes the browning of the samples. Similar patterns have been described for baked brown rice and roasted chickpeas (1, 22). Compared to BRT of milled, the 0% DOM BRT achieved maximum BI in the same baking time. This may be because 0% DOM BRT contains more free amino acids, reducing sugar and other non-enzymatic browning reaction substrate, which promoted the color reaction in the process of BRT roasting (1, 23). The color difference was relatively significant when DOM was more than 5%, suggesting that milling of brown rice significantly changes the color of BRT.

The Merad reaction produces toxic by-products such as AA and AGEs (12, 24). Notably, each milling stage resulted in a reduction of acrylamide and fluorescent AGEs content, which is not consistent with previous studies of milled chia seeds (24), AA and fluorescent AGEs are mainly formed in rice bran. Acrylamide content decreased by 52.33, 63.26, 56.60, 72.61 and 73.18%, respectively for brown rice when milled to 2, 5, 8, 11 and 13% DOM. The content of fluorescent AGEs decreased from 234.19 AU/g to 117.71 AU/g as DOM increased, with the largest decrease (31.88%) when DOM increased from 0 to 2%. This could be caused by the stripping of rice bran, which is enriched with reducing sugars, proteins and other substrates for the Merad reaction. This is consistent with the BI results.

3.2. Effect of DOM on the basic nutrients and phenolic compounds of BRT

As shown in Table 2 each grinding stage resulted in a decrease in water, lipids, protein, reducing sugars, dietary fiber and ash and an increased total starch, as previously reported (8). Dietary fiber content reduced to extent of 2.44, 2.29, 2.16, 0.70 and 0.69%, respectively for brown rice when milled to 0, 2, 5, 8 and 13% DOM. The reason for this phenomenon is that when rice is milled, the layer of rice bran containing dietary fiber is removed at the beginning (8). The reducing sugar content decreased from 0.85 to 0.67% with increasing DOM, with the greatest decrease (21.2%) when DOM increased from 0 to 2%. Reducing sugars are involved in heat-induced non-enzymatic browning reactions and their content defines the flavor, color and consumer satisfaction of baked goods (1). It is noteworthy that the moisture content decreased significantly from 2.15 to 1.20% with the increase in the DOM, which is inconsistent with the reports from the past (25). This may be due to the increase in DOM, which makes the water inside the rice more susceptible to participate in the browning reaction (26, 27). In addition, the lipid in BRT was reduced from 2.43 to 0.29%. Lipid oxidation can generate off-flavors, and this study found that milling processing significantly reduced lipids in BRT, which may inhibit the generation of off-flavors during BRT storage. The BRT without milling process contained 73.08% starch and reached a maximum starch content of 85.18% at 13% DOM, which was caused by the reduction in the proportion of other components.

Table 3 shows that polyphenols, flavonoids, and condensed tannins contained in BRT with different DOMs differ significantly ($p < 0.05$). A large proportion of the polyphenolic substances in the BRTs were in the free state, accounting for 67.2–84.76% of the TPC. 0% DOM had the greatest content of free and total phenols with 198.05 and 256.55 mg GAE/100 g. A 5% increase in DOM was observed, the TPC in BRT decreased slightly and then decreased substantially thereafter, in agreement with previous studies on the TPC of different bran fractions of black rice (17). Compared to 0% DOM, TPC decreased by 7.55, 8.54, 32.58, 45.27 and 48.12% for 2–13% DOM, respectively. Similarly, similar changes were observed in the flavonoid content of BRT. The proportion of flavonoids in the free state was the largest in the BRT of all DOMs, accounting for

TABLE 1 Variation of acrylamide, fluorescent AGEs content and color of BRT with different DOMs.

DOMs	*L**	*a**	*b**	Browning index	*ΔE*	Acrylamide(ug/kg)	Fluorescent AGEs(AU/g)
0%	72.07 ± 0.36^{d}	4.86 ± 0.04^{a}	17.60 ± 0.18^{b}	32.45 ± 0.47^{a}	–	1612.68 ± 171.56^{a}	234.19 ± 8.01^{a}
2%	75.50 ± 0.36^{c}	4.12 ± 0.11^{b}	17.35 ± 0.18^{b}	29.63 ± 0.40^{b}	3.52 ± 0.42^{c}	768.79 ± 37.93^{b}	159.54 ± 5.04^{b}
5%	75.73 ± 0.76^{c}	4.07 ± 0.12^{b}	17.56 ± 0.26^{b}	29.85 ± 0.81^{b}	3.75 ± 1.11^{c}	592.50 ± 27.43^{b}	169.46 ± 7.32^{b}
8%	77.49 ± 0.16^{b}	3.20 ± 0.07^{c}	16.49 ± 0.10^{c}	26.50 ± 0.22^{c}	5.78 ± 0.35^{b}	699.93 ± 40.44^{b}	146.41 ± 4.60^{c}
11%	80.07 ± 0.46^{a}	2.50 ± 0.038^{d}	15.32 ± 0.21^{d}	23.10 ± 0.36^{d}	8.65 ± 0.77^{a}	441.79 ± 29.14^{c}	125.24 ± 3.12^{d}
13%	80.70 ± 0.62^{a}	2.49 ± 0.15^{d}	16.15 ± 0.51^{c}	24.14 ± 1.12^{d}	9.08 ± 0.50^{a}	432.57 ± 60.72^{c}	117.71 ± 4.48^{d}

The mean ± SD values in each column with different letters are significantly different ($p < 0.05$).

TABLE 2 Basic nutrients of BRT of different DOMs.

DOMS	Moisture (g/100 g)	Lipid (g/100 g DW)	Protein (g/100 g DW)	Reducing sugars (g/100 g DW)	Dietary fiber (g/100 g DW)	Total starch (g/100 g DW)	Ash (g/100 g DW)
0%	2.15 ± 0.06^{a}	2.43 ± 0.09^{a}	9.22 ± 0.15^{a}	0.85 ± 0.05^{a}	2.44 ± 0.03^{a}	73.08 ± 4.76^{c}	1.05 ± 0.07^{a}
2%	1.79 ± 0.03^{a}	2.27 ± 0.24^{b}	8.60 ± 0.14^{b}	0.67 ± 0.04^{b}	2.29 ± 0.09^{ab}	74.40 ± 4.65^{c}	0.81 ± 0.11^{b}
5%	1.53 ± 0.04^{a}	1.97 ± 0.40^{c}	8.55 ± 0.21^{bc}	0.58 ± 0.03^{c}	2.16 ± 0.13^{b}	78.21 ± 3.40^{bc}	0.47 ± 0.17^{c}
8%	1.49 ± 0.05^{b}	1.32 ± 0.08^{cd}	8.51 ± 0.02^{bcd}	0.60 ± 0.05^{bc}	0.70 ± 0.01^{c}	80.82 ± 1.84^{ab}	0.45 ± 0.08^{c}
11%	1.44 ± 0.01^{b}	1.09 ± 0.37^{d}	8.22 ± 0.19^{cd}	0.63 ± 0.04^{bc}	0.68 ± 0.02^{c}	83.44 ± 2.35^{ab}	0.24 ± 0.08^{cd}
13%	1.20 ± 0.03^{c}	0.29 ± 0.09^{e}	8.25 ± 0.23^{d}	0.58 ± 0.03^{c}	0.69 ± 0.03^{c}	85.18 ± 0.60^{a}	0.27 ± 0.09^{d}

The mean ± SD values in each column with different letters are significantly different ($p < 0.05$).

76.05–88.95% of the total flavonoids. The TFC reached 114.44 mg CAE/100 g DW at 2% DOM, the highest at this point. Compared to the 2% DOM, the TFC of the 5 and 8% DOM decreased by 24.01 and 40.81%, and then the total flavonoid content of the 11 and 13% DOM decreased rapidly to 45.05 and 56.73%, respectively.

With Table 3 we found little variation in the proportion of free phenols and free flavonoids possessed by the BRT of all DOMs. This is the same as the contribution of free phenols and flavonoids in black rice bran (17). It's worth noting that 5% DOM had the highest bound phenolics, flavonoids and condensed tannins levels, which were 76.95 mg GAE/100 g DW, 20.82 and 29.54 mg CAE/100 g DW, respectively. Bound phenols are reported to be able to covalently bind to dietary fiber components and release them in a free state after high temperature processing (28, 29). In 0 to 5% DOM, dietary fiber content was significantly higher than in 8 to 13% ($p < 0.05$, Table 1) and the degree of browning reaction was significantly lower in 5% DOM then that in 0, 2% DOM ($p < 0.05$, Table 2), thus reduced the release of bound phenolics. This explains why BRT with 5% DOM has the most bound phenols, flavonoids and condensed tannins.

3.3. Antioxidant properties and inhibitory effect on enzyme of BRT with different DOMs

As seen in Figures 1A–C, the extracts of each BRT showed better levels of antioxidant activity. 0% DOM possessed the highest DPPH, FRAP and OH value, which were 96.55 mg Vc/100 g DW, 89.18 mg Vc/100 g DW and 45.82 mg Vc/100 g DW, respectively. Compared to 0% DOM, the DPPH, OH radical scavenging and FRAP value of 2 to 13% DOMs decreased by 18.5, 24.1, 38.5, 50.8, 52.4%; 14.9, 20.6, 36.0, 48.9, 52.9%; and 5.3, 23.9, 29.6, 37.4, 39.2%, respectively. The 0% DOM rice tea underwent the strongest browning reaction after high temperature treatment, producing more dark pigments with antioxidant activity (30). In addition, the higher free and total phenolics levels may be reasons for the highest antioxidant capacity of the 0% DOM sample (31).

Regular consumption of cereal tea has a health effect of reducing the risk of type 2 diabetes (32, 33). The α-amylase and α-glucosidase inhibitory activities of 0% DOM samples (54.3 and 53.5%, respectively) were stronger than those of other samples (46.2–48.5% and 44.7–48. 8%, respectively), indicating that retention of whole rice bran significantly ($p < 0.05$) enhanced the α-amylase and α-glucosidase inhibitory activities (Figures 1D–F). The changes of the pancreatic lipase inhibitory activities in different DOMs were similar to those of the α-amylase and α-glucosidase inhibitory activities. The inhibition of pancreatic lipase decreased from 81.9 to 72.6% with increasing DOM, with the most significant decrease (11.4%) when DOM increased from 0 to 2%, and remained relatively stable thereafter. According to previous studies that brown rice is rich in ferulic acid, coumaric acid and apigenin, all of which have good inhibitory effects on the activities of alpha-amylase, alpha-glucosidase and pancreatic lipase (20, 34, 35). This also explains the significant ability of the 0% DOM sample to inhibit several enzyme activities mentioned above.

3.4. Electronic nose detection analysis of BRT with different DOMs

3.4.1. Analysis of e-nose response values of BRT with different DOM

As shown in Figure 2, the response intensity of sensors W1W, W1S, W2W, W3S, W2W and W6S were high and did not vary significantly, indicating that the inorganic sulfide, organic sulfide,

TABLE 3 The total content of free and bound phenolics, flavonoids, and condensed tannins in different DOM samples and their percentage contribution to the total.

DOM	Phenolics (mg GAE/100 g DW)			Flavonoids (mg CAE/100 g DW)			Condensed tannins (mg CAE/g DW)
	Free	Bound	Total	Free	Bound	Total	
0%	198.05 ± 6.59a[A] (77.20)[B]	58.50 ± 4.95ab (22.80)	256.55 ± 14.55a	99.35 ± 3.95a (87.68)	13.96 ± 0.40c (12.32)	113.31 ± 3.76a	22.76 ± 0.96b
2%	177.37 ± 12.55b (74.78)	59.82 ± 3.95ab (25.22)	237.19 ± 21.84a	97.25 ± 4.21a (84.98)	17.19 ± 0.40b (15.02)	114.44 ± 4.47a	22.51 ± 1.73b
5%	157.70 ± 11.91b (67.20)	76.95 ± 6.04a (32.79)	234.65 ± 10.88a	66.14 ± 6.03b (76.05)	20.82 ± 0.81a (23.94)	86.96 ± 10.82b	29.54 ± 1.15a
8%	127.65 ± 5.88c (73.80)	45.32 ± 3.83b (26.20)	172.97 ± 15.37b	52.97 ± 1.29c (78.21)	14.76 ± 1.02c (21.79)	67.74 ± 0.73c	18.80 ± 0.38 dc
11%	117.51 ± 2.27c (83.68)	22.91 ± 1.95c (16.32)	140.42 ± 7.92c	53.38 ± 1.03c (84.88)	9.51 ± 0.81d (15.12)	62.89 ± 1.84c	19.19 ± 0.77c
13%	112.82 ± 5.13c (84.76)	20.28 ± 1.91c (15.24)	133.10 ± 5.25c	44.05 ± 2.04d (88.95)	5.47 ± 0.41e (11.05)	49.52 ± 1.23d	17.27 ± 0.38d

GAE, gallic acid equivalents; CAE, catechin equivalents. (A) The mean ± SD values in each column with different letters are significantly different ($p < 0.05$). (B) Values in parentheses indicate the percentage contribution to the total content.

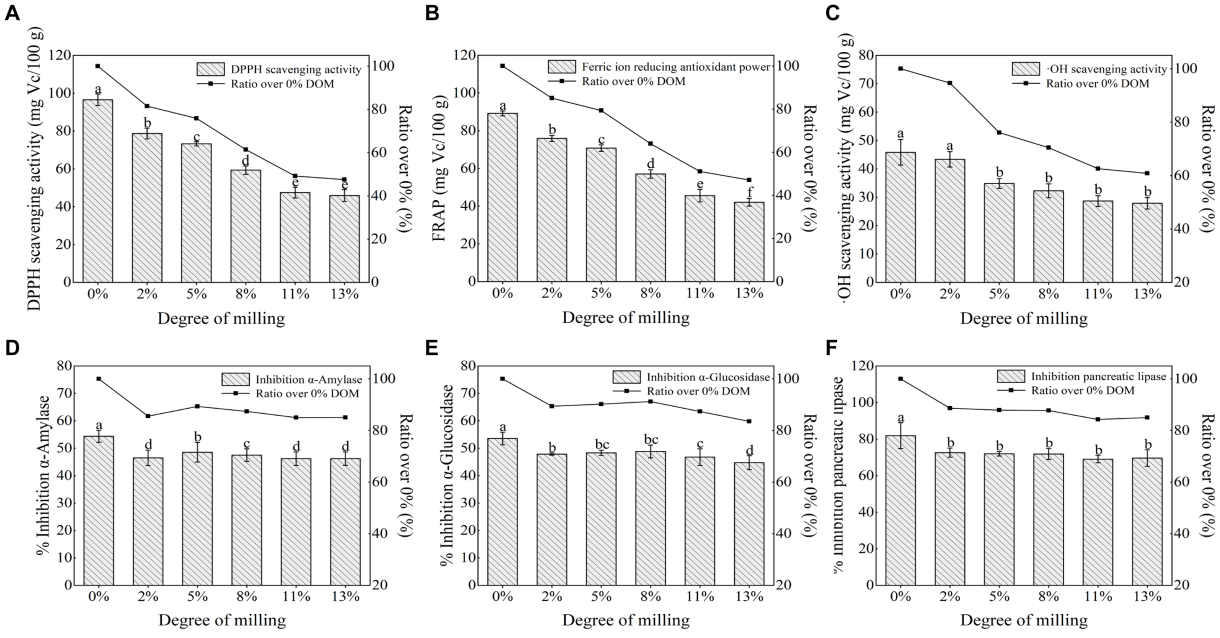

FIGURE 1
Comparison of **(A)** DPPH free radical scavenging activity, **(B)** Ferric ion reducing antioxidant power, **(C)** OH scavenging activity, **(D)** Inhibition α-amylase, **(E)** Inhibition α-glucosidase, **(F)** Inhibition Pancreatic lipase according to the DOM. Means with different letters in the same column are significantly different ($p < 0.05$).

long-chain alkanes, hydrogen, aromatic compounds and methyl components in BRT were high and DOM did not affect them significantly under different DOMs. The sensors W5S changed significantly, indicating that the length of the rice milling time had a significant effect on nitrogen oxides. The e-nose response values of BRT samples showed a tendency to decrease first with increasing DOM and then increase after 2% DOM. These results could also be related to the increase in DOM, which affected the content of free amino acids, lipids and reducing sugars in the bran layer, leading to a decrease in the degree of some non-enzymatic browning reactions, which ultimately affected the oxidative decomposition of alcohols and aldehydes (36, 37).

3.4.2. Identification of BRT subjected to different DOMs using an electronic nose

As in Figure 3, we combined PCA and FDA analysis to further distinguish the BRT volatile substance characteristics of different DOMs (37). The induction values from 95 s to 105 s were used as

eigenvalues for the analysis. Contribution of the first principal component and the second principal of BRT with different DOMs were 80.1 and 9.8%, respectively, with a cumulative contribution of 89.9%, so samples can be analyzed largely based on these two principal components. 8, 11, and 13% of DOMs m-cha were concentrated in the first and fourth quadrants, which indicated that these BRT samples contained more hydrocarbons, ketones, and nitrogen oxides. The analysis showed that the contribution of LDA1 and LDA2 of BRTs with different DOMs was 64.3 and 20.1%, respectively, with a cumulative contribution of 84.4%. These results suggest that the combination of PCA and FDA can well distinguish the BRT of different DOMs. For the 0, 2 and 5% DOM BRT samples, the distances in the PCA and FDA charts were distant from the other samples, indicating that the milling process significantly altered the odor of BRT.

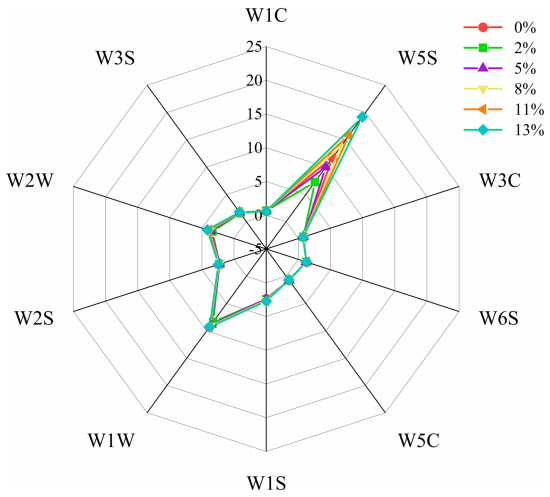

FIGURE 2
Radar fingerprinting of BRT volatile compounds under different DOMs.

3.5. GC–MS analysis of BRT with different DOM

The BRT samples with different DOM (0, 2, 5, 8, 11 and 13%) contained a total of 67 volatile compounds classified into 17 groups including 14 aldehydes, 13 pyrazines, 5 furans, 5 pyrroles, 5 alcohols, 6 alkanes, 3 ketones, 3 alkenes, 2 esters, 2 ethers, 1 phenol, 1 benzene, 1 amine and 3 thiophenes. The results in Supplementary Table SA1 and Figure 4 show that alkanes, furans, aldehydes, pyrazines and alcohols were the most abundant volatiles in BRT (0% DOM) with ratios of 22.04, 21.80, 18.52, 18.07 and 6.20%, respectively. This is consistent with previous studies on baked brown rice (21). Among these volatile compounds, furans are the main providers of sweet and aromatic flavors, pyrazines provide strong roasted and nutty odors (38), and aldehydes and alcohols usually present herbaceous, green, floral and sweet flavors (39). With increasing grinding, the content of aldehydes and ketones increased about 1-fold, the content of furans, pyrazines and alcohols showed a decreasing pattern, while the content of alkanes, pyrroles and phenols remained unchanged.

As shown in Figure 4B, the key volatile compounds of BRT in the milling process were grouped into two clusters in the clustering heat map. DOM increased from 2 to 13% and hexanal, nonanal, benzaldehyde, 2-heptanone, pyrazine, methylpyrazine, 2-pentylfuran, 3-dimethyl-2,1H-pyrrole, thiophene, and 3-methyltridecane were increased compared to BRT without milling. Hexanal is formed by the hydrolyzed oxidation of fatty acids and is the dominant aroma in green tea (40). It has an extremely low odor threshold and usually provides an herbal aroma

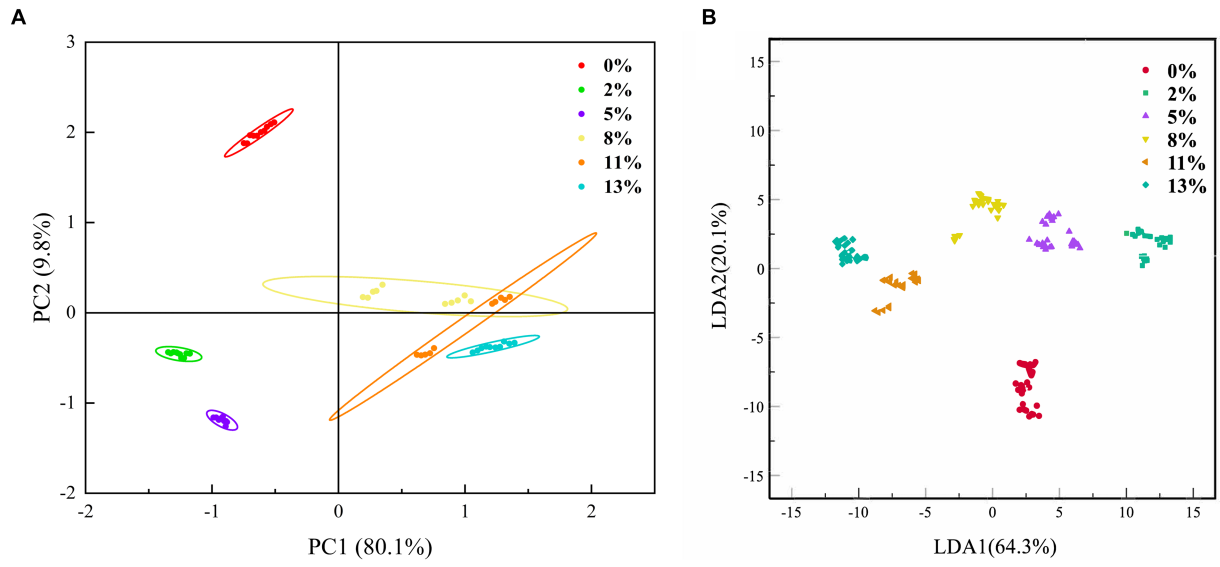

FIGURE 3
Electronic nose-based method for differentiation of BRT with different DOM. **(A)** Principal component analysis (PCA) and **(B)** Fisher discrimination analysis (FDA).

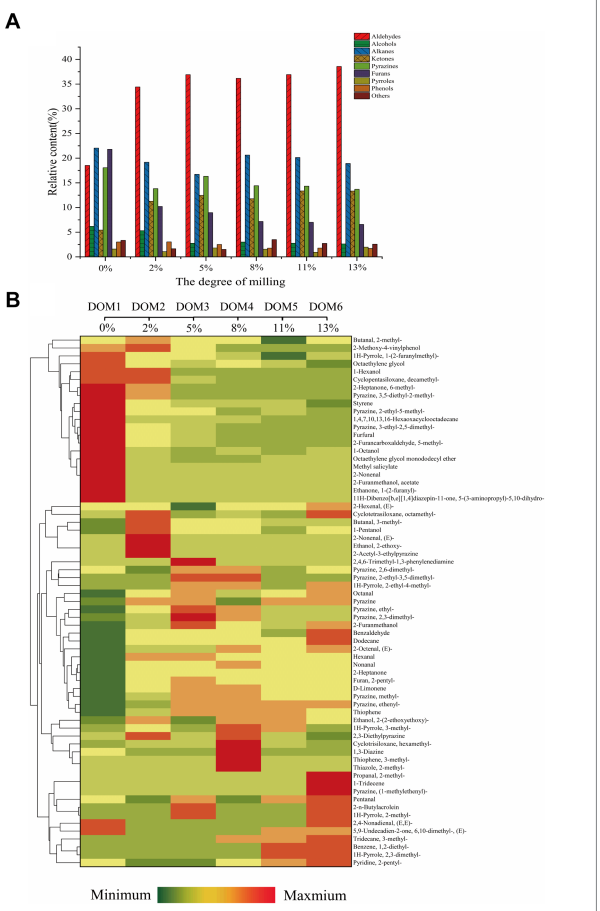

FIGURE 4
(A) Relative content of volatile substances of BRT with different DOM, **(B)** Clustering heat map of volatile compounds variation in BRT with different DOMs.

(41). Benzaldehyde is formed by Strecker degradation, which may impart a bitter perception (42). Pyrazine, methylpyrazine, 2-pentylfuran and 3-dimethyl-2,1 h-pyrrole provide roasted, nutty and floral flavors, which are desirable properties for baked goods. Nonanal is the main aroma contributor present in large quantities in unroasted BRT infusions and usually exhibits an off-flavor. It can be formed by the oxidation of oleic acid (1).

In the second group of volatiles, some of the aroma contributors of rice were ground off, like 2-ethyl-5-methylpyrazine, 3-ethyl-2,5-dimethylpyrazine, 3,5-diethyl-2-methylpyrazine, furfural, 5-methyl-2-furancarboxaldehyde, 1-(2-furanylmethyl)-1H-pyrrole, 1-octanol, (e)-2-nonenal, 6-methyl-2-heptanone, and styrene, resulting in a significant reduction in the aroma intensity of BRT. The reduction in the content of these aromas could be attributed to the removal of a large amount of non-enzymatic browning reaction substrates with the milling process (6). Furfural, 5-methyl-2-furancarboxaldehyde and 3-ethyl-2,5-dimethylpyrazine are the major furan and pyrazine volatiles in BRT. The reduction of these substances significantly reduced the roasted, cocoa and nutty aromas in the tea (43). Therefore, it can be concluded that the milling process significantly changes the concentration and diversity of flavor substances in BRT, which can significantly affect the flavor quality of BRT (5).

3.6. Descriptive discrimination of flavor substances of BRT during milling

We analyzed the changes of the grinding process on the volatile compounds of BRT by building an OPLS-DA model. OPLS-DA uses orthogonal signal correction to select signals that are strongly associated with the model classification, better separating samples between groups and making the explanatory power clearer and more credible (44). As shown in the OPLS-DA score plot in Figure 5A, the first and second components accounted for 40.5 and 13.7% of the total variables, respectively (R2Xcum = 54.2%). The results can reflect the greater the difference in the relative positions of BRTs with different DOMs in the score plot (Figure 5B). Based on the OPLS-DA model, it showed a good fit (R2Ycum = 0.962) and prediction (Q2cum = 0.782) for the identification of flavor substances in BRT during the milling process. R2 and Q2 exceeding 0.5 indicates that model fitting results are acceptable (45). We have verified it using interchange tests. To verify whether the model has overfitting problems, we performed 200 iterations of the model (R2, Q2 intercepts were 0.657 and −0.722) (Figure 5C). It can be seen that this model is able to differentiate well between samples. The predicted variable importance (VIP) values can be derived from the PLS regression model for the flavor substances of BRT during milling processing (Figure 5D). The VIP scores for 2-methyl-thiazole, 2-pentyl-pyridine, 2-ethyl-4-methyl-1 h-pyrrole, 2-methyl-1 h-pyrrole, 2,3-dimethyl-1 h-pyrrole, 2-acetyl-3-ethylpyrazine, (1-methylethenyl)-pyrazine, 2-ethyl-3,5-dimethyl-pyrazine, 2,6-dimethyl-pyrazine, 2,4,6-trimethyl-1,3-phenylenediamine, 1,2-diethyl-benzene, 2-(2-ethoxyethoxy)-ethanol, 1-tridecene, 6,10-dimethyl-(e)-5,9-undecadien-2-one, 3-methyl-tridecane, 1-hexanol, 1-pentanol, 2-ethoxy-ethanol, (E,E)-2,4-nonadienal, (E)-2-nonenal, (E)-2-hexenal, pentanal, 2-methyl-butanal and 2-methyl-propanal were > 1. These compounds can be used as an indicator to identify the degree of BRT milling (VIP > 1 and $p < 0.05$).

3.7. Sensory evaluation of BRT tea infusion and rice grains

In this study, sensory evaluation of tea infusion and rice grains from BRT made from rice with different DOMs was carried out (Table 4). The BRT samples with different DOM exhibited significant differences in color, aroma, flavor, texture and overall acceptability ($p < 0.05$). With the DOM of BRT increasing, the overall acceptance of tea infusions decreased, the mouthfeel score of rice grains decreased. This is because 0% DOM BRT contains the most dietary fiber, resulting in greater hardness and poorer taste of rice grains (46). Because of the reduced browning reaction, DOM revealed a negative correlation with the color and taste of BRT. With the higher DOM had greater intensities of sweet taste (46), so the aroma score revealed a positive correlation with DOM. In conclusion, the degree of milling of BRT can significantly change the sensory characteristics (color, texture and taste) and overall acceptability of tea infusion and rice grains. A proper level of grinding can usefully enhance the overall sensory quality and acceptance of the BRT.

4. Conclusion

Our study investigated the effects of different DOMs on BRT essential nutrients, phenolics, their distribution, biological activity,

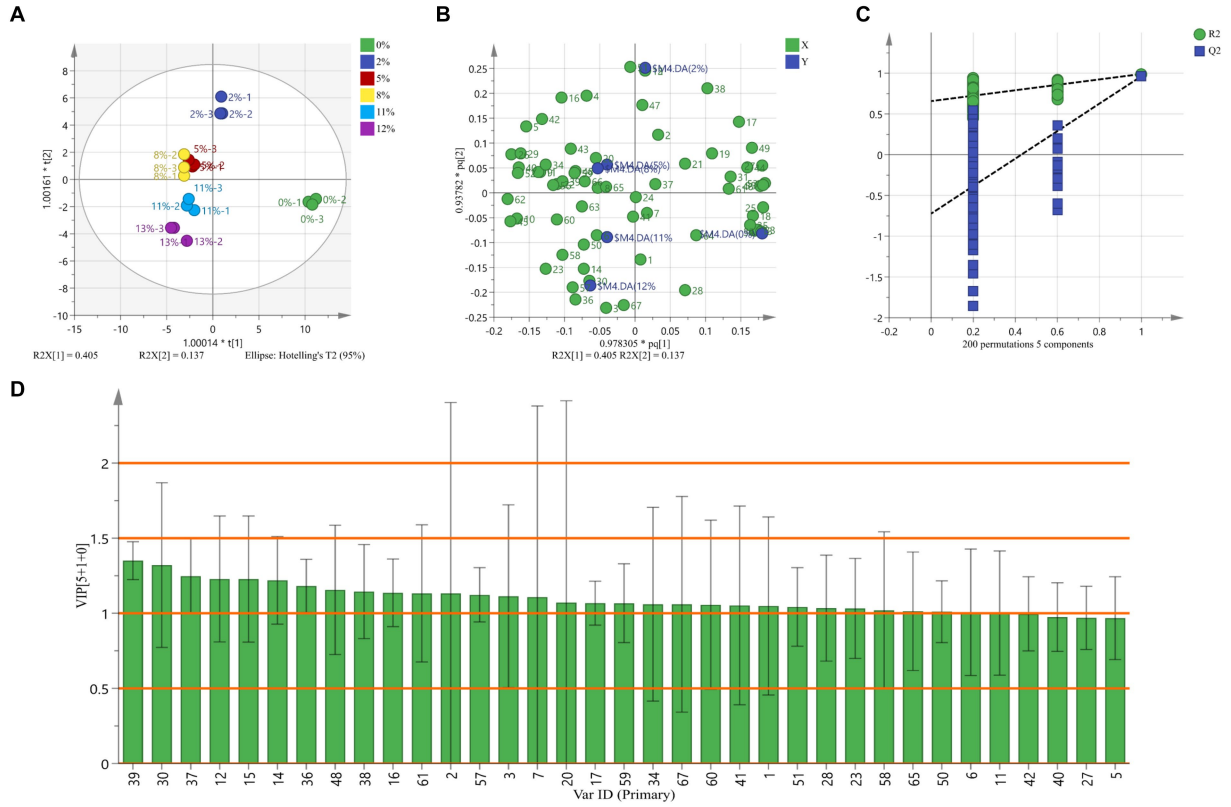

FIGURE 5
Descriptive discrimination of flavor substances of BRT during milling. **(A)** OPLS-DA results from GC–MS data of BRT at different milling stages. **(B)** The OPLS-DA score plot. **(C)** The result of 200 times permutation testing for OPLS-DA. **(D)** VIP values.

TABLE 4 Sensory characteristics of tea infusion and rice grains from BRT samples produced by different DOM.

Samples	DOMs	Color	Aroma	Taste	Overall acceptance/ Mouthfeel
Tea infusions	0%	7.61 ± 0.44^{a}	4.69 ± 0.36^{a}	7.25 ± 0.58^{a}	6.44 ± 0.31^{a}
	2%	6.93 ± 0.44^{b}	5.83 ± 0.24^{b}	6.56 ± 0.25^{b}	5.83 ± 0.55^{ab}
	5%	5.55 ± 0.38^{c}	5.48 ± 0.36^{bc}	5.49 ± 0.33^{c}	5.74 ± 0.60^{b}
	8%	5.18 ± 0.43^{cd}	5.83 ± 0.48^{bc}	4.82 ± 0.35^{d}	6.08 ± 0.61^{b}
	11%	4.93 ± 0.40^{d}	6.08 ± 0.68^{c}	4.28 ± 0.29^{e}	5.69 ± 0.33^{b}
	13%	3.93 ± 0.29^{e}	6.99 ± 0.36^{d}	3.54 ± 0.26^{f}	5.94 ± 0.57^{b}
Rice grains	0%	7.26 ± 0.38^{a}	4.01 ± 0.38^{c}	4.68 ± 0.34^{d}	2.57 ± 0.37^{e}
	2%	6.45 ± 0.36^{b}	4.16 ± 0.33^{c}	5.58 ± 0.30^{c}	4.49 ± 0.62^{d}
	5%	5.39 ± 0.49^{c}	4.62 ± 0.37^{b}	5.95 ± 0.60^{b}	5.73 ± 0.57^{c}
	8%	5.08 ± 0.73^{c}	6.27 ± 0.49^{a}	6.65 ± 0.35^{a}	6.62 ± 0.34^{b}
	11%	4.28 ± 0.38^{d}	6.33 ± 0.59^{a}	5.84 ± 0.35^{bc}	7.33 ± 0.58^{a}
	13%	3.75 ± 0.60^{e}	6.27 ± 0.64^{a}	5.68 ± 0.36^{bc}	6.69 ± 0.57^{b}

Means with different letters in the same column are significantly different ($p < 0.05$).

and volatile compound content. Acrylamide and AGEs were effectively reduced at 2% DOM. The 0% DOM samples contained noticeably higher TPC, TFC and CTC and showed stronger antioxidant and enzyme inhibitory activities compared to other DOM samples. Alkanes, furans, aldehydes, pyrazines and alcohols are the main volatile compounds in BRT. It can be concluded from the Herarchical clustering and OPLS-DA analysis that 2% DOM is the optimal milling condition, as this condition retains most of the aromatic compounds and nutrients, and the safety and taste are greatly enhanced. Finally, twenty-five aroma-active compounds may have contributed to rice type discrimination, like 1-tridecene, 2,4,6-trimethyl-1,3-phenylenediamine, (E)-2-nonenal, (E, E)-2,4-nonadienal and

2-ethoxy-ethanol. This study provides significant data to guide the appropriate processing and aroma quality of BRT.

Data availability statement

The original contributions presented in the study are included in the article/Supplementary material, further inquiries can be directed to the corresponding authors.

Author contributions

LZ: methodology, investigation, and writing. YS: investigation and funding acquisition. ZZ: investigation. SL: funding acquisition and writing – original draft. RX: writing – original draft. JW: investigation and visualization. JS: investigation. SC and TX: supervision and resources. FC: supervision, funding acquisition, and resources. XM: conceptualization, supervision, funding acquisition, and writing – review & editing. All authors contributed to the article and approved the submitted version.

Funding

This work was supported by the project of Special Project for Science and Technology Innovation of Wuhan (2022020801020344). Science and Technology Plan Project of Hubei Province (2023BBB101). The support of the National Key Research and Development Program of China (2018YFD0301306-4-2), Outstanding young and middle-aged science and technology innovation team in Hubei Province (T2020012), the Science and Technology Plan Project in Agriculture and Rural Areas of Hubei Province in 2023 were also appreciated.

Conflict of interest

The authors declare that the research was conducted in the absence of any commercial or financial relationships that could be construed as a potential conflict of interest.

Publisher's note

Supplementary material

The Supplementary material for this article can be found online at: https://www.frontiersin.org/articles/10.3389/fnut.2023.1232251/full#supplementary-material

References

1. Hyun-Jin K, Jung-Ah H, Seung-Taik L, Dong-Hwa C. Effects of germination and roasting on physicochemical and sensory characteristics of brown rice for tea infusion. *Food Chem*. (2021) 350:129240. doi: 10.1016/j.foodchem.2021.129240

2. Park J, Oh S-K, Chung H-J, Shin DS, Choi I, Park H-J. Effect of steaming and roasting on the quality and resistant starch of brown rice flour with high amylose content. *LWT*. (2022) 167:113801. doi: 10.1016/j.lwt.2022.113801

3. Park H, Puligundla P, Mok C. Cold plasma decontamination of brown rice grains: impact on biochemical and sensory qualities of their corresponding seedlings and aqueous tea infusions. *LWT*. (2020) 131:109508. doi: 10.1016/j.lwt.2020.109508

4. Lei L, Jinjie G, Ruifen Z, Zhencheng W, Yuanyuan D, Jinxin G, et al. Effect of degree of milling on phenolic profiles and cellular antioxidant activity of whole brown rice. *Food Chem*. (2015) 185:318–25. doi: 10.1016/j.foodchem.2015.03.151

5. Zhihai L, Xinyang S, Tong X, Wei D, Qu Y, Peng L, et al. Insight into the dynamic variation and retention of major aroma volatile compounds during the milling of Suxiang japonica rice. *Food Chem*. (2023) 405:134468. doi: 10.1016/j.foodchem.2022.134468

6. Sehun C, Jihyun L. Volatile and sensory profiles of different black rice (*Oryza sativa* L.) cultivars varying in milling degree. *Food Res Int*. (2021) 141:110150. doi: 10.1016/j.foodres.2021.110150

7. Nie CZP, Li Y, Guan YM, Zhang KL, Liu JX, Fan MC, et al. Highland barley tea represses palmitic acid-induced apoptosis and mitochondrial dysfunction via regulating AMPK/SIRT3/FoxO3a in myocytes. Food. *Bioscience*. (2021) 40:100893. doi: 10.1016/j.fbio.2021.100893

8. Zhiming W, Mingwei Z, Guang L, Yuanyuan D, Yan Z, Xiaojun T, et al. Effect of the degree of milling on the physicochemical properties, pasting properties and in vitro digestibility of Simiao rice. *Grain Oil Sci Technol*. (2021) 4:45–53. doi: 10.1016/j.gaost.2021.04.002

9. Hongyan L, Minghao X, Zhijun C, Jie L, Yangyang W, Yingli L, et al. Effects of the degree of milling on starch leaching characteristics and its relation to rice stickiness. *J Cereal Sci*. (2021) 98:103163. doi: 10.1016/j.jcs.2021.103163

10. Bai J, Dong M, Li J, Tian L, Xiong D, Jia J, et al. Effects of egg white on physicochemical and functional characteristics of steamed cold noodles (a wheat starch gel food). *Lebensm Wiss Technol*. (2022) 169:114057. doi: 10.1016/j.lwt.2022.114057

11. Champrasert O, Chu J, Meng Q, Viney S, Holmes M, Suwannaporn P, et al. Inhibitory effect of polysaccharides on acrylamide formation in chemical and food model systems. *Food Chem*. (2021) 363:130213. doi: 10.1016/j.foodchem.2021.130213

12. Wang S, Zheng L, Zheng X, Yang Y, Xiao D, Zhang H, et al. Chitosan inhibits advanced glycation end products formation in chemical models and bakery food. *Food Hydrocoll*. (2022) 128:107600. doi: 10.1016/j.foodhyd.2022.107600

13. Li SY, Xu H, Sui Y, Mei X, Shi JB, Cai S, et al. Comparing the LC-MS phenolic acids profiles of seven different varieties of Brown Rice (*Oryza sativa* L.). *Foods*. (2022) 11:1552. doi: 10.3390/foods11111552

14. Hongyi S, Haoxin W, Pangzhen Z, Said A, Zhongxiang F. Changes in phenolic content, antioxidant activity, and volatile compounds during processing of fermented sorghum grain tea. *Cereal Chem*. (2020) 97:612–25. doi: 10.1002/cche.10277

15. Seerat B, Balwinder S, Amritpal K, Narpinder S, Manpreet K, Supriya K, et al. Effect of infrared roasting on antioxidant activity, phenolic composition and Maillard reaction products of Tartary buckwheat varieties. *Food Chem*. (2019) 285:240–51. doi: 10.1016/j.foodchem.2019.01.141

16. Fukui M, Islm MZ, Lai HM, Kitamura Y, Kokawa M. Effects of roasting on storage degradability and processing suitability of brown rice powder. *LWT*. (2022) 161:113277. doi: 10.1016/j.lwt.2022.113277

17. Zhang S, Ma Q, Dong LH, Jia XC, Liu L, Huang F, et al. Phenolic profiles and bioactivities of different milling fractions of rice bran from black. *Food Chem*. (2022) 378:132035. doi: 10.1016/j.foodchem.2021.132035

18. Yongxu S, Tianbao L, Jicheng L. Structural characterization and hydroxyl radicals scavenging capacity of a polysaccharide from the fruiting bodies of Auricularia polytricha. *Carbohydr Polym*. (2010) 80:378–81. doi: 10.1016/j.carbpol.2009.11.033

19. Fatemeh S, Hossein Azizi M, Ahmadi Gavlighi H, Ali R. Potential benefits of Moringa peregrina defatted seed: effect of processing on nutritional and anti-nutritional properties, antioxidant capacity, in vitro digestibility of protein and starch, and inhibition of alpha-glucosidase and alpha-amylase enzymes. *Food Chem Adv*. (2022) 1:100034. doi: 10.1016/j.focha.2022.100034

20. Ruimin W, Lu W, Lin Z, Sitong W, Congfa L, Sixin L. Solvents effect on phenolics, iridoids, antioxidant activity, antibacterial activity, and pancreatic lipase inhibition activity of noni (*Morinda citrifolia* L.) fruit extract. *Food Chem*. (2022) 377:131989. doi: 10.1016/j.foodchem.2021.131989

21. Shi Y, Wang L, Fang Y, Wang H, Tao H, Pei F, et al. A comprehensive analysis of aroma compounds and microstructure changes in brown rice during roasting process. *Lebensm Wiss Technol*. (2018) 98:613–21. doi: 10.1016/j.lwt.2018.09.018

22. Jogihalli P, Singh L, Kumar K, Sharanagat VS. Novel continuous roasting of chickpea (*Cicer arietinum*): study on physico-functional, antioxidant and roasting characteristics. *LWT*. (2017) 86:456–64. doi: 10.1016/j.lwt.2017.08.029

23. Paras S, Singh GH. Effect of sand roasting and microwave cooking on antioxidant activity of barley. *Food Res Int*. (2011) 44:235–40. doi: 10.1016/j.foodres.2010.10.030

24. Mesías M, Gómez P, Olombrada E, Morales FJ. Formation of acrylamide during the roasting of chia seeds (*Salvia hispanica* L.). *Food Chem*. (2023) 401:134169. doi: 10.1016/j.foodchem.2022.134169

25. Liu KL, Zheng JB, Chen FS. Relationships between degree of milling and loss of vitamin B, minerals, and change in amino acid composition of brown rice. *LWT Food Sci Technol*. (2017) 82:429–36. doi: 10.1016/j.lwt.2017.04.067

26. Bassama J, Brat P, Bohuon P, Hocine B, Boulanger R, Gunata Z. Acrylamide kinetic in plantain during heating process: precursors and effect of water activity. *Food Res Int*. (2011) 44:1452–8. doi: 10.1016/j.foodres.2011.03.018

27. Eichner K, Karel M. Influence of water-content and water activity on sugar amino browning reaction in model systems under various conditions. *J Agric Food Chem*. (1972) 20:218–23. doi: 10.1021/jf60180a025

28. Acosta-Estrada BA, Gutierrez-Uribe JA, Serna-Saldivar SO. Bound phenolics in foods, a review. *Food Chem*. (2014) 152:46–55. doi: 10.1016/j.foodchem.2013.11.093

29. Yun X, Pangzhen Z, Jiaqian L, Johnson S, Zhongxiang F. Effect of processing on the phenolic contents, antioxidant activity and volatile compounds of sorghum grain tea. *J Cereal Sci*. (2019) 85:6–14. doi: 10.1016/j.jcs.2018.10.012

30. Ahmad Mir S, Don Bosco SJ, Ahmad Shah M, Maqbool MM. Effect of puffing on physical and antioxidant properties of brown rice. *Food Chem*. (2016) 191:139–46. doi: 10.1016/j.foodchem.2014.11.025

31. Kim SH, Yang YJ, Chung IM. The effect of degree of milling on the nutraceutical content in ecofriendly and conventional Rice (*Oryza sativa* L.). *Foods*. (2020) 9:1297. doi: 10.3390/foods9091297

32. Li W, Zhaohui H, Peiyou Q, Guixing R. Effects of processing on phytochemical profiles and biological activities for production of sorghum tea. *Food Res Int*. (2013) 53:678–85. doi: 10.1016/j.foodres.2012.07.062

33. Zhou X, Zhao GC, Sun SY, Li JY. Antihypertensive effect of giant embryo brown rice and pre-germinated giant embryo brown rice on spontaneously hypertensive rats. *Food Sci Nutr*. (2019) 7:2888–96. doi: 10.1002/fsn3.1137

34. Meng Z, Yunfeng X, Jinle X, Bailiang Z, Yuan Y, Denglin L, et al. Comparative evaluation on phenolic profiles, antioxidant properties and alpha-glucosidase inhibitory effects of different milling fractions of foxtail millet. *J Cereal Sci*. (2021) 99:103217. doi: 10.1016/j.jcs.2021.103217

35. Zheng YX, Tian JH, Yang WH, Chen SG, Liu DH, Fang HT, et al. Inhibition mechanism of ferulic acid against alpha-amylase and alpha-glucosidasee. *Food Chem*. (2020) 317:126346. doi: 10.1016/j.foodchem.2020.126346

36. Purlis E. Browning development in bakery products - a review. *J Food Eng*. (2010) 99:239–49. doi: 10.1016/j.jfoodeng.2010.03.008

37. Song FH, Xiang H, Li ZF, Li J, Li LQ, Song CF. Monitoring the baking quality of Tieguanyin via electronic nose combined with GC-MS. *Food Res Int*. (2023) 165:112513. doi: 10.1016/j.foodres.2023.112513

38. Pico J, Bernal J, Gomez M. Wheat bread aroma compounds in crumb and crust: a review. *Food Res Int*. (2015) 75:200–15. doi: 10.1016/j.foodres.2015.05.051

39. Lasekan O, Alfi K, Abbas KA. Volatile compounds of roasted and steamed malaysian tropical almond nut (*terminalia catappa* L.). *Int J Food Prop*. (2012) 15:1120–32. doi: 10.1080/10942912.2010.514086

40. Chi-Tang H, Xin Z, Shiming L. Tea aroma formation. *Food Sci Human Wellness*. (2015) 4:9–27. doi: 10.1016/j.fshw.2015.04.001

41. Lee J, Chambers DH IV, Chambers E IV, Adhikari K, Yoon Y. Volatile aroma compounds in various brewed green teas. *Molecules*. (2013) 18:10024–41. doi: 10.3390/molecules180810024

42. Supeeraya A, Chockchai T, Chockchai T. Preparation, aroma characteristics and volatile compounds of flavorings from enzymatic hydrolyzed rice bran protein concentrate. *J Sci Food Agric*. (2018) 98:4479–87. doi: 10.1002/jsfa.8972

43. Mizukami Y, Sawai Y, Yamaguchi Y. Changes in the concentrations of acrylamide, selected odorants, and catechins caused by roasting of green tea. *J Agric Food Chem*. (2008) 56:2154–9. doi: 10.1021/jf0731806

44. Liao S, Han J, Jiang C, Zhou B, Jiang Z, Tang J, et al. HS-SPME-GC*GC/MS combined with multivariate statistics analysis to investigate the flavor formation mechanism of tank-fermented broad bean paste. *Food Chem X*. (2023) 17:100556. doi: 10.1016/j.fochx.2022.100556

45. Jing Y, Chuanjian C, Shihua Z, Jiaji Z, Chuanyi P, Huimei C, et al. Use of headspace GC/MS combined with chemometric analysis to identify the geographic origins of black tea. *Food Chem*. (2021) 360:130033. doi: 10.1016/j.foodchem.2021.130033

46. Jung Kwang P, Sang Sook K, Kwang OK. Effect of milling ratio on sensory properties of cooked rice and on physicochemical properties of milled and cooked rice. *Cereal Chem*. (2001) 78:151–6. doi: 10.1094/CCHEM.2001.78.2.151

frontiers | Frontiers in Nutrition

TYPE Original Research
PUBLISHED 11 October 2023
DOI 10.3389/fnut.2023.1236216

OPEN ACCESS

EDITED BY
Yu-Chung Chang,
Washington State University, United States

REVIEWED BY
Jinyan Gong,
Zhejiang University of Science and Technology, China
Dongchao Xie,
Zhejiang A&F University, China
Xiao Chun Wan,
Anhui Agricultural University, China
Peiqiang Wang,
Qingdao Agricultural University, China

*CORRESPONDENCE
Yong-Quan Xu
✉ yqx33@126.com

†These authors have contributed equally to this work

RECEIVED 07 June 2023
ACCEPTED 21 September 2023
PUBLISHED 11 October 2023

CITATION
Jin J-C, Liang S, Qi S-X, Tang P, Chen J-X, Chen Q-S, Chen Y-F, Yin J-F and Xu Y-Q (2023) Widely targeted metabolomics reveals the effect of different raw materials and drying methods on the quality of instant tea. *Front. Nutr.* 10:1236216. doi: 10.3389/fnut.2023.1236216

Widely targeted metabolomics reveals the effect of different raw materials and drying methods on the quality of instant tea

Jian-Chang Jin[1†], Shuang Liang[2†], Shang-Xiong Qi[3], Ping Tang[4], Jian-Xin Chen[2], Quan-Sheng Chen[5], Yan-Feng Chen[6], Jun-Feng Yin[2] and Yong-Quan Xu[2*]

[1]College of Biological and Environmental Engineering, Key Laboratory of Pollution Exposure and Health Intervention of Zhejiang Province, Zhejiang Shuren University, Hangzhou, China, [2]Key Laboratory of Biology, Genetics and Breeding of Special Economic Animals and Plants, National Engineering Research Center for Tea Processing, Tea Research Institute Chinese Academy of Agricultural Sciences, Ministry of Agriculture and Rural Affairs, Hangzhou, China, [3]Eastsign Foods (Quzhou) Co., Ltd., Quzhou, China, [4]Hangzhou Vocational and Technical College, Hangzhou, China, [5]College of Ocean Food and Biological Engineering, Jimei University, Xiamen, China, [6]Unibioche Food Tech Co., Ltd., Hangzhou, China

Introduction: Instant teas are particularly rich in tea polyphenols and caffeine and have great potential as food ingredients or additives to improve the quality of food and enhance their nutritional and commercial value.

Methods: To determine the relationships between raw material, drying method, and sensory and other quality attributes, instant teas were prepared from three tea varieties, namely black, green and jasmine tea, using two drying methods, namely spray-drying (SD) and freeze-drying (FD).

Results: Both the raw tea material and drying method influenced the quality of the finished instant teas. Black tea was quality stable under two drying, while green tea taste deteriorated much after SD. Jasmine tea must be produced from FD due to huge aroma deterioration after SD. FD produced instant tea with higher sensory quality, which was attributed to the lower processing temperature. Chemical compositional analysis and widely targeted metabolomics revealed that SD caused greater degradation of tea biochemical components. The flavonoids content changed markedly after drying, and metabolomics, combined with OPLS-DA, was able to differentiate the three varieties of tea. Instant tea preparations via SD often lost a large proportion of the original tea aroma compounds, but FD minimized the loss of floral and fruity aroma compounds. Changes in the tea flavonoids composition, especially during drying, contributed to the flavor development of instant tea.

Discussion: These results will provide an practicle method for high-quality instant tea production through choosing proper raw tea material and lowering down drying temperature with non-thermal technologies like FD.

KEYWORDS

instant tea, raw tea materials, drying, flavonoids, aroma

1. Introduction

Tea has long been recognized for its unique color, flavor and health properties, and has been described as the most pleasant and popular of beverages (1). In 2022, global tea production was 6.397 million tons, a decrease of 54,000 tons compared with 2021. Traditionally, a time-consuming and complex process is needed to offer consumers a fragrant tea with sweet and mellow taste, which contains both rigorous water preparation paying attention to water quality and temperature and strict tea brewing paying attention to tea-to-water ratio and brewing time (2). To simplify tea preparation process, instant tea with characteristic flavor and satisfying solubility come into market. Instant tea is a powdered form of tea infusion, manufactured from tea leaf extracts of the six tea varieties (black, green, oolong, etc.). In addition to drinking, instant tea can also be added to other foods to improve flavor, increase nutritional quality and extend shelf-life, with great potential for new applications (3).

The sensory quality and health benefits of tea are clearly related to the inherent primary and secondary plant metabolites, such as polyphenols, amino acids, alkaloids, tea polysaccharides and tea saponins (4). Tea polyphenols, the general term for phenolic compounds in tea, are the main bioactive compounds in tea and usually comprise 18–36% of tea leaf dry weight. Due to remarkable health benefits and specific structural properties, tea polyphenols are widely used in the food industry (5). Tea flavonoids, the most studied functional phenolic components, are the important contributor to the taste and multiple health-promoting effects, particularly anti-inflammatory, antioxidant, antimicrobial, neuroprotective, antihypertensive, and anti-carcinogenic properties (6). As the most abundant secondary metabolites, tea flavonoids comprise a large group of structurally diverse compounds with a variety of basic skeleton (6), namely flavan-3-ols (such as catechins, theaflavins, thearubigins, and proanthocyanidins), flavonols (such as quercetin, kampferol, myricetin, and their glycosides) and flavones (such as luteolin and apigenin). Tea flavonoids have attracted much attention in recent years because of their major contribution as complementary and alternative medicines, and tea would be the rich source of flavonoids for daily intake (7).

Past studies on instant tea focused on the mechanisms that influence quality and sensory attributes in each procedures. During the extraction procedure, choosing processed tea (as opposed to green) as the raw material would compromise the quality of the instant tea, because the chemical components in processed tea have been degraded and modified by heat-treatment (8). One way of reducing flavor components degradation is to use fermented dhool (particles resulting from rolling of green tea leaves) as the raw material (8). Filtration and concentration of the extract resulted in decreased concentrations of geraniol, indole, *β*-damascenone, methyl jasmonate, *trans*-nerolidol, and safranal (9). Ultrafiltration of the extract before drying promoted the loss of aroma volatiles, by removing some of the tea polyphenols, which would otherwise combine with and help retain the volatiles (9).

Drying is the key step of instant tea production. The drying technology of instant tea after water extraction is well-established, usually based on three drying methods: spray-drying (SD), freeze-drying (FD), or vacuum-drying. SD uses the high temperature/very short time approach for rapid evaporation of water, which has advantages of satisfying powder characteristics, continuous production and large throughput (10). However, when processing tea infusion into instant tea powder, high temperatures involved in SD can alter the content and composition of aroma components by evaporation, oxidation and thermal degradation (8, 11, 12). By contrast, FD involves removal of water by sublimation of ice under a vacuum, at temperatures below the freezing point of water (13, 14). This low temperature minimizes thermal degradation and evaporation of flavor components (15). Although FD effectively minimizes loss of flavor components, it requires costly freezing and vacuum systems, which have much higher energy consumption and capital costs than SD.

Since high temperature is the main cause of aroma compound loss and quality deterioration, reducing the processing temperature is considered a promising way to maximize the quality of instant tea (1). Recently, electrostatic spray drying, which operates at a much lower temperature (outlet air temperature 38–42°C) than conventional SD, was shown to be comparable to FD in terms of sensory quality and productivity, although most aroma compounds were less abundant than after FD (12). In this study, three normal raw tea materials, black tea (BT), green tea (GT) and jasmine tea (JT; GT scented with jasmine flowers so the tea absorbs the jasmine scent), were subjected to analysis of the relationships between sensory quality and quality attributes when processed into instant teas (IBT, IGT, and IJT) by SD or FD. The influence of the different raw materials and drying methods on the organoleptic properties, chemical composition and physicochemical properties of instant tea was determined. Metabolomics analysis was applied to identify differential metabolites between drying methods and elucidate the relationships and interactions between flavonoids and volatile compounds. The findings will provide a theoretical and scientific basis for improved quality control of instant tea during the drying procedure.

2. Materials and methods

2.1. Reagents and materials

Black tea, green tea and jasmine tea were from Eastsign Foods (Quzhou) Co., Ltd. (Quzhou, China). Purified water was from Hangzhou Wahaha Beverage Co., Ltd. (Hangzhou, Zhejiang, China), which had a total dissolved solids of 1.768 mg/L and a pH of 6.74.

Gallic acid (GA), gallocatechin (GC), epigallocatechin (EGC), catechin (C), epicatechin (EC), gallocatechin gallate (GCG), epigallocatechin gallate (EGCG), catechin gallate (CG), epicatechin gallate (ECG), theaflavin (TF), theaflavin-3-gallate (TF-3-G), theaflavin-3-gallate (TF-3-G) and theaflavin-3,3-digallate (TFDG) were from Shanghai Yuanye Biotechnology Co., Ltd. (China) with purity ≥95%. *N*-Alkanes for linear retention index (RI) determination and internal standard solution (decanoic acid ethyl ester) were from TCI (Shanghai) Development Co., Ltd. (Shanghai, China). Ninhydrin, stannous chloride, sodium carbonate, disodium hydrogen phosphate, potassium dihydrogen phosphate and disodium EDTA were all analytical grade from local suppliers. Acetic acid and acetonitrile were chromatographic grade, from local suppliers.

2.2. Preparation of instant tea

Process parameters was set as follows. Tea-to-water ratio was 1:10, extraction temperature for BT was 90°C, and for GT and JT was 75–80°C. Tea leaves (5 kg) were put in an extraction tank (diameter of 30 cm, height of 1.2 m) and were extracted with hot water, impregnated for 30 min, then extraction started to slowly extract the impregnated. The total soaking time was 3–4 h. The resulting extract concentrations were 6% (w/v) for BT, 8% (w/v) for GT and 10% (w/v) for JT. After centrifugation, the three tea extracts were used to prepare tea powders through SD and FD. For SD, the 50-type spray drying tower (D-300, from Changsheng Dryer Manufacturing Co., Ltd., Wuxi, China) had an inlet air temperature of 170°C and an outlet air temperature of 100°C. For FD, the vacuum freeze dryer (ZG-200, from Hangznou Innovative Vacuum Freeze-drying Plant, Hangzhou, China) was set to the following parameters (Table 1), which was from a mature large-scale FD process.

2.3. Sensory evaluation

Tea solution preparation were referred to "5.3.2.7 Powdered tea (Cylindrical cup evaluation method)" in Chinese standard GB/T 23776-2018 Methodology for sensory evaluation of tea with slight modification. The three varieties of instant tea powder (0.5 g) were each mixed into 100 mL of pure water at 50°C, and stayed for 1 min. To determine the sensory differences among the instant tea, evaluation of the appearance, liquor color, aroma and taste was scored on a 100-point scale, performed by five fully trained panelists (three men and two women, 26–52 years old) with certificates (four senior and one intermediate tea assessor) for tea quality evaluation from the Tea Scientific Society of China. There were three replicate ratings for each treatment.

2.4. Chemical and physical analysis of raw materials and instant teas

The test samples were prepared according to the method "3.4.3.2 Preparation of Test Solution" in Chinese standard GB/T 8313-2018. Determination of tea polyphenols was by the Folin phenol method according to Chinese standard GB/T 8313-2018. Total amino acids were determined by the ninhydrin colorimetric method according to Chinese standard GB/T 8314-2013. Determination of theaflavins (TFs) was by high-performance liquid chromatography (HPLC) according to Chinese standard GB/T 30483-2013.

Catechins, caffeine, and gallic acid were determined by HPLC (LC-20D, Shimadzu Kyoto, Japan) (16), fitted with a Symmetry C18 column (5 µm, 4.6 mm × 250 mm; Waters, Milford, MA). The mobile phases were 2% (v/v) aqueous acetic acid (A) and acetonitrile (B). The linear elution gradient was: 0–3 min, 6.5%B; 19 min, 15%B; 25 min, 25%B; 30–35 min, 6.5%B, at a flow rate of 1 mL/min, a column temperature of 40°C, UV detection at 280 nm and injection volume 10 µL. Samples were filtered before injection using 0.45 µm microporous membrane filters.

Color differences (CIELAB L^*, a^* and b^* values) were measured by a CM-5 color difference meter (Konica Minolta, Tokyo, Japan). L^* represents brightness, a^* represents the red/green balance ($+a$ is red, $-a$ is green). b^* represents the yellow/blue balance ($+b$ is yellow, $-b$ is blue).

TABLE 1 Parameters of the vacuum freeze dryer for large-scale freeze-drying (FD) process.

Stage	Accumulated drying time/min	Operation time/min	Temperature (partition)/°C	Vacuum degree/Pa
1	30	30	20	70–100
2	90	60	30	
3	270	180	30	
4	300	30	40	
5	1,080	780	40	
6	1,110	30	50	
7	1830	720	50	

2.5. Extraction of volatiles using headspace-solid phase microextraction (HS-SPME)

The extraction of volatile compounds from green tea was performed using HS-SPME (50/30 µm divinylbenzene/carboxen/polydimethylsiloxane; CAR/PDMS/DVB) fiber (catalog No. 57328-U; Supelco, Bellefonte, PA) (17). Tea sample (0.5 g), boiling water (5 mL), and the internal standard, decanoic acid ethyl ester (10 mg/L, 10 µL), were added to 20 mL glass headspace vials by injection. The samples were kept in a water bath at 60°C to equilibrate for 5 min, then extracted with the SPME fiber for 60 min. After sampling of the headspace volatiles, the SPME fiber was inserted into the GC injector in splitless mode, and held there for 5 min to allow analyte thermal desorption at 250°C.

2.6. GC–MS analysis

According to our previous study (17), GC–MS analysis were performed on a 7890B GC, coupled with an HP-5 ms Ultra Inert capillary column (30 m × 0.25 mm × 0.25 µm) and a 7000C MS (Agilent Technologies, Santa Clara, CA). The GC analysis conditions were: Carrier gas, high-purity helium at a flow rate of 1 mL/min; injection port temperature, 250°C; temperature program, initial column temperature 50°C, held for 5 min, increased to 150°C at 5°C/min, held for 2 min, increased to 270°C at 10°C/min, maintained for 6 min; No shunting. MS analysis conditions: electron impact mode; electron energy 70 eV; ion source temperature 230°C; transmission line temperature 270°C; and quality scanning range 35–400 amu.

The volatile compounds were identified by comparing retention indices (RIs) with those of authentic standards, or mass spectra with reference spectra in the Wiley and NIST14 libraries. The RIs were determined by comparison with a homologous series of alkanes (C_5-C_{30}) and identification was achieved by comparing the mass spectra. The relative quantification of volatile compounds with internal standard (IS) was calculated using the following equation: volatile compound concentration = (volatile compound peak area/IS peak

area) × IS concentration. To compare the contribution of individual volatiles to the overall aroma profile, the relative odor activity value (rOAV) of each volatile was calculated by dividing its concentration by its olfactory threshold in water, obtained from the literature (18).

2.7. Dry sample extraction for UPLC–MS/MS analysis

The freeze-dried tea samples were ground into powder (30 Hz, 1.5 min), then powdered sample (50 mg) was extracted with pre-cooled 70% methanol/water (1,200 µL; −20°C), vortexing for 30 s, every 30 min, repeated five times. After centrifugation at 15984 *g* (or 12,000 rpm with a centrifugal radius of 10 cm) for 3 min, the supernatant was filtered using a microporous filter membrane (0.22 µm) then stored until needed for UPLC–MS/MS analysis.

2.8. UPLC–MS/MS analysis

The sample extracts were analyzed using an UPLC–MS/MS system (ExionLC AD, Sciex, Toronto, Canada).

The UPLC was fitted with an Agilent SB-C18 column (1.8 µm, 2.1 mm × 100 mm). The mobile phases were ultrapure water/0.1% formic acid (A) and acetonitrile/0.1% formic acid (B). The elution gradient was: Initially 5% B, then increased linearly to 95% B at 9 min, held for 1 min, then decreased linearly to 5% B at 11.10 min, held until 14 min. The flow rate was 0.35 mL/min, column temperature 40°C and injection volume 2 µL.

The MS/MS system had an electrospray (ESI) turbo interface (temperature 500°C; ion spray voltage 5,500 V for positive ion mode; −4,500 V for negative ion mode). The ion source gas I, gas II, and curtain gas were set to 50, 60, and 25 psi respectively, and the collision induced ionization parameters were set to high. QQQ scanning used MRM mode with the collision gas (nitrogen) set to medium. Optimization of the clustering potential (DP) and collision energy (CE) enabled determination of the DP and CE of each MRM ion pair. A specific set of MRM ion pairs was monitored, based on the metabolite eluting at any given time.

Identification of metabolites was carried out by comparing their MS2 spectra with a tea database developed in our laboratory (MWDB) and with the human metabolome database.[1] Isotopic signals, repetitive signals containing K^+ ions, Na^+ ions, and NH_4^+ ions, as well as repetitive signals of fragment ions of higher molecular weight substances were removed. Then, the data were normalized to the sample weight, before carrying out statistical analysis.

2.9. Statistical analysis

Three replicates of all samples were analyzed. Data are presented as the mean ± standard deviation and analysis of variance was performed using SPSS 25.0 software. Comparison of means between samples was performed using the Least Significant Difference (LSD) method. The biochemical compositional map of each treatment was plotted using GraphPad Prism 8 (GraphPad Software, San Diego, CA). Principal components analysis (PCA) and supervised orthogonal partial least squares-discriminant analysis (OPLS-DA) were performed using SIMCA 14.1 software (Umetrics, Umeå, Sweden). Heatmaps were produced by Multi Experiment Viewer (version 4.7.4) software.

3. Results and discussion

3.1. Effect of drying method on the sensory quality of instant teas

The sensory evaluation and solubility comparison results of instant tea powder prepared by SD and FD are shown in Table 2. FD tea powder was crystalline, whereas SD tea powder was amorphous. The solubility of FD tea powder was higher than that of SD tea powder, indicating that the two drying methods have different influence on the solid structure of tea powder. Drying with SD turned black tea powder brown and jasmine tea powder gray, indicating the existence of heat-induced damage to the tea components. The overall sensory score of SD green tea powder was slightly lower than that of FD green tea powder due to lower solubility of the former, however, the two drying methods had little effect on the color of green tea powder. Increasing the inlet temperature of SD can decrease the solubility of the resulting tea powder (19). Increasing the temperature from 145°C to 165°C increased the a^* value by 40% and decreased the L^* value by 5% (19), i.e., the tea powder darkened at higher inlet temperatures. Therefore, to minimize color changes in tea powder, the SD inlet temperature in drying procedure should be reduced while ensuring spray efficiency.

The instant tea via two drying methods was observed totally different after redissolution in water. As for liquor color, FD tea solution remained normal red color, whereas SD tea solution was reddish-brown. In addition, the aroma of all three FD tea infusions was better than the SD infusions. As for aroma, SD tea had the same aromas as the corresponding FD, but with lower intensity. Similarly, the taste quality of the FD tea was better than that of the SD as for taste. SD green tea was more bitter, with the lowest score, and SD black and jasmine tea were more astringent. FD retained more flavor and bioactive compounds in instant green tea (20), whereas that of SD tea was much weaker (21). Overall, SD produced instant tea with a browner color, lower solubility, weaker aroma and a stronger bitter taste. FD instant tea maintained the flavor quality of the teas and all sensory, thus were better than SD ones. Black tea was more stable in quality changes between two drying methods. Green tea liquor color can be well maintained while its taste deteriorates much after SD. Jasmine tea liquor color can also be well maintained, while its aroma deteriorates much more after SD. Therefore, jasmine tea must be produced from FD to maintain its characteristic aroma.

The two drying methods had significant effect on the brightness (L^*), red-green balance (a^*), and yellow-blue balance (b^*) of the instant tea solutions (Supplementary Figure S1). SD significantly increased L^* for IBT solution, but significantly decreased a^* and b^* (Supplementary Figures S1A–C), i.e., SD reduced the redness and yellowness of tea solution and decreased its quality, which is in agreement with the sensory evaluation results. SD significantly increased L^* for IJT solution, same as IBT and IGT. However, a^* and

1 http://www.hmdb.ca

TABLE 2 Sensory evaluation results of instant tea with different drying methods.

Tea varieties*	Instant tea powder			Instant tea infusion					
	Appearance	Solubility	Score	Liquor color	Score	Aroma	Score	Taste	Score
FD-Black tea	Red, uniform, crystalline	High	84	Red, little bright	87	Sweet, little high	88	Mellow, little sweet	88
SD-Black tea	Reddish brown, uniform, powdery	Low	82	Little red, little bright, clear	82	Little sweet	83	Less mellow, less sweet	84
FD-Green tea	Yellow green, uniform, crystalline	High	85	Green yellow, little bright	84	Little characteristic tea aroma	85	Less mellow, with steamed tea flavor	84
SD-Green tea	Yellow green, uniform, powdery	Low	84	Green yellow, little bright	85	Less characteristic tea aroma	81	Little coarse and astringent, bitter	79
FD-Jasmine tea	Yellow, uniform, crystalline	High	85	Yellow, little bright	88	Flowery, rich	89	Less mellow	87
SD-Jasmine tea	Yellow with gray, uniform, powdery	Low	83	Yellow, less bright	87	With flowery note	83	Less mellow, with astringent taste	82

*Tea varieties are the instant teas prepared from three tea varieties using two drying methods, namely spray-drying (SD) and freeze-drying (FD).

b^* increased significantly, i.e., the redness and yellowness of IJT solution increased, unlike IBT and IGT. SD significantly increased the L^* of IGT and significantly decreased a^* and b^*, reducing the redness and yellowness (Supplementary Figures S1A–C), but increasing the greenness, which is in agreement with the sensory evaluation results. Overall, SD reduced the color quality of IBT and IJT, but maintained the color quality of IGT solution.

3.2. Effect of drying method on the chemical components related to the quality of instant teas

SD and FD had significantly different effects on the content of tea polyphenols, amino acids, and caffeine in the three instant teas (Figure 1). The contents of tea polyphenols, amino acids and caffeine in IBT after SD were significantly lower than that after FD. SD significantly reduced the amino acids of IGT (Supplementary Figure S1D), but significantly increased the tea polyphenol and caffeine contents (Supplementary Figures S1E,F), which was consistent with the stronger bitterness and astringency of SD-GT. SD significantly decreased the content of amino acids in IJT, but significantly increased the contents of tea polyphenols and caffeine, same as IGT. Therefore, SD significantly reduced the contents of the main quality-related chemical components of IBT, compared with FD. Although SD increased the contents of tea polyphenols and caffeine in IGT and IJT, it also consequently strengthened their undesirable bitter taste.

SD and FD had significant but slightly different effect on the catechins composition of the three instant teas. SD had no significant effect on the GC content of IBT (Figure 1A), but reduced those of the other seven catechins compared with FD. For IGT (Figure 1C), the concentrations of C and GCG under FD were significantly higher than those after SD, but the concentrations of EC, EGC, CG, ECG and EGCG increased significantly after SD. The increased content of five catechins is consistent with the increased content of tea polyphenols and indicates that limited catechins oxidation occurred during SD. Neither treatment had significant effect on the GC content. Neither treatment had a significant effect on the C and CG contents of IJT (Figure 1E), whereas those of GC and EGC were higher after FD and those of EC, EC, GGC and EGCG were higher after SD. The increased astringency of IGT and IJT after SD is consistent with the increased contents of the astringent galloyl ester catechins (ECG and EGCG). The above analysis indicates that the composition changes under thermal production is complicated, but from sensory scores FD is more preferable for instant tea production.

To further analyze the effect of the temperature differences between FD and SD on the quality of instant tea powder, the generation of TFs was compared between the two treatments (Figures 1B,D,F). The concentration of four TFs in IBT after SD was lower than after FD (Figure 1B). TFs are sensitive to high temperature, and their concentration decreases with increased extraction, concentration and drying temperatures (22). In this study, since the SD temperature was much higher than that of FD, the former resulted in a greater loss of TFs. TFs appear to be further oxidized and polymerized to form thearubigins and theabrownins, thereby reducing the TF content after SD. However, the TF content after SD was higher in IGT and IJT than that after FD. Therefore, drying temperature is an important factor affecting the quality of IGT. As temperatures exceed 50°C, the concentration of catechins decreases and the loss of catechins is about 4% heating to 90°C (23). It indicates that the oxidation of catechins is accelerated by the thermal effect of SD compared with the lower treatment temperature of FD, which result in increased content of TFs. Under thermal processing like SD, catechins are easy to be oxidized and polymerized into TFs (23). Although they are still flavonoids, the bioactivity and the sensory quality have changed. To better maintain the quality attributes of three raw tea, FD is more preferable for instant tea production to preserve the flavonoids compositions.

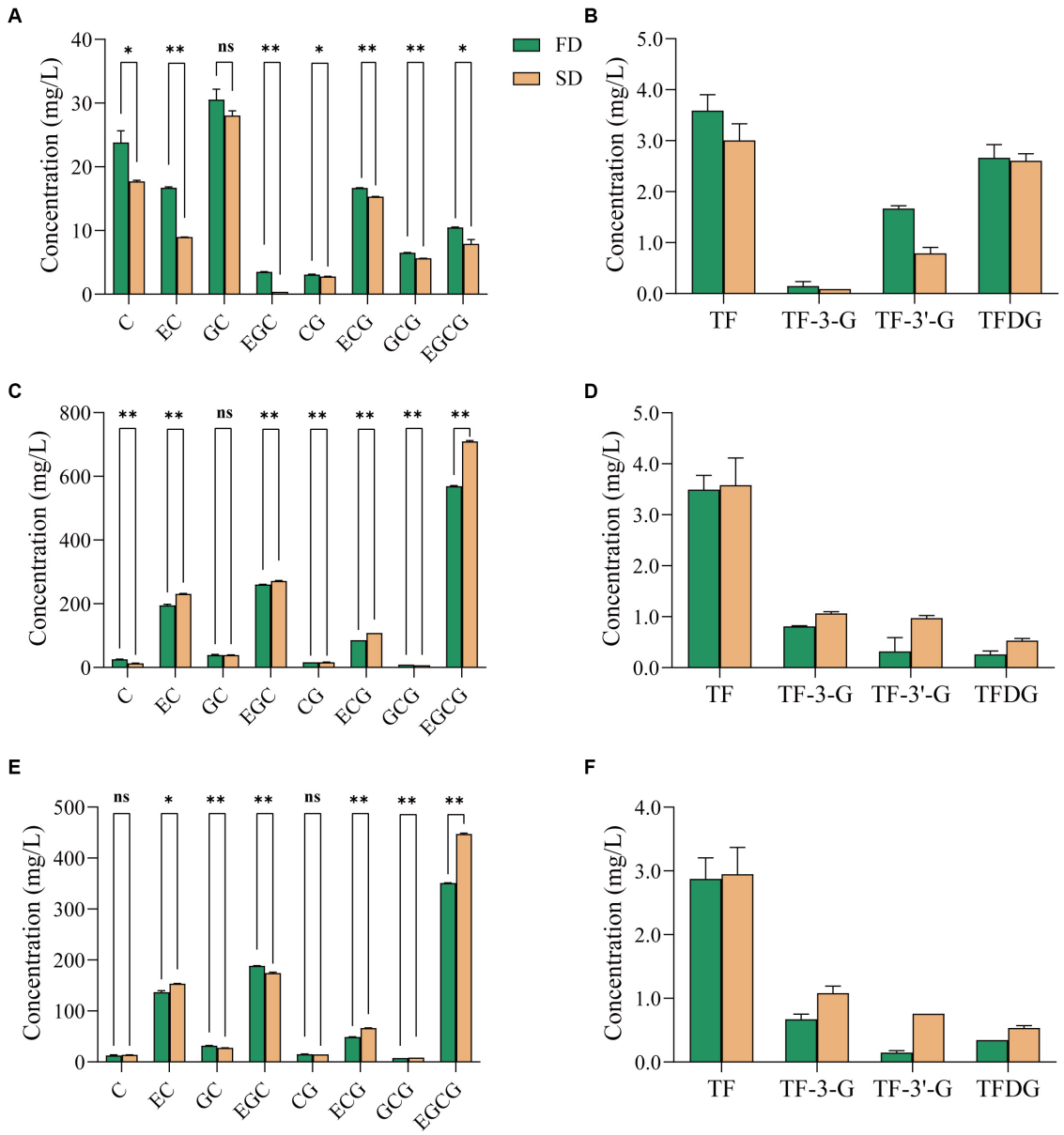

FIGURE 1
Effect of different drying methods on the content of catechins and theaflavins in instant tea powder. **(A,B)** Black tea. **(C,D)** Green tea. **(E,F)** Jasmine tea. FD, freeze drying; SD, spray drying.

3.3. Characterization of the chemical composition of instant teas made from different raw tea materials

Selection of suitable raw tea materials is essential to produce high quality instant tea, because of the differences in biochemical compositions in different tea plant varieties, growing regions, and harvest seasons (8, 24), as well as the different leaching rates of the various biochemical components from the leaves during infusion (25). The biochemical composition of the green, black and jasmine tea used here are shown in Supplementary Table S1. GT had the highest content of total polyphenols, amino acids, and caffeine, followed by JT and BT. The GC concentration was highest in BT, followed by JT and GT. The most abundant catechin in BT was EC (2.34 mg/g) and that in GT and JT were EGCG (82.32 and 59.70 mg/g, respectively). The content of ester catechins and non-ester catechins in BT was 2.38 and 5.59 mg/g respectively, a ratio of 1:2.35. The ester/non-ester ratio in GT was 1.9:1 and that of JT was 2.1:1. The lower catechin content of BT than those of GT and JT indicates that the catechins in (fermented) BT are more extensively oxidized into high molecular weight tea pigments. BT contained the highest content of the four TFs (2.69 mg/g, or 0.27%), an indicator of superior quality to bulk black tea (~0.2% TFs). JT was the second highest, at 0.33 mg/g of TFs and GT was the lowest at 0.163 mg/g. The low TF content in jasmine and green tea could be related to slow catechin oxidation under hot working conditions during processing.

In total, 878 primary metabolites (Supplementary Figure S2A) and 565 flavonoids (secondary metabolites; Supplementary Figure S2B)

were detected in the tea samples and displayed in heatmaps. Amino acids and derivatives accounted for 43.05% of the metabolites, followed by lipids (20.27%), organic acids (15.26%), and phenolic acids and tannins (0.69%) (Supplementary Figure S2A1). Flavonoids accounted for 93.32% of the polyphenols, followed by tannins (7.16%) and phenolic acids (0.35%) (Supplementary Figure S2A2). Lipids were abundant in raw tea, but decreased in both FD and SD instant tea, which can be attributed to their low water solubility (Supplementary Figure S2A1). Other primary metabolites were essentially retained in instant tea (Supplementary Figures S2A,B). Raw GT contained more flavonoids, and more was retained in IGT than in IJT and IBT (Supplementary Figure S2B).

The cluster analysis of primary metabolites (Figure 2A) showed that the raw teas had marked compositional differences. Their clusters were well separated. There was greater similarity between SD and FD instant teas of each tea variety than among the three varieties of raw tea (Figure 2A). The mixed quality control samples were clustered in the center of the principal component analysis (PCA) score plot, which indicated that the tea extraction process and LC-MS analysis were consistent and reliable. In addition, in the PCA score plot, GT and JTwere closely clustered, and GT-FD, GT-SD, JT-FD and JT-SD were closely clustered (Figure 2C). This is to be expected, as jasmine tea is made from green tea leaves with added jasmine flowers to impart a flower-like aroma. Essentially, SD and FD had little effect on the primary metabolite composition of IGT and IJT. However, BT was not only well separated from GT, JT, GT-FD, GT-SD, JT-FD and JT-SD, but also from BT-SD and BT-FD (Figure 2C). SD and FD significantly changed the primary metabolite composition of IBT from that of raw BT.

In contrast to the primary metabolites, the differences in flavonoids content (secondary metabolites) among the three tea varieties was relatively large (Figure 2B) compared with the differences in primary metabolites. Raw black, green and jasmine tea were similar to their corresponding instant teas (Figure 2B). The close clustering of SD and FD instant tea flavonoids compositions of the three varieties of tea was similar to that of primary metabolites. In the PCA score plot, GT and JT were separated by 45.46% on PC1and 14.77% on PC2 (Figure 2D), but the separation was smaller than that from BT. The PC1 separation (45.46%) clearly separated BT and IBT from both green and jasmine tea and their corresponding instant teas (Figure 2D), indicating that the flavonoids composition can be used to differentiate black tea from green tea and jasmine tea, whereas the primary metabolite composition cannot.

During its original processing, raw green tea is steamed to inactivate endogenous enzymes, such as polyphenol oxidase (PPO) and peroxidase (POD). In contrast, black tea is not steamed, so PPO

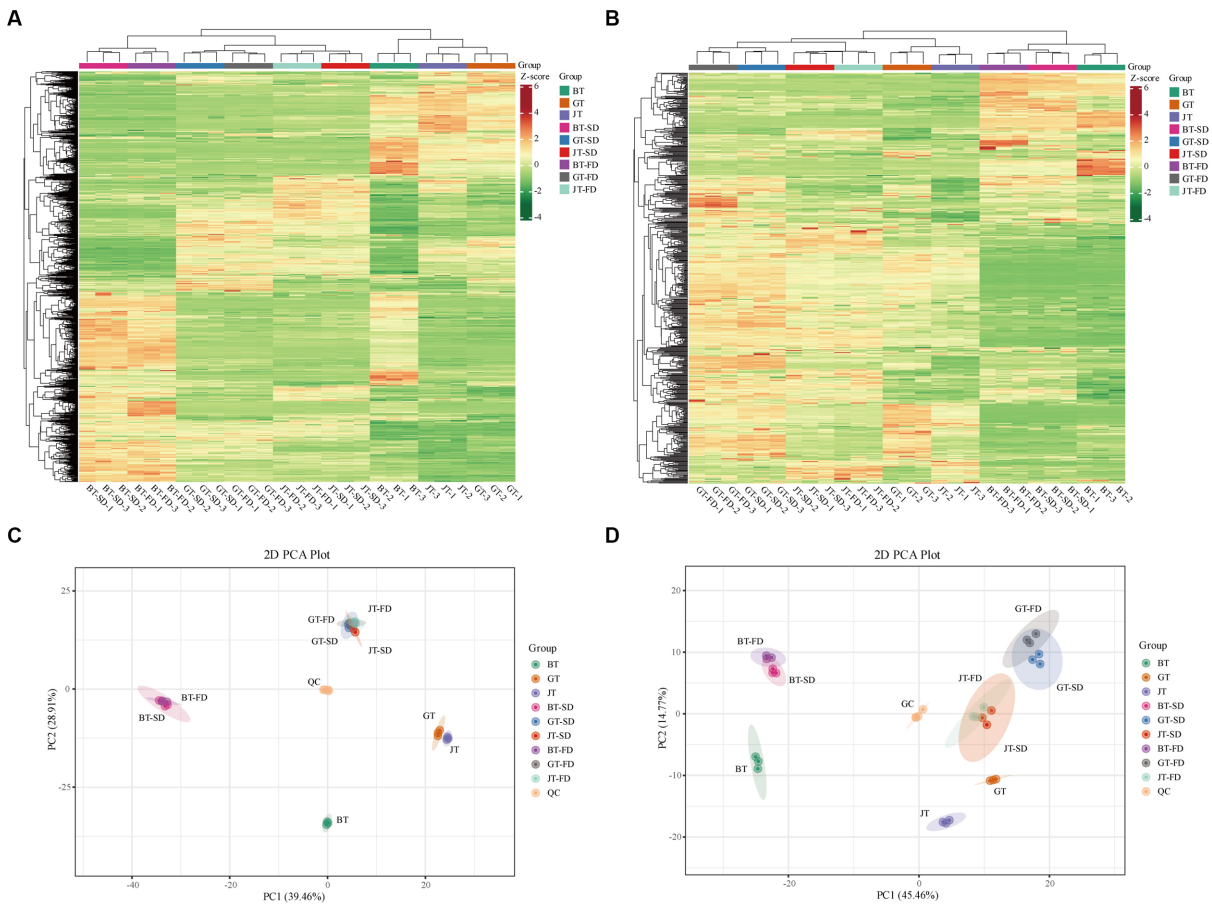

FIGURE 2
The cluster analysis and principle compound analysis of the metabolites in raw tea materials and instant tea. **(A,C)** Primary metabolites. **(B,D)** Flavonoids.

and POD can catalyze marked changes in flavonoids composition, transforming catechins (flavan-3-nols) into tea pigments (TFs, thearubigins, and theabrownins) (26, 27). To improve understanding of the mechanism of quality changes to instant tea resulting from SD and FD, subsequent work should focus on changes in flavonoids composition.

3.4. Comparison of the flavonoid composition of the different instant teas

OPLS-DA modeling was applied to the LC-MS datasets to determine which metabolites were significantly changed during the production of instant tea from different raw tea materials. After selecting the differential variables by removing the irrelevant differences, a score map of the three different raw teas was constructed (Supplementary Figure S3A). Each tea variety was clearly separated from the others, with the BT triplicate samples all grouped toward the upper right, the GT triplicate samples all grouped toward the upper left and the JT triplicate samples grouped toward the lower region. The groupings and separations were similar in the maps of the BT-SD, GT-SD and JT-SD instant teas (Supplementary Figure S3B), as well as the BT-FD, GT-FD and JT-FD instant teas (Supplementary Figure S3C). The OPLS-DA score maps showed wider separations among BT, GT and JT than was obtained from the PCA score plot.

The above OPLS-DA models were then used to construct an S-plot (Supplementary Figures S3D–F), to provide a graphical projection of specific compounds. Generally, metabolites that are far from the plot origin contribute more to the separation among different samples, and the metabolites marked as red dots at the lower left and upper right corners are significant, with variable importance in projection (VIP) values exceeding 1. In total, there were 309, 322, and 326 significantly different metabolites contributing to the separations among raw tea, SD and FD samples, respectively. Compared with PCA, OPLS-DA magnified the separation between groups, which facilitates the discovery of differential metabolites (28). These results indicate that OPLS-DA of flavonoids can be used to differentiate the three different tea varieties, either as raw tea materials or as instant teas.

SD and FD had significantly different effects on the flavonoid composition of black tea (Figure 3A1). BT-SD was separated from BT-FD. In addition, an S-plot was used to screen the differential metabolites between BT-SD and BT-FD, using VIP value analysis (Figure 3B1), and 224 metabolites with VIP > 1 were found. Of these, 76 differential metabolites with VIP > 1 and $p < 0.05$ were found between BT-SD and BT-FD (Figure 4A). Heatmap analysis characterized the relative content of the differential metabolites, of which 36 were more abundant in SD black tea and 40 were more abundant in FD black tea. Compared with FD, SD effectively protected the GCG (decrease), CG (decrease) and isoquercitrin (decrease) in black tea from being hydrolyzed to gallic acid (increase) and quercetin (increase).

Similar results were obtained by comparing GT-SD with GT-FD and JT-SD with JT-FD. Comparing the flavonoids in green tea, 244 metabolites with VIP > 1 were found by OPLS-DA and 109 metabolites with VIP > 1 and $p < 0.05$ were recognized as differential metabolites between GT-SD and GT-FD (Figures 3A2,B2), of which 52 were more abundant in SD green tea and 57 were more abundant in FD green tea (Figure 4B). Compared with FD, SD effectively promoted TFDG (decrease), GCG (decrease), and TF-3-G (decrease) in IGT. Comparing the flavonoids in jasmine tea, 239 metabolites with VIP > 1 were recognized by OPLS-DA and 88 metabolites with VIP > 1 and $p < 0.05$ were recognized as differential metabolites between JT-SD and JT-FD (Figures 3A3,B3), of which 64were more abundant in SD green tea and 24 were more abundant in FD green tea (Figure 4C). Compared with FD, SD effectively protected TF-3-G (decrease), EC (decrease), C (decrease), and EGCG (decrease) in raw JT from being hydrolyzed to GC (increase).

The changes in TFDG, and TF-3-G in GT and JT confirmed that the oxidation of catechins was accelerated by the high temperature of SD compared with the lower treatment temperature of FD, resulting the increase of TFs. FD is more suitable for instant tea production from green and jasmine tea. Important quality attributes for BT are the content of tea pigments and aroma (29). The hydrolysis of some flavone glycosides influences the appearance, color and aroma of black tea (6). Therefore, unlike GT and JT, changes in the chemical composition of BT after SD treatment appear to improve its sensory quality, compared with FD treatment.

3.5. Effect of SD and FD treatments on volatile profiles of instant teas

A total of 177 volatile compounds were detected in the three raw tea materials and their corresponding instant teas, permitting analysis of the influence of chemical compositional changes on the overall flavor. These compounds included 35 alcohols, 28 aldehydes, 39 ketones, 39 esters, 28 alkenes, six heterocyclic compounds, and two acids (Supplementary Figure S4). Comparing the three raw tea varieties, JT was clearly the most abundant in volatile compounds, followed by BT, with GT the least abundant (Supplementary Figure S4A). The same order of volatile compound abundance applied to their SD and FD instant teas. The main components in the three tea varieties were different, with aldehydes (36.06%) the major compound class in BT, ketones (37.09%) in GT, and esters (51.53%) in JT (Supplementary Figure S4B). This indicates that during the scenting process of raw GT with jasmine flowers, raw GT absorbs the floral aroma, thus the content of aroma compounds is much more abundant than BT and GT. For instant tea, using scented teas like jasmine tea can facilitate the production of fragrant tea.

After drying, the main volatile components in the JT-SD and JT-FD were still esters (48.31 and 50.65%, respectively), those in BT-SD were still aldehydes (36.42%), and those in GT-FD were still ketones (37.30%) (Supplementary Figure S4B). However, the main volatile components in BT-FD were alcohols (34.93%), and those in GT-SD were esters (34.21%). Although both SD and FD teas contained less esters and alcohols than the corresponding raw teas, FD retained more aroma compounds than SD for all three tea varieties. The low temperature of FD reduces evaporation and degradation of aroma compounds (21), compared with the high temperature of the SD tower, i.e., FD is more suitable for producing scented instant teas.

After literature and database matching, 49 aroma compounds were identified (Supplementary Table S2) and OAV analysis was used to compare the contribution of each compound to the overall tea aroma. The 15 most abundant volatiles were benzyl acetate (0.03–35.55 μg/g), methyl benzoate (0.00–8.94 μg/g), linalool

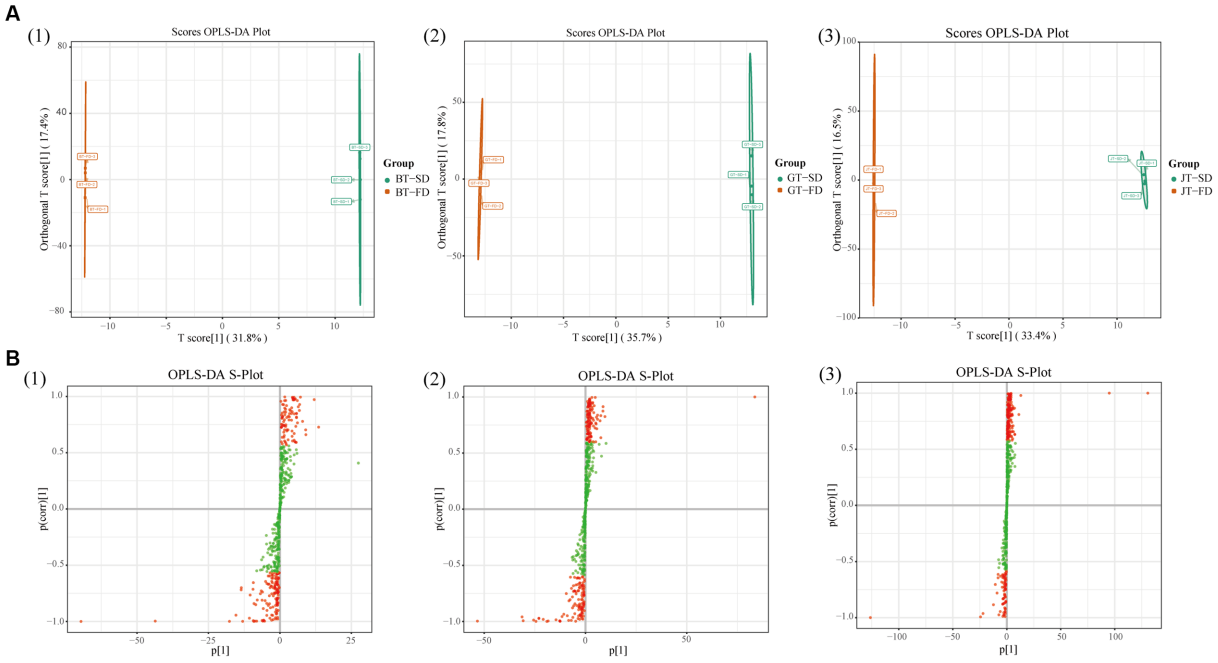

FIGURE 3
Multivariate statistical analysis of non-volatile compounds under different drying methods. Score scatter plots for the OPLS-DA models **(A)**: BT-SD vs. BT-FD; GT-SD vs. GT-FD; JT-SD vs. JT-FD; S-plots of the OPLS-DA models **(B)**: BT-SD vs. BT-FD; GT-SD vs. GT-FD; JT-SD vs. JT-FD.

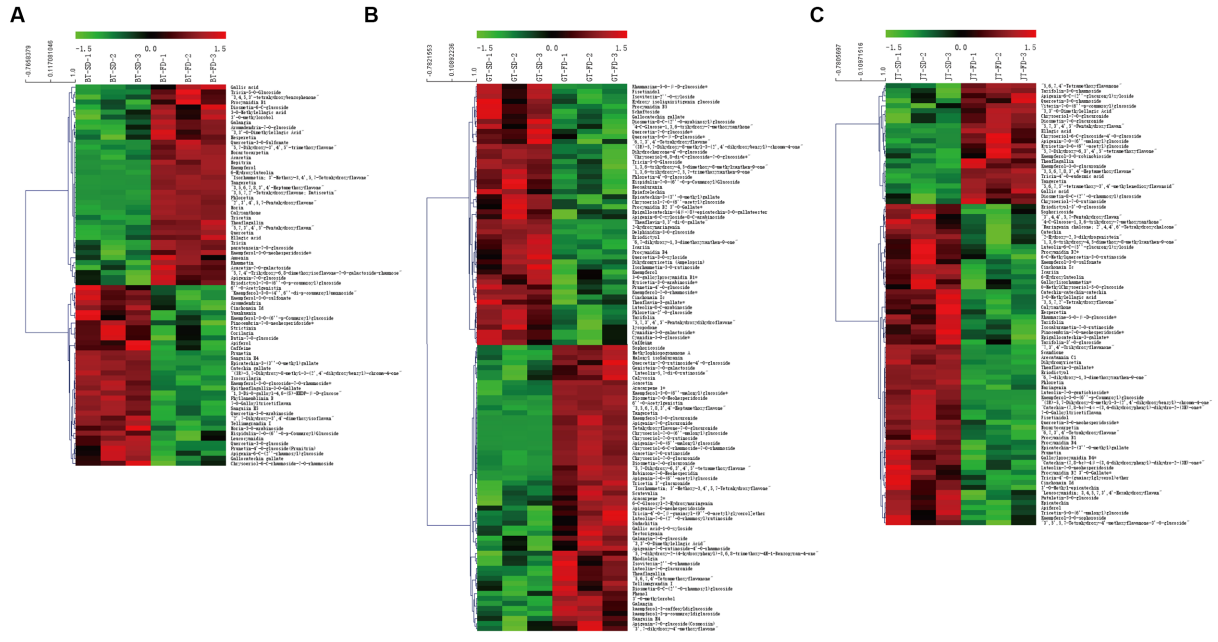

FIGURE 4
Heatmaps of key aroma compounds with VIP > 1 and $P < 0.05$ for the OPLS-DA models. Heatmaps of key aroma compounds with VIP > 1 and P < 0.05 for the OPLS-DA models. **(A)**: BT-SD vs. BT-FD; **(B)**: GT-SD vs. GT-FD; **(C)**: JT-SD vs. JT-FD.

(0.01–8.45 μg/g), benzaldehyde (0.25–7.88 μg/g), (*E*,*E*)-2,4-heptadienal (0.22–6.69 μg/g), methyl salicylate (0.05–5.56 μg/g), phenylethyl alcohol (0.14–4.18 μg/g), geraniol (0.04–3.90 μg/g), neral (0.01–3.90 μg/g), 3,5-octadien-2-one (0.06–3.73 μg/g), benzeneacetaldehyde (0.04–3.27 μg/g), benzyl alcohol (0.17–2.83 μg/g), (*Z*)-3-hexenyl acetate (0.01–2.54 μg/g), indole (0.01–1.56 μg/g) and (*E*)-2-octenal (0.02–1.03 μg/g) (Supplementary Table S2). Apart from benzyl alcohol, these major volatiles were all more abundant in the raw tea materials than in the corresponding instant teas and were more abundant in FD teas than SD teas, further elucidated that FD reduced evaporation and degradation of aroma compounds compared with SD.

The main volatiles have different odor thresholds, so their concentrations in tea infusions do not necessarily match their relative abundances. To compare the contribution of each compound to the overall tea aroma, GC–MS combined with OAV analysis identified nine compounds with rOAVs >1 (Table 3), namely *trans-β*-damascenone, linalool, benzeneacetaldehyde, geraniol, nonanal, methyl salicylate, safranal, neral, and (*Z*)-3-hexenyl acetate. The rOAVs of *trans-β*-damascenone (40.00–1200.00), linalool (0.36–768.82), benzeneacetaldehyde (0.06–16.39), geraniol (0.03–10.42), nonanal (0.55–4.89) and methyl salicylate (0.00–2.78) were the highest of the nine compounds, indicating that they are major contributors to the aroma of the three tea varieties and their corresponding instant teas.

Of these aroma compounds, *trans-β*-damascenone has the lowest odor threshold (0.002 μg/L) and its rOAV in BT is higher than those in GT and JT, contributing a strong "rose" fragrance and the main contributor to the aroma of black tea (31). Geraniol, nonanal, and neral are major floral and fruity volatiles in black tea (31, 32), and in this study their rOAVs in black teas were higher than those in jasmine and green teas. Safranal contributes the woody aroma characteristic of souchong and congou black tea (33), and it had the highest rOAV in BT, followed by JT, GT and their instant teas. This indicated that these four floral and fruity compounds were well-retained in BT, JT and GT, but efficiently released from the instant tea. Again, FD teas retained much more of these volatiles than SD teas, further evidence that FD reduces evaporation and degradation of aroma compounds, compared with SD.

Linalool has a low odor threshold (0.22 μg/L) and a sweet floral note and its rOAVs in JT and IJT were higher than those in black and green teas (32). Linalool has the highest relative abundance in jasmine tea, making it the main flavoring component (34), indicating that scenting with jasmine flowers increases the content of linalool well above that in black tea. Methyl salicylate, another jasmine flower component is well-absorbed by the tea leaves (34), has the aroma of holly leaves and mint and its content was higher in JT, followed by BT and their instant teas. (*Z*)-3-Hexenyl acetate is also present in jasmine tea and its content was higher in JT and its instant teas (Table 3). Therefore green tea absorbs linalool, methyl salicylate and (*Z*)-3-hexenyl acetate released from jasmine flowers during scenting, and this greatly strengthened the floral aroma of jasmine tea, however, their content decreased during instant tea preparation, weakening its floral aroma.

In general, BT and its instant teas contained the most floral and fruity aroma compounds, especially *trans-β*-damascenone, geraniol, nonanal, and neral. JT and its instant teas contained the much more floral linalool and fresh methyl salicylate and (*Z*)-3-hexenyl acetate. GT and its instant teas contained far less aroma compounds than BT and JT. Instant tea preparations contained less of these aroma compounds than the raw teas, but FD reduced evaporation and degradation of aroma compounds compared with SD.

3.6. Correlation analysis between flavonoid content and volatile profile of different raw tea materials

Since flavonoids have been confirmed to contribute to tea aroma (6, 35) and OPLS-DA can differentiate between the aroma profiles of IBT, IGT and IJT, changes in flavonoid content between SD and FD samples may contribute to the aroma of the instant teas. Differential metabolite analysis with VIP values and fold-change was used to generate volcano plots of the increased and decreased differential metabolites (Supplementary Figure S5).

Comparing BT-SD and BT-FD, found 76 significant differential flavonoids, of which 40 increased and 36 decreased, respectively (Supplementary Figure S5A). The above limits of fold-change found 20 significant differential metabolites between FD and SD instant black teas (Figure 5A1), namely, 6 glycosylated flavonoids, 12 flavones and 2 flavon-3-ols (procyanidin B1 and GCG). Of these, 14 were more abundant, including 10 non-glycosylated flavonoids (3,5,6,7,8,3,4-heptamethoxyflavonenepitrin, tangeretin, phloretin, quercetin, morin and isorhamnetin, 2′,3′,4′,5,7-pentahydroxyflavone, 6-hydroxyluteolin, norartocarpetin, datiscetin) and six were less abundant, including three glycosylated flavonoids (heterophylliin A, Castanoside B and kaempferol-3-*O*-glucoside-7-*O*-rhamnoside).

To statistically analyze the relationship between the volatiles with rOAV>1 and the content of the top ten differential flavonoids, Pearson's correlation coefficient was calculated and used to generate a correlation heatmap (Figure 5A2). Top ten abundant non-glycosylated flavonoids positively were correlated with the contents of six aroma compounds, linalool, geraniol, nerol, *trans-β*-damascenone, (*Z*)-hexenyl acetate, and methyl salicylate. Three glycosylated flavonoids, less abundant ones, were negatively correlated with the contents of the above six aroma compounds. This suggests that the less-abundant glycosylated flavonoids are hydrolyzed or degraded during drying stage of instant tea, resulting in the loss of glycosylated aroma compounds and gains of the corresponding non-glycosylated flavonoids. During the withering stage of congou black tea processing, the content of flavones, flavonols and flavonoid polymers (mainly consisting of TFs) increased, whereas hydrolysis of flavonoid glycosides mainly occurred during the rolling stage (35). The thermal stability of flavonoids influenced their final content, and glycosylated flavonols are less sensitive to heat treatment than aglycon ones (35). Drying stage therefore is crucial for the final aroma of instant tea.

Comparing GT-SD and GT-FD found 109 significant differential flavonoids, of which 57 increased and 52 decreased (Supplementary Figure S5B). Of the 20 significantly different flavonoids, there were 17 glycosylated flavonoids, 2 flavones and 1 flavon-3-ol (TFDG). Eighteen flavonoids were more abundant, including three non-glycosylated flavonoids (6"-*O*-acetylgenistin, arteanoflavone, tangeretin), and two flavonoids were less abundant including two glycosylated flavonoids (narcissin and reynoutrin) (Figure 5B1). From correlation analysis (Figure 5B2), three more abundant non-glycosylated flavonoids were positively correlated with the contents of linalool, geraniol, nerol, *trans-β*-damascenone, (*Z*)-hexenyl acetate, methyl salicylate and neral. Two glycosylated flavonoids, less abundant ones, were negatively correlated with the contents of the above seven aroma compounds.

Comparing JT-SD and JT-FD found 88 significant differential flavonoids, of which 24 increased and 64 decreased (Supplementary Figure S5C). Of the 20 significantly different flavonoids, there were 10 glycosylated flavonoids, nine flavones and one flavon-3-ol (TFDG). Eight flavonoids were more abundant including three non-glycosylated flavonoids (3,5,6,7,8,3″,4- heptamethoxyflavone, tangeretin and arteanoflavone), and 12 flavonoids were less abundant, including five glycosylated flavonoids (lonicerin, 3′,5′,5,7-tetrahydroxy-4′-methoxyflavanone-3'-*O*-glucoside, luteolin-6-*C*-(5″-glucuronyl) xyloside, patuletin-3-*O*-glucoside and luteolin-7-*O*-gentiobioside) (Figure 5C1). From correlation analysis, three increased non-glycosylated

TABLE 3 OAV analysis of volatiles in the instant teas with different tea varieties and drying methods.

No	Compound	Odor description[a]	Odor type[b]	Odor threshold in water (μg/L)[c]	RI	rOAV								
						BT[¶]	GT[¶]	JT[¶]	BT-SD[§]	GT-SD[§]	JT-SD[§]	BT-FD[§]	GT-FD[§]	JT-FD[§]
Alcohols														
1	Linalool	Floral, sweet	Floral	0.22	1087.902	237.27	45.00	768.82	1.84	0.36	24.41	90.75	22.70	161.84
2	Geraniol	Rose-like, sweet, honey-like	Floral	7.5	1274.734	10.42	0.52	0.87	0.09	0.03	0.04	1.20	0.19	0.21
Aldehydes														
3	Benzeneacetaldehyde	Floral, rose, cherry-like	Floral	4	1033.525	16.39	1.28	0.23	5.32	0.50	0.41	1.85	0.27	0.06
4	Nonanal	Fatty and herbal smell	Floral	1.1	1115.703	4.89	1.95	1.95	0.82	1.02	0.76	0.95	0.55	1.62
5	Safranal	Woody, spicy, phenolic	Woody	3	1237.296	1.66	1.07	1.14	0.56	0.23	0.24	0.23	0.21	0.21
6	Neral	Lemon	Fruity	53	1264.188	1.47	0.02	0.01	0.00	0.00	0.00	0.02	0.00	0.00
Ketones														
7	*trans*-*β*-Damascenone	Rose, honey	Floral	0.002	1392.773	1200.00	290.00	300.00	137.50	47.50	40.00	325.00	87.50	82.50
Esters														
8	(*Z*)-3-Hexenyl acetate	Green, banana	Green	31	1004.607	0.05	0.29	1.64	0.00	0.01	0.01	0.02	0.02	0.13
9	Methyl salicylate	Fresh, faint gingery, grass and milky	Green	40	1162.976	1.45	0.17	2.78	0.01	0.00	0.09	0.44	0.08	0.65

[a, b, c] Odor descriptions, types and thresholds were found in the database (http://www.flavornet.org/) and literatures (18, 30). [¶]rOAVs of raw tea materials were converted based on a tea to water ratio of 1: 50 for brewing. [§]rOAVs of the instant teas were converted based on a tea to water ratio of 1:200 for brewing.

10.3389/fnut.2023.1236216

10.3389/fnut.2023.1236216

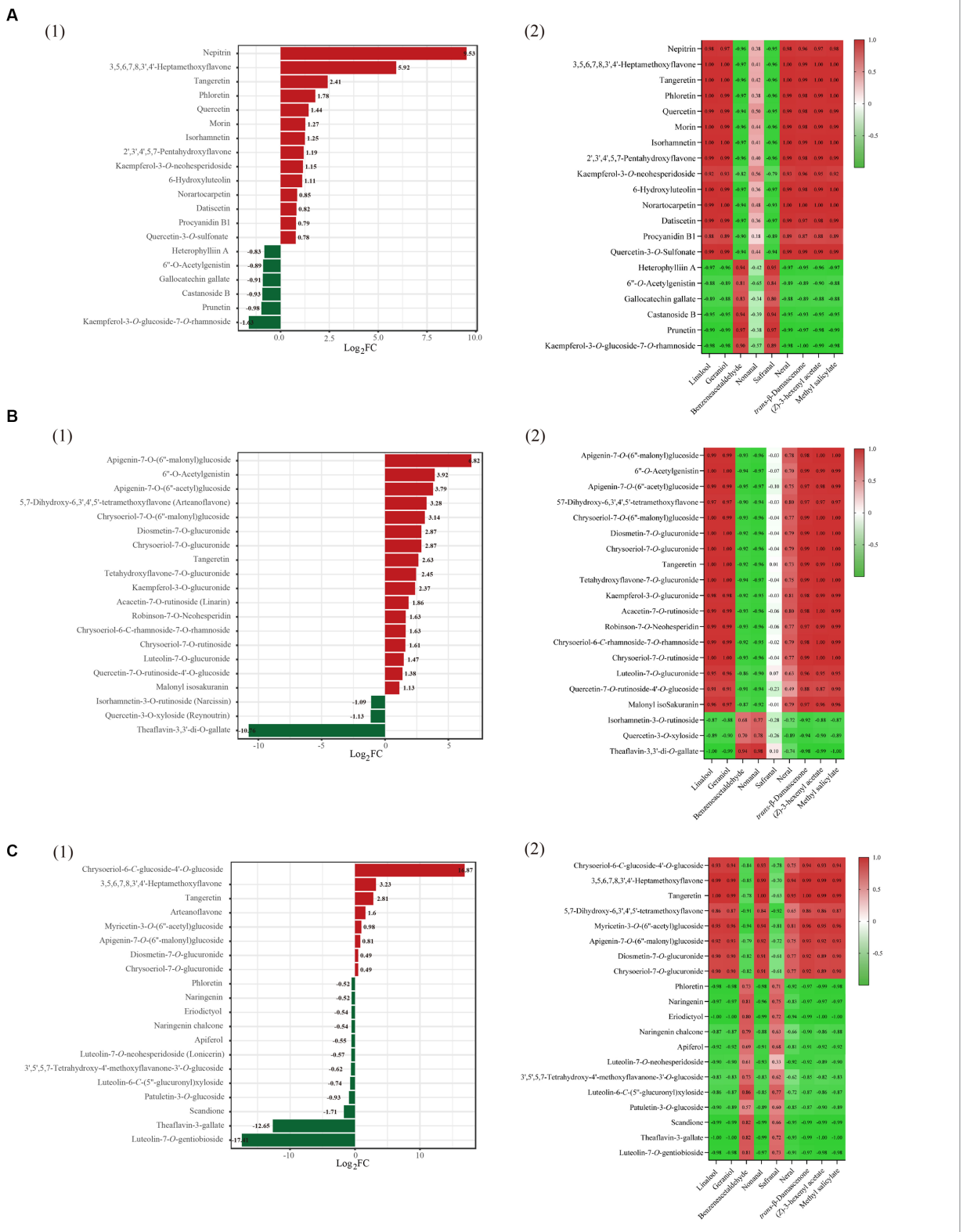

FIGURE 5
Multivariate statistical analysis of flavonoids and volatile compounds in three tea varities. Group **(A)** refers to instant black tea, group **(B)** refers to instant green tea, and group **(C)** refers to instant jasmine tea. Dynamic distribution map of differences in the content of the top 10 substances, up and down, in three instant teas (SD vs. FD) (group 1); heatmap of the pearson correlation coefficient of the volatiles (rOAV > 1) and the content of the top 10 substances (group 2).

flavonoids were positively correlated with the contents of linalool, geraniol, nerol, *trans*-*β*-damascenone, (*Z*)-hexenyl acetate, methyl salicylate, nonanal and neral (Figure 5C2). Five decreased glycosylated flavonoids were negatively correlated with the contents of the above eight aroma compounds.

Many aroma components exist in tea in the form of glycoside precursors, including monoterpene alcohols (linalool, linalool oxides, and geraniol), aromatic alcohols (benzyl alcohol and phenylethanol), and some non-alcoholic volatile aromas such as benzaldehyde and *β*-damascenone (36, 37). These glycosidically bound volatile aromas take more steps than glycosidically bound alcoholic volatiles to release free volatile aromas (38). Besides, a strong acidic condition (pH 2.0) with a high temperature (90°C) favors the hydrolysis of glycosidic bonds (38). From Table 3 we can see that FD instant teas contains more alcohol aromas including linalool and geraniol. From the above results and Supplementary Table S1 we can see that gallic acid content increase from raw tea to drying stage when flavonoids like EGCG and ECG decrease. Flavonoids degrade at different rates during the drying of black tea, because of their thermal instability, for example, luteolin-7-*O*-glucoside is more sensitive to heat treatment than its aglycone form luteolin (39). Anthocyanins and procyanidin A3 are especially unstable and may also be thermally degraded by oxidation and cleavage of covalent bonds (39, 40). This may indicate that the high temperature (over 90°C) in SD accelerates the hydrolysis of flavonoids and glycoside precursors of monoterpene alcohols, both of which form the final aroma of instant tea. Further analysis on the contributions of these changed glycosylated flavonoids to aroma is in need to facilitate instant tea drying. Besides, the correlations between glycosylated flavonoids and aroma compounds during drying of instant tea need further research. In summary, tea flavonoids change markedly during instant tea manufacturing, especially during drying, which contributes directly to the formation of flavor.

4. Conclusion

With an aim to elucidate the impact of drying methods and raw materials on the organoleptic and physicochemical properties of instant tea, we prepared instant teas from three tea varieties using two drying methods, with a focus on the inherent primary and secondary plant metabolites through widely targeted metabolomics. The raw tea materials and the drying methods strongly influenced the quality of instant tea. Sensory evaluation and physicochemical characterization revealed that freeze-drying (FD) can better maintain the sensory quality of instant teas made from black, green and jasmine raw tea materials. All sensory evaluation scores of FD samples were better than spray-dried (SD) instant tea. Black tea was more stable in quality changes between two drying methods. Green tea liquor color can be well maintained while its taste deteriorates much after SD. Jasmine tea liquor color can also be well maintained, while its aroma deteriorates much more after SD. Therefore, jasmine tea must be produced from FD to maintain its characteristic aroma. Chemical compositional analysis found that SD significantly decreased the abundance of the main flavor and quality components of black tea. SD promoted the formation of theaflavins (TFs) at high temperature. Widely targeted metabolomics revealed that the flavonoids composition changed markedly after drying and flavonoids analysis by OPLS-DA helped differentiate black tea from green and jasmine tea. Volatile compositional analysis found that drying to produce instant tea results in loss of tea volatile compounds, but FD retained more of the main floral and fruity compounds in the instant tea than SD. There were major compositional changes in the tea flavonoids during drying procedure of instant tea production, which contributed directly to the formation of the flavor of instant tea. These results provide an practicle method for high-quality instant tea production through choosing proper raw tea material like jasmine tea and lowering down drying temperature with non-thermal technologies like FD.

Data availability statement

The original contributions presented in the study are included in the article/Supplementary material, further inquiries can be directed to the corresponding author.

Author contributions

J-CJ: funding acquisition, investigation, data curation, and writing – original draft. SL: methodology, investigation, data curation, writing – original draft, and writing – review and editing. S-XQ, PT, J-XC, and Y-FC: investigation. Q-SC: writing – review and editing. J-FY: investigation and writing – review and editing. Y-QX: funding acquisition, investigation, and writing – review and editing. All authors contributed to the article and approved the submitted version.

Funding

This research was supported by the Basic Public Welfare Research Program of Zhejiang Province (LGN22C200024), the Key Research and Development Program of Guangdong (2022B0202040002), and the Central Public-interest Scientific Institution Basal Research Fund (Y2023XK11).

Conflict of interest

S-XQ was employed by Eastsign Foods (Quzhou) Co., Ltd. Y-FC was employed by Unibioche Food Tech Co., Ltd.

The remaining authors declare that the research was conducted in the absence of any commercial or financial relationships that could be construed as a potential conflict of interest.

Publisher's note

Supplementary material

The Supplementary material for this article can be found online at: https://www.frontiersin.org/articles/10.3389/fnut.2023.1236216/full#supplementary-material

References

1. Kraujalyte V, Pelvan E, Alasalvar C. Volatile compounds and sensory characteristics of various instant teas produced from black tea. *Food Chem*. (2016) 194:864–72. doi: 10.1016/j.foodchem.2015.08.051

2. Cao QQ, Wang F, Wang JQ, Chen JX, Yin JF, Li L, et al. Effects of brewing water on the sensory attributes and physicochemical properties of tea infusions. *Food Chem*. (2021) 364:130235. doi: 10.1016/j.foodchem.2021.130235

3. Lin S, Jiang Q, Lin Q, Xu Y, Li L, Weng S, et al. The change of aroma during the processing of instant tea of Baiyaqilan. *Food Sci*. (2023)

4. Pastoriza S, Mesías M, Cabrera BC, Rufián-Henares JA. Healthy properties of green and white teas: an update. *Food Funct*. (2017) 8:2650–62. doi: 10.1039/C7FO00611J

5. Li H, Guo H, Luo Q, Wu DT, Zou L, Liu Y, et al. Current extraction, purification, and identification techniques of tea polyphenols: an updated review. *Crit Rev Food Sci*. (2021) 63:3912–30. doi: 10.1080/10408398.2021.1995843

6. Shi J, Yang GZ, You QS, Sun SL, Chen RH, Lin Z, et al. Updates on the chemistry, processing characteristics, and utilization of tea flavonoids in last two decades (2001-2021). *Crit Rev Food Sci*. (2021) 63:4757–84. doi: 10.1080/10408398.2021.2007353

7. He HF, Wei K, Yin JF, Ye Y. Insight into tea flavonoids: composition and chemistry. *Food Rev Int*. (2021) 37:812–23. doi: 10.1080/87559129.2020.1721530

8. Perera G, Amarakoon A, Illeperuma D, Muthukumarana P. Effects of raw material on the chemical composition, organoleptic properties, antioxidant activity, physical properties and the yield of instant black tea. *LWT Food Sci Technol*. (2015) 63:745–50. doi: 10.1016/j.lwt.2015.03.060

9. Li Y, Wang W, Wang J, Hu Y, Ren D, Yi L. Analysis of variations in contents of extractable components and taste quality of Pu-erh raw tea with different brewing cycles. *Food Sci*. (2022) 43:210–3. doi: 10.7506/spkx1002-6630-20210519-237

10. Akbarbaglu Z, Peighambardoust SH, Sarabandi K, Jafari SM. Spray drying encapsulation of bioactive compounds within protein-based carriers; different options and applications. *Food Chem*. (2021) 359:129965. doi: 10.1016/j.foodchem.2021.129965

11. An T, Shen S, Zu Z, Chen M, Wen Y, Chen X, et al. Changes in the volatile compounds and characteristic aroma during liquid-state fermentation of instant dark tea by Eurotium cristatum. *Food Chem*. (2023) 410:135462. doi: 10.1016/j.foodchem.2023.135462

12. Wang C, Li J, Zhang Y, He Z, Zhang Y, Zhang X, et al. Effects of electrostatic spray drying on the sensory qualities, aroma profile and microstructural features of instant Pu-erh tea. *Food Chem*. (2021) 373:131546. doi: 10.1016/j.foodchem.2021.131546

13. Chakraborty R, Saha AK, Bhattacharya P. Modeling and simulation of parametric sensitivity in primary freeze-drying of foodstuffs. *Sep Purif Technol*. (2006) 49:258–63. doi: 10.1016/j.seppur.2005.10.008

14. Tian Y, Zhao Y, Huang J, Zeng H, Zheng B. Effects of different drying methods on the product quality and volatile compounds of whole shiitake mushrooms. *Food Chem*. (2016) 197:714–22. doi: 10.1016/j.foodchem.2015.11.029

15. Chumroenphat T, Somboonwatthanakul I, Saensouk S, Siriamornpun S. Changes in curcuminoids and chemical components of turmeric (*Curcuma longa* L.) under freeze-drying and low-temperature drying methods. *Food Chem*. (2021) 339:128121. doi: 10.1016/j.foodchem.2020.128121

16. Liang S, Wang F, Chen J, Daniel G, Li L, Yin JF, et al. Optimization of a tannase-assisted process for obtaining teas rich in theaflavins from *Camellia sinensis* leaves. *Food Chem X*. (2022) 13:100203. doi: 10.1016/j.fochx.2022.100203

17. Liang S, Wang F, Granato D, Zhong X, Xiao AF, Ye Q, et al. Effect of β-glucosidase on the aroma of liquid-fermented black tea juice as an ingredient for tea-based beverages. *Food Chem*. (2023) 402:134201. doi: 10.1016/j.foodchem.2022.134201

18. Guo X, Ho C-T, Wan X, Zhu H, Liu Q, Wen Z. Changes of volatile compounds and odor profiles in wuyi rock tea during processing. *Food Chem*. (2021) 341:128230. doi: 10.1016/j.foodchem.2020.128230

19. Şahin-Nadeem H, Dinçer C, Torun M, Topuz A, Özdemir F. Influence of inlet air temperature and carrier material on the production of instant soluble sage (*Salvia fruticosa* miller) by spray drying. *LWT Food Sci Technol*. (2013) 52:31–8. doi: 10.1016/j.lwt.2013.01.007

20. Quan V, Vuong JBG, Minh HN, Paul DR. Production of caffeinated and decaffeinated green tea catechin powders from underutilised old tea leaves. *J Food Eng*. (2011) 110:1–8. doi: 10.1016/j.jfoodeng.2011.12.026

21. Roshanak S, Rahimmalek M, Goli SAH. Evaluation of seven different drying treatments in respect to total flavonoid, phenolic, vitamin C content, chlorophyll, antioxidant activity and color of green tea (*Camellia sinensis* or *C. assamica*) leaves. *J Food Sci Tech Mys*. (2016) 53:721–9. doi: 10.1007/s13197-015-2030-x

22. Liang S, Granato D, Zou C, Gao Y, Zhu Y, Zhang L, et al. Processing technologies for manufacturing tea beverages: from traditional to advanced hybrid processes. *Trends Food Sci Tech*. (2021) 118:431 (PA): 431-446–46. doi: 10.1016/j.tifs.2021.10.016

23. Li N, Taylor LS, Ferruzzi MG, Mauer LJ. Kinetic study of catechin stability: effects of pH, concentration, and temperature. *J Agric Food Chem*. (2012) 60:12531–9. doi: 10.1021/jf304116s

24. Dalpathadu KAP, Rajapakse HUKDZ, Nissanka SP, Jayasinghe CVL. Improving the quality of instant tea with low-grade tea aroma. *Arab J Chem*. (2022) 15:104147. doi: 10.1016/j.arabjc.2022.104147

25. Ye D, Zhang L, Sun S, Chen J, Fang T. Production of high-aroma instant tea powder using various novel technologies. *J Food Process Eng*. (2014) 37:273–84. doi: 10.1111/jfpe.12083

26. Sang S, Yang CS, Ho C-T. Peroxidase-mediated oxidation of catechins. *Phytochem Rev*. (2004) 3:229–41. doi: 10.1023/B:PHYT.0000047794.45076.7c

27. Ke L, Xu W, Gao J, Gao G, Wang H, Zhou J, et al. Isolation and characterization of thermo-tolerant polyphenol oxidases in a black tea infusion. *Food Control*. (2021) 119:107465. doi: 10.1016/j.foodcont.2020.107465

28. Zhang K, Ren T, Liao J, Wang S, Zou Z, Ma Y, et al. Targeted metabolomics reveals dynamic changes during the manufacturing process of Yuhua tea, a stir-fried green tea. *Beverage Plant Res*. (2021) 1:1–11. doi: 10.48130/BPR-2021-0006

29. Fan J, Wang Q, Qin D, Fang K, Zhu H, Jiang X, et al. Recent progress in black tea quality and related biochemical factors. *Food Sci*. (2020) 41:246–53. doi: 10.7506/spkx1002-6630-20190217-077

30. Liu Z, Chen F, Sun J, Ni L. Dynamic changes of volatile and phenolic components during the whole manufacturing process of Wuyi rock tea (Rougui). *Food Chem*. (2022) 367:130624. doi: 10.1016/j.foodchem.2021.130624

31. Yin X, Huang J, Huang J, Wu W, Tong T, Liu S, et al. Identification of volatile and odor-active compounds in Hunan black tea by SPME/GC-MS and multivariate analysis. *LWT Food Sci Technol*. (2022) 164:113656. doi: 10.1016/j.lwt.2022.113656

32. Niu Y, Zhang Y, Xiao Z, Zhu J, Zhang F, Chen F. Release effect of aroma compounds of Keemun black tea brewed with deuterium-depleted water with different deuterium content. *LWT Food Sci Technol*. (2023) 173:114382. doi: 10.1016/j.lwt.2022.114382

33. Zeng L, Wang J, Liu Y, Luo L, Ma M. Comparative analysis of quality characteristics of souchong and congou. *Food Sci*. (2016) 37:51–6. doi: 10.7506/spkx1002-6630-201620009

34. Ye Q, Yu W, Zheng S, Zeng X, Chen F, Hao Z. Correlation analysis of moisture content and aroma quality in the scenting process of jasmine tea. *Food Sci*. (2022) 43:266–72. doi: 10.7506/spkx1002-6630-20220322-265

35. Liu F, Wang Y, Corke H, Zhu HK. Dynamic changes in flavonoids content during congou black tea processing. *LWT Food Sci Technol*. (2022) 170:114073. doi: 10.1016/j.lwt.2022.114073

36. Ogawa K, Ijima Y, Guo W, Watanabe N, Usui T, Dong S, et al. Purification of a β-primeverosidase concerned with alcoholic aroma formation in tea leaves (Cv. Shuixian) to be processed to oolong tea. *J Agric Food Chem*. (1997) 45:877–82. doi: 10.1021/jf960543l

37. Zhou Y, Dong F, Kunimasa A, Zhang Y, Cheng S, Lu J, et al. Occurrence of glycosidically conjugated 1-phenylethanol and its hydrolase β-primeverosidase in tea (*Camellia sinensis*) flowers. *J Agric Food Chem*. (2014) 62:8042–50. doi: 10.1021/jf5022658

38. Ho C-T, Zheng X, Li S. Tea aroma formation. *Food Sci Hum Well*. (2015) 4:9–27. doi: 10.1016/j.fshw.2015.04.001

39. Chaaban H, Ioannou I, Chebil L, Slimane M, G'erardin C, Paris C, et al. Effect of heat processing on thermal stability and antioxidant activity of six flavonoids. *J Food Process Pres*. (2017) 41:e13203. doi: 10.1111/jfpp.13203

40. Khanal RC, Howard LR, Prior RL. Procyanidin content of grape seed and pomace, and total anthocyanin content of grape pomace as affected by extrusion processing. *J Food Sci*. (2009) 74:H174–82. doi: 10.1111/j.1750-3841.2009.01221.x

frontiers | Frontiers in Nutrition

TYPE Original Research
PUBLISHED 10 November 2023
DOI 10.3389/fnut.2023.1290221

OPEN ACCESS

EDITED BY
Peng Wang,
Shaanxi Normal University, China

REVIEWED BY
Jianhui Wang,
Changsha University of Science and Technology, China
Jianyin Miao,
South China Agricultural University, China

*CORRESPONDENCE
Zuodong Qin
✉ dong6758068@163.com

RECEIVED 07 September 2023
ACCEPTED 30 October 2023
PUBLISHED 10 November 2023

CITATION
Quan Q, Zhang Y, Nawaz A, Feng L and Qin Z (2023) Effects of taro [*Colocasia esculenta* (L.) Schott] slices on nutritional quality, sensory quality, and shelf life of Chinese pickled and steamed pork belly.
Front. Nutr. 10:1290221.
doi: 10.3389/fnut.2023.1290221

Effects of taro [*Colocasia esculenta* (L.) Schott] slices on nutritional quality, sensory quality, and shelf life of Chinese pickled and steamed pork belly

Qinguo Quan[1], Yexuan Zhang[2], Asad Nawaz[1], Luya Feng[1] and Zuodong Qin[1]*

[1]Hunan Engineering Technology Research Center for Comprehensive Development and Utilization of Biomass Resources, College of Chemistry and Bioengineering, Hunan University of Science and Engineering, Yongzhou, China, [2]School of Food Science and Engineering, Central South University of Forestry and Technology, Changsha, China

This study aimed to investigate the influence of different ratios of taro slices (TS) on the nutritional quality, sensory quality, and shelf life of Chinese pickled and steamed pork belly (CPSPB). The study examined various aspects of CPSPB, including its proximate components, fat oxidation, fatty acid composition, protein hydrolysis, oxidation reaction, and induction period (IP). Additionally, the sensory quality and texture analysis were compared simultaneously. The results showed that the addition of TS to CPSPB significantly improved water and lipid loss ($p < 0.05$), increased the unsaturated/saturated ratio of fatty acids, and reduced lipid and protein oxidation. Additionally, the incorporation of TS extended the IP and enhanced the shelf life of CPSPB. Particularly, the addition of a specific amount of TS (60%) to CPSPB resulted in the highest organoleptic quality. Therefore, these results emphasize the positive impact of TS on the overall quality of CPSPB, highlighting its potential to enhance the nutritional value, sensory attributes, and shelf life.

KEYWORDS

fatty acid, lipid oxidation, protein oxidation, shelf life, *Colocasia esculenta* (L.) schott, pickled and steamed pork belly

1. Introduction

Chinese pickled and steamed pork belly (CPSPB), also known as kou rou in China, holds a significant place as a traditional dish among the Chinese population (1–3). The industry of prepared dishes in China is currently experiencing rapid development in both provincial and urban areas, with a focus on crucial aspects, such as quality, flavor, nutritional safety, traceability, and technical equipment (4). The CPSPB production processes use natural raw materials, mainly pork belly, similar to other traditional meat dishes. These are accompanied by vegetable ingredients like dried mustard, fermented soybean, and taro (3, 5, 6). Chinese pickling aims to enhance the flavor and prolong the shelf life of food by employing various methods (6). Steaming, as a hot processing technique, serves the dual purpose of sterilization and enhancing the formation of aromatic compounds (7). However, it is important to note that commercially available CPSPB currently exhibit variations in quality, have a limited shelf life, and lack

standardized processing methods. Therefore, addressing these issues is of utmost importance to facilitate the efficient industrial production and meet the growing consumer demand for CPSPB.

Taro [*Colocasia esculenta* (L.) Schott] is primarily cultivated in the southern province of China (8–10). Moreover, it is grown in various regions and countries including the Caribbean, Hawaii, the Solomons, American Samoa, Western Samoa, the Philippines, Fiji, Sri Lanka, India, Nigeria, Indonesia, New Hebrides, Tonga, Niue, Papua New Guinea, and Egypt (11). The primary chemical components of it are starch, with smaller amounts of protein and lipids, along with trace mineral elements and vitamins (12). CPSPB with taro slices (TS) is a popular Chinese delicacy. It consists of pork belly, taro slices, and various additives, which are then steamed. The resulting steamed dish offers a delightful taste and a satisfying sensation of fullness. However, there is a lack of published research investigating the effects of TS on CPSPB. Specifically, the impact of TS on the chemical composition of CPSPB, which is closely associated with its nutritional, sensory, and preservative properties, remains unknown.

Frozen meat deteriorates during storage due to the degradation of lipids and proteins, as reported by Ali et al. (13). The oxidation and hydrolysis reactions of these components are critical in determining the quality and shelf life of meat and meat-based products. Oxidative reactions occur during various stages of meat processing, such as mincing, cooking, and salting, as well as during storage and processing of meat and meat-base products. These reactions promote the formation of reactive oxygen species (ROS) and increase the oxidative susceptibility of the end products (14). Therefore, it is important to scavenge ROS, in order to inhibit or suppress lipid and protein peroxidation and oxidation, TS contain antioxidant compounds, such as phenolic compounds (polyphenols chlorogenic acid, catechin, epicatechin, epigallocatechin (flavan-3-01s), gallic acid and proanthocyanidins), resistant starch, and polysaccharides (15, 16), which have the potential to scavenge ROS. Therefore, it is necessary to assess the oxidation of lipids and proteins, including the fatty acid composition of CPSPB to evaluate the effectiveness of TS in meat-based products.

To determine the optimal amount of TS used to interfere with CPSPB nutritional quality, sensory quality, and shelf life. The purpose of this study was to determine the proximate components, fat oxidation, fatty acid composition, protein hydrolysis, and oxidation reaction, as well as the induction period (IP) of CPSPB under the addition of 0%–100% mass ratio TS. The sensory quality and texture analysis of these samples were concurrently compared. In line with this, the findings of this study are intended to serve as a valuable reference for domestic and industrial production, providing insights into the benefits of incorporating TS into CPSPB. Additionally, these results can be utilized as a foundation for expanding the utilization of TS, with potential economic benefits in various applications.

2. Materials and methods

2.1. Raw materials and sample preparation

Taro and pork belly with a lean-to-fat ratio of approximately 1:2 were purchased from a local food market in Yongzhou, Hunan Province, China. They were immediately transported in an ice box to the laboratory within 30 min after purchase. To ensure freshness, the taro and pork belly were stored in a plastic container with crushed ice at the bottom, maintaining a transport temperature of 5°C–10°C. The samples were prepared using traditional Chinese household cooking methods.

Firstly, the fresh pork belly was pre-cooked in boiling water for 2 min using a pork-to-water ratio of 1:5 (w/v). After removing any remaining pig hairs from the skin and rinsing off surface impurities and blood with tap water, approximately 200 grams of pre-cooked pork belly were placed in a bowl and cut into pieces measuring 2.5 cm × 3.5 cm × 0.8 cm (length × width × height). These slices were then pickled for 30 min in a pickling jar containing a solution composed of 2% soy sauce, 2% sugar, 2% salt, and 0.1% monosodium glutamate. Next, the taro was carefully selected, peeled, and then cut into fillets of the same size as the pork belly using a slicing machine (QN-200, Henan Qineng Machinery Equipment Co., Ltd., China). It was important for the taro slices to be of uniform size and show no signs of rot on the surface. Different amounts of taro slices, ranging from 0 to 200 g in increments of 40 g, were combined with 200 g of pork in each sample. Finally, all ingredients were thoroughly mixed to ensure that the sample was well-blended for testing purposes.

The samples were prepared and placed in a pressure cooker (Joyoung, China) for 15 min, where they were subjected to high-pressure steaming on an induction cooker (2,200 W). After the steaming process, the samples were left to cool for 5 min before the pressure cooker was opened and the samples were separated. The cooled samples were then either used for textural profile analysis and sensory evaluation or minced using a mincer (Midea, China) to ensure homogeneity and obtain representative samples for further analysis. Finally, the minced samples were stored at −20°C until analysis.

For all the steaming experiments, seven groups were formed. These groups include: (I) The control group, which consisted of raw pickled pork belly. Following this, (II) CPSPB alone was examined. Subsequently, CPSPB was treated with different concentrations of TS. These concentrations included (III) 20% TS, (IV) 40% TS, (V) 60% TS, (VI) 80% TS, and (VII) 100% TS. For each determination, three replicates were conducted for all the treatments.

2.2. Determination of proximate components

The determination of moisture, crude protein, ash, crude fat, and sodium chloride content followed the guidelines outlined in the AOAC methods (2006) and were followed precisely during the analysis. The standard reference numbers and brief descriptions of the determination methods were as follows: moisture content was determined by oven drying the samples at 105°C by AOAC 950.46. Crude protein was determined using the Kjeldahl method, wherein the nitrogen-to-protein conversion factor of 6.25 was applied, as specified in AOAC 928.08. Ash content was determined by heating 3 g samples in an oven at 550°C until a constant weight was achieved, following the procedure outlined in AOAC 920.153. Crude lipids was determined through Soxhlet extraction, as described in AOAC 991.36. Moreover, NaCl contents was determined by Mohr method (AOAC 935.43, 33.7.10: 2000). The parameters were measured using the appropriate units specified in the standard, such as percentages or milligrams per gram.

2.3. Determination of fatty acids

Total lipids were extracted from minced pork belly using the method of Wu et al. (17) with minor modifications. The minced pork belly was homogenized with a 2:1 chloroform-methanol solution (Tianjin Damao Chemical Reagent Co., Ltd., Tianjin, China) at a final dilution of 10 times the sample volume. The extraction was carried out in a water bath at 60°C for 15 min, followed by filtration. For conversion to methyl esters, a sulfuric acid-methanol solution (12.5%, w/v) (Tianjin Damao Chemical Reagent Co., Ltd., China) was used. The samples obtained were analyzed using a GC7890A gas chromatograph (Agilent) equipped with an autosampler, split/splitless injector, a silica capillary column (DB-23; 30 m length × 0.32 mm id × 0.25 μm film thickness; Agilent), and a flame ionization detector. To calibrate the analysis, a 37-fatty acid methyl ester (FAME) mixed standard (Sigma-Aldrich Co., LLC) was run under the same conditions.

The following GC conditions were used for the experiment: nitrogen was employed as the carrier gas at a flow rate of 9 mL/min and a pressure of 6.6016 psi. The split ratio was set to 5:1. The injector temperature was set to 270°C with an injection volume of 1 μL, while the temperature of the flame ionization detector was maintained at 280°C. The temperature ramp-up procedure was as follows: a five-minute duration at 120°C, followed by an increase to 190°C at a rate of 5°C/min and hold for 12 min. Then, there was a further increase to 210°C at a rate of 2.5°C/min, and the temperature was held at 210°C for 10 min.

2.4. Determination of lipid oxidation

The lipid oxidation coefficient was estimated using peroxide value (POV) determinations and thiobarbituric acid (TBA). The TBA determination method was adapted from Sorensen et al. (18) with minor modifications. To begin, 10 g of the ground sample were homogenized with 50 mL of 7.5% trichloroacetic acid (TCA) solution containing 0.1% ethylenediaminetetraacetic acid (EDTA) using a BRS-500-B homogenizer (Anhui Bojin Instrument Factory, China) at 15,000 rpm for 30 s. Next, a 5 mL filtrate obtained through pipette filtration was transferred to a stoppered plastic tube. After that, 5 mL of 0.02 M TBA aqueous solution was added. The sample was adequately mixed and then incubated in a water bath at 100°C for 1 h. Subsequently, it was cooled down in cold water. Using a UV spectrophotometer (model 912A1113; Thermo Fisher Scientific, Germany), the absorbance of the sample was measured at a wavelength of 532 nm. The TBA content of the sample was determined by converting it using the 1,1,3,3-tetraethoxypropane (TEP) standard curve. The results were expressed as milligrams of malondialdehyde (MDA) per kilogram of pork belly sample. The pork belly sample's POV levels were evaluated using the AOAC method 965.33 and expressed in milliequivalents (meq) of peroxide per kilogram.

2.5. Determination of protein hydrolysis and oxidation

2.5.1. Determination of soluble protein extraction and concentration

Two grams of minced pork belly were transferred to a pre-weighed centrifuge tube. Then, 10 mL of 20 mM sodium phosphate buffer (pH 6.8) was added to the tube. The mixture was homogenized twice with a homogenizer at 15,000 rpm and 4°C for 30 s. Afterward, the mixture was allowed to stand for 1 h, and subsequently filtered through Whatman No. 1 filter paper. The filtrate was stored at −20°C until further analysis. Finally, the protein concentration in the filtrate was determined using the BCA kit (Sigma), with bovine serum albumin used as the standard for calibration.

2.5.2. Determination of protein hydrolysis

The degree of hydrolysis of the protein sample was assessed using the TNBS assay, as described by Adlernissen (19) with slight modifications. Initially, 20 μL of the protein extraction sample was mixed with 980 μL of sodium phosphate buffer (pH 8.0) in a centrifuge tube. Subsequently, 1 mL of 1.0% TNBS solution was added to the tube, which was then vortexed. The resulting mixture was heated in a water bath at 50°C for 60 min. After 60 min of the water bath reaction, 2 mL of 0.1 N hydrochloric acid was added to the sample. The absorbance of the mixed sample was measured at 320 nm using a UV spectrophotometer (912A1113; Thermo Fisher Scientific, Germany). To construct a standard curve, glycine was used as the standard substance. The degree of hydrolysis of the protein sample was then calculated based on the standard curve. Finally, the results were expressed as the number of free amino groups per gram of soluble pork belly protein.

2.5.3. Determination of protein oxidation

Protein oxidation was assessed by measuring protein carbonyl and sulfhydryl levels. Protein carbonyl levels were determined using the method described by Ali et al. (13) with slight modifications. Briefly, 0.7 mL of the protein extract sample was mixed with 0.3 mL of 10 mmol/L 2,4-dinitrophenylhydrazine (DNPH) and allowed to stand for 1 h at room temperature. To facilitate protein precipitation and purification, three successive additions of 1 mL of 40% trichloroacetic acid (TCA) and 1 mL of an ethanol/ethyl acetate mixture (1:1) were made. The resulting protein was then dissolved in 3 mL of 6 mol/L guanidine hydrochloride. The absorbance at 370 nm, corresponding to carbonyl levels, and the protein content at 280 nm were measured using an ultraviolet spectrophotometer (model 912A1113; Thermo Fisher Scientific, Germany). Results are expressed as the ratio of the absorbance at 370 nm to that at 280 nm. For the determination of sulfhydryl content, the method of Srinivasan et al. (20) was modified. Briefly, 1 mL of protein sample extract was dissolved in 2 mL of sodium phosphate buffer (pH 8.0) in a plastic tube. Subsequently, 0.5 mL of 10 mmol/L 5,5′-dithiobis (2-nitrobenzoic acid) (DTNB) reagent was added to the mixture. The mixture was then incubated in the shade for 1 h. After calibrating the UV spectrophotometer using the phosphate buffer solution, the absorbance of the sample was measured at 412 nm. The sulfhydryl content was expressed as millimoles of total free sulfhydryl groups per gram of soluble pork belly protein.

2.6. Texture profile analysis

Texture profile analysis (TPA) was performed using a texture analyzer (Universal TA; Shanghai Tengba Instrument Technology Co., Ltd., China) equipped with a 5 mm diameter cylindrical probe according to Bourne's method (21). Samples of pickled pork belly,

measuring approximately 1.0 cm in length, width, and height, were prepared for each treatment. The samples were compressed to 50% of their original height at a crosshead speed of 1.0 mm/s for two cycles. Parameters such as hardness, gumminess, and chewiness were calculated for each sample.

2.7. Sensory evaluation

The evaluation team consisted of 16 members, evenly distributed between the sexes (8 men and 8 women), aged 20–25 years. All team members had received professional training in food science and sensory evaluation. For the sensory evaluation, quantitative descriptive analysis following the method established by Morita et al. (22) was used. Each team member was allocated 10 g of pork belly samples, which were weighed and randomly numbered. To ensure no residual sensory characteristics from previous samples, the samples were placed on a glass plate. The team then engaged in a group discussion to establish standardized sensory descriptions for four attributes: color, aroma, taste, and texture. Subsequently, each team member rated the samples on a scale of 1–25 for each attribute (Table 1). The entire evaluation process took place in separate compartments within the same room, under white light at a temperature of 22°C–25°C. Higher scores on the scale indicated better organoleptic quality of the samples, approaching the standard descriptions.

2.8. OXITEST analysis

The oxidation tests were performed using the OXITEST reactor (Velp Scientifica, Usmate, Milan, Italy) as described by Verardo et al. (24). Each chamber of the reactor was filled with 6 g of minced pork belly samples. The test temperatures were set at 80°C, 90°C, and 100°C, while the initial oxygen pressure was maintained at 6 atm. The minced pork belly samples were placed in the OXITEST reactor to determine the induction period (IP). The IP values were determined in triplicate for each treatment.

2.9. Statistical analysis

Results from all experiments were presented as mean ± standard deviation. These experiments were performed in triplicate, with a sample size of three ($n = 3$). Treatment effects were analyzed using SPSS 19.0 (SPSS Inc., Chicago, IL) and one-way analysis of variance (ANOVA). The separation of means was determined through Duncan's multiple-range test. Statistical significance was defined as $p < 0.05$, while $p < 0.01$ was considered statistically highly significant.

3. Results and discussion

3.1. Proximate composition

Following the steaming process, the proximate composition of CPSPB was affected by TS, as shown in Table 2. Significant increases in moisture and crude protein contents of pork belly were observed ($p < 0.05$) due to the pressure difference from the high-pressure steaming system, which caused lipids melting and liquefaction, and inorganic salt dissolution. Conversely, there was a significant decrease in the total lipids, ash contents and NaCl contents ($p < 0.05$) to 32.28 ± 0.60%, 2.94 ± 0.03% and 1.97 ± 0.02%, respectively. The alteration in fat content appeared to have the most significant influence on the composition of other components, which aligns with previous studies (23, 25). The initial moisture, crude protein, total fat, ash, and NaCl contents of raw pork belly were 40.05 ± 0.76%, 20.46 ± 0.89%, 35.49 ± 1.42%, 3.12 ± 0.04%, and 2.24 ± 0.06%, respectively.

Additionally, there was a gradual decrease in the moisture, total lipid, sodium chloride, and ash contents of pork belly, leading to a gradual increase in total protein content. The inclusion of 60% or

TABLE 1 Reference of sensory evaluation on CPSPB.

Items	Describes of different scores				
	Dislike (5)	Slightly dislike (10)	Nor like nor dislike (15)	Slightly like (20)	Like very much (25)
Color	Brown is not the dominant color	Local small black or white patches cause uneven coloration	Mostly brown with a smattering of black or white spots	Uniform brown	Glossy, full, brown color with no black or white
Aroma	The smell is distinct, pungent, and even nauseating	An unusual or off-flavor characterized by its raw, burnt, or abnormal taste	The smell of steamed pork and taro dish is a little incongruous, or there is a small amount of off flavors	The normal steamed pork and taro dish has no off flavors or abnormal smell	Characterized by the rich aroma of steamed pork and taro, without any burnt paste taste, raw meat taste, or other unusual smells
Taste	Difficult to gulp	Greasy, raw, or salty taste	The flavor is acceptable, but not enjoyable	Taro and pork exhibit a delicious, pure flavor without any unpleasant notes	The taste of taro and pork is harmonious, mellow, and delicious, devoid of any sour or bitter flavors
Texture	The pattern is generally scattered	A small amount of deformation or ground meat	Slightly harder or softer, with some incomplete grain	Clear and solid in structure, both soft and firm	Fat without greasiness, thin without being wooden, soft and sticky skin and flesh, and clear lines

10.3389/fnut.2023.1290221

TABLE 2 Effects of TS on proximate composition of CPSPB (g/100 g fresh weight).

Treatments	Contents (%)				
	Moisture	Crude protein	Total lipids	Ash	NaCl content
Control (raw)	40.05 ± 0.76^{b}	20.46 ± 0.89^{d}	35.49 ± 1.42^{a}	3.12 ± 0.04^{a}	2.24 ± 0.06^{a}
0% TS	42.74 ± 0.95^{a}	22.15 ± 0.91^{d}	32.28 ± 0.60^{b}	2.94 ± 0.03^{b}	1.97 ± 0.02^{b}
20% TS	40.12 ± 1.16^{b}	26.14 ± 0.67^{c}	29.61 ± 0.47^{c}	2.65 ± 0.13^{c}	1.40 ± 0.12^{c}
40% TS	38.31 ± 1.29^{b,c}	29.30 ± 1.04^{b}	28.25 ± 0.92^{c,d}	2.32 ± 0.05^{d}	1.15 ± 0.03^{d}
60% TS	36.98 ± 0.73^{c}	32.36 ± 0.72^{a}	27.04 ± 0.34^{d}	2.26 ± 0.08^{d,e}	1.12 ± 0.08^{d}
80% TS	36.54 ± 0.54^{c}	32.49 ± 1.13^{a}	26.57 ± 0.73^{d}	2.09 ± 0.03^{e}	0.98 ± 0.02^{d,e}
100% TS	36.37 ± 0.39^{c}	32.84 ± 0.53^{a}	26.74 ± 0.56^{d}	2.14 ± 0.04^{e}	0.90 ± 0.06^{e}

Different letters within a column are significantly different ($p < 0.05$).

more TS demonstrated no significant difference ($p > 0.05$) in moisture, total lipid, and protein content. This indicates that the addition of 60% or more TS stabilized the major components' content in the pork belly samples, possibly due to the physical barrier and diffusion-driven physicochemical properties of TS. It is plausible that some of the diffused salt from CPSPB may have transferred to the TS during the steaming process, leading to a reduction in the saltiness and graininess of the pork belly, thereby harmonizing its texture. Throughout the steaming process, the moisture contents of pork belly decreased from 42.74 ± 0.95% to 36.98 ± 0.73%, whereas the total lipids contents decreased from 32.28 ± 0.60% to 27.04 ± 0.34%. This reflects the capacity of TS to bind water and lipids, resulting in reduced moisture and lipid content of pork belly, thereby contributing to the extended shelf life of CPSPB.

3.2. Lipid oxidation

Figure 1 illustrates that CPSPB samples treated with TS exhibited a significant decrease ($p < 0.05$) in both POV and TBA values compared to the original samples. This reduction can be attributed to the exposure of the pork belly samples to the antioxidant agents such as phenolic compounds, resistant starch, and polysaccharides (14, 15) present in TS, as well as the reduction in the exposed surface area of the pork belly to air, achieved by covering it with TS. The POV represents the number of primary oxidation products generated when ROS attack the double bonds of fatty acids. On the other hand, the TBA value measures the amount of secondary lipid oxidation products, which predominantly consist of aldehydes, known to contribute to off-flavors in meat products (21). Consequently, the addition of TS shows potential in extending the shelf life of CPSPB by effectively reducing the degree of lipid oxidation (26, 27).

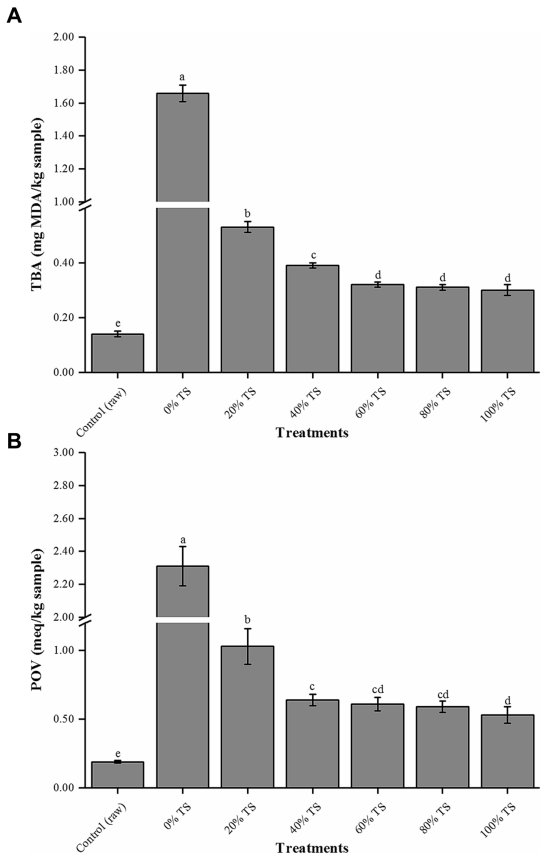

FIGURE 1
Levels of thiobarbituric acid (TBA, **A**) and peroxides levels (POVs, **B**) of CPSPB with different amounts of added of TS. Values are presented as mean ± SD. Bars with different letters are significantly different ($p < 0.05$).

3.3. Fatty acid profile

Table 3 demonstrates that the raw pork belly samples had the highest content of saturated fatty acids (SFA, 40.63 ± 0.16%), followed by monounsaturated fatty acids (MUFA, 37.01 ± 0.13%) and polyunsaturated fatty acids (PUFA, 22.36 ± 0.02%). The primary fatty acids in the raw samples were palmitic acid (C16:0, 23.06 ± 0.09%), stearic acid (C18:0, 16.13 ± 0.07%), oleic acid (C18:1n9c, 34.86 ± 0.14%), and linoleic acid (C18:2n6c, 18.27 ± 0.03%). These findings align with previous data obtained (3, 28, 29). Steaming resulted in a significant decrease in PUFA and a significant increase in MUFA and SFA ($p < 0.05$) in the pork belly samples. The increase in medium/short-chain MUFA and SFA may be attributed to the degradation of long-chain PUFA during autoclaving. However, Li et al. (30) demonstrated that prolonged cooking caused a significant decrease ($p < 0.01$) in the SFA content of pork, as it melted into the broth. Moreover, according to Zhang et al. (28), steaming did not

10.3389/fnut.2023.1290221

TABLE 3 Effects of TS on fatty acid profiles of CPSPB (area % of total fatty acids).

Retention time (min)	Fatty acid	Treatment						
		Control (raw)	0% TS	20% TS	40% TS	60% TS	80% TS	100% TS
8.57	C12:0	0.08 ± 0.00^{a}	0.10 ± 0.01^{a}	0.09 ± 0.01^{a}	0.08 ± 0.02^{a}	0.10 ± 0.01^{a}	0.10 ± 0.01^{a}	0.10 ± 0.01^{a}
12.30	C14:0	0.86 ± 0.01^{b}	0.89 ± 0.03^{b}	0.87 ± 0.02^{b}	0.91 ± 0.01^{b}	0.98 ± 0.03^{a}	1.01 ± 0.05^{a}	0.99 ± 0.02^{a}
15.45	C16:0	23.06 ± 0.09^{c}	26.05 ± 0.47^{a}	24.76 ± 0.47^{b}	23.90 ± 0.55^{b}	20.16 ± 0.18^{d}	20.04 ± 0.06^{d}	19.97 ± 0.11^{d}
17.12	C17:0	0.32 ± 0.01^{a}	0.30 ± 0.01^{a}	0.29 ± 0.01^{a}	0.25 ± 0.02^{b}	0.20 ± 0.03^{c}	0.13 ± 0.00^{d}	0.13 ± 0.01^{d}
18.23	C18:0	16.13 ± 0.07^{a}	16.42 ± 0.63^{a}	16.19 ± 0.20^{a}	15.28 ± 0.46^{b}	11.94 ± 0.31^{c}	10.81 ± 0.03^{d}	$10.90 \pm 0.21^{c,d}$
21.82	C20:0	0.24 ± 0.01^{c}	$0.26 \pm 0.03^{b,c}$	$0.27 \pm 0.04^{b,c}$	0.30 ± 0.01^{b}	0.36 ± 0.04^{a}	$0.33 \pm 0.02^{a,b}$	0.30 ± 0.01^{b}
	∑SFA	40.63 ± 0.16^{b}	44.01 ± 1.05^{a}	$42.48 \pm 0.49^{a,b}$	40.70 ± 0.34^{b}	33.72 ± 0.15^{c}	32.42 ± 0.02^{c}	32.38 ± 0.07^{c}
14.36	C15:1	0.11 ± 0.00^{c}	0.20 ± 0.06^{a}	0.19 ± 0.07^{a}	0.15 ± 0.04^{b}	0.10 ± 0.01^{c}	$0.08 \pm 0.03^{c,d}$	0.06 ± 0.00^{d}
16.20	C16:1	1.09 ± 0.04^{c}	1.45 ± 0.03^{b}	1.43 ± 0.01^{b}	$1.49 \pm 0.03^{a,b}$	1.58 ± 0.02^{a}	1.60 ± 0.01^{a}	1.51 ± 0.00^{a}
17.67	C17:1	0.18 ± 0.00^{a}	0.17 ± 0.02^{a}	$0.15 \pm 0.03^{a,b}$	0.14 ± 0.02^{b}	0.11 ± 0.00^{c}	0.10 ± 0.01^{c}	0.09 ± 0.00^{c}
19.31	C18:1n9c	34.86 ± 0.14^{c}	38.02 ± 0.54^{b}	$38.87 \pm 0.21^{a,b}$	$39.74 \pm 0.43^{a,b}$	40.37 ± 0.08^{a}	40.30 ± 0.15^{a}	40.39 ± 0.02^{a}
23.09	C20:1	0.78 ± 0.01^{b}	0.85 ± 0.02^{a}	0.76 ± 0.05^{b}	0.67 ± 0.03^{c}	$0.60 \pm 0.01^{c,d}$	0.57 ± 0.04^{d}	0.58 ± 0.03^{d}
	∑MUFA	37.01 ± 0.13^{c}	40.67 ± 0.25^{b}	$41.40 \pm 0.15^{a,b}$	42.18 ± 0.38^{a}	42.76 ± 0.34^{a}	42.65 ± 0.11^{a}	42.62 ± 0.01^{a}
20.17	C18:2n6t	1.89 ± 0.01^{b}	2.26 ± 0.06^{a}	2.07 ± 0.13^{a}	1.26 ± 0.13^{c}	0.10 ± 0.01^{d}	0.10 ± 0.00^{d}	0.09 ± 0.01^{d}
20.71	C18:2n6c	18.27 ± 0.03^{b}	12.90 ± 0.13^{e}	14.73 ± 0.21^{d}	16.08 ± 0.30^{c}	20.23 ± 0.12^{a}	20.14 ± 0.05^{a}	20.76 ± 0.02^{a}
21.69	C18:3n3	0.82 ± 0.01^{c}	0.73 ± 0.07^{c}	0.81 ± 0.01^{c}	0.95 ± 0.03^{b}	1.34 ± 0.06^{a}	1.37 ± 0.01^{a}	1.39 ± 0.02^{a}
24.32	C20:2	0.84 ± 0.01^{b}	0.69 ± 0.01^{c}	0.79 ± 0.03^{b}	0.86 ± 0.08^{ab}	0.96 ± 0.01^{a}	0.94 ± 0.01^{a}	0.93 ± 0.01^{a}
25.73	C20:3n3	0.41 ± 0.01^{c}	0.67 ± 0.04^{a}	0.58 ± 0.13^{b}	0.45 ± 0.02^{c}	0.32 ± 0.01^{d}	0.29 ± 0.01^{d}	0.28 ± 0.02^{d}
26.54	C20:4n6	0.13 ± 0.02^{b}	0.07 ± 0.03^{c}	$0.14 \pm 0.02^{a,b}$	0.18 ± 0.02^{a}	0.20 ± 0.01^{a}	0.18 ± 0.02^{a}	0.20 ± 0.00^{a}
	∑PUFA	22.36 ± 0.02^{a}	17.32 ± 0.17^{c}	19.12 ± 0.19^{b}	19.77 ± 0.34^{c}	23.15 ± 0.10^{a}	23.02 ± 0.14^{a}	23.65 ± 0.02^{a}
	∑UFA	$59.37 \pm 0.12^{b,c}$	57.99 ± 0.28^{c}	60.52 ± 0.18^{b}	61.95 ± 0.43^{b}	65.91 ± 0.28^{a}	65.67 ± 0.10^{a}	66.27 ± 0.00^{a}
	UFA/SFA	$1.46 \pm 0.01^{c,d}$	1.32 ± 0.07^{d}	1.42 ± 0.02^{d}	1.52 ± 0.04^{c}	1.95 ± 0.02^{b}	2.03 ± 0.01^{a}	2.05 ± 0.00^{a}

significantly ($p > 0.05$) affect the fatty acid composition of grass carp fillets, but led to a slight increase in SFA. Thus, it is suggested that the specifics of the heating process, rather than the sample characteristics and heating method, may influence the fatty acid composition of meat products.

The addition of various percentages of TS influenced the fatty acid composition of CPSPB in this study. The proportion of MUFAs (40.67 ±0.25%-42.76 ±0.34%) and PUFAs (17.32 ±0.17%-23.65 ±0.02%) gradually increased, while the proportion of SFAs (44.01 ±1.05%-32.38 ±0.07%) continued to decrease. The UFA/SFA ratio changed from 1.32 ±0.07 to 2.05 ± 0.00 with the sequential addition of TS from 0 to 100% of the sample proportion. When TS exceeded 60% of the sample proportion, MUFAs constituted the majority of fatty acids compared to SFAs, while PUFAs remained the least abundant. The predominant fatty acid changes driving this trend were the decrease in C16:0, C17:0, and C18:0, and the increase in C18:1n9c, C18:2n6c, C18:3n3, and C20:2. Along with the Maillard reaction products (especially melanin) of CPSPB with TS, TS contains several naturally occurring antioxidant constituents that are absorbed by the samples during steaming (23, 31). They contribute to inhibiting the autoxidation of unsaturated fatty acids. As a result, delaying the steaming process leads to a significant decrease in PUFAs and a significant increase in MUFAs and SFAs. Furthermore, the presence of C18:1n9c, C18:2n6c, and C18:3n3 in taro can combine with CPSPB during the steaming process, thereby increasing the overall fatty acid content (11). It is interesting to observe that the changes in MUFA, PUFA, and SFA were not significant ($p > 0.05$) when 60% or more TS was added. The alterations in fatty acid composition were generally consistent with the lipid oxidation indices (POV and TBA) observed in this study, further supporting the potential of TS as an effective lipid antioxidant when added to CPSPB.

3.4. Protein hydrolysis and oxidation

The results demonstrated a significantly lower content of free amino groups in raw pork belly compared to the other treatments ($p < 0.05$) (Figure 2A). This suggests that the application of high temperature during cooking led to thermal denaturation of the proteins, which may explain the observed increase in free amino acid content in the tested samples (32). Additionally, the content of free amino acids displayed a concentration-dependent response to the addition of TS. Increasing the TS concentration from 0 to 60% resulted in a significant increase in free amino acid content from 3.31 ±0.17 to 4.17 ±0.15 mmol/g soluble protein ($p < 0.05$). However, further increasing the TS additions to 80% and 100% did not significantly influence the free amino acid content ($p > 0.05$). These findings suggest that within a certain range, TS positively affects the hydrolysis process of pork belly proteins. This beneficial effect can be attributed to the Maillard reaction that takes place between the glucose present in TS

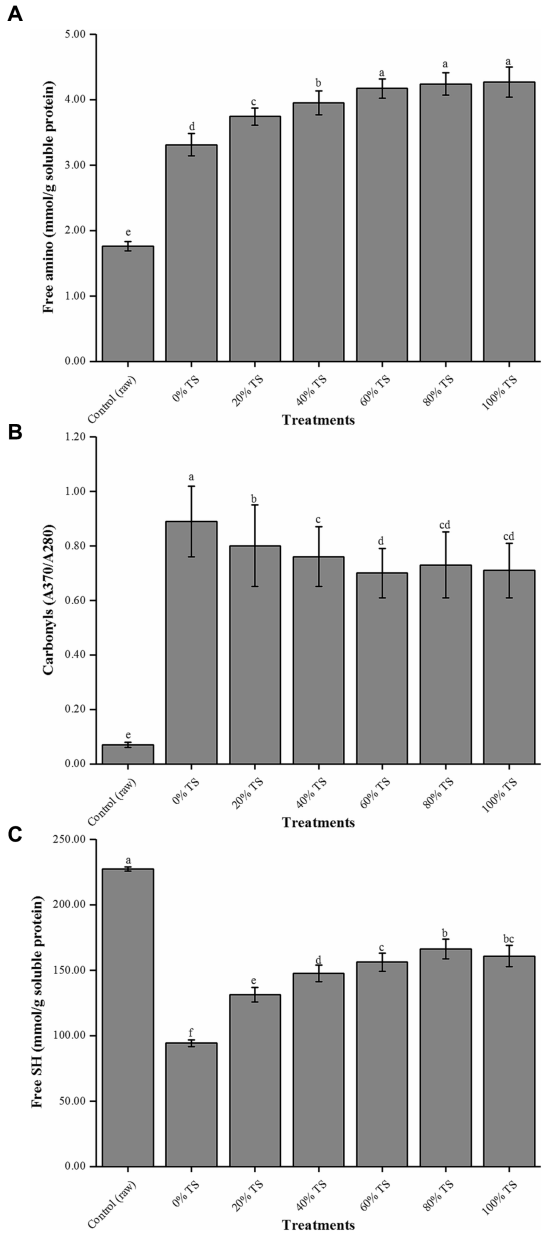

FIGURE 2
Free amino **(A)**, carbonyl **(B)** and free SH values **(C)** of CPSPB with different levels of TS added. Values are expressed as mean ± SD. Bars with different letters are significantly different from each other ($p < 0.05$).

and the hydrolysate of pork belly protein during the steaming process, facilitating the hydrolysis reaction.

To evaluate the degree of protein oxidative degradation in the samples, carbonyl (Figure 2B) and free sulfhydryl (SH; Figure 2C) counts were measured (13). Steaming significantly promoted the oxidation of proteins in the samples ($p < 0.05$). The carbonyl value increased from 0.07 ± 0.01 to 0.89 ± 0.13, while free SH decreased from 227.41 ± 1.59 to 94.25 ± 2.61 mmol/g soluble protein. These findings align with previous studies that reported higher protein oxidation in cooked samples compared to raw samples exposed to different time/temperature cooking combinations (33, 34). Although a slight negative correlation was observed between the amount of TS added and the degree of protein oxidation, both values were significantly higher than those of the raw samples ($p < 0.05$). Among all TS treatments, the lowest carbonyl value was 0.71 ± 0.10 (100% TS), and the highest free SH was 166.13 ± 7.46 mmol/g soluble protein (80% TS). These results, consistent with the findings on fat oxidation in this study, strongly suggest that the addition of TS affects protein oxidation in pork belly. It is worth noting that adding more than 60% TS did not contribute to further improvements in the protein oxidation of CPSPB. Therefore, it is plausible that protein oxidation occurs concurrently with lipid oxidation, as previous reports indicated the relationship between the primary and secondary lipid oxidation products as substrates for protein oxidation (35, 36). Moreover, the inhibitory effect of TS on lipid oxidation may explain the lower level of protein oxidation observed in CPSPB (13).

3.5. Sensory quality

The addition of varying levels of TS significantly improved the sensory quality (color, aroma, flavor, and texture) of CPSPB compared to the untreated samples ($p < 0.01$) (Figure 3A), as demonstrated by the sensory evaluation conducted by the panelists. The untreated pork belly received the lowest mean score (TS = 64.00), indicating its inferior sensory attributes. The incorporation of TS with CPSPB resulted in a pronounced flavor profile and contributed to the desirable color, aroma, and flavor of the pork belly samples. The total mean score increased from 71.30 to 85.78 as the percentage of TS increased from 20% to 60%, but decreased to 74.79 when 100% TS was added. This trend was also observed for the four sensory quality attributes. The samples with the highest mean scores for each attribute (color = 22.03, aroma = 20.65, taste = 21.26, texture = 21.84) and a total mean score of 85.78 displayed the most favorable sensory characteristics when 60% TS was added to CPSPB. Conversely, when TS was added at lower levels (<60%), there was no significant reduction in the brown color of CPSPB, nor was the full combination of TS and belly able to produce a noticeable strong flavor perceived by the panelists. Furthermore, the presence of relatively high lipid content in the CPSPB, which was insufficient to be absorbed by TS, resulted in a pronounced greasiness that could be overwhelming to the senses. Similarly, the aroma and flavor of CPSPB were not distinctly perceived, and the color became lighter and somewhat earthy when excessive TS (>60%) was added. The excessive loss of moisture and fat led to a tough texture. These findings align with the results obtained by Lorido et al. (37), who reported that the texture of a product is often influenced by its composition, specifically moisture and intramuscular lipid content. Moreover, by assessing the hardness, gumminess, and chewiness of the CPSPB at different TS levels, it was observed that the lowest values were achieved with the addition of 60% TS, resulting in soft, smooth, and tender CPSPB (Figure 3B). In conclusion, the addition of an appropriate level of TS (60%) yielded the most favorable organoleptic qualities in CPSPB (see Figure 3).

3.6. Shelf life

The OXITEST reactor is characterized by its simplicity, as it does not require sample pretreatment (24). It achieves predicting the shelf

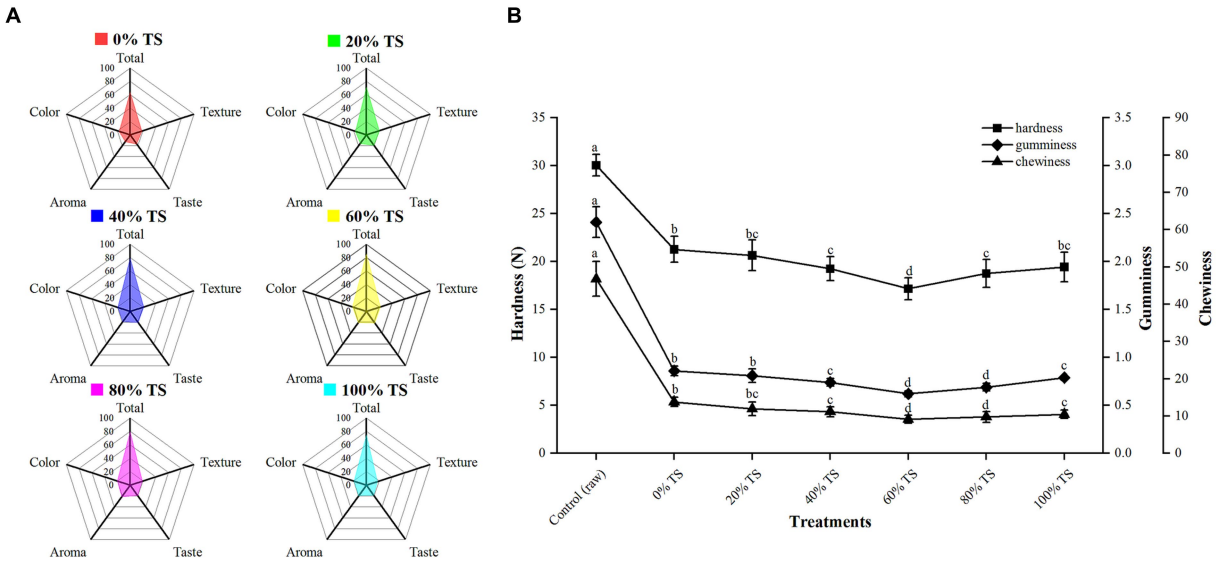

FIGURE 3
Sensory parameters **(A)** and TPA **(B)** of CPSPB with different levels of added TS. Values are presented as mean scores of each attribute.

TABLE 4 **Effects of TS on induction period (IP) of CPSPB.**

Treatments	IP (h)—T (°C)	R^2	Estimated IP25 (days:hour:min)
Control	ln(IP) = −0.090213 T + 8.971427	0.9987	34:09:36
0% TS	ln(IP) = −0.086359 T + 8.405716	0.9991	21:12:20
20% TS	ln(IP) = −0.088567 T + 9.692105	0.9972	73:16:35
40% TS	ln(IP) = −0.090273 T + 10.022361	0.9959	98:05:55
60% TS	ln(IP) = −0.092546 T + 10.167948	0.9992	107:08:47
80% TS	ln(IP) = −0.093695 T + 10.328024	0.9989	122:10:29
100% TS	ln(IP) = −0.094723 T + 10.491137	0.9993	140:11:20

life of lipid-rich foods by measuring the oxygen consumption required to oxidize fats and oils. The reactor offers a rapid and accurate process for determining the rancidity of fats and oils. Moreover, this method allows for the complete assessment of fat and oil rancidity without the need to isolate lipids from the food matrix. Additionally, the OXITEST reactor enables the prediction of the induction period (IP) of the autoxidation process for different foods at various temperatures.

The IP values for CPSPB from different treatments at three induction temperatures: 80°C, 90°C, and 100°C are presented in Table 4. The observed behavior showed that the natural logarithm of IP displayed a linear relationship with increasing induction temperature ($R^2 > 0.99$). These lines exhibited negative slopes and positive intersections, indicating that as temperature rose, the IP decreased, resulting in reduced oxidative stability and shorter preservation times for the samples. These findings support previous reports (35, 38) that storing meat at low temperatures can help prevent fat and protein oxidation during frozen storage.

To estimate the IP at room temperature (25°C), a linear model derived from the OXITEST reactor calculations was employed. The IP at 25°C (IP 25) for CPSPB without added TS was found to be shorter (IP 25 = 21:12:20, days: hours: minutes) compared to the raw product (IP 25 = 34:09:36, days: hours: minutes). This discrepancy may be due to the induction of fat and protein oxidation during the heating process, as cooked samples generally exhibit lower oxidative stability than raw meat (39). With increasing TS addition (from 20% to 100%), the IP 25 values increased (from 73:16:35 to 144:11:20, days: hours: minutes), indicating an extended storage period for the samples. Furthermore, the addition of TS affected the IP values, as evidenced by changes in the slope of the linear model. These results align with the findings of fat and protein oxidation in this study, highlighting the positive impact of TS treatment on the oxidative stability of CPSPB.

4. Conclusion

Trao (TS) plays a pivotal role in enhancing the nutritional quality, sensory attributes, and shelf life of CPSPB, as a precursor to its industrial production. Our study revealed that the addition of TS resulted in the reduction of moisture content, total fat content, ash content, and NaCl content, while simultaneously increasing the crude protein content of CPSPB. Furthermore, our findings confirmed that TS effectively mitigated fat oxidation in CPSPB, as evidenced by the decreased levels of TBA and POV, along with an elevated ratio of UFA to SFA. Additionally, TS exhibited a certain degree of promotion of protein hydrolysis and inhibition of protein oxidation in CPSPB. The OXITEST analysis demonstrated a

prolonged shelf life of CPSPB when higher levels of TS were added at the same induction temperature. Moreover, the chemical composition changes resulting from the addition of TS significantly influenced the organoleptic and nutritional qualities of CPSPB. While the inclusion of 100% TS maximized the shelf life of the samples, the addition of 60% TS yielded the best organoleptic quality of CPSPB, as determined by TPA and sensory evaluations. These results provide a solid foundation for investigating the preservation mechanisms facilitated by TS. More research is required to study changes in odor and taste and determine the optimal organoleptic properties of CPSPB prepared using a 60% TS.

Data availability statement

The original contributions presented in the study are included in the article/supplementary material, further inquiries can be directed to the corresponding author.

Author contributions

QQ: Data curation, Methodology, Software, Writing – original draft, Writing – review & editing. YZ: Data curation, Software, Writing – original draft. AN: Methodology, Writing – review & editing. LF: Writing – review & editing. ZQ: Funding acquisition, Project administration, Resources, Supervision, Validation, Writing – review & editing.

Funding

The author(s) declare financial support was received for the research, authorship, and/or publication of this article. This research was supported by the Ministry of Science and Technology Young Foreign Talent Program, China (QN2022029001).

Conflict of interest

The authors declare that the research was conducted in the absence of any commercial or financial relationships that could be construed as a potential conflict of interest.

Publisher's note

All claims expressed in this article are solely those of the authors and do not necessarily represent those of their affiliated organizations, or those of the publisher, the editors and the reviewers. Any product that may be evaluated in this article, or claim that may be made by its manufacturer, is not guaranteed or endorsed by the publisher.

References

1. Wang X, Wang X, Muhoza B, Feng T, Xia S, Zhang X. Microwave combined with conduction heating effects on the tenderness, water distribution, and microstructure of pork belly. *Innov Food Sci Emerg Technol*. (2020) 62:102344. doi: 10.1016/j.ifset.2020.102344

2. Bi J, Li Y, Yang Z, Li B, Gao Y, Ping C, et al. Analysis of the effect of steaming times on lipid composition of pork belly based on lipidomics technology. *J Food Compos Anal*. (2023) 117:105143. doi: 10.1016/j.jfca.2023.105143

3. Shen Q, Wang M, Tian J, Hu L, Ren S, Chen J, et al. Effects of Chinese pickled and dried mustard on nutritional quality, sensory quality, and shelf life of steamed pork belly. *Food Sci Nutr*. (2018) 6:747–56. doi: 10.1002/fsn3.612

4. Li D, Zhang X, Bi J, Zhang Y, Zhu B. Inheritance and innovation of Chinese prepared dishes industry. *Chin J Food*. (2022) 22:1–8. doi: 10.16429/j.1009-7848.2022.10.001

5. Zhao S, Sai Y, Liu W, Zhao H, Bai X, Song W, et al. Flavor characterization of traditional fermented soybean pastes from Northeast China and Korea. *Foods*. (2023) 12:3294. doi: 10.3390/foods12173294

6. Carrión M, Corripio M, Contreras J, Marrón M, Olán G, Cázares A. Optimization and characterization of taro starch, nisin and sodium alginate based biodegradable films: antimicrobial effect in chicken meat. *Poult Sci*. (2023) 102:103100. doi: 10.1016/j.psj.2023.103100

7. Jiang C, Chen Y, Li S, Shang S, Fu B, Wang L, et al. Ready-to-eat fish cake processing methods and the impacts on quality and flavor. *Foods*. (2022) 11:3321. doi: 10.3390/foods11213321

8. Jianchu X, Yongping Y, Yingdong P, Ayad W, Eyzaguirre P. Genetic diversity in taro (*Colocasia esculenta* Schott, Araceae) in China: an ethnobotanical and genetic approach. *Econ Bot*. (2001) 55:14–31. doi: 10.1007/bf02864543

9. Zeng F, Liu H, Liu G. Physicochemical properties of starch extracted from *Colocasia esculenta* (L.) Schott (bun-long taro) grown in Hunan, China. *Starch*. (2014) 66:142–8. doi: 10.1002/star.201300039

10. Wang X, Reddy C, Xu B. A systematic comparative study on morphological, crystallinity, pasting, thermal and functional characteristics of starches resources utilized in China. *Food Chem*. (2018) 259:81–8. doi: 10.1016/j.foodchem.2018.03.121

11. Maga JA. Taro: composition and food uses. *Food Rev Intl*. (1992) 8:443–73. doi: 10.1080/87559129209540948

12. Nip W. Taro In: *The processing vegetables*. London; New York: Routledge (2023). 355–88.

13. Ali S, Zhang W, Rajput N, Khan M, Li C, Zhou G. Effect of multiple freeze–thaw cycles on the quality of chicken breast meat. *Food Chem*. (2015) 173:808–14. doi: 10.1016/j.foodchem.2014.09.095

14. Nakyinsige K, Sazili A, Aghwan Z, Zulkifli I, Goh Y, Bakar F, et al. Development of microbial spoilage and lipid and protein oxidation in rabbit meat. *Meat Sci*. (2015) 108:125–31. doi: 10.1016/j.meatsci.2015.05.029

15. Kapcum C, Pasada K, Kantiwong P, Sroysang B, Phiwtawee J, Suphantharika M, et al. Effects of different cooking methods on chemical compositions, in vitro starch digestibility and antioxidant activity of taro (*Colocasia esculenta*) corms. *Int J Food Sci Technol*. (2022) 57:5144–54. doi: 10.1111/ijfs.15823/v1/review1

16. Ribeiro Pereira P, Bertozzi de Aquino Mattos É, Nitzsche Teixeira Fernandes Corrêa AC, Afonso Vericimo M, Margaret Flosi Paschoalin V. Anticancer and immunomodulatory benefits of Taro (*Colocasia esculenta*) corms, an underexploited tuber crop. *Int J Mol Sci*. (2020) 22:265. doi: 10.3390/ijms22010265

17. Wu H, Ge M, Chen H, Jiang S, Lin L, Lu J. Comparison between the nutritional qualities of wild-caught and rice-field male Chinese mitten crabs (*Eriocheir sinensis*). *LWT*. (2020) 117:108663. doi: 10.1016/j.lwt.2019.108663

18. Sorensen G, Jorgensen S. A critical examination of some experimental variables in the 2-thiobarbituric acid (TBA) test for lipid oxidation in meat products. *Z Lebensm Unters Forsch*. (1996) 202:205–10. doi: 10.1007/BF01263541

19. Adlernissen J. Determination of the degree of hydrolysis of food protein hydrolysates by trinitrobenzenesulfonic acid. *J Agric Food Chem*. (1979) 27:1256–62. doi: 10.1021/jf60226a042

20. Srinivasan S, Hultin H. Chemical, physical, and functional properties of cod proteins modified by a nonenzymic free-radical-generating system. *J Agric Food Chem*. (1997) 45:310–20. doi: 10.1021/jf960367g

21. Bourne M. Texture profile analysis. *Food Technol*. (1978) 32:62–6.

22. Morita K, Kubota K, Aishima T. Comparison of aroma characteristics of 16 fish species by sensory evaluation and gas chromatographic analysis. *J Sci Food Agric*. (2003) 83:289–97. doi: 10.1002/(ISSN)1097-0010

23. Li Y, Li C, Li H, Lin X, Deng S, Zhou G. Physicochemical and fatty acid characteristics of stewed pork as affected by cooking method and time. *Int J Food Sci Technol*. (2016) 51:359–69. doi: 10.1111/ijfs.12968

24. Verardo V, Riciputi Y, Sorrenti G, Ornaghi P, Marangoni B, Caboni M. Effect of nitrogen fertilisation rates on the content of fatty acids, sterols, tocopherols and phenolic

compounds, and on the oxidative stability of walnuts. *LWT*. (2013) 50:732–8. doi: 10.1016/j.lwt.2012.07.018

25. Biandolino F, Parlapiano I, Denti G, Di Nardo V, Prato E. Effect of different cooking methods on lipid content and fatty acid profiles of *Mytilus galloprovincialis*. *Foods*. (2021) 10:416. doi: 10.3390/foods10020416

26. Nguimbou R, Njintang N, Makhlouf H, Gaiani C, Scher J, Mbofung C. Effect of cross-section differences and drying temperature on the physicochemical, functional and antioxidant properties of giant taro flour. *Food Bioprocess Technol*. (2013) 6:1809–19. doi: 10.1007/s11947-012-0846-1

27. Shanta S, Ahmed T, Jubayer M, Sharma M, Sridhar K, Hoque M, et al. Effect of Taro corm mucilage and black seed oil as edible coatings on the shelf-life and quality of fresh guava. *Agronomy*. (2023) 13:538. doi: 10.3390/agronomy13020538

28. Zhang K, Li D, Zang M, Zhang Z, Li X, Wang S, et al. Comparative characterization of fatty acids, reheating volatile compounds, and warmed-over flavor (WOF) of Chinese indigenous pork and hybrid pork. *LWT*. (2022) 155:112981. doi: 10.1016/j.lwt.2021.112981

29. Soro A, Harrison S, Whyte P, Bolton D, Tiwari B. Impact of ultraviolet light and cold plasma on fatty acid profile of raw chicken and pork meat. *J Food Compos Anal*. (2022) 114:104872. doi: 10.1016/j.jfca.2022.104872

30. Li Y, Li C, Zhao F, Lin X, Bai Y, Zhou G. The effects of long-duration stewing combined with different cooking and heating methods on the quality of pork belly. *J Food Process Preserv*. (2016) 40:94–102. doi: 10.1111/jfpp.12587

31. Zhang J, Wu D, Liu D, Fang Z, Chen J, Hu Y, et al. Effect of cooking styles on the lipid oxidation and fatty acid composition of grass carp (*Ctenopharynyodon idellus*) fillet. *J Food Biochem*. (2013) 37:212–9. doi: 10.1111/j.1745-4514.2011.00626.x

32. Zou J, Xu M, Zou Y, Yang B. Chemical compositions and sensory characteristics of pork rib and silkie chicken soups prepared by various cooking techniques. *Food Chem*. (2021) 345:128755. doi: 10.1016/j.foodchem.2020.128755

33. Traore S, Aubry L, Gatellier P, Przybylski W, Jaworska D, Kajak-Siemaszko K, et al. Effect of heat treatment on protein oxidation in pig meat. *Meat Sci*. (2012) 91:14–21. doi: 10.1016/j.meatsci.2011.11.037

34. Mitra B, Lametsch R, Akcan T, Ruiz-Carrascal J. Pork proteins oxidative modifications under the influence of varied time-temperature thermal treatments: a chemical and redox proteomics assessment. *Meat Sci*. (2018) 140:134–44. doi: 10.1016/j.meatsci.2018.03.011

35. Soyer A, Özalp B, Dalmış Ü, Bilgin V. Effects of freezing temperature and duration of frozen storage on lipid and protein oxidation in chicken meat. *Food Chem*. (2010) 120:1025–30. doi: 10.1016/j.foodchem.2009.11.042

36. Al-Dalali S, Li C, Xu B. Effect of frozen storage on the lipid oxidation, protein oxidation, and flavor profile of marinated raw beef meat. *Food Chem*. (2022) 376:131881. doi: 10.1016/j.foodchem.2021.131881

37. Lorido L, Ventanas S, Akcan T, Estévez M. Effect of protein oxidation on the impaired quality of dry-cured loins produced from frozen pork meat. *Food Chem*. (2016) 196:1310–4. doi: 10.1016/j.foodchem.2015.10.092

38. Zhang C, Li Y, Xia X, Sun Q, Sun F, Kong B. Changes in protein oxidation, structure, and thermal stability of chicken breast subjected to ultrasound-assisted immersion freezing during frozen storage. *Food Chem*. (2023) 398:133874. doi: 10.1016/j.foodchem.2022.133874

39. Roldan M, Antequera T, Armenteros M, Ruiz J. Effect of different temperature–time combinations on lipid and protein oxidation of sous-vide cooked lamb loins. *Food Chem*. (2014) 149:129–36. doi: 10.1016/j.foodchem.2013.10.079

frontiers | Frontiers in Nutrition

TYPE Original Research
PUBLISHED 10 November 2023
DOI 10.3389/fnut.2023.1285590

OPEN ACCESS

EDITED BY
Peng Wang,
Shaanxi Normal University, China

REVIEWED BY
Ma Lukai,
Zhongkai University of Agriculture and Engineering, China
Filipa Mandim,
Centro de Investigação de Montanha (CIMO), Portugal
Ye Liu,
Beijing Technology and Business University, China

*CORRESPONDENCE
Jiluan Chen
✉ chenjiluan@163.com

RECEIVED 30 August 2023
ACCEPTED 30 October 2023
PUBLISHED 10 November 2023

CITATION
Pei L, Liu W, Jiang L, Xu H, Liu L, Wang X, Liu M, Abudureheman B, Zhang H and Chen J (2023) Effect of high hydrostatic pressure on aroma volatile compounds and aroma precursors of Hami melon juice.
Front. Nutr. 10:1285590.
doi: 10.3389/fnut.2023.1285590

Effect of high hydrostatic pressure on aroma volatile compounds and aroma precursors of Hami melon juice

Longying Pei[1], Wei Liu[2], Luxi Jiang[1], Heng Xu[1], Luping Liu[1], Xiaoyu Wang[1], Manli Liu[1], Buhailiqiemu Abudureheman[1], Heng Zhang[1] and Jiluan Chen[3]*

[1]College of Food Science and Engineering, Xinjiang Institute of Technology, Aksu, Xinjiang Province, China, [2]College of Food Science and Engineering, Tarim University, Alar, Xinjiang Province, China, [3]School of Food Science and Technology, Shihezi University, Shihezi, Xinjiang Province, China

High hydrostatic pressure (HHP) treatment is an effective technique for processing heat-sensitive fruits and causes changes in volatile compounds and their precursors while maintaining quality. We investigated the changes and correlations of volatile compounds, related enzyme activities and precursor amino acids, and fatty acids in Hami melon juice under 350–500 MPa pressure. The application of HHP treatment resulted in a considerable reduction of esters and a substantial increase in aldehydes and alcohols in C6 and C9. Activities of lipoxygenase (*LOX*), alcohol acyltransferase (*AAT*), and phospholipase A2 (*PLA2*) were lower than those of the untreated group, alcohol dehydrogenase (*ADH*) activity was reversed. When compared to fresh cantaloupe juice, there was an increase in both the types and contents of amino acids with lower total fatty acid contents than the control group. Positive correlations were observed among six ester-related substances and eight alcohol-related substances. Additionally, the correlations between volatile compounds and fatty acids were more substantial compared to those between volatile compounds and amino acids. HHP treatment increases Hami melon flavor precursors and is an effective way to maintain the aroma volatile compounds and flavor of Hami melon juice.

KEYWORDS

Hami melon juice, high hydrostatic pressure, aroma enzymes, aroma volatile compounds, amino acids, fatty acids

1. Introduction

Hami melon (*Cucumis melo* L. var. reticulatus naud.) is a characteristic fruit of Xinjiang Uygur Autonomous Region, a melon with a thick skin, oval shape, reticulated rind, sweet taste and pleasant aroma. In addition, the unique geographical environment facilitates photosynthesis of the fruit during the day, reduces respiratory consumption, and deposits more nutrients at night, such as long daylight hours and a DIF (diurnal temperature difference) of about 15°C, which is particularly suitable for cultivation and development of Hami melon (1). As a special agricultural product of Xinjiang, the annual production of this melon is about 2.34 million tons, but it is rather intolerant to storage and transportation. In addition, it is a heat-sensitive fruit that causes severe flavor losses during thermal processing, such as a 20% reduction in total esters and a large reduction in the content of C6 and C9 alcohols and aldehydes after heat treatment

(2), so it is important to find an innovative food process to preserve its nutritional and unique flavor.

High hydrostatic pressure (HHP) is a non-thermal processing technology that uses water as a medium to treat raw materials under ultrahigh pressure (100–1,000 MPa) at room temperature or under mild conditions, raw materials treated in this way can effectively avoid the loss of nutrients and retain their freshness, flavor and color (1). HHP can be able to destroy cellular tissue, inactivate microorganisms, in fruit and vegetable processing is mainly used to sterilize (3), improve the extraction rate of bioactive substances (4) and passivation of enzyme activity (5). Furthermore, HHP treatment can be carried out at room temperature, which reduces the heating and cooling of the required energy consumption, and not in direct contact with the processing equipment, avoiding the occurrence of secondary contamination after pasteurization, and can achieve the recycling of pressure transfer media, it also has the advantages of lower energy consumption and pollution, is a relatively environmentally friendly processing technology (6). Mild heating is another way to improve the efficiency of high pressure enzyme inactivation, study have shown that a better degree of microbial and enzyme inactivation can be achieved at lower pressures (300–500 MPa) combined with mild heating (40–70°C) treatment. Moreover, the retention and activation of enzymes by high pressure also contribute to improving the texture of processed fruit and vegetable products, creating new structures that are different from those achieved by thermal processing (7), this was demonstrated in our previous study, in which Hami melon juice treated at 45°C significantly controlled the level of microbial and some enzyme activities by combining HHP treatment with different temperatures (25–55°C), while maintaining the original good quality (8). The changes in aroma components and catalytic reactions of flavor enzymes when fruit and vegetable juices are treated under ultrahigh pressure inevitably have their characteristics and patterns (9, 10). On the one hand, the form and structure of aroma components in fruit and vegetable juices treated by ultrahigh pressure underwent different degrees of change (11, 12). On the other hand, flavor enzymes in fruit and vegetable juices treated with HHP are partially inactivated or activated, further influencing the composition and content of the catalyst (13). The effect of residual enzyme activity on the actual fruit system during or after HHP may be a contributing factor (14).

Some compounds of the aliphatic series or aromatic groups, including esters, alcohols, acids, and aldehydes, are products or intermediates in the metabolism of amino acids, are usually found in animals and plants in the form of protein structures, bound to other macromolecules or free amino acids. Differences in food system processing and storage conditions, such as temperature, time, pressure, and substrate, will result in different changes in amino acid and protein structures (15). Fatty acids are precursors of many flavor substances and play a key role in the flavor changes of fruits. Fatty acids mainly produce some branched chain fatty alcohols, aldehydes, ketones and esters during their metabolism. The fresh odor in fruits and vegetables comes from C6 and C9 aldehydes and alcohols, which are converted from fatty acids to hydroperoxides by *LOX* and then converted to the corresponding aldehydes and alcohols by oxidation, dissociation and dehydrogenation to form esters, among others (16).

To assess the alterations in the aroma substances of Hami juice following HHP treatment, we researched the correlation between the juice's aroma compounds, precursors (fatty acids and amino acids), and associated changes in enzyme activity. Four different pressures were employed to treat Hami melon juice. The study analyzed the changes in aroma precursors, the enzymes involved in relevant metabolic pathways and the volatile compounds. Furthermore, the correlation between the four substances throughout the metabolic process was explored using correlation analysis. This provides a theoretical basis for the effect of HHP treatment on the flavor substances of Hami melon juice.

2. Materials and methods

2.1. Preparations of melon samples and melon juice

Nine boxes of Hami melons were selected at random from "Fruit and Vegetable Wholesale Market" in Shihezi City. These late-maturing melons were grown in Jiashi County, Xinjiang province, and were fully mature, with no visible lesions or rot. The soluble solid content of melons was approximately 12% with a pH range of 5.6 to 5.8. The melons were then placed in pre-sterilized cold storage at 4°C, to keep them fresh for later use. Hami melon juice was processed using a HHP machine (HHP.L.2–600/0.6, Huatai Senmiao Biotechnology Co., Tianjin, China).

2.2. High hydrostatic pressure treatment

Using water as the pressure transmission medium, four pressure gradients were set, 350, 400, 450 and 500 MPa, the temperature and pressure were kept at 45°C and 15 min, and the sub-packed Hami melon juice was put into the autoclave after the temperature of the ultrahigh pressure sterilizer was raised to 45°C by hot water circulation, then its water level was adjusted, and the pressure was set for 15 min, then the pressurization started, and after completion release the pressure automatically. Put the processed samples into the refrigerator at 4°C and stand for no more than 4 h from placement to measurement.

2.3. Extraction of volatiles compounds and analysis of GC–MS

After HHP processing, volatiles were extracted from juice by HS-SPME, by using SPME (Supelco, Inc.) after preprocessing polydimethylsiloxane (PDMS) fiber at 250°C for 30 min. Eight mL juice was transferred quickly to a headspace bottle (15 mL) containing 2.1 g NaCl, the juice was equilibrated through magnetic heating plate (HMS-901D, Bdjk Biotechnology Co., Ltd.) at 40°C for 10 min. The volatile components in the headspace were extracted at 40°C for 30 min by a stable flex PDMS fiber placed at 1 cm away from the liquid surface under 100 rpm/min magnetic stirring.

GC–MS analysis was performed by GC–MS (HP 7890/5975, Agilent Technologies) equipped with DB-5 (5% cross-linked phenylmethyl silicone) column (30 m × 0.25 mm i.d. × 0.25 μm, Agilent Technologies). The fiber was inserted into the sample hole and desorbed at 250°C for 1 min and run for 30 min. The fiber head is held for 5 min to remove impurities in the sample hole, injected in

splitless mode. The carrier gas (He, 99.999%) is added for 1 min and the flow rate was set to 40 cm/s. The initial temperature of the GC is maintained at 50°C for 1 min, then raised to 100°C (5°C/min), then raised to 250°C (10°C/min) and maintained for 9 min. The carrier gas was Helium (1.2 mL/min) with splitless injection. The quadrupole mass spectrometer was utilized in 70 eV electron ionization mode, with an ion source temperature of 200°C, a quadrupole temperature of 106°C, and a continuous scan range of 33–350 m/z.

2.4. Determining method of *ADH* activity

The *ADH* crude enzyme extract was extracted with a modification of the method described by Ntsoane et al. (17), combing Hami melon juice (4 mL) and 12 mL *ADH* extraction solution containing 10 mL of MES buffer (100 mM, pH = 6.5), 2 mM DTT, 1% (w/v) PVPP in a centrifuge tube, then stirred well to digestion (4°C, 30 min). The solution was centrifuged (GR21G, Hitachi Koki Co., Ltd., Tokyo, Japan) for 30 min (12,000 × g, 4°C), the supernatant as crude enzyme extract stored at 4°C for use. Two-point five mL MES buffer (100 mM pH = 6.5), 0.15 mL NADH (1.6 mM), 0.15 mL acetaldehyde (80 mM) and finally 0.3 mL of crude enzyme extract were added and completely mixed. The *ADH* activity was determined by measuring the change in absorbance value at 340 nm (recorded every 20 s for 3 min).

2.5. Determination method of *LOX* activity

According to Zhang et al. (18) methodology with modifications. Briefly, The *LOX* assay utilized sodium linoleate as a substrate. To prepare, 60 μL linoleic acid (LA) is extracted and placed in nitrogen gas at 15°C, degassed distilled water (4 mL) was added to the LA together with Tween 20 (120 μL), then 60 μL NaOH (5 M) is added and the solution is diluted to 25 mL with distilled water. Next, a mixture of Hami melon juice (3 mL) and 3 mL of *LOX* extraction buffer [with 1% (*w/v*)TritonX-100, 1% (*w/v*) PVP, 0.05 M phosphate buffer at pH = 6.8] was combined and left for 30 min. The supernatant was stored at 4°C after subjecting the mixture to centrifugation (12,000 rpm/min, 4°C, 10 min). Next, enzyme extract (0.02 mL) was added into a quartz cuvette containing the reacting mixture, which consisted of sodium linoleate (0.1 mL) and 2.88 mL of borate buffer (0.05 M, pH = 6.8). The *LOX* activity was determined by measuring the change in absorbance value at 234 nm (recorded every 20 s for 3 min).

2.6. Determination method of *ATT* activity

The *AAT* crude enzyme extract was extracted and assayed by the Zhu et al. (19) method with modifications. Hami melon juice (8 mL), potassium phosphate solution (16 mL, 100 mM, pH = 7.5) and 2.5 g PVPP were mixed thoroughly and digested (4°C, 30 min), then centrifuged for 30 min (12,000 × g, 4°C), the supernatant as crude enzyme extract stored at 4°C for use. Two point two 5 mL potassium phosphate buffer (100 mM, pH = 7.5), 0.3 mL DTNB (10 mM), 0.03 mL $MgCl_2$ (1 M), 0.06 mL isoamyl alcohol (20 mM), 0.06 mL acetyl coenzyme (50 mM) and finally 0.3 mL of crude enzyme extract were mixed thoroughly. The *ATT* activity was determined by measuring the change in absorbance value at 234 nm (recorded every 20 s for 3 min).

2.7. Determination method of *PLA2* activity

Hami melon juice (3 mL) was homogenized in 5 mL of pre-cooled 0.1 M phosphate buffered saline ($Na_2HPO_4{\cdot}12H_2O$, $NaH_2PO4{\cdot}2H_2O$). The mixture was centrifuged (12,000 × g, 4°C, 2 min). The supernatant was immediately collected as crude enzyme extract, and *PLA2* activity was detected by ELISA kit (DUMABIO, Shanghai, China). During the unit time, the absorbance variation 0.001 of 1 mL of enzyme solution was defined as 1 mL of *PLA2* activity.

2.8. Analysis of amino acids

Hami melon juice sample's amino acid content was analyzed using an amino acid analyzer (L-8900, Hitachi) in accordance with the Chinese Standard (GB/T 5009.124–2016). Following hydrolysis into free amino acids using HCl, the proteins in the juice samples were derivatized with ninhydrin solution, separated on an ion-exchange column, and their spectrophotometric absorbance was measured at 440/570 nm. To determine the amino acid content (g/100 g), the retention time of each amino acid was measured and compared to the standard mixed solution.

2.9. Analysis of fatty acids

The fatty acids were determined using the third method outlined in the Chinese Standard (GB/T 5009.168–2016), the specific methodology is based on our previous research (8). For total lipid extraction, 50 mL of the juice was mixed with 10 mL of 95% ethanol. The resulting mixture was then transferred using a separatory funnel containing a 50 mL mixture of ethyl ether/petroleum ether and shaken for 5 min before being left to settle for 10 min. The extract from the ether layer was gathered in a 250 mL flask and dried using rotary evaporation, resulting in the fat extract. The fat extract was mixed with an 8 mL solution of 2% (*w/v*) NaOH in methanol, thereafter converting the total fatty acid into fatty acid methyl esters. The organic phase was dried using nitrogen stream, upon which 20 mL of n-heptane was added and shaken for 2 min, followed by the addition of saturated aqueous NaCl. After allowing the mixture to stand and stratify, 5 mL of the upper heptane extraction solution was transferred into a 25 mL test tube. Around 3–5 g of anhydrous sodium sulfate was added, shaken for 1 min, and left untouched for 5 min, before transferring the upper phase of the solution into the sample bottle.

Fatty acid analysis was performed using a Shimadzu GC-2010, which was equipped with a capillary column (100 m × 0.2 μm × 0.25 mm i.d). The detector and sample injector were set to temperatures of 280°C and 270°C, respectively. The heating protocol proceeded as follows: the initial temperature was set to 100°C and maintained for 13 min, then increased to 180°C (10°C/min), then held for 6 min. Subsequently, the temperature was further raised to 200°C (1°C/min) and held for a duration of 20 min. Finally, the temperature was increased to 230°C (4°C/min) and kept for a total of 10.5 min. The results of the analysis of fatty acids were presented in percentage content (percentage of certain fatty acids to total fat).

2.10. Statistical analysis

Data analysis utilized SPSS to analyze variance, Origin was adopted for charting. and all experiments were repeated three times. GC–MS Data was acquired using HP ChemStation software (Agilent Technologies) and compared to a NIST library to determine the composition. Spectral library was used initially to determine the composition, while retention times, mass spectra, actual compositions, and retention indices were used for determine most compositions, quantification of the components was achieved by adding n-heptanol as an internal standard at a certain concentration. Relative quantification was then performed using the area normalization method. Moreover, the principal component analysis used the ade4 package of R-3.5.3 language for drawing, and thermograph adopted the complex heatmap package of the R-3.5.3 language for charting. Correlation analysis made use of spearman for correlation analysis and cytoscape for visualization.[1]

3. Results

3.1. Change in aroma volatile compounds

As shown in Table 1, there were 30 compounds in the untreated group, mainly including 20 esters, 4 alcohols, 3 aldehydes and 3 ketones. There were 30, 31, 29 and 25 categories of compounds in the group from 350 to 500 MPa. The 350 MPa group contained 18 esters, 4 alcohols, 5 aldehydes, 3 ketones. The 400 MPa group contained 18 esters, 4 alcohols, 6 aldehydes, 3 ketones, the 450 MPa group contained 17 esters, 4 alcohols, 5 aldehydes, 3 ketones, the 500 MPa group contained 15 esters, 3 alcohols, 4 aldehydes, 3 ketones. Compared to the untreated group, at different pressures, the treated groups were reduced by 2 to 4 esters and their content decreased significantly. Additionally, the content of alcohols and aldehydes increased after treatment at different pressures, but the content of alcohols decreased with increasing pressure and the content of aldehydes increased significantly.

3.2. Changes in enzyme activity

The major enzymes generated by the metabolism of aromatic substances included *ADH*, *LOX*, *AAT* and *PLA2*. Compared with untreated group, all the activities of *ADH* (Figure 1A) increased significantly ($p < 0.05$) under HHP treatments, of which the activity was highest under 350 MPa (13.4 U/mL), the activity of *ADH* decreased with increasing pressure. The activity of *LOX* after HHP treatment was lower than that of the untreated group and decreased with increasing pressure (Figure 1B). The activity of *ADH* decreased in samples between 400 MPa and 450 MPa, while it decreased significantly in samples at 500 MPa ($p < 0.05$), with an activity of 6.7 U/mL. The activity of *AAT* after HHP treatment was much lower than in the untreated group. Furthermore, the activity of *AAT* (Figure 1C) was obviously different between 4 types of pressure ($p < 0.05$), of which the activity of *AAT* was highest in the 400 MPa (18.6 U/mL). In addition, the activity of *PLA2* (Figure 1D) was greatly reduced ($p < 0.05$), and it also showed a downward trend with increasing pressure, but got some upturn at 500 MPa.

3.3. Change in amino acid contents

As shown in Figure 2, untreated Hami melon juice is rich in 11 amino acids, namely aspartic acid (Asp), threonine (Thr), serine (Ser), glutamic acid (Gly), proline (Pro), glycine (Glu), alanine (Ala), valine (Val), leucine (Leu), phenylalanine (Phe) and arginine (Arg). Among these, there are 4 essential amino acids and 7 non-essential amino acids. The number of amino acids increases with increasing pressure. 350 MPa treatment contained 14 amino acids, with increases in histidine (His), isoleucine (Iso) and lysine (Lys) compared to the untreated group. 400 MPa and 450 MPa treatments contained 13 amino acids with increases in Iso and Lys. 500 MPa treatment contained 12 amino acids, with a higher level of Lys. Across all treatments, Glu, Asp and Ala had notably higher contents when compared to other amino acids. However, the concentrations of Pro, Glu, Lys and Phe remained unchanged as pressure increased. Essential and non-essential amino acids, as well as total amino acids, experienced a marked increase in HHP treated groups. Nevertheless, there was an observed tendency toward decreasing contents with greater pressure, with the 400 and 450 MPa treatment groups demonstrating a decreasing trend, no significant differences were found between the 400 and 450 MPa treatment groups.

3.4. Change in fatty acids contents

Hami melon juice was analyzed for its fatty acid composition and a total of nine fatty acids were identified, comprising five unsaturated and four saturated fatty acids (Figure 3). Within the untreated group, palmitic acid and linoleic acid had the highest fatty acid content, 20.53 and 20.33% respectively, and were significantly reduced after HHP treatment ($p < 0.05$), heptadecanoic acid had the lowest content (2.65%), accounting for only 3.55% of the total fatty acid content. In the HHP treatment group, linoleic acid had the highest quantity followed by palmitic acid and α-linolenic acid in underwent treatment at 450 MPa. When the pressure was increased from 350 MPa to 500 MPa, the levels of palmitoleic, linoleic acid and α-linolenic acid significantly rose, with the exception of 450 MPa. Conversely, the levels of other fatty acids declined with an increase in pressure.

3.5. Correlation analysis

Figure 4 shows the correlation between aroma volatile compounds, amino acids, fatty acids and enzymes, with the red line indicating a positive correlation and the blue line a negative correlation. *PLA2* had the most related volatile compounds (nine esters, three alcohols, two aldehydes and two ketones), of which 10 were positively and 6 negatively correlated. Lys was associated with 12 volatile compounds, 11 of which were negatively correlated while

1 http://www.cytoscape.org

10.3389/fnut.2023.1285590

TABLE 1 Aroma volatile compounds in Hami melon juice under HHP treatments.

Volatile compound	Retention time (min)	Untreated	350 MPa	400 MPa	450 MPa	500 MPa
Eaters						
Methyl acetate	1.43	2.03 ± 0.57	ND	ND	ND	ND
Ethyl acetate	1.65	10.09 ± 0.43 ^{a}	26.23 ± 0.99 ^{b}	30.17 ± 1.5 ^{c}	29.51 ± 0.91 ^{c}	28.6 ± 1.11 ^{c}
Propyl acetate	2.25	1.56 ± 0.42 ^{a}	2.31 ± 0.19 ^{bc}	3.09 ± 0.62 ^{c}	2.97 ± 0.15 ^{c}	2.76 ± 0.64 ^{c}
Methyl butyrate	2.38	1.92 ± 0.49	ND	ND	ND	ND
Isobutyl acetate	2.67	3.91 ± 0.34 ^{c}	1.80 ± 0.04 ^{ab}	1.71 ± 0.02 ^{a}	2.06 ± 0.12 ^{b}	2.10 ± 0.16 ^{b}
2-methyl propyl acetate	2.8	8.22 ± 1.87 ^{c}	5.45 ± 0.38 ^{b}	4.21 ± 1.07 ^{b}	ND	4.91 ± 1.31 ^{b}
Methyl 2-methylbutyrate	2.86	4.93 ± 0.87	ND	ND	ND	ND
Ethyl butanoate	3.25	5.69 ± 0.78 ^{a}	5.98 ± 0.13 ^{a}	5.84 ± 0.13 ^{a}	6.8 ± 0.1 ^{b}	5.79 ± 0.15 ^{a}
Ethyl benzoate	3.45	1.08 ± 0.03 ^{a}	0.98 ± 0.12 ^{a}	0.96 ± 0.08 ^{a}	0.98 ± 0.12 ^{a}	0.98 ± 0.12 ^{a}
Methyl valerate	3.64	0.09 ± 0.02	ND	ND	ND	ND
Ethyl 2-methylbutanoate	3.87	3.40 ± 0.57 ^{a}	4.18 ± 0.23 ^{b}	4.67 ± 0.46 ^{bc}	4.36 ± 0.18 ^{bc}	4.93 ± 0.12 ^{c}
2-methyl butyl acetate	4.36	11.7 ± 2.55 ^{b}	5.33 ± 0.31 ^{a}	3.45 ± 0.65 ^{a}	4.33 ± 0.56 ^{a}	4.77 ± 1.24 ^{a}
Methyl ethyl thioacetate	6.65	0.05 ± 0.01^{a}	1.79 ± 0.15 ^{b}	2.16 ± 0.38 ^{b}	2.12 ± 0.29 ^{b}	ND
Ethyl caproate	6.99	4.83 ± 0.78 ^{b}	1.68 ± 0.21 ^{a}	1.54 ± 0.44 ^{a}	1.67 ± 0.23 ^{a}	1.65 ± 0.42 ^{a}
3-hexenol acetate	7.02	ND	1.16 ± 0.09 ^{d}	0.66 ± 0.16 ^{b}	0.86 ± 0.13 ^{c}	0.1 ± 0.02 ^{a}
Hexyl acetate	7.79	9.39 ± 0.83 ^{c}	0.15 ± 0.03 ^{a}	0.17 ± 0.15 ^{a}	0.17 ± 0.03 ^{a}	2.30 ± 0.49 ^{b}
2,3-butanediol diacetate	8.68	0.29 ± 0.04 ^{b}	1.16 ± 0.05 ^{c}	0.20 ± 0.02 ^{a}	0.24 ± 0.03 ^{ab}	0.19 ± 0.03 ^{a}
2-butanol-2 methyl acetate	8.83	ND	0.18 ± 0.03 ^{c}	ND	0.11 ± 0.03 ^{b}	0.1 ± 0.03 ^{b}
Heptyl acetate	9.95	0.17 ± 0.03	ND	ND	ND	ND
Methyl phenylacetate	11.34	3.99 ± 0.16 ^{a}	2.34 ± 0.44 ^{c}	1.54 ± 0.03 ^{b}	0.74 ± 0.57 ^{a}	1.29 ± 0.01 ^{ab}
Dimethyl 2-methylpropionate	15.4	ND	0.46 ± 0.04 ^{c}	0.52 ± 0.08 ^{c}	0.38 ± 0.03 ^{b}	ND
Butyl butyrate	15.42	ND	1.18 ± 0.03 ^{d}	0.56 ± 0.07 ^{c}	0.44 ± 0.06 ^{b}	0.4 ± 0.09 ^{b}
Diethyl phthalate	18.64	0.15 ± 0.01 ^{b}	0.13 ± 0.02 ^{ab}	0.10 ± 0.03 ^{a}	0.13 ± 0.03 ^{ab}	0.24 ± 0.04 ^{c}
Isopropyl palmitate	34.11	0.26 ± 0.05	ND	ND	ND	ND
Alcohols						
Ethanol	1.34	ND	6.40 ± 0.25 ^{d}	3.29 ± 0.13 ^{b}	4.36 ± 0.22 ^{c}	ND
2-ethyl-1-hexanol	7.64	0.68 ± 0.13 ^{a}	1.37 ± 0.08 ^{b}	1.38 ± 0.03 ^{b}	1.39 ± 0.06 ^{b}	1.38 ± 0.07 ^{b}
Nonanol	9.36	0.44 ± 0.07	ND	ND	ND	ND
(*Z*)-3-nonen-1-ol	11.5	ND	2.24 ± 0.12 ^{b}	2.46 ± 0.03 ^{c}	2.49 ± 0.07 ^{c}	2.59 ± 0.06 ^{c}
(*Z*)-6-nonen-1-ol	11.94	1.93 ± 0.10	ND	ND	ND	ND
2,7-octanediol	12.15	2.05 ± 0.15 ^{a}	3.01 ± 0.07 ^{b}	3.02 ± 0.08 ^{b}	3.42 ± 0.08 ^{c}	3.48 ± 0.06 ^{c}
Aldehydes						
2,4-pentadienal	3.31	6.13 ± 0.22	ND	ND	ND	ND
Hexanal	4.93	ND	0.11 ± 0.06 ^{b}	0.15 ± 0.03 ^{b}	ND	ND
Heptanal	7.86	ND	0.24 ± 0.04 ^{b}	0.30 ± 0.05 ^{b}	0.44 ± 0.10 ^{c}	ND
Nonanal	9.82	1.3 ± 0.06 ^{d}	ND	0.14 ± 0.01 ^{b}	0.22 ± 0.02 ^{c}	0.14 ± 0.02 ^{b}
(*E*)-6-nonenal	10.12	ND	7.52 ± 0.08 ^{b}	9.39 ± 0.01 ^{c}	10.51 ± 0.04 ^{d}	11.6 ± 0.35 ^{e}
Benzaldehyde	10.23	ND	0.12 ± 0.01 ^{b}	0.22 ± 0.03 ^{d}	0.15 ± 0.01 ^{b}	0.16 ± 0.01 ^{b}
(2*E*,6*Z*)-nonadienal	11.65	ND	3.15 ± 0.07 ^{b}	3.15 ± 0.15 ^{b}	4.55 ± 0.11 ^{c}	3.15 ± 0.02 ^{b}
Ketones						
6-methyl-5-heptene-2-one	7.34	0.16 ± 0.01 ^{a}	0.16 ± 0.01 ^{a}	0.15 ± 0.01 ^{a}	0.15 ± 0.02 ^{a}	0.15 ± 0.01 ^{a}
6,10-dimethylundeca-5,9-dien-2-one	16.96	0.25 ± 0.05 ^{c}	0.20 ± 0.02 ^{b}	0.19 ± 0.01 ^{ab}	0.16 ± 0.01 ^{ab}	0.15 ± 0.02 ^{a}
2,2,6-trimethyl-3-butanedione	17.52	0.17 ± 0.03 ^{c}	0.16 ± 0.02 ^{c}	0.15 ± 0.01 ^{bc}	0.12 ± 0.01 ^{ab}	0.11 ± 0.02 ^{a}

Results are presented in relative percentages and mean values ± standard deviation, $n = 3$. Volatile compound content is the relative percentage (%). ND, not detected. Different letters in the same raw correspond to significant differences ($p < 0.05$).

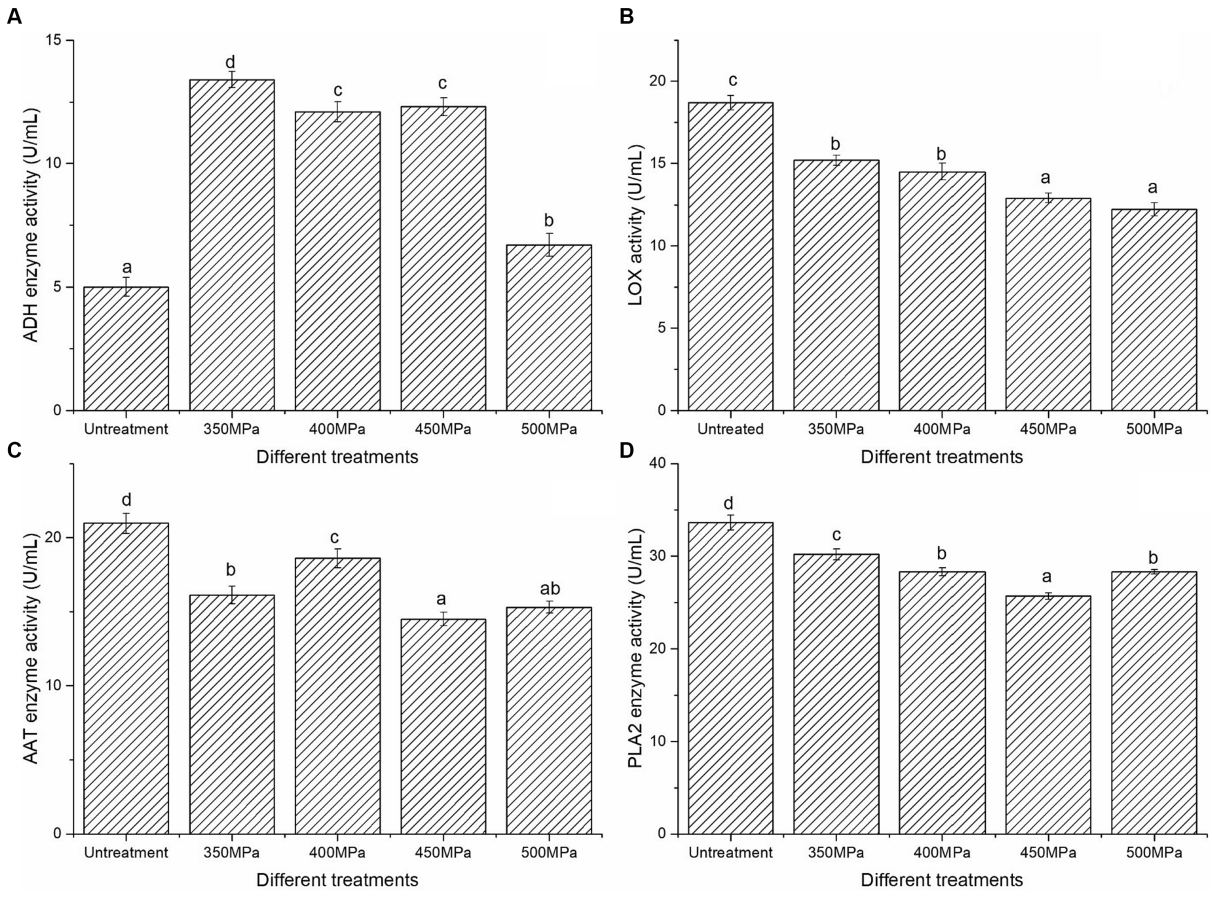

FIGURE 1
Effect of ADH **(A)**, LOX **(B)**, AAT **(C)** and PLA2 **(D)**.

only one exhibited a positive correlation, namely *2E*, *6Z*-nonadienal. Palmitic acid was found to have a correlation with 11 volatile compounds, of which six showed a negative correlation, while five showed a positive correlation. Based on the analysis in the right circle, *ADH* displayed positive associations with Asp., Thr, and Ser, as well as with Iso and stearic acid (FA9). Meanwhile, *LOX* exhibited positive correlations with palmitic acid (FA1), arachidonic acid (FA6), lauric acid (FA7), and heptadecanoic acid (FA8). These findings indicate that *ADH* mainly relates to amino acid metabolism while *LOX* is primarily involved in fatty acid metabolism. In addition, there is a correlation between six substances and esters, with three showing a positive correlation (FA8, *AAT*, *PLA2*) and the remaining three displaying a negative correlation (Lys, Pro, Asp). Eight substances are associated with alcohol, all of which demonstrate a positive correlation. As for aldehydes, Leu is positively correlated with eight substances, while *LOX*, *AAT*, *PLA2*, FA1, FA3, FA6, and FA7 exhibit negative correlations.

Table 2 shows a ranked list of correlations between enzymes, amino acids, fatty acids and volatile compounds. The most notable correlations were observed between enzymes and volatile compounds, with a coefficient of 0.85. Fatty acids came in second with a correlation coefficient of 0.77, followed by amino acids with 0.65. The greater *r* value noted in fatty acids than that of amino acids suggests a more robust metabolic response to fatty acid exposure compared to amino acids, following HHP processing in Hami melon juice.

4. Discussion

In comparison with the untreated group, the number of esters in HHP treatment decreased significantly, possibly because the pressure increased the decomposition reaction of the solvent, which nucleophilically attacked the esters and promoted their hydrolysis into various acids and alcohols (20). Similar findings have been reported in previous studies, such as the research conducted by Yi et al. (21), which indicated a significant reduction in ester levels in turbid apple juice following HHP treatment. Furthermore, HHP treatment resulted in altered levels of alcohols and aldehydes in Hami melon juice at different pressures. In contrast to other studies, Liu et al. (22) found that *6Z*-nonenal (*3E*,*6Z*)-nonadienol had no significant changes ($p > 0.05$), and (*2E*,*6Z*)-nonadienal as well as *2E*-nonenal had an obvious increase, making the cucumber odor fresher, which agreed with our results. Viljanen et al. (23) investigated the effects of 800 MPa treatment on tomatoes, revealing changes in key flavor compounds such as *3Z*-hexenal and *2Z*-pentenal. Two reasons were given for the changes in flavor caused by HHP treatment, firstly, the content of flavor compounds may have increased after pressure was applied,

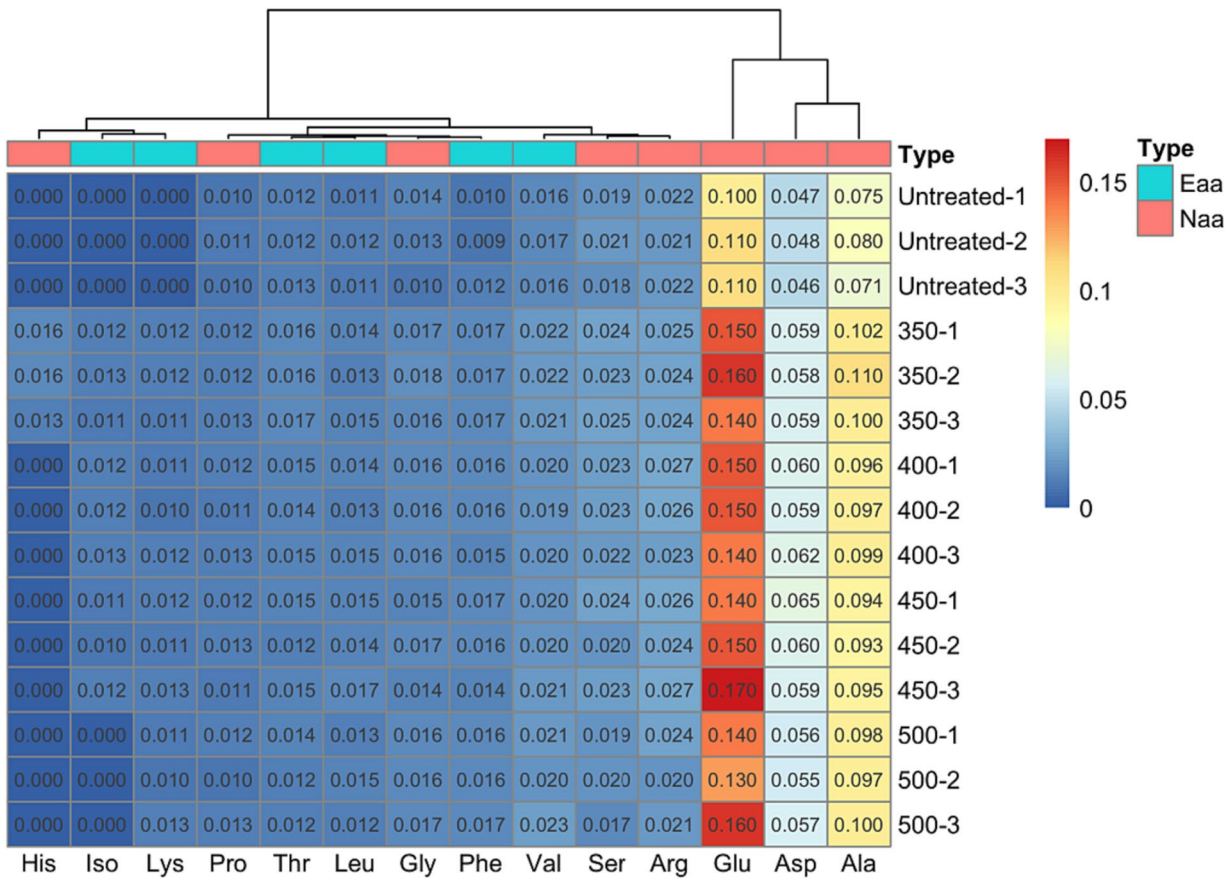

FIGURE 2
Changes of amino acids under different treatments.

resulting in increased contact between enzymes and their substrates and automatic oxidation of lipids (24). Secondly, HHP treatment is likely to impact the interaction between protein and flavor compounds (21).

The changes in *LOX* observed in this study were consistent with those reported in other studies, for instance, *LOX* in tomato juice lost more activity at higher pressures (550 MPa, 12 min/600 MPa, 10 min) according to the research of Rodrigo et al. (25), the activity of *ADH* was highest after ultrahigh pressure treatment, but decreased with increasing pressure. The research conducted by Denoya et al. (26) supports our conclusion regarding the *ADH* of two varieties of freshly cut peaches. The study determined that pressure has an impact on the activity of *ADH*, with a significant decrease observed when the pressure increased from 500 MPa to 700 MPa. Enzyme activity changes aligned not only with external factors such as pressure, temperature, and duration but with enzyme properties and internal factors such as substances like ethylene and tannin in fruit. Our results, similar to previous research, were substantiated by the crucial *AAT* that transformed alcohols to esters (10, 27). Shan et al. (28) found close links between the activity of the *AAT* in various melon cultivars and their aroma compounds. They showed that this activity directly impacted the production of volatile aldehydes and alcohols.

The HHP treatment process influenced the functioning of metabolic substrates such as amino acids and fatty acids, as well as enzymes related to volatile compounds, resulting in the modification of aroma substances. According to findings by Contreras et al. (29), differences in processing methods were able to alter the release of volatile compounds by affecting the correlation between factors in amino acid and fatty acid metabolism. For instance, the compounds, such as hexyl alcohol, hexyl ester, and caproic aldehyde, along with their metabolites, originated from the actions of *LOX* on linoleic acid. Moreover, *LOX* on linolenic acid predominantly resulted in the production of *3Z*-hexenal and *2E*-hexenal. El-Hadi et al. (30) discovered that the monomer amino acids contributing to fruit aroma metabolism primarily consisted of Val, Leu, Iso, Ala, Cys, and Phe, which are consistent with the results of our study. The association of numerous amino acids with flavor substances arose primarily due to the involvement of amino acid invertase in breaking them down, which was released during protein hydrolysis, and its activities led to the production of various volatile compounds (31, 32). Zhang et al. (33) reported that some alcohols of synthetic linear esters were also derived from *LOX*, which acted on aldehydes produced by fatty acids and was reduced to alcohols with the participation of *ADH*. In Shi et al.'s study (34), the decrease in aromatic ester showed a positive correlation with the change in *ADH* activity and the levels of oleic acid and linoleic acid, and a negative correlation with the activities of lipase, phospholipase D (*PLD*), *LOX*, and the rate of membrane permeability. Wang et al. (35) found that the *LOX* in tomatoes exerted large impacts on saturated and unsaturated C6 and C9 alcohols and aldehydes, by studying the effects of high-pressure treatment on

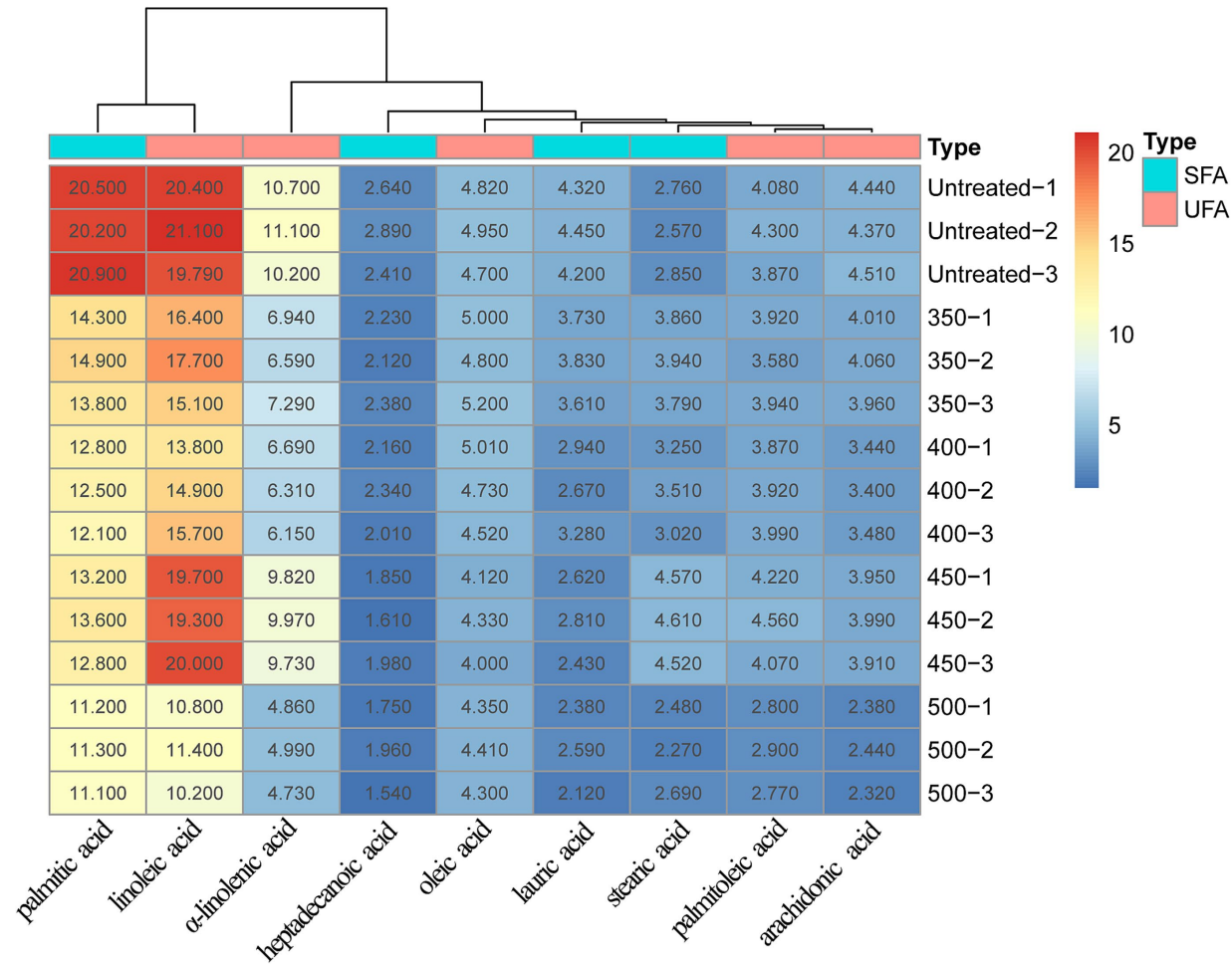

FIGURE 3
Changes of fatty acids under different treatments.

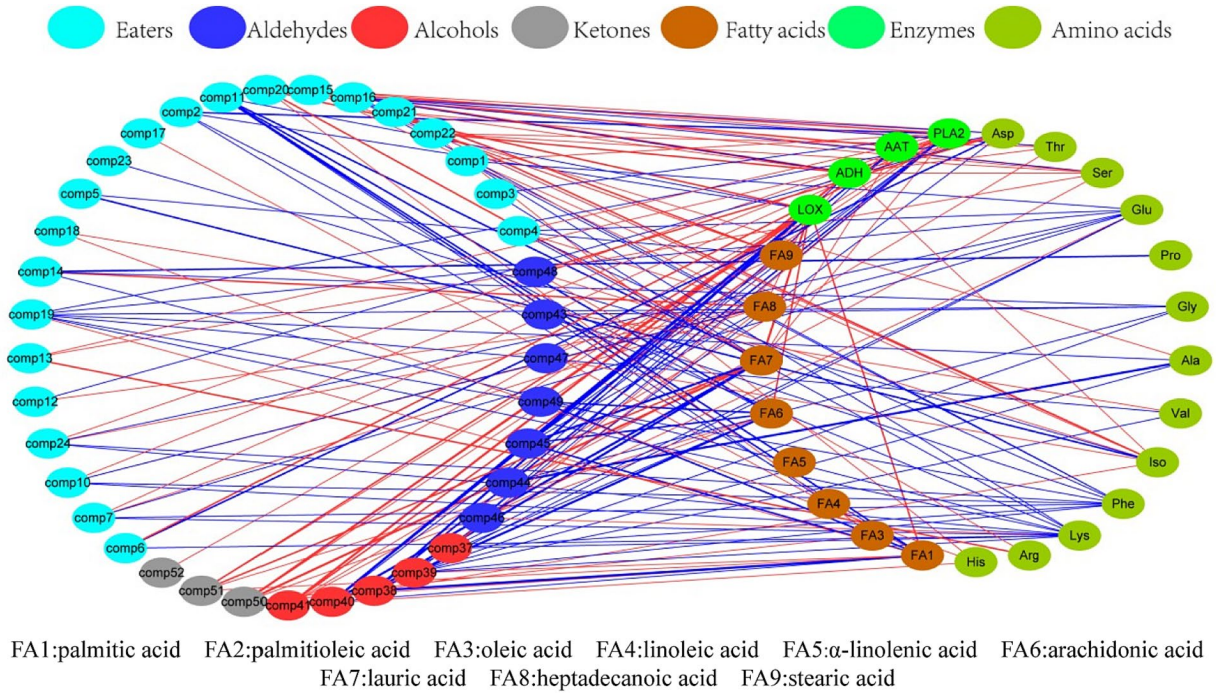

FIGURE 4
Correlation analysis of volatile compounds, amino acids, fatty acids and enzymes.

TABLE 2 Correlation analysis of aroma volatile compounds and precursors in HHP treatments.

Index	*r*	*p*
Enzymes	0.85 ± 0.02	0.002
Amino acids	0.65 ± 0.03	0.006
Fatty acids	0.77 ± 0.02	0.005

volatile ingredients and odors in tomatoes. The literature suggests that specific enzymes and substrates can influence the aroma in metabolic processes, which supports our conclusions.

5. Conclusion

HHP treatment had an effect on the species and contents of esters, alcohols and aldehydes in the volatile compounds of juice, mainly a substantial decrease in esters and a substantial increase in aldehydes and C6 and C9 alcohols. HHP treatment decreased the activities of four vital enzymes, of which *PLA2* and *AAT* activities were similar to *LOX*, and the activity of *ADH* was opposite to *LOX*. the activity of *ADH* was significantly increased, but decreased with the increase of pressure. The types and contents of amino acids in Hami melon juice increased, and the total amount of amino acids was also elevated, although the total amount of fatty acids decreased. By correlation analysis, there were six ester-related substances and eight alcohol-related, ketone-related and aldehyde-related substances in high pressure-treated Hami melon juice, and the correlation between fatty acids and volatile compounds was greater than the correlation between amino acids and volatile flavor compounds.

Data availability statement

The original contributions presented in the study are included in the article/supplementary material, further inquiries can be directed to the corresponding author.

Author contributions

LP: Methodology, Validation, Writing – original draft, Data curation, Investigation. WL: Data curation, Investigation, Writing – review & editing, Formal analysis, Validation. LJ: Conceptualization, Data curation, Writing – review & editing, Visualization. HX: Conceptualization, Data curation, Formal analysis, Writing – review & editing. LL: Data curation, Software, Visualization, Validation, Writing – review & editing. XW: Data curation, Formal analysis, Software, Writing – review & editing. ML: Software, Visualization, Writing – review & editing. BA: Investigation, Writing – review & editing, Validation. HZ: Investigation, Writing – review & editing. JC: Funding–acquisition, Methodology, Project–administration, Writing – review & editing.

Funding

The author(s) declare financial support was received for the research, authorship, and/or publication of this article. This work gained support from the National Science Foundation of China (31560461) and Xinjiang Institute of Technology project (ZT202101).

Conflict of interest

The authors declare that the research was conducted in the absence of any commercial or financial relationships that could be construed as a potential conflict of interest.

Publisher's note

References

1. Gómez-García R, Campos DA, Aguilar CN, Madureira AR, Pintado M. Valorization of melon fruit (*Cucumis melo* L.) by-products: phytochemical and biofunctional properties with emphasis on recent trends and advances. *Trends Food Sci Technol*. (2020) 99:507–19. doi: 10.1016/j.tifs.2020.03.033

2. Luo D, Pan X, Zhang W, Bi S, Wu J. Effect of glucose oxidase treatment on the aroma qualities and release of cooked off-odor components from heat-treated Hami melon juice. *Food Chem*. (2022) 371:131166. doi: 10.1016/j.foodchem.2021.131166

3. Li F, Chen G, Zhang B, Fu X. Current applications and new opportunities for the thermal and non-thermal processing technologies to generate berry product or extracts with high nutraceutical contents. *Food Res Int*. (2017) 100:19–30. doi: 10.1016/j.foodres.2017.08.035

4. García-Parra J, Ramírez R. New preservations technologies: hydrostatic high pressure processing and high pressure thermal processing. *Ref Module Food Sci*. (2018). 473–480. doi: 10.1016/b978-0-08-100596-5.22428-1

5. Grassino AN, Ostojić J, Miletić V, Djaković S, Bosiljkov T, Zorić Z, et al. Application of high hydrostatic pressure and ultrasound-assisted extractions as a novel approach for pectin and polyphenols recovery from tomato peel waste. *Innov Food Sci Emerg Technol*. (2020) 64:102424. doi: 10.1016/j.ifset.2020.102424

6. Zhang S, Zheng Z, Zheng C, Zhao Y, Jiang Z. Effect of high hydrostatic pressure on activity, thermal stability and structure of horseradish peroxidase. *Food Chem*. (2022) 379:132142. doi: 10.1016/j.foodchem.2022.132142

7. Huang H, Hsu P, Wang C. Healthy expectations of high hydrostatic pressure treatment in food processing industry. *J Food Drug Anal*. (2020) 28:1–13. doi: 10.1016/j.jfda.2019.10.002

8. Pei L, Hou S, Wang L, Chen J. Effects of high hydrostatic pressure, dense phase carbon dioxide, and thermal processing on the quality of Hami melon juice. *J Food Process Eng*. (2018) 41:e12828. doi: 10.1111/jfpe.12828

9. Zhu D, Zhang Y, Kou C, Xi P, Liu H. Ultrasonic and other sterilization methods on nutrition and flavor of cloudy apple juice. *Ultrason Sonochem*. (2022) 84:105975. doi: 10.1016/j.ultsonch.2022.105975

10. Terefe NS, Buckow R, Versteeg C. Quality-related enzymes in fruit and vegetable products: effects of novel food processing technologies, part 1: high-pressure processing. *Crit Rev Food Sci Nutr*. (2014) 54:24–63. doi: 10.1080/10408398.2011.566946

11. Zhou L, Bi X, Xu Z, Yang Y, Liao X. Effects of high-pressure CO2 processing on flavor, texture, and color of foods. *Crit Rev Food Sci Nutr*. (2015) 55:750–68. doi: 10.1080/10408398.2012.677871

12. Yang Y, Xia Y, Wang G, Tao L, Yu J, Ai L. Effects of boiling, ultra-high temperature and high hydrostatic pressure on free amino acids, flavor characteristics and sensory profiles in Chinese rice wine. *Food Chem*. (2019) 275:407–16. doi: 10.1016/j.foodchem.2018.09.128

13. Dars AG, Hu K, Liu Q, Abbas A, Xie B, Sun Z. Effect of thermo-sonication and ultra-high pressure on the quality and phenolic profile of mango juice. *Foods*. (2019) 8:298. doi: 10.3390/foods8080298

14. Wang C, Huang H, Hsu C, Yang B. Recent advances in food processing using high hydrostatic pressure technology. *Crit Rev Food Sci Nutr*. (2016) 56:527–40. doi: 10.1080/10408398.2012.745479

15. Zeng X, Jiao D, Yu X, Chen L, Sun Y, Guo A, et al. Effect of ultra-high pressure on the relationship between endogenous proteases and protein degradation of yesso scallop (Mizuhopecten yessoensis) adductor muscle during iced storage. *Food Chem X*. (2022) 15:100438. doi: 10.1016/j.fochx.2022.100438

16. Yue J, Zhang Y, Jin Y, Deng Y, Zhao Y. Impact of high hydrostatic pressure on non-volatile and volatile compounds of squid muscles. *Food Chem*. (2016) 194:12–9. doi: 10.1016/j.foodchem.2015.07.134

17. Ntsoane M, Luca A, Zude-Sasse M, Sivakumar D, Mahajan PV. Impact of low oxygen storage on quality attributes including pigments and volatile compounds in "Shelly" mango. *Sci Hortic*. (2019) 250:174–83. doi: 10.1016/j.scienta.2019.02.041

18. Zhang C, Jin Y, Liu J, Tang Y, Cao S, Qi H. The phylogeny and expression profiles of the lipoxygenase (LOX) family genes in the melon (*Cucumis melo* L.) genome. *Sci Hortic*. (2014) 170:94–102. doi: 10.1016/j.scienta.2014.03.005

19. Zhu Y, Rudell DR, Mattheis JP. Characterization of cultivar differences in alcohol acyltransferase and 1-aminocyclopropane-1-carboxylate synthase gene expression and volatile ester emission during apple fruit maturation and ripening. *Postharvest Biol Technol*. (2008) 49:330–9. doi: 10.1016/j.postharvbio.2008.03.01

20. González-Cebrino F, García-Parra J, Contador R, Tabla R, Ramírez R. Effect of high-pressure processing and thermal treatment on quality attributes and nutritional compounds of "Songold" plum purée. *J Food Sci*. (2012) 77:C866–73. doi: 10.1111/j.1750-3841.2012.02799.x

21. Yi J, Kebede BT, Hai Dang DN, Buvé C, Grauwet T, van Loey A, et al. Quality change during high pressure processing and thermal processing of cloudy apple juice. *Lebensm Wiss Technol*. (2017) 75:85–92. doi: 10.1016/j.lwt.2016.08.041

22. Liu F, Zhang X, Zhao L, Wang Y, Liao X. Potential of high-pressure processing and high-temperature/short-time thermal processing on microbial, physico- chemical and sensory assurance of clear cucumber juice. *Innov Food Sci Emerg Technol*. (2016) 34:51–8. doi: 10.1016/j.ifset.2015.12.030

23. Viljanen K, Lille M, Heiniö R-L, Buchert J. Effect of high-pressure processing on volatile composition and odor of cherry tomato purée. *Food Chem*. (2011) 129:1759–65. doi: 10.1016/j.foodchem.2011.06.046

24. Terefe NS, Buckow R, Versteeg C. Quality-related enzymes in plant-based products: effects of novel food-processing technologies part 3: ultrasonic processing. *Crit Rev Food Sci Nutr*. (2015) 55:147–58. doi: 10.1080/10408398.2011.586134

25. Rodrigo D, Jolie R, Loey AV, Hendrickx M. Thermal and high pressure stability of tomato lipoxygenase and hydroperoxide lyase. *J Food Eng*. (2007) 79:423–9. doi: 10.1016/j.jfoodeng.2006.02.005

26. Denoya GI, Vaudagna SR, Chamorro VC, Godoy MF, Budde CO, Polenta GA. Suitability of different varieties of peaches for producing minimally processed peaches preserved by high hydrostatic pressure and selection of process parameters. *LWT-Food Sci Technol*. (2017) 78:367–72. doi: 10.1016/j.lwt.2017.01.006

27. Kumar P, Kermanshahi-Pour A, Brar SK, He QS, Rainey JK. Influence of elevated pressure and pressurized fluids on microenvironment and activity of enzymes. *Biotechnol Adv*. (2023) 68:108219. doi: 10.1016/j.biotechadv.2023.108219

28. Shan W, Zhao C, Fan J, Cong H, Liang S, Yu X. Antisense suppression of alcohol acetyltransferase gene in ripening melon fruit alters volatile composition. *Sci Hortic*. (2012) 139:96–101. doi: 10.1016/j.scienta.2012.03.010

29. Contreras C, Tjellström H, Beaudry RM. Relationships between free and esterified fatty acids and LOX-derived volatiles during ripening in apple. *Postharvest Biol Technol*. (2016) 112:105–13. doi: 10.1016/j.postharvbio.2015.10.00

30. El-Hadi MA, Zhang FJ, Wu FF, Zhou CH, Tao J. Advances in fruit aroma volatile research. *Molecules*. (2013) 18:8200–29. doi: 10.3390/molecules18078200

31. Bas D, Kendirci P, Salum P, Govce G, Erbay Z. Production of enzyme-modified cheese (EMC) with ripened white cheese flavor: I-effects of proteolytic enzymes and determination of their appropriate combination. *Food Bioprod Process*. (2019) 117:287–301. doi: 10.1016/j.fbp.2019.07.016

32. Espino-Díaz M, Sepúlveda DR, González-Aguilar G, Olivas GI. Biochemistry of apple aroma: a review. *Food Technol Biotechnol*. (2016) 54:375–97. doi: 10.17113/ftb.54.04.16.4248

33. Zhang L, Wang J, Li G, Zhou X, Fu WW, Jiang YG, et al. Exogenous ATP alleviated aroma fading by regulating LOX pathway and fatty acids synthesis in "Nanguo" pears after refrigeration. *Sci Hortic*. (2018) 240:522–9. doi: 10.1016/j.scienta.2018.06.062

34. Shi F, Zhou X, Zhou Q, Tan Z, Yao M, Wei B, et al. Transcriptome analyses provide new possible mechanisms of aroma ester weakening of "Nanguo" pear after cold storage. *Sci Hortic*. (2018) 237:247–56. doi: 10.1016/j.scienta.2018.04.013

35. Wang X, Chen F, Ma L, Liao X, Hu X. Non-volatile and volatile metabolic profiling of tomato juice processed by high-hydrostatic-pressure and high-temperature short-time. *Food Chem*. (2022) 371:131161. doi: 10.1016/j.foodchem.2021.131161

frontiers | Frontiers in Nutrition

TYPE Original Research
PUBLISHED 05 January 2024
DOI 10.3389/fnut.2023.1321938

OPEN ACCESS

EDITED BY
Dandan Pu,
Beijing Technology and Business University, China

REVIEWED BY
Changyu Zhou,
Ningbo University, China
Alejandro Bielli,
University of the Republic, Uruguay

*CORRESPONDENCE
Xiang-Yun Rui
✉ 965347604@qq.com
Ming-Yue Wei
✉ weimingyue@stu.xmu.edu.cn
Bin Zhang
✉ zhangbin207@163.com

†These authors have contributed equally to this work

RECEIVED 15 October 2023
ACCEPTED 11 December 2023
PUBLISHED 05 January 2024

CITATION
Li H, Feng Y-H, Xia C, Chen Y, Lu X-Y, Wei Y, Qian L-L, Zhu M-Y, Gao G-Y, Meng Y-F, You Y-L, Tian Q, Liang K-Q, Li Y-T, Lv C-T, Rui X-Y, Wei M-Y and Zhang B (2024) Physiological and transcriptomic analysis dissects the molecular mechanism governing meat quality during postmortem aging in Hu sheep (*Ovis aries*). *Front. Nutr.* 10:1321938. doi: 10.3389/fnut.2023.1321938

Physiological and transcriptomic analysis dissects the molecular mechanism governing meat quality during postmortem aging in Hu sheep (*Ovis aries*)

Huan Li[1†], Yan-Hui Feng[2†], Chao Xia[1], Yu Chen[1], Xin-Yi Lu[1], Yue Wei[1], Le-Le Qian[1], Meng-Yao Zhu[1], Guo-Yv Gao[1], Ya-Fei Meng[1], Yv-Le You[1], Qi Tian[1], Kun-Qi Liang[1], Yun-Tao Li[1], Chao-Tian Lv[1], Xiang-Yun Rui[1*], Ming-Yue Wei[3*] and Bin Zhang[1*]

[1]College of Food and Bio-engineering, Bengbu University, Bengbu, Anhui, China, [2]College of Food Engineering, Anhui Science and Technology University, Chuzhou, Anhui, China, [3]School of Ecology, Resources and Environment, Dezhou University, Dezhou, Shandong, China

Introduction: Hu sheep, known for its high quality and productivity, lack fundamental scientific research in China.

Methods: This study focused on the effects of 24h postmortem aging on the meat physiological and transcriptomic alteration in Hu sheep.

Results: The results showed that the 24h aging process exerts a substantial influence on the mutton color, texture, and water content as compared to untreated group. Transcriptomic analysis identified 1,668 differentially expressed genes. Functional enrichment analysis highlighted the importance of glycolysis metabolism, protein processing in endoplasmic reticulum, and the FcγR-mediated phagocytosis pathway in mediating meat quality modification following postmortem aging. Furthermore, protein-protein interaction analysis uncovered complex regulatory networks involving glycolysis, the MAPK signaling pathway, protein metabolism, and the immune response.

Discussion: Collectively, these findings offer valuable insights into the molecular mechanisms underlying meat quality changes during postmortem aging in Hu sheep, emphasizing the potential for improving quality control strategies in mutton production.

KEYWORDS

lamb meat, post-slaughter storage, aging process, transcript profiles, regulatory network

1 Introduction

Mutton holds great value in Chinese culinary culture and offers numerous benefits. Its exceptional taste, high protein content, balanced fat levels, and low cholesterol levels

contribute to its consumer appeal (1). Consequently, there is a growing demand for lamb meat. Additionally, the improvement in living standards and changes in dietary preferences have led consumers to expect better quality mutton. However, meeting these expectations poses challenges due to the large market supply and demand. Therefore, it becomes essential to conduct thorough research on the post-slaughter quality of mutton.

Postmortem aging is an essential stage in mutton processing, and extensive research has demonstrated its significant enhancement of meat quality (2–5). This improvement is primarily due to anaerobic respiration during post-slaughter storage, resulting in the generation of lactic acid. Under controlled conditions of temperature, humidity, and airflow, lactic acid is enzymatically decomposed into carbon dioxide and water. And the intracellular adenosine triphosphate is hydrolyzed into the flavor-enhancing substance inosine monophosphate. Moreover, the altered pH not only increases tenderness but also aids digestion and absorption. Edible quality is a key determinant of meat quality, focusing on sensory attributes such as color, tenderness, and water retention. The duration of maturation after slaughter significantly affects the edible quality of the meat. Abdullah and Qudsieh (2) studied the quality changes in mutton stored for 24 and 168 h, and found that the meat within 168 h-treated exhibited increased brightness (L*) and redness (a*), as well as improved tenderness. Gao et al. (4) found that Jinta mutton that underwent aging process under optimal conditions (0–4°C, 90% humidity, hung for 16–20 h, then frozen at −20°C and matured on the second day) had superior meat color, pH, and flavor compared to untreated mutton. Martínez-Cerezo et al. (5) observed that postmortem aging affected the texture of Rasa Aragonesa, Churra, and Spanish Merino lambs, especially in the first 4 days, and the effect continued until day 16, but with a slower tenderization rate. In addition, Choe et al. (3) found that increasing the aged temperature (3 or 7°C) for lamb loin significantly shortened the required treatment time before freezing while maintaining equivalent quality characteristics, such as tenderness, drip loss, and shelf life, as 14 days aged-treated loin at −1.5°C. Despite significant research on the physiological and biochemical effects of postmortem aging on mutton, further investigation is needed to decipher the underlying transcriptional expression profiles and molecular mechanisms.

Transcriptomics is an effective means of studying gene expression and regulatory patterns to reveal biological pathways and molecular mechanisms. It is widely used in animal research, especially for identifying candidate genes related to meat quality in livestock. For instance, Fernández-Barroso et al. (6) identified 200 differentially expressed genes and 245 novel isoforms in Iberian pigs with varying tenderness levels. Muniz et al. (7) using RNA-Sequencing (RNA-Seq) found newly mRNA isoforms linked to beef tenderness, involving oxidative processes, energy production, and striated muscle contraction. Damon et al. (8) discovered that breed differences in pigs' muscle gene expressions and chemical composition are linked to energy metabolism, lipid deposition, and the role of cytoskeleton and contractile fibers in determining muscle and meat phenotypes. This technology has also been applied to research in mutton. Miao et al. (9) observed significant down-regulation of metabolic processes, particularly lipid metabolism, in Small Tail Han sheep's adipose tissue compared to Dorset sheep, potentially explaining disparities in fat deposition. Moreover, mitochondrial genes ATP synthase F0 subunit 6, cytochrome c oxidase subunit I, II, and cytochrome b were identified as core tenderness-related genes in Tan sheep meat (10). RNA-Seq, therefore, offers robust technical support for understanding molecular mechanisms after postmortem aging of mutton at the transcriptional level.

The Hu sheep (*Ovis aries*) of China is well-known for its early maturity, high productivity, and excellent meat production (11). This local variety, with a breeding history of over 800 years, also shows resilience to high temperatures and humidity (12). It is preferred for factory-scale meat sheep production and its market sales are on the rise. However, research on Hu sheep is still in its early stages, indicating significant potential for development. Thus, this study was performed to explore the potential mechanisms related to meat quality during postmortem aging using physiological, transcriptomic, and bioinformatic approaches.

2 Materials and methods

2.1 Sample preparation and treatment

In October 2022, nine 6-month-old male Hu sheep (*O. aries*) from a pasture located at Anhui Zhenghua Yang Ye Co., Ltd. in China, with comparable body weights (45 ± 1.62 kg) and feeding protocols, were selected for this study. Fresh lamb muscles between the 12th and 13th ribs on either side were meticulously packed in an insulated container and transported to the laboratory under controlled temperature conditions ranging between 0 and 4°C (13). The Hu sheep meat batch was then segregated into two distinct groups: a control group designated as before the aging process (BA) and an experimental group referred to as after the aging process (AA). The Hu sheep meat samples in the BA group underwent no treatment and were directly collected for index testing. On the other hand, the Hu sheep meat samples in the AA group underwent a refrigerated aging process at a temperature of 4°C for 24 h prior to conducting the assays. A portion of the Hu sheep meat samples were selected for physiological analysis such as color and pH measurements, determination of textural profile and cooking loss, and assessment of nuclear magnetic properties. The remaining samples weighing 0.2 g were immediately cryopreserved in liquid nitrogen for future transcriptome sequencing studies, with three biological repeats.

2.2 Color and pH measurement

To ensure accurate color measurement, only areas without any apparent imperfections that could potentially impact the consistency of color readings were selected (14). To measure meat color, the surface of meat samples was scanned using an NR10QC Color Meter from Shenzhen ThreeNH Technology Co., Ltd., which provided readings for lightness (L*), redness (a*), and yellowness (b*) in accordance with the manufacturer's instructions. pH values in the muscle tissue were measured by inserting a calibrated pH probe (PHs-2F from Shanghai INESA Scientific Instrument Co., Ltd.) to a depth of 2 cm in postmortem meat at random locations (15).

2.3 Textural profile determination and cooking loss analysis

The TA. XT Express texture analyzer (Stable Micro Systems, United Kingdom) was used to analyze the texture of the Hu sheep meat before and after the aging process, following the method of Dong et al. (11) with slight modifications. Hardness (N) and chewiness (mJ) values were obtained by setting the parameters of the texture analyzer, including a pre-test speed of 5 mm/s, a test speed of 1.5 mm/s, a post-test speed of 5 mm/s, a 5-s pause time between compressions, and a trigger force of 5 g. The cooking loss is performed with the method of Wang et al. (12). In brief, high-quality meat samples were precisely weighed and measured to ensure a consistent thickness. A thermometer was inserted into the center of each sample and sealed in a steaming bag. The samples were heated in a controlled 80°C water bath until the core temperature reached 75°C. The heating process was stopped after 20 min of constant temperature. Once cooled to room temperature, the surface was carefully dried, and each sample was weighed. The cooking loss was determined by quantifying the weight difference of Hu sheep meat before and after cooking, under both BA and AA treatment conditions. The resulting values were then expressed as a percentage (%).

2.4 Magnetic resonance imaging measurement

Magnetic resonance imaging (MRI) measurements were conducted based on the method of Dong et al. (11) with alterations. The sample was placed in the center of the coil for MRI testing. A SPIN ECHO sequence was employed and the main parameters of the magnetic imaging (MRI) were average = 2, slice width (mm) = 3.0, slice gap (mm) = 2.0, waiting time (TR) = 500 ms, echo time (TE) = 20 ms, phase size = 192, and read size = 256.

2.5 Low-field nuclear MR analysis

The acquisition of transverse (T_2) relaxation in Low-field nuclear MR (LF-NMR) was carried out following the method of Zheng et al. (16), with modifications. Water distribution of the Hu sheep meat samples was measured with the NMR analysis software. A sample of approximately 2 g of Hu sheep meat was placed in the center of the coil for nuclear magnetic testing, and the center frequency of the sample was obtained by an FID sequence. The CPMG sequence was then used for the subsequent detection. The main parameters of the T_2 test included SF (MHz) = 21, RFD (ms) = 0.02, O_1 (Hz) = 328,606.75, RG1 (db) = 10.0, P1 (μs) = 14.00, DRG1 = 3, TD = 120,012, PRG = 3, TW (ms) = 4,500.00, NS = 16, TE (ms) = 0.200, and NECH = 3,000. After information was collected, data inversion was performed to obtain the transverse relaxation time T_2 of the sample.

2.6 RNA extraction, sequencing, and data processing

The samples of Hu sheep meat underwent cryogenic grinding in liquid nitrogen. Total RNA was extracted from each sample using a Quick RNA isolation kit (Bioteke Corporation, Beijing, China). The quality assessment of the extracted total RNA was carried out using the NanoDrop 2000 (Thermo Fisher Scientific, USA), Qubit 2.0 fluorometer (Life Technologies, USA), and Agilent 2,100 bioanalyzer (Agilent, USA) (17). Subsequently, the total RNA was sent to Beijing Novel Bioinformatics Co., Ltd. for the construction of cDNA libraries and *de novo* transcriptome sequencing using the Illumina NovaSeq 6,000 platform, which resulted in the generation of 150 bp paired-end reads (18). The raw sequencing data were archived in the Sequence Read Archive with the accession number SRR25065590-SRR25065595. After rigorous quality control, the clean reads were utilized for subsequent analyses. Differential gene expression analysis was performed using FPKM values and DESeq2 (19, 20). Genes meeting the criteria of having a value of $p < 0.05$ and $|\log2FoldChange| > 0$ were deemed as differentially expressed genes (DEGs) (21, 22). The potential molecular functions and biochemical pathways were determined via Gene Ontology (GO) enrichment analysis with a significance threshold of value of $p < 0.05$, and Kyoto Encyclopedia of Genes and Genomes (KEGG) metabolic pathway enrichment analysis with a corrected value of $p < 0.01$, following the method of Young et al. (23) and Mao et al. (24).

2.7 Statistical analysis

The One-way ANOVA analysis, followed by Duncan's multiple range test with a significance threshold of $p < 0.05$, was used to perform significance analysis on the data presented in the figures and tables of the experiment using SPSS software (Version 21) (18). The means ± SE were used to represent all data depicted in the figures. Venn diagrams and hierarchical clustering were analyzed on the Novogene online platform.[1] Additionally, other graphical representations were generated using GraphPad Prism software (Version 9.0.2).

3 Results

3.1 Changes in mutton color and pH of Hu sheep after postmortem aging

To investigate the impact of postmortem aging on the physicochemical properties of Hu sheep, color and pH measurements were conducted before and after the aging process (Figure 1). The results showed substantial variations in both color and pH levels between the untreated and treated samples. Notably, the aging process significantly increased the values of Lightness (L*), Redness (a*), and Yellowness (b*) in Hu sheep meat (Figures 1A–C). Compared to the non-aging-treated group, the values of L*, a* and b* were 2.4, 7.2 and 14.2% higher, respectively. Among these, the b * values changed the most. In contrast, the pH value significantly decreased as a result of the aging process (Figure 1D).

1 https://magic.novogene.com

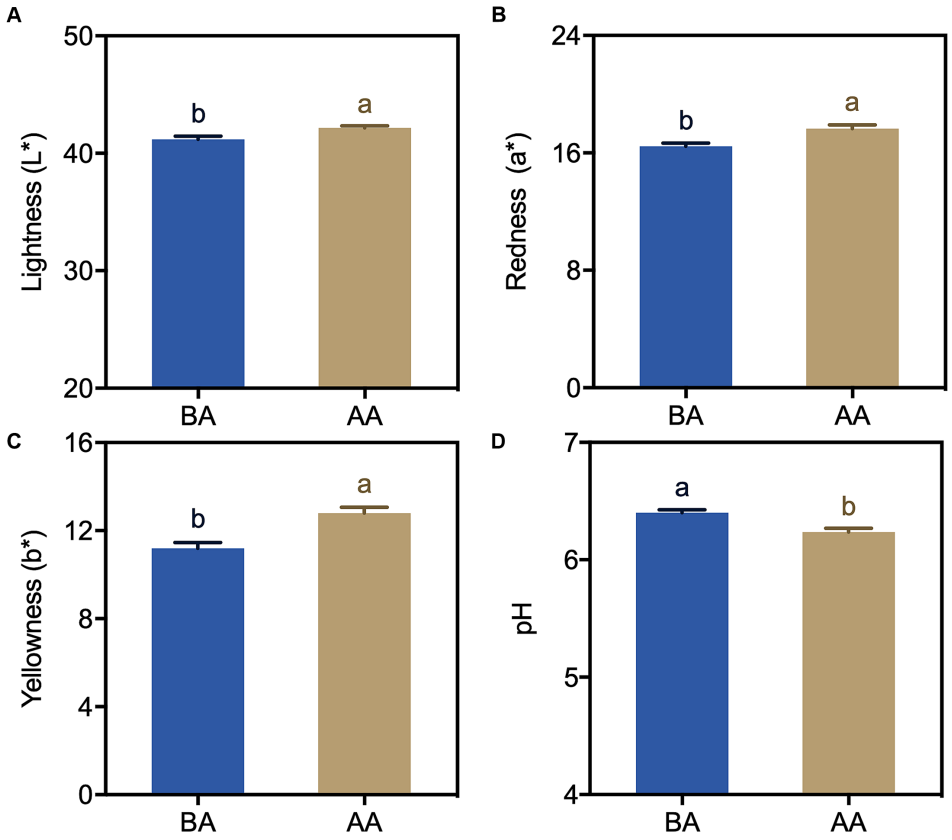

FIGURE 1
Color **(A–C)** and pH **(D)** changes in Hu sheep meat before (BA) and after the aging process (AA), with significance at $p < 0.05$ (one-way ANOVA) indicated by different lowercase letters above each column.

3.2 Effect of aging process on the mutton textural characteristics of Hu sheep

Textural characteristics are an important aspect in determining the sensory presentation of meat. To explore the relationship between the aging process and the textural characteristics of the meat products, the hardness and chewiness of the samples were examined. The obtained findings, as illustrated in Figure 2, demonstrated a marked elevation in the hardness of Hu sheep meat subsequent to the aging process compared to controlled samples. Furthermore, a substantial alteration in chewiness was observed under aging conditions, showing a significant surge of 75.6% relative to the controlled level.

3.3 Cooking loss analysis and water distribution analysis of Hu sheep meat utilizing magnetic resonance imaging and low-field nuclear MR relaxometry

To know the effect of the aging process on the moisture of Hu sheep meat, the cooking loss rates of meat samples were determined. A significant difference in the cooking loss of Hu sheep meat between the BA and AA group was found (Figure 3). This difference was evident in the marked increase observed after the aging process. Specifically, the loss rate of the AA group was more than 30%, which indicated that the water retention of Hu sheep meat decreased after the aging process.

The water distribution in the BA and AA-treated meat samples was visualized using magnetic resonance imaging (MRI). By applying pseudocolor processing, the spatial distribution of water molecules in Hu sheep meat could be distinctly observed (Figure 4A). Typically, the red color in the image represents a high proton density, the blue color represents the low proton density. As shown in Figure 4A, the total signal intensity of aging Hu sheep meat decreased and the red area was unevenly distributed, with a reduction of red in the center. This suggests a decrease in water content and a change in its distribution, with water shifting from the center of the meat outward. In Figure 4B, the hydrogen proton signal intensity also significantly decreased after the aging process, indicating a reduction in water content in Hu sheep meat. This is consistent with the results observed in hydrogen proton nuclear magnetic imaging and further confirms that the aging process reduces the water holding capacity of mutton.

The analysis of multi-component relaxation characteristics revealed the presence of four distinct water populations in both BA and AA-treated mutton samples. These water populations had T_2 relaxation times ranging from 0.1 to 1, 1 to 10, 10 to 100, and 100 to 1,000 ms, corresponding to bound water (T_{2b} and T_{21}), immobilized

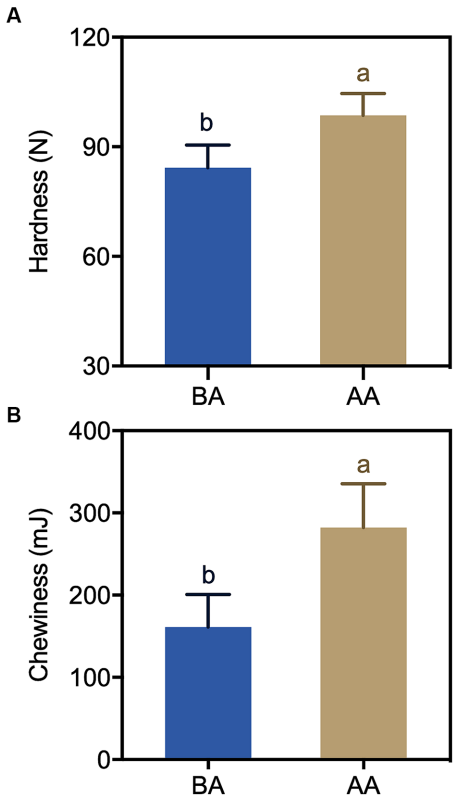

FIGURE 2
Comparison of hardness **(A)** and chewiness **(B)** of Hu sheep meat before (BA) and after the aging process (AA), with significance at $p < 0.05$ (one-way ANOVA) indicated by different lowercase letters above each column.

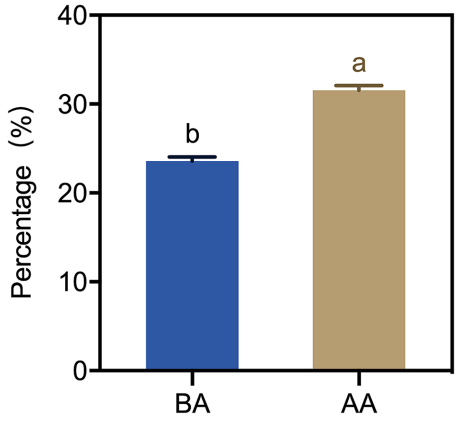

FIGURE 3
Cooking loss of Hu sheep meat before (BA) and after the aging process (AA), with significance at $p < 0.05$ (one-way ANOVA) indicated by different lowercase letters above each column.

water (T_{22}), and free water (T_{23}) (Figures 4C,D). In addition, the analysis showed that both BA and AA treated mutton exhibited the lowest P_{2b} and P_{21}, while manifesting the highest P_{22}, followed by P_{23}. Consequently, immobilized water was the main water phase of mutton. Furthermore, it was observed that P_{23} exhibited a decreasing trend, indicating a significant loss of free water (Figure 4C).

3.4 Assembly, differentially expressed genes selection, and enrichment analysis of GO and KEGG metabolic pathways

In order to gain deeper insights into the molecular mechanism behind the aging process of the Hu sheep meat quality, subsequent transcriptomic investigations were undertaken. The sequencing and assembly results are presented in Table 1. Upon raw read filtration, a total of 40,593,128-44,781,602 clean reads were successfully obtained. The Q20 and Q30 values were calculated to be 97.46–97.72% and 93.12–93.57%, respectively. Furthermore, the GC content ranged from 44.49 to 49.98% (Table 1).

The transcriptomic analysis of Hu sheep yielded a comprehensive set of 12,915 genes (Figure 5A). Detailed analysis of the expression profiles of meat samples from the control and AA groups facilitated the generation of a heatmap, demonstrating the hierarchical clustering among Unigenes (Figure 5B). It is noteworthy that 10,998 genes were found to be present in both treatment groups. Moreover, specifically in the AA and BA treated groups, there were 965 and 952 genes, respectively, that were exclusively obtained. Further analysis uncovered a total of 1,668 genes exhibiting differential expression. Among these, 920 genes displayed a down-regulated pattern, while 748 genes were observed to be up-regulated (Figure 5C).

To explore the functional distribution characteristics of DEGs and their corresponding metabolic pathways, we conducted GO and KEGG enrichment analyses. The GO analysis results showed that there were 22 significantly affected biological pathways under aging conditions (Figure 6). Among them, there was a substantial enrichment of DEGs within specific biological processes, namely catabolic process, organic substance catabolic process, and cellular catabolic process. Furthermore, in the categories of iron ion homeostasis, cellular ion homeostasis, cellular iron ion homeostasis, cellular chemical homeostasis, transition metal ion homeostasis, and cellular metal ion homeostasis, only four upregulated DEGs were identified. Similarly, in the categories of negative regulation of the cell cycle and cell cycle process, only four and six down-regulated DEGs were found.

Further investigation conducted through KEGG pathway analysis revealed a notable enrichment of up-regulated DEGs within crucial pathways (Figure 7), such as glycolysis and FcγR-mediated phagocytosis. Conversely, the down-regulated DEGs displayed a conspicuous enrichment in the protein processing in endoplasmic reticulum. Specific analysis showed that 13 DEGs were involved in the glycolysis metabolic pathway (Figure 8). Out of these, 10 DEGs were found to participate in the biosynthesis of pyruvate and exhibited an up-regulated expression. Furthermore, 2 DEGs (one up-regulated and one down-regulated) and 1 DEG (up-regulated) were discovered to participate in the subsequent synthesis of lactic acid and alcohol (Figure 8), respectively. In FcγR-mediated phagocytosis, a total of 18 DEGs were identified, with 16 up-regulated and 2 down-regulated (Figure 8). In the metabolic pathway of protein processing in the endoplasmic reticulum, a comprehensive total of 25 DEGs were identified. It is noteworthy that the majority of these

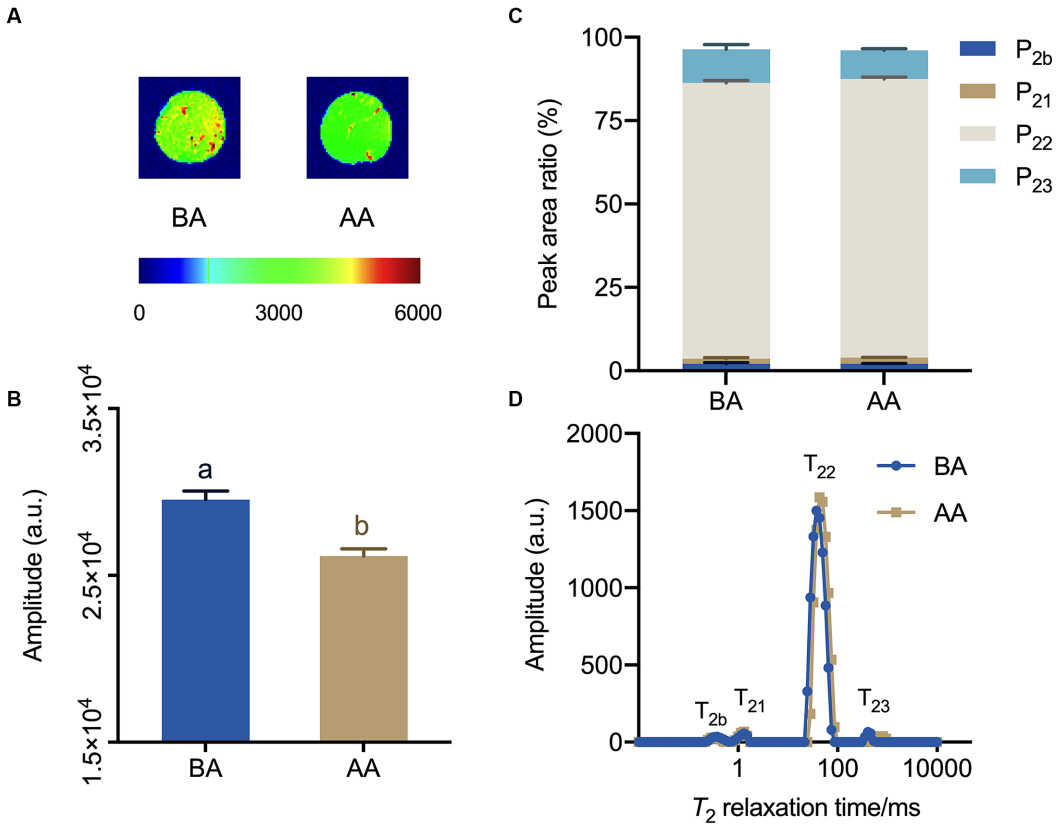

FIGURE 4
Exploration of the effects of the aging process on Hu sheep meat through magnetic resonance imaging (MRI) and Low-field nuclear MR (LF-NMR) relaxometry. **(A)** proton density-weighted images and **(B)** corresponding quantitative signal intensity histogram, **(C)** water distribution, **(D)** low-field relaxometry distributed T_2 relaxation times, with statistically significant differences at $p < 0.05$ (one-way ANOVA) indicated by different lowercase letters above each column.

TABLE 1 **Summary of assembly results of Hu sheep meat before (BA) and after aging process (AA).**

Sample	Raw reads	Clean reads	Clean bases	Error (%)	Q20 (%)	Q30 (%)	GC (%)
BA1	45,553,662	44,101,392	6.62G	0.03	97.72	93.57	44.49
BA2	47,197,656	44,781,602	6.72G	0.03	97.53	93.32	46.67
BA3	41,230,828	40,593,128	6.09G	0.03	97.51	93.34	49.98
AA1	46,748,564	46,072,050	6.91G	0.03	97.59	93.48	49.09
AA2	45,088,868	44,475,286	6.67G	0.03	97.57	93.37	46.65

The Q20 and Q30 percentages indicate the proportions of nucleotides with quality values greater than 20 and 30, respectively.

DEGs exhibited a significant down-regulation, while only a mere 3 genes displayed an up-regulated pattern (Figure 8). These genes play diverse roles, to varying extents, in essential biological processes including protein synthesis and degradation, such as the ubiquitination-mediated degradation of misfolded proteins.

3.5 Construction and modular analysis of protein–protein interaction network

By utilizing the STRING online database and the Cytoscape software, we successfully generated a PPI network in order to elucidate potential functional modules pertaining to Hu sheep meat quality after the aging process. The findings from the protein–protein interaction (PPI) analysis unveiled that, upon undergoing the aging process, a total of 54 nodes and 177 edges were acquired. Moreover, the PPI analysis discerned the existence of an intricate regulatory network interconnecting glycolysis, Fc gamma R-mediated phagocytosis, and protein metabolism throughout the course of the aging process (Figure 9; Supplementary Table S1).

Additionally, the implementation of the MCODE plugin led to the identification of three distinct functional modules, as depicted in Figure 10 and Supplementary Table S2. Cluster 1 encompasses a total of 11 nodes and 37 edges, with HSPA5 serving as the seed node. The proteins within Cluster 1 primarily exhibit associations with protein processing and carbohydrate metabolism. Cluster 2 consists of 8 nodes and 18 edges, with

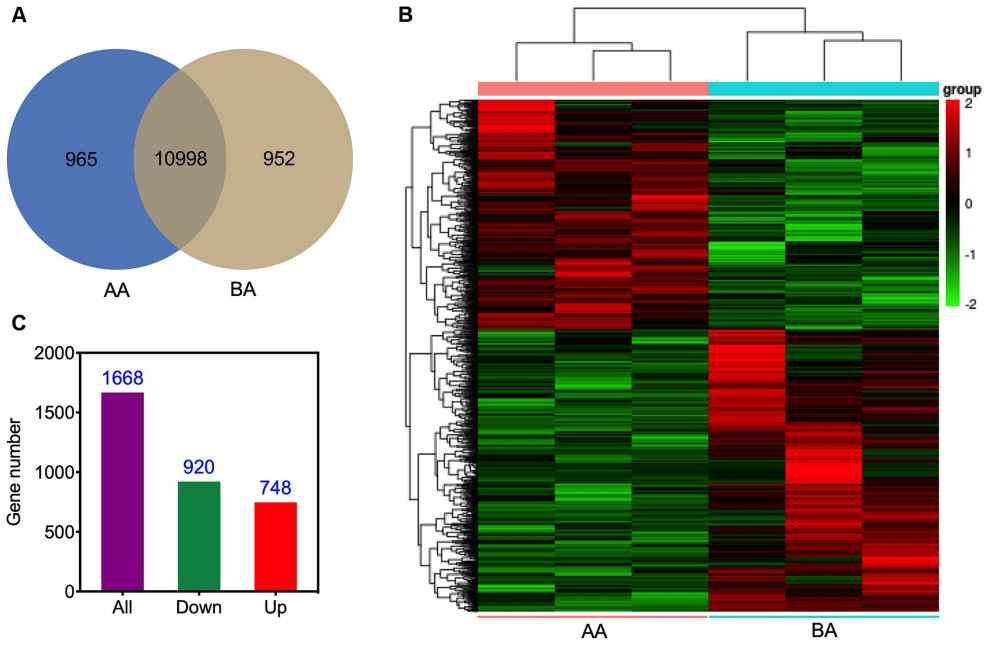

FIGURE 5
Visual representations illustrating the unigenes of Hu sheep meat before (BA) and after the aging process (AA): Venn diagram **(A)**, and hierarchical clustering **(B)**, accompanied by the histogram **(C)**, presenting the profiles of DEGs.

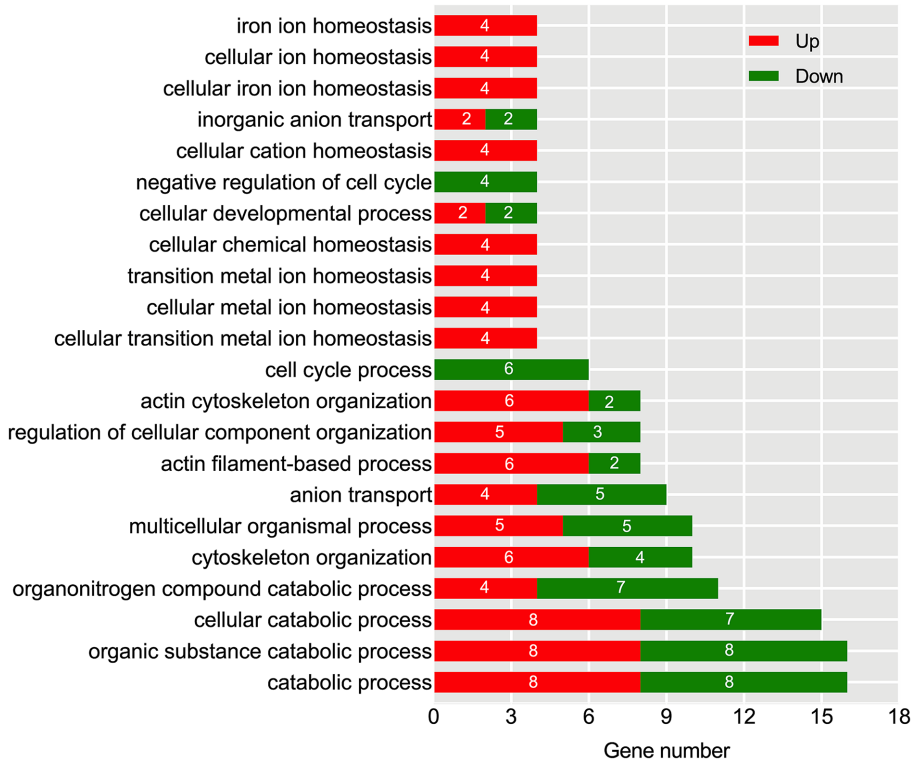

FIGURE 6
Identification of significantly enriched GO terms based on biological process after the aging process. The x-axis represents the number of DEGs, while the left y-axis displays various functional groups. Up-regulated DEGs are highlighted in red, and down-regulated DEGs are highlighted in green.

GAPDH as the seed node, predominantly participating in glycolysis, the mitogen-activated protein kinase (MAPK) cascade, and protein metabolism. Cluster 3 comprises 4 nodes and 6 edges, with FCGR1A acting as the seed node. The proteins within this particular module mainly exhibit involvement in Fc gamma R-mediated phagocytosis.

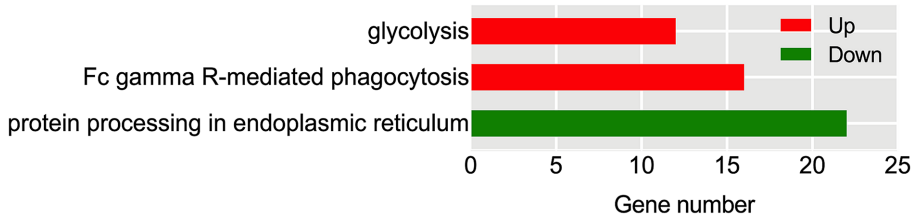

FIGURE 7
KEGG enrichment analysis of Hu sheep meat after the aging process. The x-axis represents the number of DEGs, while the left y-axis reflects the diversity of functional groups. KEGG pathways related to up-regulated DEGs are highlighted in red, and those associated with down-regulated DEGs are highlighted in green.

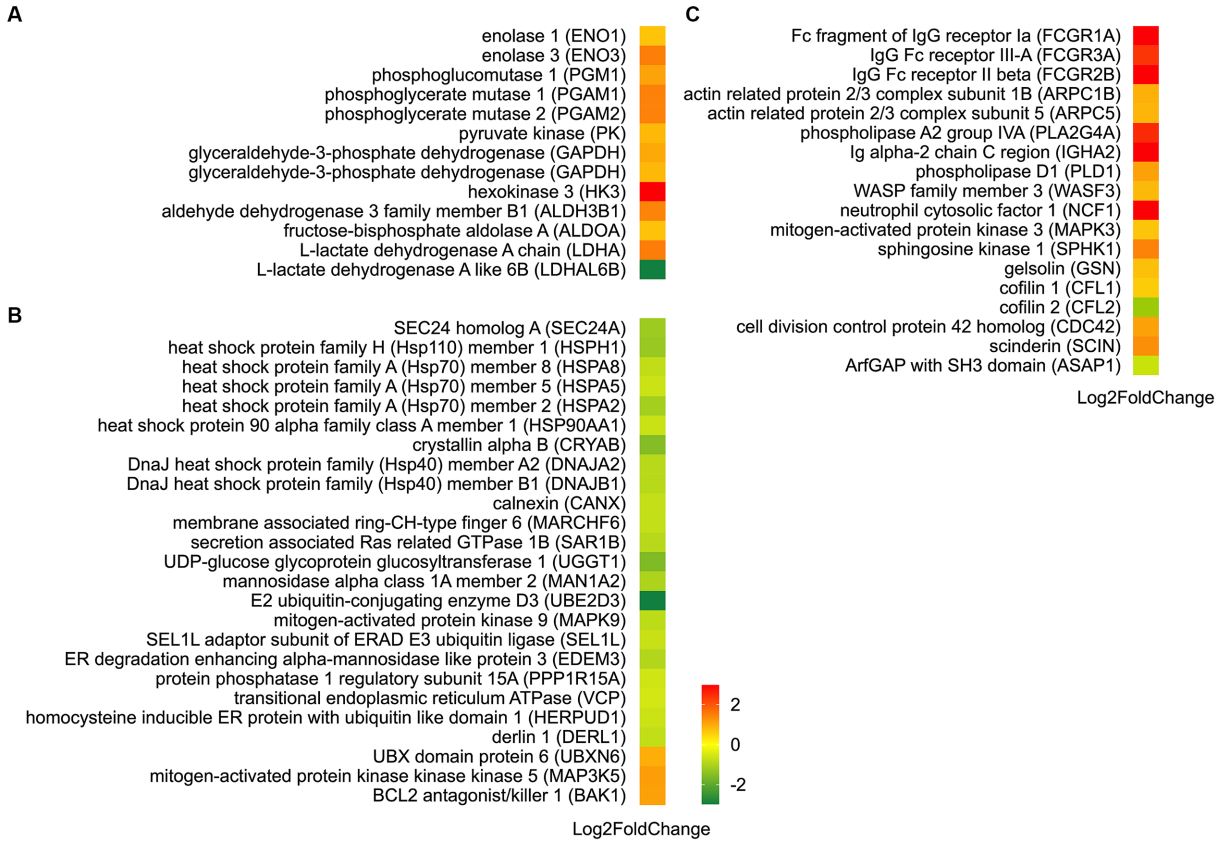

FIGURE 8
Identification of DEGs in metabolic pathways: glycolysis **(A)**, protein processing in endoplasmic reticulum **(B)**, and FcγR-mediated phagocytosis **(C)**. Up-regulated DEGs are denoted in red, whereas down-regulated DEGs are represented in green. The color bar in the lower left corner signifies the intensity of gene expression profiling.

4 Discussion

Hu sheep (*O. aries*) is a crucial breed in China's efforts to conserve domesticated ovine genetic resources. It is essential in the Taihu Plain and known for its excellent qualities, such as high lamb yield, favorable wool characteristics, rapid growth, and optimal meat output (11, 12). Currently, frozen storage is the primary method for mutton preservation, as it inhibits the growth of surface microorganisms and slows down biochemical reactions, and thus plays a vital role in the circulation, sales, and storage process (15, 25). Improper freezing methods can deteriorate mutton quality by accelerating protein denaturation through prolonged freezing time and thawing, thereby reducing its edibility. It was reported that the appropriate aging process subsequent to livestock slaughter is widely recognized as a pivotal factor in the establishment of optimal meat quality (2, 4). However, due to limited genetic resources, research on Hu sheep is still at its preliminary stages. To enhance the understanding of the molecular mechanisms governing postmortem aging-induced changes in meat quality in Hu sheep, transcriptomics analysis is crucial. Our study findings elucidate the fundamental involvement of glycolysis, protein processing in endoplasmic reticulum, and the FcγR-mediated phagocytosis

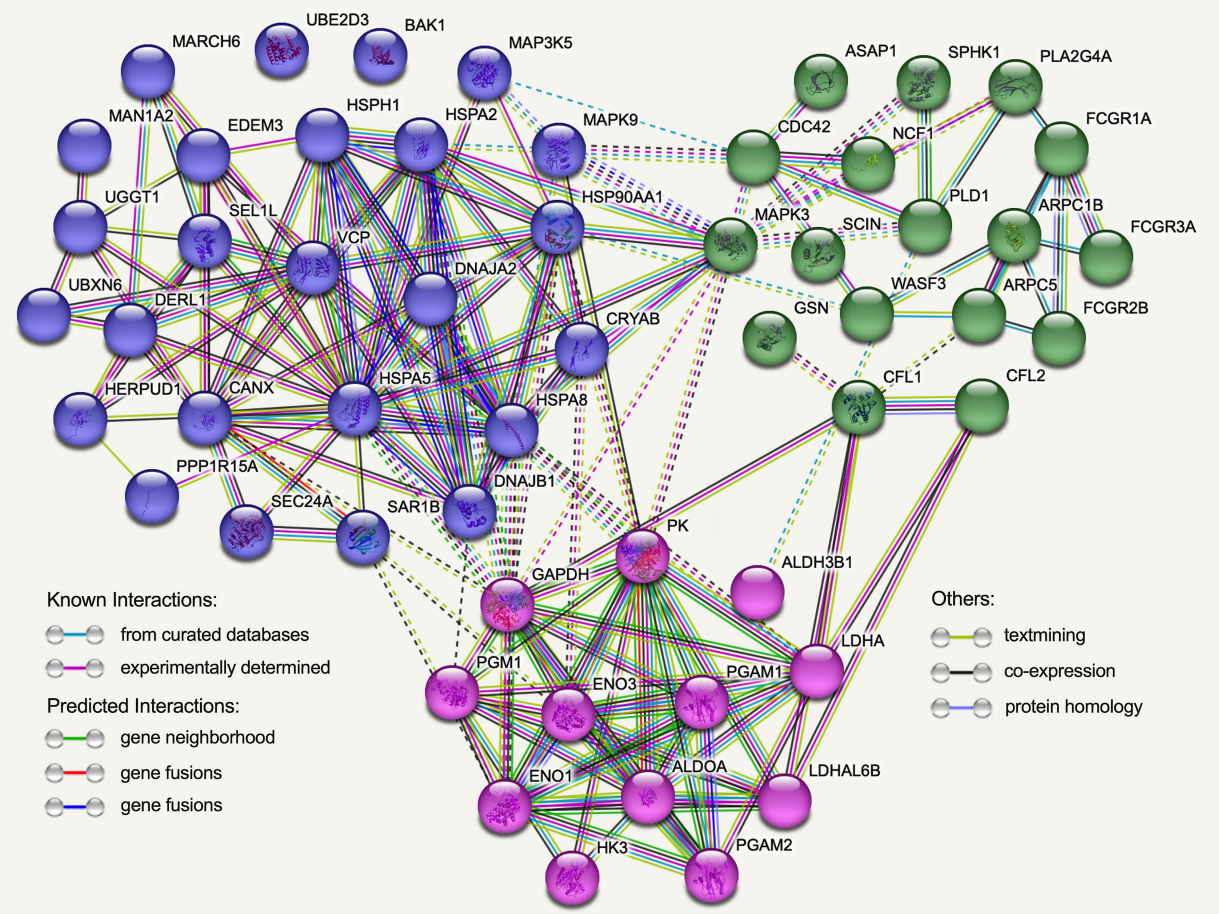

FIGURE 9
The protein–protein interaction (PPI) network was established using the functional enrichment analysis conducted on Hu sheep after the aging process. Each node in the network corresponds to DEGs encoding proteins, and the edges symbolize associations between these proteins. Blue nodes specifically represent proteins linked to protein processing in endoplasmic reticulum, while green nodes represent proteins associated with Fc gamma R-mediated phagocytosis, and red nodes indicate proteins associated with glycolysis.

pathway in the determination of meat quality following postmortem aging in Hu sheep.

4.1 Implication of aging process in quality alterations of Hu sheep meat through glycolysis-related gene expression regulation

Appearance color is the most direct indicator for evaluating the edible quality of meat, exerting a considerable influence on consumers' purchasing inclination (26). In this study, the color of Hu sheep meat changed during the post slaughter aging process (Figure 1). Specifically, the lightness (L*) exhibited a significant augmentation (Figure 1A), potentially attributable to the enzymatic degradation of mutton proteins leading to protein structure deterioration and enhanced light dispersion. Additionally, both the redness (a*) and yellowness (b*) values demonstrated noteworthy increments when compared to the control group (Figures 1B,C). Previous research has established the association between the a* and b* values with the oxidation–reduction state of myoglobin and lipid oxidation, respectively (27). The increased a* and b* values in this study could potentially stem from the generation of oxymyoglobin (OxyMb) through the oxygen bonding with myoglobin (Mb) under aerobic conditions, along with the accumulation of metmyoglobin (MetMb).

The pH dynamics greatly affect meat quality, impacting important aspects such as color, tenderness, and water holding capacity (28). After slaughter, animal pH levels start neutral or slightly alkaline and gradually decline. Our study found that pH significantly decreased under aging process (Figure 1D). The accumulation of lactic acid resulting from glycolysis during the early postmortem period emerged as a significant contributing factor to the decline in muscle pH levels (29). Another reason might be due to ATP depletion, resulting in a lower ATP threshold. It was also reported that the conversion between ATP and ADP, impacting muscle fiber cross-linking and meat hardening (10, 30). This explains the increased hardness and chewiness observed in the present study (Figure 2). These findings are consistent with Abdullah and Qudsieh (2)'s research, which showed a significant pH decrease within 24 h after postmortem aging in lamb meat.

Water retention in muscles and their products is vital for the juiciness of meat. In fact, it is established that meat contains approximately 75% water, serving as its principal constituent and

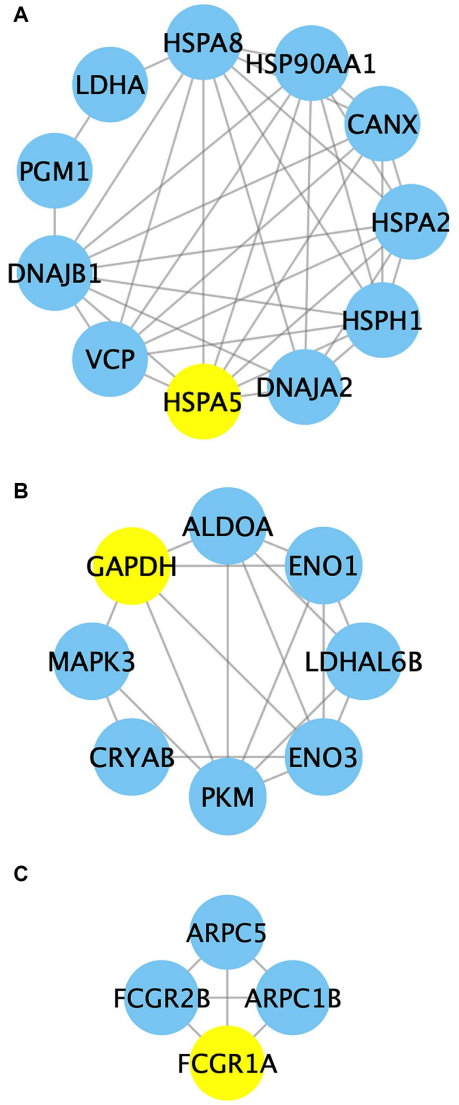

FIGURE 10
The PPI network analysis of identified proteins in clusters 1–3. Nodes in the network represent the relevant proteins, while edges symbolize the associations between them. Yellow circles highlight the predicted seed nodes within each cluster.

exerting pivotal influence on both its functional attributes and textural characteristics (31). In this study, the cooking loss rate of AA-treated mutton significantly increased compared to controlled samples, which may be attributed to muscle stiffness and contraction after slaughter, as well as reduced protein space and muscle water retention. Additionally, moisture in meat predominantly occurs as bound water, free water, and immobilized water. After complex biochemical changes post-slaughter, the structures of muscles undergo alterations that impact the distribution and state of these three water types.

Research has shown that Low-field NMR relaxometry is an effective tool for quantifying water distribution and mobility, and its relationship to meat quality (31, 32). The MRI images of AA-treated mutton showed reduced brightness and quantitative signal intensity (Figures 4A,B). Moreover, T_{22} increased (Figures 4C,D), suggesting elevated flowability of immobilized water after the 24 h aging process. This enhancement contributes to the continuous improvement of mutton quality during subsequent aging.

Our transcriptome analysis confirmed the above findings, identifying 13 DEGs related to glycolysis (Figure 8). Among these genes, 12 were up-regulated, including genes encoding hexokinase 3 (HK3), phosphoglucomutase 1 (PGM1), fructose bisphophase aldolase A (ALDOA), glyceraldehyde-3-phosphate dehydrogenase (GAPDH), phosphoglycerate mutase (PGAM), enolase (ENO), pyruvate kinase (PK), aldehyde dehydrogenase 3 family member B1 (ALDH3B1), and L-lactate dehydrogenase A (LDHA). HK and PK are recognized as key enzymes in the glycolysis pathway. HK facilitates the conversion of glucose (Glu) into glu-6-phosphate (G6P). Previous research has indicated a potential correlation between HK2 and carcass traits and meat quality in pigs (33). PK catalyzes the final rate-limiting step of glycolysis, converting phosphoenolpyruvate and ADP into pyruvic acid and ATP. PK activity has been observed to be 10 times higher in pale, soft, and exudative (PSE) pork than that of normal meat (34). However, another study did not find a significant association between PK activity and meat quality traits such as muscle pH, L*, and drip loss (35). In our investigation, the upregulation of *HK* and *PK* expression after the aging process implies their possible role in meat quality formation of Hu sheep. The relationship between other enzymes in the glycolysis metabolic pathway and meat quality has also been extensively studied. Such as, PGM can reversibly catalyze the transfer of phosphate groups between the G1P and G6P. Silva et al. (36) found that phosphorylation of PGM1 in the early postmortem period speeds up the decline in pH, resulting in a longer sarcomere length. Wei et al. (37) used iTRAQ proteomics to study goat meat quality and found that LDH can be used to indicate tenderness, while GAPDH detects fat content. In non-aged beef, the brightness is positively correlated with PGM1, while the tenderness is negatively correlated with PGAM2 and annexin 2 (38). ALDHs are enzymes that facilitate the conversion of aldehydes into corresponding carboxylic acids. Gagaoua et al. (39) investigated 29 protein biomarkers using reverse phase protein arrays and identified the ALDH1A1 as a significant biomarker associated with beef tenderness and juiciness. This highlights its importance in assessing beef quality. The protein ENO3 plays a crucial role in muscle development and regeneration by catalyzing the conversion of 2-phospho-D-glycerate to phosphoenol-pyruvate. Guillemin et al. (40) revealed that ENO3 exhibits higher expression levels and more glycolytic in the muscles of steers compared to bulls. Moreover, previous studies have established a positive correlation between ENO and shear force (37, 41) as well as redness (42, 43). In this study, the up-regulated expression of these genes demonstrated enhanced glycolysis which is attributed to the respiratory arrest following slaughter and the subsequent interruption of oxygen supply in the muscles. Consequently, glycolysis becomes the dominant reaction, leading to the continuous conversion of glycogen into lactic acid. However, lactic acid produced by glycolysis cannot be transported to the liver or excluded from circulation, accumulating in muscles and causing a decrease in meat pH (37). These pH decline dynamics after slaughter remarkably impact meat quality. The rate of pH decrease determines the occurrence of PSE meat, while the extent of decline affects meat tenderness, water retention, color, and cooking loss (37, 44).

In summary, the 24 h aging process can up-regulate the expression of genes related to glycolysis metabolism, such as *HK*, *PGM1*, *ALDOA*, *GAPDH*, *PGAM*, *ENO*, *PK*, and *ALDH*, regulating the changes in pH,

color, hardness, chewiness, and water content, thereby affecting the meat quality of Hu sheep.

4.2 Aging process influences endoplasmic reticulum pathway-associated gene expression for Hu sheep meat quality regulation

The endoplasmic reticulum (ER) serves as the site for synthesizing almost all lipids, secreted proteins, and transmembrane proteins. Initially, intracellular protein synthesis begins with free ribosomes in the cytoplasm. Some proteins then move to the ER membrane for further extension to complete protein synthesis. In this study, a total of 25 DEGs associated with the protein processing in the endoplasmic reticulum pathway were identified (Figure 8). Notably, calnexin (CANX), mannosidase alpha class 1A member 2 (MAN1A2), and UDP glucose glycoprotein glucose transfer 1 (UGGT1) are involved in the folding of newly synthesized glycoproteins. Secretion associated Ras related GTPase 1B (SAR1B) and SEC24 homolog A (SEC24A) play roles in the assembly and transport of COPII-coated vesicles. Research has demonstrated the importance of CANX as an ER molecular chaperone for glycoprotein folding and modification, crucial for maintaining correct folding and reducing misfolded protein accumulation (45). UGGT is a key participant in ER quality control, recognizing nearly folded proteins lacking glucose in N-oligosaccharide and catalyzing reglycosylation using UDP-Glu as a substrate. Additionally, glucosidase II removes the Glu residue. The glycosylation and deglycosylation cycle continues until the glycoproteins are correctly folded or targeted for degradation (46). SAR1, a samll GTPase, acts as a molecular switch regulating selective substance transport from ER to Golgi via SAR1-GDP/SAR1-GTP formation, playing a vital role in COPII-coated vesicle mediated protein transportation (47). Down-regulation of *CANX*, *MAN1A2*, *UGGT1*, *SAR1B*, and *SEC24A* indicates the impact of aging process on protein assembly, COPII-coated vesicle assembly and transport, ultimately influencing protein synthesis.

Abnormal protein synthesis can trigger a cascade of reactions, including dysfunction of the ER and an imbalance in calcium levels. This leads to the accumulation of unfolded or misfolded proteins in the ER, activating signaling pathways and causing ER stress (ERS) response. Three genes, protein phosphatase 1 regulatory subunit 15A (PPP1R15A), mitogen-activated protein kinase kinase 5 (MAP3K5, ASK1) and mitogen-activated protein kinase 9 (MAPK9, JNK2) (Figure 8), were found to be involved in the ERS process. The role of ER stress sensor protein kinase (PERK) in ER stress is well-established. Activation of the PERK pathway leads to phosphorylation of the eukaryotic translation initiation factor 2a (eIF2a), which inhibits protein synthesis and triggers apoptosis. Phosphorylated eIF2a selectively translates activating transcription factor 4 (ATF4), resulting in the expression of downstream proteins like GADD34. GADD34, in turn, dephosphorylates eIF2a, restoring protein synthesis and preventing inhibition (48). This study found that the expression of the *PPP1R15A* gene, which encodes GADD34, was down-regulated, suggesting that the 24 h aging process can regulate protein translation initiation through the PERK signaling pathway, leading to protein synthesis inhibition. ASK1 and JNK have been implicated in the unfolded protein response (UPR). Overexpressing *ASK1* induces apoptosis through mitochondrial-dependent caspase activation (49), whereas deletion of *ASK1* in mice inhibits NF and H_2O_2-induced apoptosis in $ASK1^{-/-}$ cells (50). ASK1 can activate JNK, which impedes the anti-apoptotic function of BCL2. Deactivating BCL2 can activate BAX/BAK-mediated apoptosis (51). In this study, *BAK1*, *ASK1* and *JNK2* were differentially expressed in AA-treated mutton as compared to BA (Figure 8). This finding indicates that the 24 h aging process mainly modulates apoptosis through regulating *ASK1* and *BAK1*. Under severe stress and unrecovered ER function, cells undergo programmed cell death (52). Moreover, the ER-associated protein degradation (ERAD) pathway regulates the transport of misfolded proteins from the ER for degradation through the ubiquitin proteasome system. This study identified 16 DEGs involved in ERAD, associated with processes like substrate recognition, ubiquitination, and retrograde transport (Figure 8). These findings suggest that the 24 h aging process can potentially impact ERAD function and be linked to post-mortem metabolic disorders, such as considerable inhibition of ATP-producing aerobic metabolism.

Taken together, the 24 h aging process can affect protein synthesis, ERS response, and ERAD pathway by down-regulating the proteins processed in endoplasmic reticulum, thus having an impact on the meat quality of Hu sheep.

4.3 FcγR-mediated phagocytosis-associated genes were involved in Hu sheep meat quality changes after aging process

Phagocytosis is a vital mechanism for host immune defense, providing a direct route for digesting external substances. Fcγ-receptors (FcγRs), categorized as activating or inhibitory receptors, transmit appropriate signals through immunoreceptor tyrosine-based activation motifs or inhibitory motifs (53). FcγR-mediated phagocytosis involves phagocytic cup formation through actin cytoskeletal rearrangements, engulfment of particles, and release of proinflammatory mediators like cytokines and reactive oxygen species (ROS). This process is tightly regulated by activating and inhibitory FcγRs and intracellular signaling molecules (54). In this study, three FcγR genes were identified, including two genes encoding activating receptor proteins: Fc fragment of IgG receptor Ia (FCGR1A) and IgG Fc receptor III-A (FCGR3A); and one gene encoding an inhibitory receptor protein: IgG Fc receptor II beta (FCGR2B) (Figure 8). The increased expression of *FCGR1A* and *FCGR2B* signifies the activation of the FcγR-mediated phagocytosis metabolic pathway, suggesting a potential mechanism by which the aging process influences immune response and cellular clearance.

In addition, the transcriptome analysis revealed the presence of 14 additional genes inked to FcγR-mediated phagocytosis (Figure 8), and their functions have been investigated. For instance, studies have demonstrated that PLD catalyzes the hydrolysis of phosphatidylcholine, generating the lipid second messenger phosphatidic acid (PA) and choline (55). PLD is involved in various cellular functions, including intracellular protein transport and cell cytoskeleton dynamics (55, 56). SPHK, a member of the DAG kinase family, has been well characterized for its activity and function in animals and yeast. In mammals, both SPHK and its product sphingosine-1-phosphate (S1P) play essential roles in regulating numerous cellular processes (57). NCF1 ($p47^{phox}$) is a vital NADPH oxidase subunit that, upon appropriate stimulation, assembles protein subunits, leading to ROS

generation. These ROS, in turn, initiate crucial intracellular signals that govern the cell's response to functional effects including phagocytosis (58). Extracellular signal-regulated kinases 1 and 2 (ERK1/2) are members of the mitogen-activated protein kinase (MAPK) family, involved in signal cascades and transmitting extracellular signals to intracellular targets. Research has indicated that the ERK cascade reaction involves several kinases in the MAP3K layer, including Ras/Raf/MAPK (MEK) 1/2 in the MAPKK layer, ERK1/2 (MAPK3/1) in the MAPK layer, and seveal MAPKAPKs within PLA2 in the subsequent layer. The highly regulated ERK cascade is responsible for fundamental cellular processes (59). This study suggests that the aging process could affect the cellular signaling transduction network through ROS-mediated signal transduction and the ERK cascade, as indicated by the up-regulation of *NCF1*, *MAPK3* and *PLA2G4A* genes. Cell cytoskeleton rearrangement is a well-known phenomenon that occurs in various cellular activities, enabling the transition between gel and sol states of the cytoplasm. This reversible process involves multiple proteins, including gelsolin (GSN), a crucial member of the gelsolin superfamily. GSN binds to actin and regulates its polymerization and depolymerization, playing a significant role in actin dynamics, cell movement, apoptosis, and phagocytosis (60). Another member of this family, scinderin (SCIN), shows the closest similarity to GSN. SCIN is found in all secretory cells and participates in the remodeling of the actin cytoskeleton during secretion processes (60, 61). Cdc42, discovered in yeast, belongs to the Rho subfamily of small GTPases. It acts as a potent regulator of actin cytoskeleton dynamics, cell adhesion interactions, and motility, while also playing vital roles in gene expression, proliferation, and apoptosis (62). In addition, studies have shown that Arp2/3 nucleates branched actin filaments and is important for cell motility, endocytosis, and phagocytosis. This activity is stimulated by nucleation promoting factors including Wiskott-Aldrich syndrome protein (WASP) and ASP family verprolin-homologous protein (WAVE) (63). The WAVE family proteins have the function of regulating the actin cytoskeleton (64). In our study, we observed an up-regulation of *GSN*, *SCIN*, *CDC42*, *ARPC1B*, *ARPC5*, and *WASF3* (*WAVE3*), implying an important role of cytoskeleton remodeling in the quality formation of Hu sheep meat.

Collectively, the 24 h aging process can modulate the immune response, cellular clearance, and cell cytoskeleton rearrangement by enhancing the expression of FcγR-mediated phagocytosis-associated genes, ultimately impacting the meat quality of Hu sheep.

4.4 Protein–protein interaction network

Protein complexes in cells play crucial roles in various cellular processes (65, 66). PPI analysis is an influential approach for investigating the intricate functionality of proteins and their networks at a network-based level (65). In this study, the interaction networks of DEGs were analyzed and visualized using the STRING online database and Cytoscape software. Subsequently, the MCODE plugin was applied to identify potential functional modules within the network, leading to the discovery of three clusters (Figure 10; Supplementary Table S2). In cluster 1, there are 11 nodes and 37 edges that are primarily associated with protein metabolism and glycolysis. Among them, 70 kDa heat shock protein 5 (HSPA5) serves as the seed node. HSPA5 is located within the ER lumen and plays a dual role as a typical HSP70 chaperone. It assists in the folding and assembly of proteins while also acting as a key regulator of ER homeostasis (67). Previous studies have investigated the correlation between HSPs and meat quality. Zhang et al. (68) observed decreased levels of HSP90 in the *Longissimus dorsi* muscle of pigs with low pH and discovered a significant negative correlation between HSP90 levels and cooking loss, drip loss, and brightness. Sanchez, et al. (67) proposed HSPA5 as a potential biomarker for heat stress in Guang Ming Broilers. Laville et al. (69) found the absence of HSP27 in samples of the PSE zones in pig semimembranosus muscle compared to the normal treatment group. Our analysis indicates that the main interaction involving HSPA5 and the nearby proteins was obtained from curated databases, suggesting that HSPA5 might function as a master regulator in this sub-network. In cluster 2, GAPDH, ALDOA, ENO1, ENO3, LDHAL6B, and PKM participate in glycolytic metabolism. MAPK3 is involved in the MAPK signaling pathway, while CRYAB acts as a molecular chaperone in protein metabolism. This suggests a close connection between glycolysis, the MAPK signaling pathway, and protein metabolism. Additionally, GAPDH acts as the seed node in this cluster. It has been reported that GAPDH is a key enzyme that converts 3-phosphoglycerate (3-PGA) to glyceraldehyde 3-phosphate (G3P) (70). Along with other endogenous enzyme systems, GAPDH is believed to play important roles in postmortem protein hydrolysis and meat tenderization (71). A recent study revealed that GAPDH, ATP-dependent 6-phosphofructokinase (PFKM), and PKM may directly interact with other differentially expressed proteins, affecting glycolytic muscle characteristics (72). The interactions among these proteins highlight the vital role of GAPDH in interacting with adjacent proteins like PKM, and thus participating in regulating the quality changes in mutton. Cluster 3 proteins are primarily engaged in FcγR-mediated phagocytosis, with FCGR1A being predicted as the seed node. FcγRs play a vital role in both humoral and cellular immune responses due to their interaction with the Fc region of IgG (53). FCGR1A is the only high-affinity receptor for IgG and functions in both innate and adaptive immune responses. In this study, FCGR1A may participate in the immune response and contribute to the quality maintenance of mutton in Hu sheep through its interaction with adjacent proteins. Taken together, PPI analysis reveals an intricate regulatory network connecting glycolysis, the MAPK signaling pathway, protein metabolism, and immune response during the aging process in Hu sheep meat. Nevertheless, further investigation is warranted to elucidate the specific regulatory mechanisms involved.

5 Conclusion

This study was conducted with the aim of investigating the impacts of a 24 h aging process on the physiological and transcriptomic changes of Hu sheep meat. The results obtained from our study demonstrate that the application of the aging process leads to significant increases in the L*, a*, b* values, as well as its hardness and chewiness, while concurrently causing a notable decrease in pH value. Furthermore, the aging process has a discernible influence on the water content. Through transcriptomic analysis, it has been revealed that the primary effects of the 24 h aging process predominantly

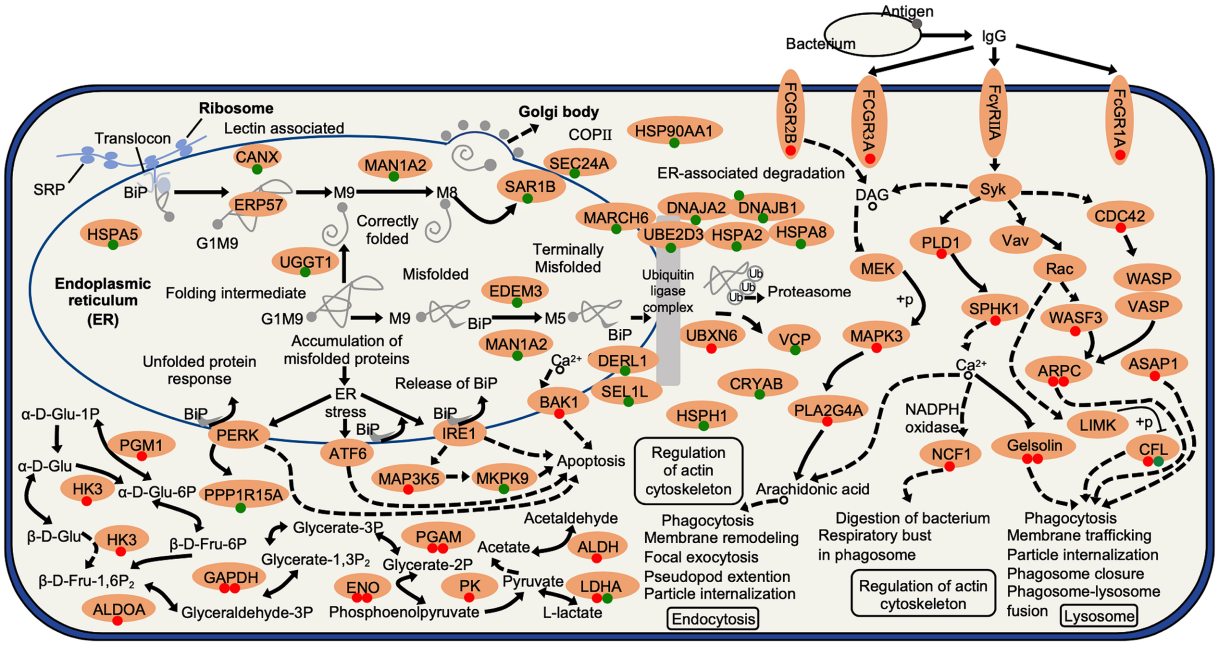

FIGURE 11
Schematic presentation of the aging process effects on Hu sheep meat. The expression profiles of DEGs are highlighted and denoted by circles, with red and green colors signifying up- and down-regulated expression levels. ALDH, aldehyde dehydrogenase; ALDOA, fructose-bisphosphate aldolase A; ARPC, actin related protein 2/3 complex; ASAP1, ArfGAP with SH3 domain; ATF6, activating transcription factor 6; BAK1, BCL2 antagonist/killer 1; CANX, calnexin; CDC42, cell division control protein 42 homolog; CFL, cofilin; CRYAB, crystallin alpha B; DAG, Diacylglycerol; DERL1, derlin 1; α-D-Glu-1-P, α-D-Glucose-1-phosphate; β-D-Fru-1,6P_2, β-D-Fructose-1,6-diphosphate; DNAJA2, DnaJ heat shock protein family (Hsp40) member A2; DNAJB1, DnaJ heat shock protein family (Hsp40) member B1; ENO, enolase; ERP57, protein disulfide-isomerase A3; FCGR1A, Fc fragment of IgG receptor Ia; FCGR3A, IgG Fc receptor III-A; FCGR2B, IgG Fc receptor II beta; FcγRIIA, low affinity immunoglobulin gamma Fc region receptor II-A; GAPDH, glyceraldehyde-3-phosphate dehydrogenase; Glyceraldehyde-3P, glyceraldehyde 3-phosphate; Glycerate-1,3P_2, glycerate-1,3-bisphosphate; HK3, hexokinase 3; HSP, heat shock protein; IgG, Immunoglobulin G; IRE1, inositol-requiring enzyme-1; MAN1A2, mannosidase alpha class 1A member 2; MAP3K5, mitogen-activated protein kinase kinase kinase 5; MAPK9, mitogen-activated protein kinase 9; MEK, mitogen-activated protein kinase kinase 1; NCF1, neutrophil cytosolic factor 1; LDHA, L-lactate dehydrogenase A; LIMK, LIM domain kinase 1; PERK, PKR-like endoplasmic reticulum kinase; PGAM, phosphoglycerate mutase; PGM, phosphoglucomutase; PK, pyruvate kinase; PLD1, phospholipase D1; PLA2G4A, phospholipase A2 group IVA; PPPIR15A, protein phosphatase 1 regulatory subunit 15A; Rac, Ras-related C3 botulinum toxin substrate 1; SAR1B, secretion associated Ras related GTPase 1B; SEC24A, SEC24 homolog A; SEL1L, SEL1L adaptor subunit of ERAD E3 ubiquitin ligase; SRP, signal recognition particle; Syk, spleen tyrosine kinase; UBE2D3, E2 ubiquitin-conjugating enzyme D3; VASP, vasodilator-stimulated phosphoprotein; Vav, guanine nucleotide exchange factor VAV; VCP, transitional endoplasmic reticulum ATPase; WASF3, WASP family member 3; WASP, Wiskott-Aldrich syndrome protein.

involve the modulation of glycolysis metabolism, protein processing in endoplasmic reticulum, and the FcγR-mediated phagocytosis pathway, thereby facilitating changes in the mutton quality attributes. In light of these discoveries, a schematic diagram has been devised to visually depict the observed 24 h aging process effects on Hu sheep (Figure 11).

Data availability statement

The supporting data is publicly available in NCBI SRA with the accession numbers SRR25065590-SRR25065595.

Ethics statement

The animal study was approved by Animal Ethics Committee of the Bengbu University. The study was conducted in accordance with the local legislation and institutional requirements.

Author contributions

HL: Conceptualization, Methodology, Software, Data curation, Formal analysis, Funding acquisition, Investigation, Project administration, Resources, Supervision, Visualization, Writing – original draft, Writing – review & editing. Y-HF: Methodology, Writing – review & editing, Conceptualization, Software, Supervision. CX: Supervision, Validation, Writing – review & editing. YC: Supervision, Validation, Writing – review & editing. X-YL: Supervision, Validation, Writing – review & editing. YW: Supervision, Validation, Writing – review & editing. L-LQ: Writing – original draft, Validation. M-YZ: Validation, Supervision, Writing – review & editing. G-YG: Supervision, Validation, Writing – review & editing. Y-FM: Writing – review & editing, Supervision, Validation. Y-LY: Writing – review & editing, Supervision, Validation. QT: Writing – review & editing, Supervision. K-QL: Writing – review & editing, Supervision, Validation. Y-TL: Writing – review & editing, Supervision, Validation. C-TL: Writing – review & editing, Supervision, Validation. X-YR: Writing – review & editing, Conceptualization, Funding acquisition,

Methodology, Project administration, Software, Supervision. M-YW: Data curation, Formal analysis, Investigation, Resources, Visualization, Writing – original draft, Writing – review & editing, Conceptualization, Funding acquisition, Methodology, Project administration, Software, Supervision. BZ: Conceptualization, Funding acquisition, Methodology, Project administration, Software, Supervision, Writing – review & editing.

Funding

The author(s) declare financial support was received for the research, authorship, and/or publication of this article. This research was funded by the Key Research Foundation of Education Bureau of Anhui Province (2022AH051917), the Key Research and Development Program of Anhui Province (202004a06020010), the Talent Introduction Project of Bengbu University (BBXY2020KYQD01), and Industry-University-Institute Cooperation (2023340306000004 and 2022340306000167).

Acknowledgments

We thank the Project of Anhui Science and Technology Mission for the Hu Sheep Industry Development in Guzhen (2023tpt034) for their funding and technology support. We would like to express our sincere appreciation to the reviewers and editor for their perceptive comments and invaluable suggestions.

Conflict of interest

The authors declare that the research was conducted in the absence of any commercial or financial relationships that could be construed as a potential conflict of interest.

Publisher's note

Supplementary material

The Supplementary material for this article can be found online at: https://www.frontiersin.org/articles/10.3389/fnut.2023.1321938/full#supplementary-material

References

1. Sun MX, Chen MY, Li SY, Dai CP, Chen YR. Study on structure and properties of hu sheep wool. *J Nat Fibers*. (2023) 20:2160405. doi: 10.1080/15440478.2022.2160405

2. Abdullah AY, Qudsieh RI. Effect of slaughter weight and aging time on the quality of meat from Awassi ram lambs. *Meat Sci*. (2009) 82:309–16. doi: 10.1016/j.meatsci.2009.01.027

3. Choe JH, Stuart A, Kim YHB. Effect of different aging temperatures prior to freezing on meat quality attributes of frozen/thawed lamb loins. *Meat Sci*. (2016) 116:158–64. doi: 10.1016/j.meatsci.2016.02.014

4. Gao YC, Bai YJ, Chen XJ, Wang ZL, Wu ZF. Research on the optimal time for acid excretion of Jinta muton and analysis of related influencing factors. *J Anim Sci Vet Med*. (2022) 41:227–30.

5. Martínez-Cerezo S, Sañudo C, Panea B, Medel I, Delfa R, Sierra I, et al. Breed, slaughter weight and ageing time effects on physico-chemical characteristics of lamb meat. *Meat Sci*. (2005) 69:325–33. doi: 10.1016/j.meatsci.2004.08.002

6. Fernández-Barroso MA, Caraballo C, Silió L, Rodríguez C, Nuñez Y, Sánchez-Esquiliche F, et al. Differences in the loin tenderness of Iberian pigs explained through dissimilarities in their transcriptome expression profile. *Animals*. (2020) 10:1715. doi: 10.3390/ani10091715

7. Muniz MMM, Fonseca LFS, Silva DBD, de Oliveira HR, Baldi F, Chardulo AL, et al. Identification of novel mRNA isoforms associated with meat tenderness using RNA sequencing data in beef cattle. *Meat Sci*. (2021) 173:108378. doi: 10.1016/j.meatsci.2020.108378

8. Damon M, Wyszynska-Koko J, Vincent A, Hérault F, Lebret B. Comparison of muscle transcriptome between pigs with divergent meat quality phenotypes identifies genes related to muscle metabolism and structure. *PLoS One*. (2012) 7:e33763. doi: 10.1371/journal.pone.0033763

9. Miao XY, Luo QM, Qin XY, Guo YT, Zhao HJ. Genome-wide mRNA-seq profiling reveals predominant down-regulation of lipid metabolic processes in adipose tissues of small tail Han than Dorset sheep. *Biochem Bioph Res Co*. (2015) 467:413–20. doi: 10.1016/j.bbrc.2015.09.129

10. Ji C, Liu JJ, Luo RM. Regulatory role of mitochondrial genes in the tenderisation of lamb meat during postmortem ageing. *Int J Food Sci Tech*. (2022) 57:3544–55. doi: 10.1111/ijfs.15678

11. Dong X, He S, Li HT, Zhang JH, Wei YQ, Zhang B. Effects of compound preservative treatment on the quality of Hu mutton. *J Shanxi Datong Univ (Nat Sci Ed)*. (2022) 38:79–85.

12. Wang HJ, Wang WT, Du PF, He HJ, Liu YB, Gong JJ, et al. Changes in quality of mutton during post-slaughter storage. *Shandong Agric Sci*. (2023) 55:140–6. doi: 10.14083/j.issn.1001-4942.2023.02.019

13. He S, Zhang B, Dong X, Wei YQ, Li HT, Tang B. Differentiation of goat meat freshness using gas chromatography with ion mobility spectrometry. *Molecules*. (2023) 28:3874. doi: 10.3390/molecules28093874

14. Al-Hijazeen M, Lee EJ, Mendonca A, Ahn DU. Effects of tannic acid on lipid and protein oxidation, color, and volatiles of raw and cooked chicken breast meat during storage. *Antioxidants*. (2016) 5:19. doi: 10.3390/antiox5020019

15. Tao YM, Ma L, Li DD, Tian YT, Liu J, Liu DH. Proteomics analysis to investigate the effect of oxidized protein on meat color and water holding capacity in Tan mutton under low temperature storage. *LWT Food Sci Technol*. (2021) 146:111429. doi: 10.1016/j.lwt.2021.111429

16. Zheng HB, Xiong GY, Han MY, Deng SL, Xu XL, Zhou GH. High pressure/thermal combinations on texture and water holding capacity of chicken batters. *Innov Food Sci Emerg*. (2015) 30:8–14. doi: 10.1016/j.ifset.2015.06.002

17. Wei MY, Li H, Zhong YH, Shen ZJ, Ma DN, Gao CH, et al. Transcriptomic analyses reveal the effect of nitric oxide on the lateral root development and growth of mangrove plant *Kandelia obovata*. *Plant Soil*. (2022) 472:543–64. doi: 10.1007/s11104-021-05271-7

18. Li H, Lv CT, Li YT, Gao GY, Meng YF, You YL, et al. RNA-sequencing transcriptome analysis of *Avicennia marina* (Forsk.) Vierh. Leaf epidermis defines tissue-specific transcriptional response to salinity treatment. *Sci Rep*. (2023) 13:7614–4. doi: 10.1038/s41598-023-34095-x

19. Love MI, Huber W, Anders S. Moderated estimation of fold change and dispersion for RNA-seq data with DESeq2. *Genome Biol*. (2014) 15:550. doi: 10.1186/s13059-014-0550-8

20. Trapnell C, Williams BA, Pertea G, Mortazavi A, Kwan G, van Baren MJ, et al. Transcript assembly and quantification by RNA-Seq reveals unannotated transcripts and isoform switching during cell differentiation. *Nat Biotechnol*. (2010) 28:511–5. doi: 10.1038/nbt.1621

21. Zhang HL, Feng JH, Lin ZG, Wang SY, Wang Y, Dai SM, et al. Identification and analysis of genes underlying bone mineral density by integrating microarray data of osteoporosis. *Front Cell Dev Biol*. (2020) 8:798. doi: 10.3389/fcell.2020.00798

22. Zhang KK, Li WP, Ju YL, Wang XH, Sun XY, Fang YL, et al. Transcriptomic and metabolomic basis of short- and long-term post-harvest UV-C application in regulating grape berry quality development. *Foods*. (2021) 10:625. doi: 10.3390/foods10030625

23. Young MD, Wakefield MJ, Smyth GK, Oshlack A. Gene ontology analysis for RNA-seq: accounting for selection bias. *Genome Biol*. (2010) 11:R14. doi: 10.1186/gb-2010-11-2-r14

24. Mao XZ, Cai T, Olyarchuk JG, Wei LP. Automated genome annotation and pathway identification using the KEGG Orthology (KO) as a controlled vocabulary. *Bioinformatics*. (2005) 21:3787–93. doi: 10.1093/bioinformatics/bti430

25. Liu Q, Wang R, Kong BH, Zhang YG. Effect of superchilling storage on quality characterizes of beef as compared with chilled and frozen preservation. *Adv Mater Res*. (2012) 554-556:1195–201. doi: 10.4028/www.scientific.net/AMR.554-556.1195

26. Mancini RA, Hunt MC. Current research in meat color. *Meat Sci*. (2005) 71:100–21. doi: 10.1016/j.meatsci.2005.03.003

27. Gutzke D, Trout GR. Temperature and pH dependence of the autoxidation rate of bovine, ovine, porcine, and cervine oxymyoglobin isolated from three different muscles-*longissimus dorsi*, *gluteus medius*, and *biceps femoris*. *J Agr Food Chem*. (2002) 50:2673–8. doi: 10.1021/jf0112769

28. Lytras GN, Geileskey A, King RD, Ledward DA. Effect of muscle type, salt and pH on cooked meat haemoprotein formation in lamb and beef. *Meat Sci*. (1999) 52:189–94. doi: 10.1016/s0309-1740(98)00167-3

29. Ryu YC, Choi YM, Kim BC. Variations in metabolite contents and protein denaturation of the longissimus dorsi muscle in various porcine quality classifications and metabolic rates. *Meat Sci*. (2005) 71:522–9. doi: 10.1016/j.meatsci.2005.04.034

30. Neath KE, Del Barrio AN, Lapitan RM, Herrera JRV, Cruz LC, Fujihara T, et al. Difference in tenderness and pH decline between water buffalo meat and beef during postmortem aging. *Meat Sci*. (2007) 75:499–505. doi: 10.1016/j.meatsci.2006.08.016

31. Bertram HC, Andersen HJ. NMR and the water-holding issue of pork. *J Anim Breed Genet*. (2007) 124:35–42. doi: 10.1111/j.1439-0388.2007.00685.x

32. Bertram HC, Kohler A, Bocker U, Ofstad R, Andersen HJ. Heat-induced changes in myofibrillar protein structures and myowater of two pork qualities. A combined FT-IR spectroscopy and low-field NMR relaxometry study. *J Agr Food Chem*. (2006) 54:1740–6. doi: 10.1021/jf0514726

33. Wang J, Deng CY, Xiong YZ, Zuo B. Association analysis of polymorphism in intron-10 of porcine *HK2* gene with meat quality and carcass traits. *J Anim Vet Adv*. (2012) 11:1158–61. doi: 10.3923/javaa.2012.1158.1161

34. Schwägele F, Haschke C, Honikel KO, Krauss G. Enzymological investigations on the causes for the PSE-syndrome, I. Comparative studies on pyruvate kinase from PSE- and normal pig muscles. *Meat Sci*. (1996) 44:27–40. doi: 10.1016/s0309-1740(96)00046-0

35. Allison CP, Bates RO, Booren AM, Johnson RC, Doumit ME. Pork quality variation is not explained by glycolytic enzyme capacity. *Meat Sci*. (2003) 63:17–22. doi: 10.1016/s0309-1740(02)00046-3

36. Silva LHP, Rodrigues RTS, Assis DEF, Benedeti PDB, Duarte MS, Chizzotti ML. Explaining meat quality of bulls and steers by differential proteome and phosphoproteome analysis of skeletal muscle. *J Proteome*. (2019) 199:51–66. doi: 10.1016/j.jprot.2019.03.004

37. Wei YC, Li X, Zhang DQ, Liu YF. Comparison of protein differences between high- and low-quality goat and bovine parts based on iTRAQ technology. *Food Chem*. (2019) 289:240–9. doi: 10.1016/j.foodchem.2019.03.052

38. Antonelo DS, Gómez JFM, Silva SL, Beline M, Zhang X, Wang YF, et al. Proteome basis for the biological variations in color and tenderness of longissimus thoracis muscle from beef cattle differing in growth rate and feeding regime. *Food Res Int*. (2022) 153:110947. doi: 10.1016/j.foodres.2022.110947

39. Gagaoua M, Bonnet M, Ellies-Oury MP, De Koning L, Picard B. Reverse phase protein arrays for the identification/validation of biomarkers of beef texture and their use for early classification of carcasses. *Food Chem*. (2018) 250:245–52. doi: 10.1016/j.foodchem.2018.01.070

40. Guillemin N, Jurie C, Cassar-Malek I, Hocquette JF, Renand G, Picard B. Variations in the abundance of 24 protein biomarkers of beef tenderness according to muscle and animal type. *Animal*. (2011b) 5:885–94. doi: 10.1017/s1751731110002612

41. Guillemin N, Bonnet M, Jurie C, Picard B. Functional analysis of beef tenderness. *J Proteome*. (2011a) 75:352–65. doi: 10.1016/j.jprot.2011.07.026

42. Joseph P, Nair MN, Suman SP. Application of proteomics to characterize and improve color and oxidative stability of muscle foods. *Food Res Int*. (2015) 76:938–45. doi: 10.1016/j.foodres.2015.05.041

43. Joseph P, Suman SP, Rentfrow G, Li ST, Beach CM. Proteomics of muscle-specific beef color stability. *J Agr Food Chem*. (2012) 60:3196–203. doi: 10.1021/jf204188v

44. Scheffler TL, Scheffler JM, Kasten SC, Sosnicki AA, Gerrard DE. High glycolytic potential does not predict low ultimate pH in pork. *Meat Sci*. (2013) 95:85–91. doi: 10.1016/j.meatsci.2013.04.013

45. Bedard K, Szabo E, Michalak M, Opas M. Cellular functions of endoplasmic reticulum chaperones calreticulin, calnexin, and ERp57. *Int Rev Cytol*. (2005) 245:91–121. doi: 10.1016/S0074-7696(05)45004-4

46. Blanco-Herrera F, Moreno AA, Tapia R, Reyes F, Araya M, D'Alessio C, et al. The UDP-glucose: glycoprotein glucosyltransferase (UGGT), a key enzyme in ER quality control, plays a significant role in plant growth as well as biotic and abiotic stress in *Arabidopsis thaliana*. *BMC Plant Biol*. (2015) 15:127. doi: 10.1186/s12870-015-0525-2

47. van der Verren SE, Zanetti G. The small GTPase Sar1, control centre of COPII trafficking. *FEBS Lett*. (2023) 597:865–82. doi: 10.1002/1873-3468.14595

48. Halliday M, Hughes D, Mallucci GR. Fine-tuning PERK signaling for neuroprotection. *J Neurochem*. (2017) 142:812–26. doi: 10.1111/jnc.14112

49. Hatai T, Matsuzawa A, Inoshita S, Mochida Y, Kuroda T, Sakamaki K, et al. Execution of apoptosis signal-regulating kinase 1 (ASK1)-induced apoptosis by the mitochondria-dependent caspase activation. *J Biol Chem*. (2000) 275:26576–81. doi: 10.1074/jbc.M003412200

50. Tobiume K, Matsuzawa A, Takahashi T, Nishitoh H, Morita K, Takeda K, et al. ASK1 is required for sustained activations of JNK/p38 MAP kinases and apoptosis. *EMBO Rep*. (2001) 2:222–8. doi: 10.1093/embo-reports/kve046

51. O'Neill KL, Huang K, Zhang JJ, Chen Y, Luo X. Inactivation of prosurvival Bcl-2 proteins activates Bax/Bak through the outer mitochondrial membrane. *Genes Dev*. (2016) 30:973–88. doi: 10.1101/gad.276725.115

52. Malila Y, Uengwetwanit T, Thanatsang KV, Arayamethakorn S, Srimarut Y, Petracci M, et al. Insights into transcriptome profiles associated with wooden breast myopathy in broilers slaughtered at the age of 6 or 7 weeks. *Front Physiol*. (2021) 12:691194. doi: 10.3389/fphys.2021.691194

53. Lu JH, Ellsworth JL, Hamacher N, Oak SW, Sun PD. Crystal structure of fc gamma receptor I and its implication in high affinity gamma-immunoglobulin binding. *J Biol Chem*. (2011) 286:40608–13. doi: 10.1074/jbc.M111.257550

54. Joshi T, Butchar JP, Tridandapani S. Fc gamma receptor signaling in phagocytes. *Int J Hematol*. (2006) 84:210–6. doi: 10.1532/ijh97.06140

55. Gomez-Cambronero J. New concepts in phospholipase d signaling in inflammation and cancer. *TheScientificWorldJOURNAL*. (2010) 10:1356–69. doi: 10.1100/tsw.2010.116

56. Exton JH. Regulation of phospholipase D. *FEBS Lett*. (2002) 531:58–61. doi: 10.1016/s0014-5793(02)03405-1

57. Strub GM, Maceyka M, Hait NC, Milstien S, Spiegel S. Extracellular and intracellular actions of sphingosine-1-phosphate. *Adv Exp Med Biol*. (2010) 688:141–55. doi: 10.1007/978-1-4419-6741-1_10

58. Nambooppha B, Photichai K, Wongsawan K, Chuammitri P. Quercetin manipulates the expression of genes involved in the reactive oxygen species (ROS) process in chicken heterophils. *J Vet Med Sci*. (2018) 80:1204–11. doi: 10.1292/jvms.17-0112

59. Guo YJ, Pan WW, Liu SB, Shen ZF, Xu Y, Hu LL. ERK/MAPK signalling pathway and tumorigenesis. *Exp Ther Med*. (2020) 19:1997–2007. doi: 10.3892/etm.2020.8454

60. Silacci P, Mazzolai L, Gauci C, Stergiopulos N, Yin HL, Hayoz D. Gelsolin superfamily proteins: key regulators of cellular functions. *Cell Mol Life Sci*. (2004) 61:2614–23. doi: 10.1007/s00018-004-4225-6

61. Vitale ML, Delcastillo AR, Tchakarov L, Trifaró JM. Cortical filamentous actin disassembly and scinderin redistribution during chromaffin cell stimulation precede exocytosis, a phenomenon not exhibited by gelsolin. *J Cell Biol*. (1991) 113:1057–67. doi: 10.1083/jcb.113.5.1057

62. Pichaud F, Walther RF, de Almeida FN. Regulation of Cdc42 and its effectors in epithelial morphogenesis. *J Cell Sci*. (2019) 132:jcs217869. doi: 10.1242/jcs.217869

63. Rotty JD, Wu CY, Bear JE. New insights into the regulation and cellular functions of the ARP2/3 complex. *Nat Rev Mol Cell Bio*. (2013) 14:7–12. doi: 10.1038/nrm3492

64. Suetsugu S, Miki H, Takenawa T. Identification of two human WAVE SCAR homologues as general actin regulatory molecules which associate with the Arp2/3 complex. *Biochem Bioph Res Co*. (1999) 260:296–302. doi: 10.1006/bbrc.1999.0894

65. Krogan NJ, Cagney G, Yu HY, Zhong GQ, Guo XH, Ignatchenko A, et al. Global landscape of protein complexes in the yeast *Saccharomyces cerevisiae*. *Nature*. (2006) 440:637–43. doi: 10.1038/nature04670

66. Li H, Ghoto K, Wei MY, Gao CH, Liu YL, Ma DN, et al. Unraveling hydrogen sulfide-promoted lateral root development and growth in mangrove plant *Kandelia obovata*: insight into regulatory mechanism by TMT-based quantitative proteomic approaches. *Tree Physiol*. (2021) 41:1749–66. doi: 10.1093/treephys/tpab025

67. Sanchez ALB, Wang Q, Thiam M, Wang ZX, Zhang J, Zhang Q, et al. Liver transcriptome response to heat stress in Beijing you chickens and guang ming broilers. *Genes*. (2022) 13:416. doi: 10.3390/genes13030416

68. Zhang MH, Wang DY, Geng ZM, Bian H, Liu F, Zhu YZ, et al. The level of heat shock protein 90 in pig *Longissimus dorsi* muscle and its relationship with meat pH and quality. *Food Chem*. (2014) 165:337–41. doi: 10.1016/j.foodchem.2014.05.111

69. Laville E, Sayd T, Sante-Lhoutellier V, Morzel M, Labas R, Franck M, et al. Characterisation of PSE zones in semimembranosus pig muscle. *Meat Sci*. (2005) 70:167–72. doi: 10.1016/j.meatsci.2004.12.008

70. Chintakovid N, Maipoka M, Phaonakrop N, Mickelbart MV, Roytrakul S, Chadchawan S. Proteomic analysis of drought-responsive proteins in rice reveals photosynthesis-related adaptations to drought stress. *Acta Physiol Plant*. (2017) 39:240. doi: 10.1007/s11738-017-2532-4

71. Laville E, Sayd T, Morzel M, Blinet S, Chambon C, Lepetit J, et al. Proteome changes during meat aging in tough and tender beef suggest the importance of apoptosis and protein solubility for beef aging and tenderization. *J Agr Food Chem*. (2009) 57:10755–64. doi: 10.1021/jf901949r

72. Tan XF, He Y, He YQ, Yan ZW, Chen J, Zhao RX, et al. Comparative proteomic analysis of glycolytic and oxidative muscle in pigs. *Genes*. (2023) 14:361. doi: 10.3390/genes14020361

frontiers | Frontiers in Nutrition

TYPE Original Research
PUBLISHED 06 February 2024
DOI 10.3389/fnut.2024.1325886

OPEN ACCESS

EDITED BY
Dandan Pu,
Beijing Technology and Business University, China

REVIEWED BY
Jinwang Li,
Beijing Technology and Business University, China
Heny Herawati,
National Research and Innovation Agency (BRIN), Indonesia

*CORRESPONDENCE
Jing Gan
ganjing@ytu.edu.cn

RECEIVED 22 October 2023
ACCEPTED 15 January 2024
PUBLISHED 06 February 2024

CITATION
Du M, Yu W, Ding N, Jian M, Cheng Y and Gan J (2024) Antioxidant, aroma, and sensory characteristics of Maillard reaction products from *Urechis unicinctus* hydrolysates: development of food flavorings. *Front. Nutr.* 11:1325886. doi: 10.3389/fnut.2024.1325886

Antioxidant, aroma, and sensory characteristics of Maillard reaction products from *Urechis unicinctus* hydrolysates: development of food flavorings

Mengdi Du[1], Wei Yu[1,2], Ning Ding[1,2], Mengqi Jian[1,2], Yongqiang Cheng[2] and Jing Gan[1]*

[1]College of Life Science, Yantai University, Yantai, Shandong, China, [2]Beijing Key Laboratory of Functional Food from Plant Resources, College of Food Science and Nutritional Engineering, China Agricultural University, Beijing, China

To develop food flavorings with a delicious taste and an anti-oxidation effect, in this study, the glucose Maillard reaction was used for hydrolysates of *Urechis unicinctus*. The various biological activities of Maillard reaction products (MRPs) and their antioxidant capacity were evaluated. The results showed that the unique fishy odor substances of seafood in MRPs were reduced, indicating that the Maillard reaction improved the flavor of the hydrolysate of *Urechis unicinctus*. Meanwhile, MRPs exhibited more competitive radical scavenging activities compared to the hydrolysate. Moreover, MRPs demonstrated a considerable potential to protect against 2,2′-Azobis (2-methylpropionamidine) dihydrochloride (AAPH)-induced oxidative stress in a cell model *in vitro* and in a zebrafish model *in vivo*. Finally, a novel food flavoring was produced with MRPs as raw material, while the sensory qualities were deemed acceptable. In consequence, during industrial production, MRPs of *Urechis unicinctus* hydrolysate act as a high-quality raw material for functional flavorings and provide an effective way for the utilization of marine resources.

KEYWORDS

***Urechis unicinctus*, the Maillard reaction, ROS, antioxidation, functional condiment**

1 Introduction

Flavorings are usually food ingredients that are used to be added in small quantities to other foods to improve their flavor (deodorize, enhance freshness, relieve grease, etc.) (1). The flavoring industry has a wide range of products and a large sales volume, especially in China and other south-central Asian countries. The flavoring industry is developing rapidly, and the annual production of flavoring can be more than ten million tons. Especially in recent years, with the rapid development of society, people's living standards are improving at lightning speed, and the majority of consumers on the requirements for seasonings are also on the rise. Compared with the popular flavorings sold in the market now, people's requirements for flavorings are not only reflected in the color and flavor but also in being natural and environmentally friendly, green and safe, with specific nutritional properties. Therefore, seasonings with certain functions have become a hot spot for research in the food industry and the mainstream development direction of China's seasoning industry. Aquatic seasoning

is becoming more and more popular because it retains the original unique flavor of aquatic products (2), and contains rich amino acids, nucleotides, small peptides, and other active ingredients, and it has shown a rapid growth trend in international market demand. The production and consumption of aquatic seasonings in foreign countries are mainly distributed in Southeast Asia, Japan, and the northern Philippines. At present, seafood seasonings account for about 60% of the Japanese seasoning market, and gradually replace traditional seasonings such as monosodium glutamate in Southeast Asia. Aquatic seasoning has gradually become the mainstream development direction of international condiments. China is rich in marine resources, and the development of functional marine food is the strategic goal of our country's future development. Making full use of marine animal protein resources is an urgent problem for the aquatic product processing industry.

Urechis unicinctus, also known as the sea intestine, is a long cylindrical annelid. Its protein content is rich, accounting for about 71.01% of its dry weight, which is much higher than that of other aquatic products (mussel protein accounted for 58.5% and oyster protein accounted for 47.21%), and it also contains peptides, polysaccharides, and other physiologically active substances (3), which have the hypoglycemic effect, antihypertensive and antioxidant activity (4, 5). The muscle hydrolysate of *Urechis unicinctus* contained 18 amino acids, comprising five types of umami amino acids and eight types of necessary amino acids. The composition of amino acids was reasonable, and the umami amino acids representing 53.63% of the total amino acids. Therefore, *Urechis unicinctus* is an excellent source for the development of functional condiments. What's more, the processing and utilization of *Urechis unicinctus* in China and other Southeast Asian countries is still in its infancy, mainly in the form of cooking. There are relatively few studies on flavor, especially in the development of seasonings. The development of seafood seasoning is one of the effective way to realize the high value utilization of marine resources, so the preparation of *Urechis unicinctus* seafood seasoning products has become the trend of the *Urechis unicinctus* industry. However, in general, as the freshness of seafood decreases, it will produce a unique smell, which may have a negative impact on the flavor of *Urechis unicinctus*. Therefore, improving this bad flavor is a prerequisite for the development of *Urechis unicinctus* seasoning. There are many methods to improve this unpleasant odor, such as adsorption, extraction, biological deodorization, and the Maillard reaction (MR), among which MR method is deeply favored by the food industry. The use of MR technology to treat the protein hydrolysate of aquatic products is a simple and low-cost process, and the purpose of deodorization and flavor enhancement can be achieved at the same time.

The Maillard reaction (MR), additionally referred as non-enzymatic browning, is a non-enzymatic reaction that takes place between the carbonyl group of reducing sugar and the amino group of amino acids, peptides, or proteins (6, 7), which can improve the disagreeable taste of food (8–12). The Maillard reaction has been extensively used in food processing, flavor chemistry, and other realms (13–15) and is essential for increasing the flavor and color of food products, resulting in distinctive color and flavor in pastry, cocoa bakery, and meat processing products (16). The Maillard reaction can not only improve flavor but also effectively improve antioxidant activity (17). For instance, Guérard et al. (18) reported that when casein peptone and cod offal hydrolysates were heated in the presence of glucose, the free radical scavenging effect increased by 75%. Some researchers have broadly divided the factors influencing the change in antioxidant activity into two categories: the type of reactants and the generation of some reaction products. Firstly, Hwang et al. (19) studied MRPs of more than 20 amino acids under the same conditions and found that MRPs produced by alanine, tyrosine, tryptophan, and asparagine had stronger free radical scavenging ability. Second, some antioxidant compounds are formed after the Maillard reaction, such as phenolics and acids (20–22). Consequently, we attempted to enhance the flavor and antioxidant capacity of the hydrolysate of *Urechis unicinctus* by means of the Maillard reaction, which supplied a foundation for the development of functional seasonings.

In this research, the enzymatic solution of *Urechis unicinctus* was reacted with glucose at 120°C for 2 h to prepare Maillard reaction products (MRPs). Compared to the hydrolysates, the components of MRPs may change. To evaluate these changes, high-performance liquid chromatography (HPLC) and gas chromatography–mass spectrometry (GC–MS) were utilized to detect the amino acid composition and flavor substances in the hydrolysates and MRPs (23). The antioxidant property of MRPs was evaluated by chemical approaches as well as the construction of L_{02} cells and zebrafish oxidative stress models. In addition, functional seasonings were prepared based on the Maillard reaction products of *Urechis unicinctus* hydrolysates.

2 Materials and methods

2.1 Materials

Urechis unicinctus were obtained from Yantai Laishan District Aquatic Products Market (Shandong, China). Fetal bovine serum (FBS) was acquired from Zhejiang Tianhang Biotechnology Co., Ltd. (Zhejiang, China). 3-(4,5-dimethyl-2-thiazolyl) -2,5-diphenyl-2H-tetra-zolium bromide (MTT), dimethyl sulfoxide (DMSO), Acridine Orange, 1,3-bis (diphenylphosphine) propane (DPPP), and 2,2′-Azobis (2-methylpropionamidine) dihydrochloride (AAPH) were procured from Sigma-Aldrich (St Louis, MO, USA). Amino Acids Mixture Standard Solution was obtained from KGaA (Darmstadt, Germany). GSH assay kits and MDA assay kits were bought from Nanjing Jiancheng Bioengineering Institute (Nanjing, China). BCA Protein Assay Kit was supplied by the Beyotime Institute of Biotechnology (Beijing, China). Dulbecco's Eagle's medium (DMEM), phosphate-buffered solution (PBS, pH 7.2–7.4, 0.01 M), L-ascorbic acid, 2′,7′-dichlorodihydrofluorescein diacetate (DCFH-DA), HO• scavenging activity assay kit, DPPH• scavenging activity assay kit, ABTS• scavenging activity assay, and alkaline protease were procured from Solarbio Science & Technology Co., Ltd. (Beijing, China). Pepsin was obtained from Macklin Biochemical Co., Ltd. (Shanghai, China). Trypsin, papain, and flavourzyme were acquired from Aladdin Reagent Co., Ltd. (Shanghai, China). Salt, sodium glutamate, disodium nucleotide, yeast extract, and white granulated sugar were obtained from Yantai New world Department Store (Shandong, China).

2.2 Preparation of enzymatic hydrolysate of *Urechis unicinctus*

After the viscera were removed, the fresh *Urechis unicinctus* was washed and stored in a refrigerator at −80°C. The cryopreserved *Urechis unicinctus* was placed in a freezing dryer. After 24 h, it was

ground and crushed (24). A measured amount of distilled water was added and the pH was adjusted. After the hydrolysis was completed, the enzyme was killed at 95°C, cooled, centrifuged, and the supernatant was taken. The free amino acid was measured by the neutral formaldehyde method, and the total nitrogen content was detected by the Kjeldahl method (25). Based on the degree of hydrolysis, three proteases with the highest degree of hydrolysis were selected. Using the software Design-Expert1, the Simplex lattice experimental design method was utilized to identify the optimal ratio of compound protease. Then the optimal ultrasonic conditions and enzymatic hydrolysis conditions (4) were optimized by single factor test and response surface experiment. The enzymatic hydrolysate prepared under the optimal conditions was freeze-dried and placed in a refrigerator at −20°C for subsequent use.

2.3 Preparation of Maillard reaction products (MRPs)

Under the optimal conditions MRPs of the hydrolysate of *Urechis unicinctus* were prepared from the lyophilized powder of the enzymatic hydrolysate. The powder (10 g) was solved in 100 mL of water at a proportion of 1:10 (w/v), and then the glucose (4 g) was incorporated into the Maillard reaction mixture. Followed by heating at 120°C for 2 h (26), the samples were promptly freeze-dried and kept at −20°C for subsequent use.

2.4 Bioactive compound analysis of Maillard reaction products

2.4.1 Amino acid composition analysis of MRPs

The composition of amino acids was tested by HPLC utilizing a C18 column (5 μm, 4.6 × 250 mm). With this method, the composition of amino acids was analyzed separately for the Maillard reaction solution and the enzymatic digestion solution. The chromatographic conditions were as follows: Test wavelength was 254 nm, determination of column temperature was 40°C, injection volume was 10 μL, mobile phase: A phase was 0.1 mol/L sodium acetate solution (pH 6.50): acetonitrile = 93: 7, B phase was water: acetonitrile = 20: 80, gradient elution procedure: 0–0.01 min, 100% A; 0.01–35 min, 100 ~ 0% A; 35–42 min, 100% B; 42–45 min, 0–100% A, flow rate was 1.0 mL/min, and the total elution time was 60 min.

2.4.2 Analysis of flavor substances of MRPs By GC–MS

The changes in flavor substances of the hydrolysate and MRPs were determined separately by GC–MS. The samples were subjected to solid-phase microextraction at 80°C for 40 min and sorption at 250°C for 3 min, which were tested afterwards. The GC–MS analysis was carried out on a DB-5MS column under the following conditions: The temperature of the injection port was 250°C, the split ratio was 10:1, and the carrier gas was high-purity helium 6.0 flowing at a rate of 1 mL/min. The temperature program was adapted as follows: maintain 40°C for 2 min, rise to 200°C at 6°C/min, then rise to 300°C at 15°C/min for 2 min. The temperature of the ion source was 220°C, the surface temperature was 280°C, and the m/z scan range was 33 to 500 for the full scan.

2.5 Determination of antioxidant activities with chemical methods

2.5.1 DPPH radical scavenging activity

The method of Li et al. (27) was utilized to evaluate the DPPH radical scavenging capacity of hydrolysates and MRPs with minor adjustment. DPPH working solution is obtained by dissolving DPPH powder in ethanol. The 20 μL sample was combined with 180 μL DPPH working solution (0.2 mM) and incubated in darkness at room temperature for 30 min. Subsequently, the absorbance of the mixed solution was detected at 517 nm utilizing a microplate with L-ascorbic acid as a positive control. The DPPH free radical scavenging rate is calculated as follows:

DPPH radical scavenging activity (%) = $\{[A_{blank} - (A_{sample} - A_{control})]/A_{blank}\} \times 100\%$.

2.5.2 ABTS radical scavenging activity

A minor modification was adapted to the procedure reported by Tan et al. (28) for sake of assessing ABTS radical scavenging capacity. The $ABTS^+$ solution was formulated by combining 2.45 mM potassium persulfate solution and 7 mM ABTS mother liquor in an equal volume, which was then incubated for 12–16 h at room temperature away from light. PBS was applied to dilute the solution to an absorbance of 0.70 ± 0.02 at 734 nm, and the ABTS working solution was obtained. Subsequently, 200 μL of ABTS working solution was combined with 8 μL of the sample solution. The mixture was incubated under darkness at room temperature for 10 min before the absorbance was tested at 734 nm with L-ascorbic acid as the positive reference. The results of the calculations are expressed as the percentage of the scavenging rate using the following formula:

$$\text{ABTS radical scavenging activity}(\%) = \left\{\left[A_{blank} - \left(A_{sample} - A_{control}\right)\right] / A_{blank}\right\} \times 100\%$$

2.5.3 HO radical scavenging activity

HO• scavenging activity was determined with reference to the testing means used by Liu et al. (29) with light revision. The HO• radical was produced by $FeSO_4$ and H_2O_2, which was detected by its ability to hydroxylate salicylate. The reaction system (0.2 mL) included 50 μL $FeSO_4$ (9 mM), 50 μL H_2O_2 (9 mM), 50 μL sodium salicylate (9 mM), and 50 μL different concentrations of hydrolysate or MRPs. After 1 h of incubation at 37°C, the absorbance at 520 nm was tested, and ascorbic acid was utilized as a positive control. The following is how the percentage elimination effect was computed:

$$\text{HO radical scavenging activity}(\%) = \left\{\left[A_{blank} - \left(A_{sample} - A_{control}\right)\right] / A_{blank}\right\} \times 100\%$$

2.6 To evaluate the antioxidant effect of MRPs in the L_{02} cell model

2.6.1 Cell culture

L_{02} cells were cultivated in DMEM with 1% antibiotics (100 U/mL penicillin and 100 g/mL streptomycin) and 10% fetal bovine serum

(FBS) at 37°C in a moist environment with 5% CO_2. 0.25% trypsin was applied to subculture the cells when their confluence reached 80–90%.

2.6.2 Cell viability assay

The viability of L_{02} cells induced by AAPH was assessed by the MTT method. The cells (1×10^5/mL) were inoculated into 96-well plates and cultivated for 24 h. After that, the medium was renewed, and the cells were cultured in various doses of MRPs for 1 h. Afterwards, the cells were treated for 16 h in the absence or presence of AAPH (15 mM) (30). The final step was to incorporate 10 μL MTT solution (5 mg/mL). After 3 h of incubation, the purple formazan crystals were resolved in dimethyl sulfoxide (150 μL). With the use of a microplate reader (Molecular Devices, San Jose, CA, USA), the absorbance was measured at 570 nm.

2.6.3 Determination of ROS levels

Cells were inoculated in 96-well plates at a density of 1×10^4 per well and grown for 24 h. Cells were subsequently recieved treatment with AAPH (15 mM, 16 h) and pre-incubated with MRPs for 1 h. After that, according to the instructions for the ROS detection kit, the cells were covered with DCFH-DA (10 mM). After 30 min, the intracellular ROS content was assessed by quantifying the fluorescence emitted by DCFH-DA oxidation to 2′, 7′-dichlorofluorescein. A microplate reader was applied to examine the fluorescence intensity at wavelengths of 485 nm for the excitation and 525 nm for the emission.

2.7 Antioxidant evaluation of MRPs in oxidative stress model *in vivo*

To estimate the antioxidative effect of the MRPs, we constructed a zebrafish model of oxidative stress. Zebrafish embryos were cultivated in 6-well plates. The 24 hpf zebrafish embryos were firstly treated with various doses of MRPs (0, 25, 50, 100, 200, 400 μg/mL) with the aim of determining the concentration of MPRs used in subsequent experiments. After that, the concentration of AAPH-induced oxidative damage in 24 hpf zebrafish embryos was screened.

2.7.1 Determination of zebrafish heart rate

The selected 24 hpf zebrafish embryos were placed in 6-well plates, and the water was replaced once a day. The number of zebrafish heartbeats per minute was counted by microscope after 72 hpf of continuous administration and oxidative induction, and the average value was calculated.

2.7.2 ROS, apoptotic cell staining, and lipid peroxidation staining experiment of zebrafish

Specific fluorescent probes were, respectively, used to stain zebrafish embryos with the purpose of detecting zebrafish cell mortality (acridine orange), intracellular ROS production rate (DCFH-DA), and lipid peroxidation production rate (DPPP). Zebrafish were rinsed with fresh embryonic medium after being incubated for a period of time in a dye-containing medium, then they were anesthetized. After that, we observed with a fluorescence microscope (Leica DMi8, Wetzlar, Germany), and images were taken with a digital camera. Finally, employing Image J software (National Institutes of Health, Bethesda, MD, USA), the fluorescence intensity of individual zebrafish was quantified.

2.7.3 Behavioral analysis

After 96 h of exposure to MRPs in the presence or absence of AAPH, the spontaneous movement of embryos was tracked for 10 min in a 96-well plate at 27.5 ± 1°C between 9 a.m. and 12 a.m. under particularly suitable light conditions. The zebrafish behavior tracking system (Danio Vision, Noldus, Wageningen, Netherlands) was used to record the number of tail coil alternations every 10 min, and the spontaneous movement distance of 7 dpf embryos per minute was calculated.

2.7.4 MDA and GSH assay

The larvae were cleaned three times using pre-cooled PBS, and then 10 larvae were homogenized. After centrifugation at 4°C, based on the manufacturer's instructions, the levels of malondialdehyde (MDA) and reductive glutathione (GSH) were detected by the assay kit supplied by Nanjing Jiancheng Bioengineering Institute (Nanjing, China).

2.8 Preparation and sensory evaluation of condiments

2.8.1 Process optimization of condiments

To obtain high-quality seasonings, the enzymatic hydrolysate was used as raw material to prepare seasoning by adding salt, sodium glutamate, disodium nucleotide, yeast extract, and white granulated sugar. For purpose of exploring the concentration of raw materials in the composite seasoning, we first determined the optimum concentration of each raw material by single factor test. Then, MRPs, salt, white granulated sugar, and sodium glutamate were used as factors to do four-factor and three-level orthogonal experiments to determine the best compounding ratio. The ingredients were mixed in proportion, and the seafood seasoning was obtained after canning and sterilizing.

2.8.2 Sensory evaluation of the condiment

The evaluation of sensory was carried out in the way presented by Fu et al. (31) with minor changes. In the sensory evaluation process, the explanation of the sensory panel should be included: demographic characteristics of the panel, recruitment and training characteristics, and performance analysis results (32).

Select sensory evaluators based on interest, sensitivity, and familiarity with the sample. Sensory evaluators are not allergic to seafood products and pass olfactory and taste sensitivity tests. Sensory training was conducted for sensory evaluators a total of eight times, for about two hours each time, to establish consistent descriptive terms, improve the evaluators' perception of descriptive words, and standardize the use of sensory scales. In the subsequent simulation test, 10 sensory evaluation team members (5 females and 5 males) were selected based on the difference of no more than 20% between individual team members.

Sensory evaluation indexes included taste, flavor, saltiness, total acceptance and so on. The samples were placed in a 50 mL sanitary cup, and the team members tasted the samples and scored them. Before evaluating each sample, team members were asked to rest for 30 s and were given clean water to rinse their mouths. In each test, 10 team members tested different samples three times.

2.9 Statistical analysis

All the data were displayed as means ± SD of three to six separate experiments. GraphPad Prism 8 software (GraphPad Software, San Diego, CA, USA) was applied to conduct statistical analyses using one-way ANOVA. $p < 0.05$ was deemed significant.

3 Results

3.1 Optimization of enzymatic hydrolysis process of *Urechis unicinctus*

Under the optimum conditions, trypsin, alkaline protease, papain, pepsin, and flavorzyme were used to hydrolyze *Urechis unicinctus*. The three proteases with the highest degree of hydrolysis were trypsin, flavorzyme, and alkaline protease (Supplemenatry Figure S1). Then the simple lattice experimental design was used to obtain the best ratio of complex protease: trypsin: alkaline protease = 21.2: 8.8. Finally, the ultrasonic enzymolysis conditions were determined by the single factor experiment and the response surface experiment. The ultrasonic enzymolysis time was 54.95 min, the ratio of liquid to material was 52: 1, and the amount of enzyme was 3.17%. The optimum enzymatic hydrolysis conditions were that the enzymatic hydrolysis time was 3.16 h, the pH was 8.58, and the enzymatic hydrolysis temperature was 50.48°C. At this time, the degree of hydrolysis (DH) was 34.19%.

3.2 Amino acid compositions of *Urechis unicinctus* hydrolysate and *Urechis unicinctus* hydrolysate MRPs

The hydrolysate of *Urechis unicinctus* was modified by the Maillard reaction when mainly amino acids were engaged in the reaction, which would lead to a significant change in amino acid composition. In this experiment, the amino acid composition of *Urechis unicinctus* hydrolysate was established by HPLC before and after the Maillard reaction. The changes in amino acid composition are shown in Table 1, where the total amino acid content of the hydrolysate of *Urechis unicinctus* decreased from 486.65 mg to 310.7 mg after MR, which occurred between reducing sugars and amino acids and gave the food its unique flavor. Studies have shown that bitter amino acids (leucine, lysine, valine, methionine, etc.) were consumed in large quantities during the Maillard reaction (33), so the content of bitter amino acids in the Maillard reaction products was significantly reduced.

3.3 GC–MS analysis of *Urechis unicinctus* hydrolysate and hydrolysate MRPs

GC–MS analysis was employed to study the changes of flavor substances in MRPs of enzymatic hydrolysates and hydrolysates of *Urechis unicinctus*. By comparing with the mass spectrometry database, we speculated on the types of flavor substances contained in the enzymatic hydrolysates and MRPs of enzymatic hydrolysates and analyzed the relative content changes of flavor substances in the enzymatic hydrolysate and the enzymatic hydrolysate MRPs with 2-methyl-3-heptanone as internal standard substance. It can be observed from Table 2 that the content of aldehydes decreased significantly after MR (from 14.21 to 3.33%), among which heptanal, hexanal, octanal, and 2-methyl-2-pentenal all decreased to 0%, nonanal decreased from 3.42 to 0.89%, and acetaldehyde decreased from 2.84 to 0.32%. The content of ketones also decreased (from 6.2 to 1.27%), especially acetone, nonanone, and undecane, which decreased to 0%.

The content of acid compounds raised after the Maillard reaction (from 24.91 to 34.9%), and the proportion of acid compounds contained in the enzymatic hydrolysate increased to a certain extent. Alcohols also increased from 16.54 to 27.88%, and the most significant change was ethanol (from 0.48 to 5.22%). In addition, phenolic compounds were achieved from nothingness to being, maltol (from 0 to 5.32%) and 5-methyl-2-isopropylphenol (from 0 to 2.23%) increased significantly.

3.4 Determination of antioxidant activity

The antioxidant properties of MRPs and *Urechis unicinctus* hydrolysate were determined by three methods, and it was observed that the scavenging ability of hydrolysates enhanced after MR and showed a concentration dependence (Figures 1A–C). In addition, it was shown that the difference between the antioxidant property of MRPs and the hydrolysate increased with growing concentration. For example, the enzymatic digest of 4 mg/mL showed no apparent difference after MR, and then it became larger. The results obtained by the three methods are consistent with each other, so they can be good proof of the enhanced antioxidant activity of the hydrolysate after the Maillard reaction.

3.5 MRPs attenuate of AAPH-induced oxidative damage in L_{02} cells

To verify the antioxidant activity of the *Urechis unicinctus* hydrolysate MRPs, we established an AAPH-induced damage model based on previous studies (34, 35). AAPH is a free radical promoter that disintegrates at 37°C to form two free radicals with carbon atoms as the core. In the presence of oxygen, this triggers a free radical chain reaction to generate ROS, leading to cell damage. Cell viability after treatment with varying concentrations of MRPs was first measured using the MTT assay. MRPs did not show cytotoxicity at concentrations below 200 μg/mL compared to the control group (Figure 2A). MRPs at non-toxic concentrations were utilized in subsequent experiments to detect their protective effects against oxidative damage. Cells were incubated with varying doses of MRPs samples (0, 25, 50, 100, and 200 μg/mL) for 1 h, preceded by the addition of 15 μM AAPH for 16 h. As shown in Figure 2B, cell viability was drastically decreased in the AAPH group, and pretreatment of MRPs led to a positive response to the cell viability of oxidative stress injury in a concentration-dependent manner. Particularly, the cell viability treated with 200 μg/mL MRPs was markedly raised compared to the AAPH group.

In addition, endo cellular ROS generation was assessed employing DCFH-DA fluorescence staining. In Figures 3B,C, the fluorescence intensity of the AAPH-exposed group was 98,963, which was

TABLE 1 The amino acid composition of *Urechis unicinctus* hydrolysate and *Urechis unicinctus* hydrolysate MRPs.

Amino acid	*Urechis unicinctus* Hydrolysates (mg/g)	Content (%)	*Urechis unicinctus* Hydrolysates MRPs (mg/g)	Content (%)
Asparticacid	56.540 ± 3.852^{a}	5.654	37.296 ± 4.176^{bc}	3.730
Glutamicacid	72.810 ± 8.481^{a}	7.281	47.111 ± 6.178^{bc}	4.741
Hydroxy-proline	6.264 ± 0.310^{a}	0.626	3.863 ± 0.091^{b}	0.386
Serine	25.114 ± 0.223^{a}	2.511	15.396 ± 1.020^{b}	1.540
Glycine	68.025 ± 1.152^{a}	6.803	37.632 ± 2.586^{bc}	3.763
Histidine	7.177 ± 0.426^{a}	0.718	4.087 ± 0.430^{b}	0.409
Arginine	35.365 ± 2.718^{a}	3.537	24.702 ± 1.804^{b}	2.470
Threonine	15.485 ± 0.562^{a}	1.549	10.497 ± 0.365^{b}	1.050
Alanine	60.785 ± 5.936^{a}	6.079	43.973 ± 3.963^{b}	4.397
Proline	15.485 ± 0.497^{a}	1.549	10.497 ± 0.238^{b}	1.050
Tyrosine	12.425 ± 0.825^{a}	1.242	7.710 ± 1.053^{b}	0.771
Valine	15.553 ± 0.370^{a}	1.555	10.062 ± 0.411^{b}	1.006
Methionine	12.012 ± 1.543^{a}	1.201	5.346 ± 0.243^{b}	0.535
Cystine	0.605 ± 0.062^{a}	0.06	0.645 ± 0.087^{a}	0.065
Isoleucine	12.546 ± 0.375^{a}	1.255	8.106 ± 0.211^{b}	0.0811
Leucine	29.416 ± 3.407^{a}	2.942	18.724 ± 2.705^{b}	1.872
Phenylalanine	13.385 ± 0.753^{a}	1.339	8.137 ± 0.621^{b}	0.814
Lysine	27.859 ± 0.343^{a}	2.786	17.425 ± 4.481^{b}	1.742

Different subscript letters in the same line indicate significantly different ($p < 0.05$).

dramatically higher than that in the control group. As expected, pretreatment with different dosages of MRPs remarkably reduced ROS overaccumulation in a dose-dependent manner, with fluorescence intensities reduced to 311,060, 253,936, 232,131, and 223,833, respectively. The results suggest that *Urechis unicinctus* hydrolysate MRPs can protect L_{02} cells by attenuating oxidative damage. The *Urechis unicinctus* hydrolysate MRPs could be a potential biomolecular candidate to inhibit cell oxidative stress and ROS generation.

3.6 Protective effect of MRPs On oxidative damage *in vivo*

3.6.1 Construction of AAPH oxidative damage model *in vivo*

The antioxidant properties of an active substance can be verified by *in vitro* chemical methods, but these methods are not sufficient to support whether the substance has antioxidant properties *in vivo*. Therefore, an *in vivo* model of zebrafish was further used to investigate the protective impact of MRPs on AAPH-induced oxidative strain. The mortality rate of zebrafish embryos increased with increasing AAPH concentration in a dose-dependent manner. The survival rate of zebrafish embryos decreased to less than 50% when induced with 25 mM and 30 mM doses and was unsuitable for further index testing (Figure 3A). Zebrafish yolk sac size also increased with increasing AAPH concentration, showing distinct enlargement at 20 mM (Figure 3B). The fluorescence detection results of cellular ROS formation and cell death in zebrafish showed that AAPH induction could increase the ROS level in zebrafish, and the ROS generation rate was higher with increasing induction concentration (Figures 3B,C). The cell death rate of zebrafish also increased sharply with the increase of concentration (Figure 3D). In summary, we selected 20 mM AAPH to establish a zebrafish oxidative stress induction model for subsequent evaluation of the antioxidant property of MRPs.

3.6.2 Screening of MRPs concentration In zebrafish

The following methods were utilized to observe the impact of MRPs at various doses (25, 50, 100, 200 and 400 μg/mL) on the viability of zebrafish. MRPs in the dose range of 0–200 μg/mL had little effect on the zebrafish embryo survival rate, and the survival rate decreased when the concentration attained 400 μg/mL (Figure 4A). The heartbeat rate of zebrafish was significantly increased at a dose of 400 μg/mL compared to the control group (Figure 4B). As demonstrated in Figures 4B,C, in comparison with the control group, there was no obvious change in zebrafish cell mortality after treatment with MRPs below 200 μg/mL, while MRPs at 400 μg/mL caused a significant increase. Therefore, 25, 50, 100, and 200 μg/mL of MRPs were chosen for the subsequent experiments.

3.6.3 Protective effects of MRPs against AAPH-induced oxidative stress in zebrafish

Oxidative injury may eventually result in cell death, overproduction of ROS and lipid peroxidation. In this study, the improved impacts of MRPs against AAPH-induced cell death, reduced locomotor activity, ROS production, and lipid peroxidation in zebrafish were examined. As indicated in Figures 5A,B), in comparison with the model group, zebrafish embryo survival and cell mortality were markedly reduced when MRPs were administered in a dose-dependent manner. The zebrafish heart rate and zebrafish yolk sac size

TABLE 2 Comparison of flavor substances between *Urechis unicinctus* hydrolysate and hydrolysate MRPs.

Category	Compound	*Urechis unicinctus* hydrolysates			*Urechis unicinctus* Hydrolysates MRPs		
		Content (μg/g)	Percentage (%)	SI	Content (μg/g)	Percentage (%)	SI
Alcohol	1-Octen-3-ol	63.11 ± 1.17^{a}	5.88	88	66.66 ± 2.26^{a}	6.21	91
	Ethyl alcohol	5.15 ± 0.12^{c}	0.48	92	56.03 ± 0.19^{d}	5.22	87
	Cyclopentyl alcohol	9.55 ± 0.69^{a}	0.89	88	28.02 ± 0.60^{c}	2.61	90
	tert-Butyl alcohol	16.10 ± 0.65^{c}	1.50	96	22.86 ± 0.67^{b}	2.13	97
	1-Pentene-3-ol	3.76 ± 0.26^{c}	0.35	91	23.08 ± 0.35^{a}	2.15	93
	2-Pentene-1-ol	2.47 ± 0.24^{c}	0.23	87	18.14 ± 0.26^{a}	1.69	90
	Isopropanol	3.11 ± 0.12^{a}	0.29	97	3.76 ± 0.21^{a}	0.35	95
	Diphenylsilanediol	11.16 ± 0.65^{c}	1.04	89	4.72 ± 0.31^{b}	0.44	90
	N-amyl alcohol	3.11 ± 0.38^{a}	0.29	96	3.33 ± 0.12^{a}	0.31	87
	Methanol	14.28 ± 0.71^{b}	1.33	99	15.24 ± 0.57^{b}	1.42	95
	Phenylethyl alcohol	23.08 ± 1.82^{c}	2.15	93	31.99 ± 2.17^{b}	2.98	88
	Furfuralcohol	22.65 ± 1.69^{a}	2.11	96	25.44 ± 1.98^{a}	2.37	94
	Sum	177.54 ± 8.50	16.54		299.26 ± 9.69	27.88	
Acid	Adipic acid	25.55 ± 1.13^{c}	2.38	89	33.38 ± 1.36^{b}	3.11	95
	Caproic acid	8.37 ± 0.27^{a}	0.78	87	14.81 ± 0.40^{b}	1.38	93
	Pelargonic acid	37.89 ± 1.86^{c}	3.53	95	45.30 ± 2.09^{c}	4.22	92
	Alanine	9.66 ± 0.11^{b}	0.90	94	6.23 ± 0.34^{b}	0.58	87
	Fumaric acid	1.29 ± 0.05^{a}	0.12	91	9.45 ± 0.28^{b}	0.88	96
	Acetic acid	102.29 ± 3.57^{a}	9.53	97	130.52 ± 3.82^{b}	12.16	96
	Propionic acid	41.54 ± 2.24^{c}	3.87	92	53.36 ± 2.47^{b}	4.99	97
	Oleic acid	14.60 ± 0.45^{a}	1.36	97	32.42 ± 0.68^{b}	3.02	94
	Myristic acid	7.30 ± 0.17^{b}	0.68	91	14.60 ± 0.20^{a}	1.36	88
	Palmitic acid	10.30 ± 0.31^{a}	0.96	86	18.78 ± 0.45^{b}	1.75	91
	Benzoic acid	2.58 ± 0.06^{a}	0.24	90	8.16 ± 0.29^{b}	0.76	86
	Phenylacetic acid	6.01 ± 0.12^{c}	0.56	97	28.87 ± 0.34^{a}	2.69	99
	Sum	267.38	24.91		396.08	36.90	
Aldehyde	Heptanal	14.17 ± 0.38^{a}	1.32	96	-	-	
	Hexanal	10.20 ± 0.54^{a}	0.95	95	-	-	
	Acetaldehyde	30.48 ± 1.02^{c}	2.84	93	3.43 ± 0.07^{a}	0.32	96
	Benzaldehyde	20.72 ± 0.72^{a}	1.93	97	5.96 ± 0.10^{b}	0.53	96
	Heptanal	9.23 ± 0.30^{a}	0.86	96	-	-	
	Octanal	11.81 ± 0.41^{c}	1.10	97	-	-	
	Nonanal	36.71 ± 1.33^{c}	3.42	96	9.55 ± 0.21^{b}	0.89	96
	2-Methyl-2-pentenal	13.42 ± 0.27^{a}	1.25	90	-	-	
	Butylaldehyde	5.80 ± 0.09^{c}	0.54	91	17.07 ± 0.19^{b}	1.59	93
	Sum	152.53	14.21		35.74	3.33	
Ketone	2,6-dimethyl-4-pyranone	1.40 ± 0.08^{a}	0.13	87	6.23 ± 0.09^{b}	0.58	90
	2-Heptanone	3.11 ± 0.11^{a}	0.29	91	7.94 ± 0.13^{b}	0.74	86
	1-Pentene-3-one	13.52 ± 0.19^{c}	1.26	96	3.86 ± 0.07^{b}	0.36	92
	Butanone	9.88 ± 0.15^{c}	0.92	98	1.82 ± 0.03 ^{b}	0.17	99
	Acetone	9.23 ± 0.43^{a}	0.86	87	-	-	
	Nonanone	10.41 ± 0.28^{a}	0.97	82	-	-	
	Undecanone	20.39 ± 0.79^{c}	1.90	95	-	-	
	Sum	66.55	6.20		13.63	1.27	

(Continued)

10.3389/fnut.2024.1325886

TABLE 2 (Continued)

Category	Compound	*Urechis unicinctus* hydrolysates			*Urechis unicinctus* Hydrolysates MRPs		
		Content (μg/g)	Percentage (%)	SI	Content (μg/g)	Percentage (%)	SI
Hydrocarbon	Dodecane	21.25 ± 0.73a	1.98	95	3.22 ± 0.17^{c}	0.30	83
	Tetradecane	28.77 ± 1.01^{c}	2.68	96	3.65 ± 0.11^{a}	0.34	95
	Hexadecane	27.48 ± 0.36^{a}	2.56	94	2.79 ± 0.02^{c}	0.26	91
	Heptadecane	1.50 ± 0.03^{c}	0.14	92	4.94 ± 0.10^{c}	0.46	95
	Eicosane	12.67 ± 0.12^{c}	1.18	96	5.37 ± 0.06^{c}	0.50	93
	Styrene	48.73 ± 3.43^{a}	4.54	99	-	-	
	Tridecane	21.47 ± 0.81^{c}	2.00	84	-	-	
	Pentadecane	19.54 ± 0.63^{a}	1.82	89	-	-	
	Tetracosane	6.76 ± 0.21^{c}	0.63	91	4.83 ± 0.08^{c}	0.45	89
	Sum	188.16	17.53		24.79	2.31	
Phenol	Maltol	-	-		57.10 ± 1.98^{c}	5.32	99
	5-Methyl-2-isopropylphenol	-	-		23.94 ± 0.76^{c}	2.23	97
	2,4-Di-tert-butylphenol	-	-		1.61 ± 0.03^{a}	0.15	90
	Sum		0.00		82.65	7.70	

Different subscript letters in the same line indicate significantly different ($p < 0.05$). "-" means not detected.

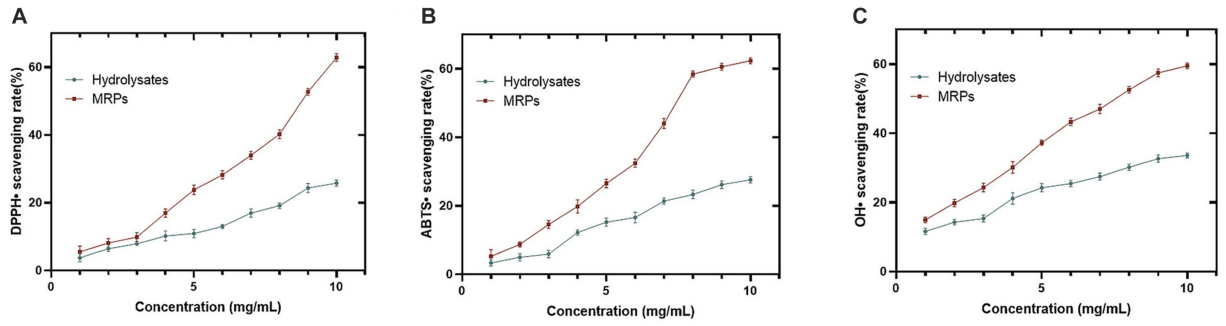

FIGURE 1
Comparison of antioxidant ability between *Urechis unicinctus* hydrolysate and hydrolysate MRPs. DPPH• **(A)**, ABTS• **(B)**, and OH• **(C)** scavenging activity of hydrolysate and hydrolysate MRPs. n = 3, Data are expressed as mean ± SD.

could reflect the survival status of zebrafish. Treatment with MRPs reversed the increased heart rate and enlarged yolk sac size of zebrafish caused by AAPH. After treatment with only AAPH, the total distance of zebrafish movement was obviously decreased. However, MRPs showed a good improvement in locomotor activity in zebrafish (Figures 5B,C). The effects of MRPs on AAPH-induced ROS production and lipid peroxidation levels are indicated in Figures 5D,E), respectively. When zebrafish embryos were treated with MRPs in advance of AAPH treatment, a dose-dependent reduction in ROS and lipid peroxidation production was observed. Moreover, MRPs pretreatment ameliorated the increased MDA content and reduced GSH content in zebrafish caused by AAPH treatment (Figures 5F,G). These data indicated that MRPs pretreatment inhibited ROS generation and lipid peroxidation to protect zebrafish from oxidative injury.

3.7 Preparation of seasonings

There is no doubt that the most critical factor in seasoning is flavor. The single-factor experiment showed that the change of I + G and yeast extract content had little effect on the sensory scores. The main and secondary factors affecting the sensory score were salt, MRPs, sodium glutamate, and white sugar (Figure 6). The content of I + G was 0.8%, and yeast extract was 1.5% for subsequent experiments. With MRPs, salt, white sugar, and sodium glutamate as factors, the orthogonal experiment of four factors and three levels (Table 3) was conducted to determine the best formula process. The data showed that the optimal combination was MRPs (11%), sugar (11%), salt (25%), sodium glutamate (25%), I + G (0.8%), and yeast extract (1.5%) (Table 4). Finally, a high-end seasoning with hygienically qualified, white powder, unique seafood flavor, and pleasant taste was obtained.

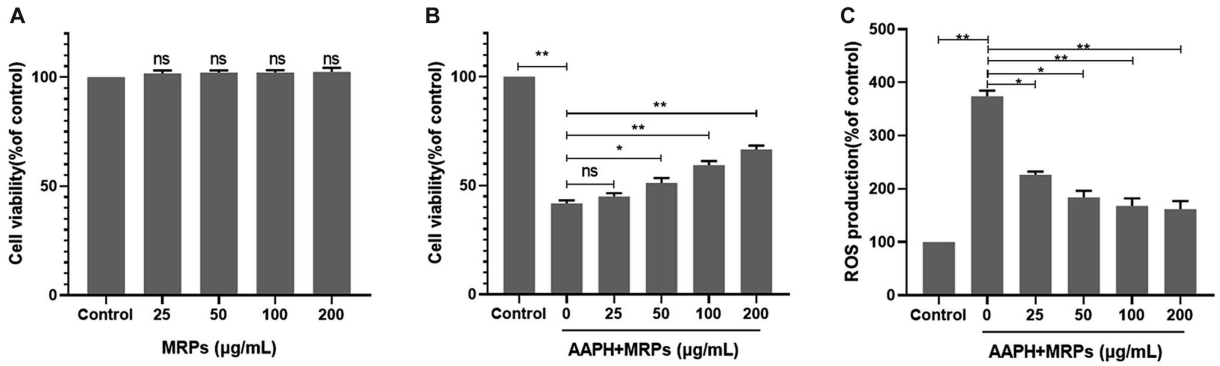

FIGURE 2
MRPs attenuated AAPH-induced cell injury and ROS generation in L_{02} cells. **(A)** MTT assay to verify whether different concentrations of MRPs (25, 50, 100, 200 μg/mL) had cytotoxicity. **(B)** MRPs were added 1 h before AAPH. Effect of MRPs on AAPH-induced cell viability. **(C)** Effect of MRPs on the ROS levels of AAPH-induced L_{02} cells. n = 4, Data are expressed as mean ± SD. * $p < 0.05$, ** $p < 0.01$ vs. AAPH group, ns, not significant.

4 Discussion

With the improvement of people's living standards, aquatic condiments with health care functions are becoming more popular (2). *Urechis unicinctus*, also known as "naked sea cucumber," has the potential to prepare seafood condiments because of its low fat and high protein content. However, the hydrolysate of *Urechis unicinctus* has a bitter taste that is unique to seafood. MR can improve the flavor and color of food and in some cases, can enhance protein functionality (36, 37). Therefore, we attempted to use the enzymatic hydrolysate of *Urechis unicinctus* for MR with glucose and found that the bad flavor of the enzymatic hydrolysate was improved after the reaction. MRPs showed prosperous antioxidant capacity and the ability to alleviate oxidative damage *in vitro* and *in vivo*. Then, an umami-rich, nutritious, and healthy seasoning was prepared from the Maillard reaction product of *Urechis unicinctus* hydrolysate.

Urechis unicinctus has the potential to develop functional seafood seasonings due to its rich protein content, reasonable amino acid composition, and biological activities such as antioxidant and hypoglycemic. However, the enzymatic hydrolysate of *Urechis unicinctus* has the characteristic fishy flavor of aquatic products. Therefore, improving this unsatisfactory flavor has become the key to the preparation of *Urechis unicinctus* seasoning. The Maillard reaction treatment of aquatic product protein hydrolysates can achieve the purpose of deodorization and aroma enhancement, which is favored by the food industry. Therefore, firstly, in this study, the hydrolysate was reacted with glucose at 120°C for 2 h to obtain the MRPs of *Urechis unicinctus* hydrolysate. The total amino acid content decreased after the reaction, which was to be attributed to the fact that MR takes place mainly between reducing sugars and amino acids, giving the food a unique flavor (7, 37). Among them, leucine, lysine, methionine, valine, and other amino acids that produce a bitter taste (38, 39) were apparently reduced, which was similar to the findings obtained by Lan and Liu et al. in the study of the xylose-soybean peptide maillard reaction system (40). Hexanal, heptanal, octanal, nonanal, etc., which are responsible for the fishy smell of seafood (41, 42), were markedly reduced after MR, which was consistent with the study of Zhao et al. (43). After MR, the content of short-chain fatty acids such as acetic acid and propionic acid increased, and their thresholds were lower, which had a cheese flavor and could play a certain modification role. Additionally, the content of acetic acid and propionic acid increased after MR. Alcohols are mainly derived from amino acid reduction and fat oxidation, which usually have plant fragrances (44). Phenolic compounds are beneficial in encouraging the release of fishy odor components, reducing the fishy odor of aquatic products significantly (45), and harmonizing the overall flavor of the food. In summary, the findings indicated that MR enhanced the flavor of the hydrolysates of *Urechis unicinctus*.

Simultaneously, the MRPs showed more competitive free radical scavenging capacity in contrast to that of the hydrolysates. We speculated that the increase in free radical scavenging capacity might be related to changes in the composition of the hydrolysates, especially the increase in acids and phenolics in the MRPs. The antioxidant activity of phenolics and acids has been widely reported. Dini et al. (46) added 5-methyl-2-isopropyl phenol to polylactic acid at a certain concentration, and found that its antioxidant capacity in water was enhanced. Wang et al. (47) found that the antioxidant property of chitosan modified by fumaric acid increased from 63 to 85% in ionic liquid solution by the DPPH free radical scavenging method. Furthermore, oyster protein hydrolysate showed superior free radical scavenging ability due to the increased phenolic and acid content after MR (48). Therefore, we concluded that MR improved the antioxidant properties of the hydrolysates, and the change in composition was essential for the increase in antioxidant capacity.

L_{02} cells have been validated as an ideal cellular model for evaluating antioxidant activity (49, 50). For the sake of further verifying the antioxidant capacity of MRPs, we utilized L_{02} cells to evaluate their intracellular antioxidant efficacy. AAPH is a free radical initiator applied extensively in mimicking oxidative stress states (51). Therefore, AAPH was employed in this study to induce oxidative strain L_{02} cells. The viability of L_{02} cells exposed to AAPH was markedly reduced. This might be due to the fact that cellular damage attributed to ROS-induced oxidative stress usually impairs biomolecular functions and results in cell death (52, 53). However, cell death was inhibited with MRPs, indicating that MRPs can protect cells

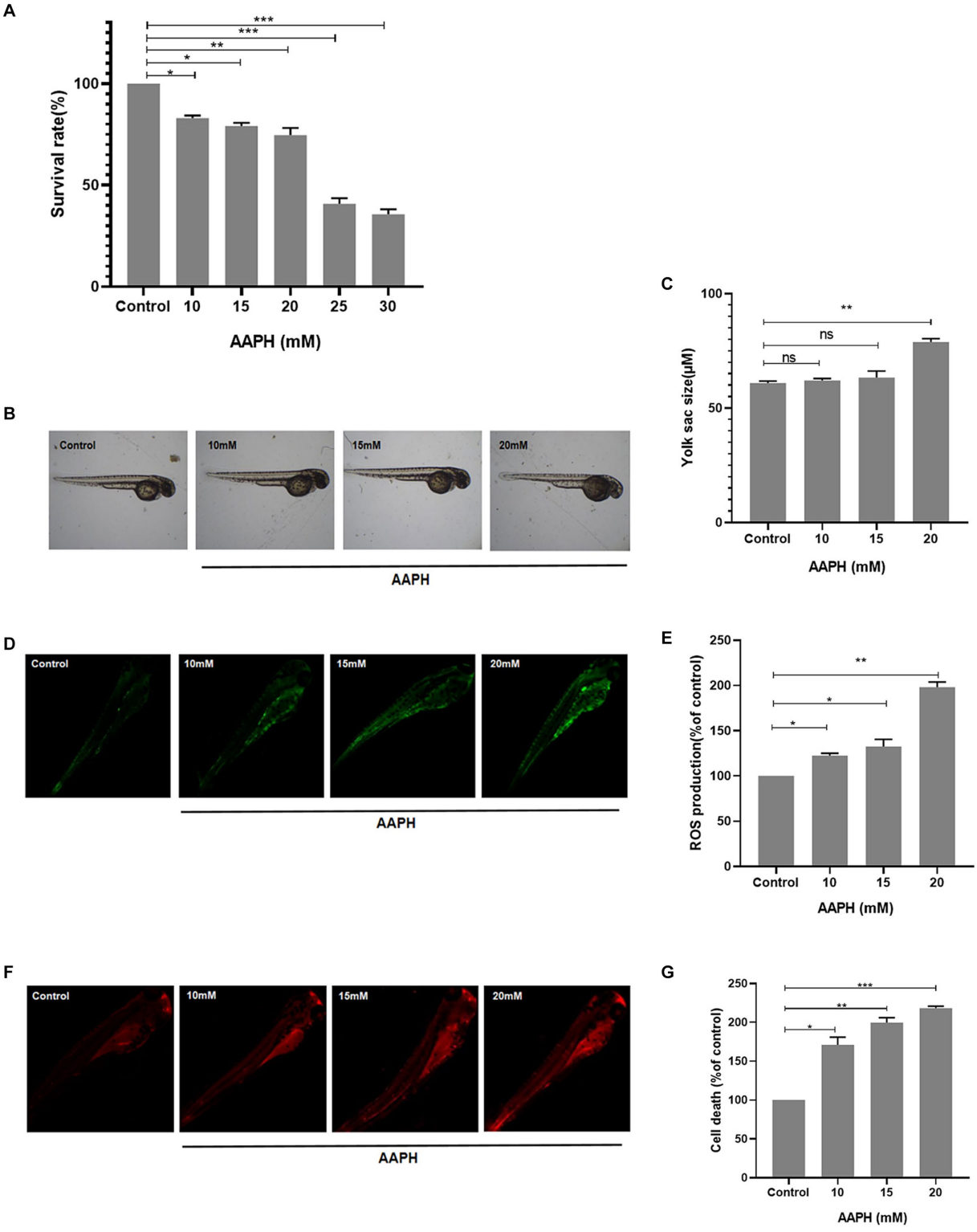

FIGURE 3
Construction of AAPH-induced oxidative stress model *in vivo*. The effects of different concentrations of AAPH on the survival rate **(A)**, yolk sac size **(B,C)**, ROS production rate **(D,E)** and cell death rate **(F,G)** of zebrafish. $n = 10$, Data are presented as means ± SD and analyzed by one-way ANOV A followed. * $p < 0.05$, ** $p < 0.01$ vs. control, ns, not significant.

from AAPH-induced cytotoxicity. We utilized an oxidant-sensitive DCFH-DA fluorescence sensor to quantify the level of ROS generation in cells and determined that MRPs block AAPH-induced ROS generation and subsequent oxidative stress. These findings demonstrated that MRPs played a protective role in ROS-induced oxidative stress, thereby reducing cellular damage.

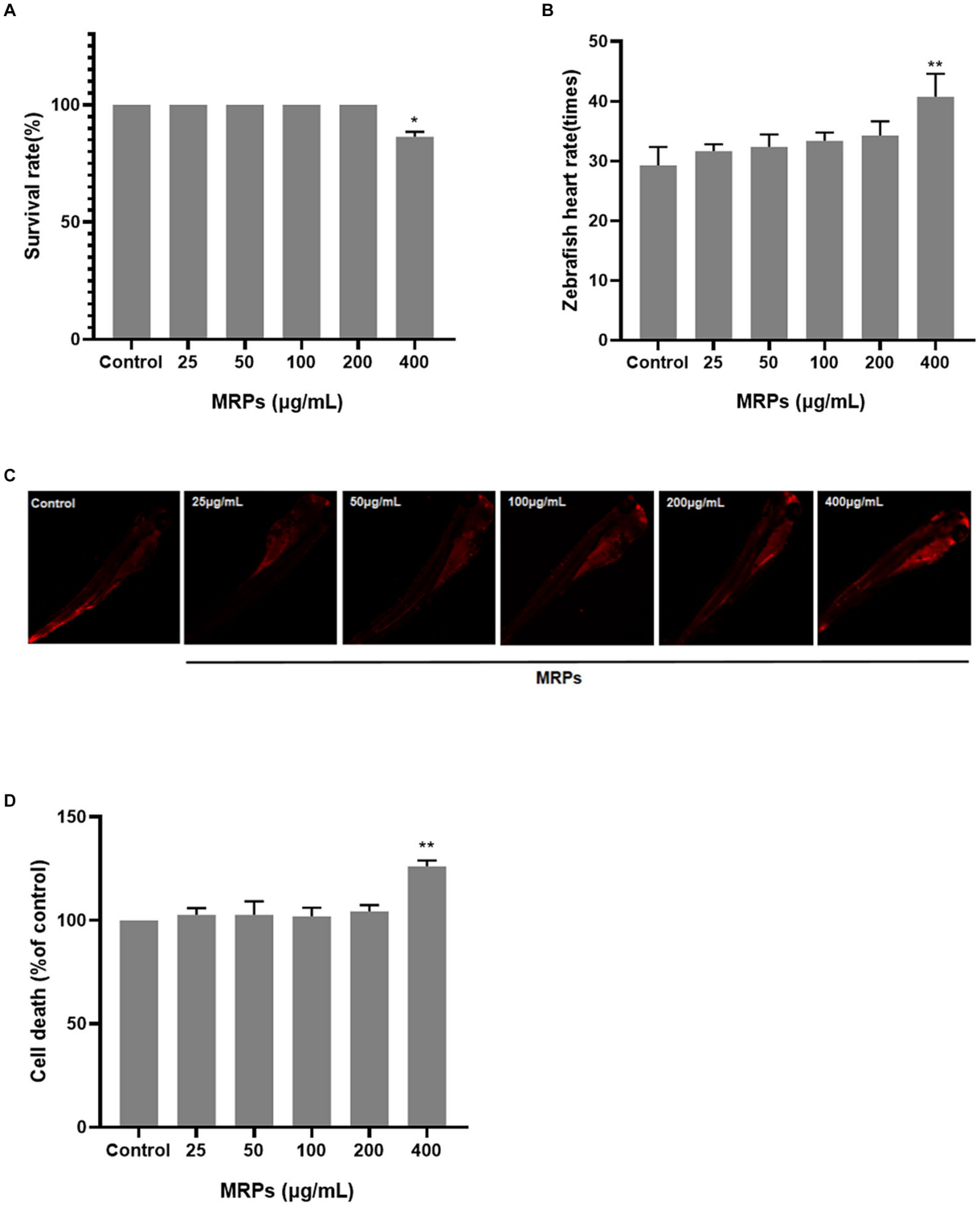

FIGURE 4
Screening of MRPs concentration. The effects of different concentrations of MRPs on the survival rate **(A)**, heart rate **(B)** and cell death rate of zebrafish **(C,D)**. $n = 10$, Data are presented as means ± SD and analyzed by one-way ANOV A followed. * $p < 0.05$, ** $p < 0.01$ vs. control, ns, not significant.

In accordance with recent reports, zebrafish can be utilized as a quick and straightforward model to evaluate anti-oxidative stress activity *in vivo* (34, 35). As a consequence, in this research, we made use of the zebrafish oxidative damage model to explore the antioxidant effect of MRPs *in vivo*. The outcomes indicated that AAPH dramatically raised cell death and ROS levels in zebrafish embryos. In contrast, MRPs suppressed this phenomenon. In the research, AAPH treatment significantly increased lipid peroxidation in zebrafish

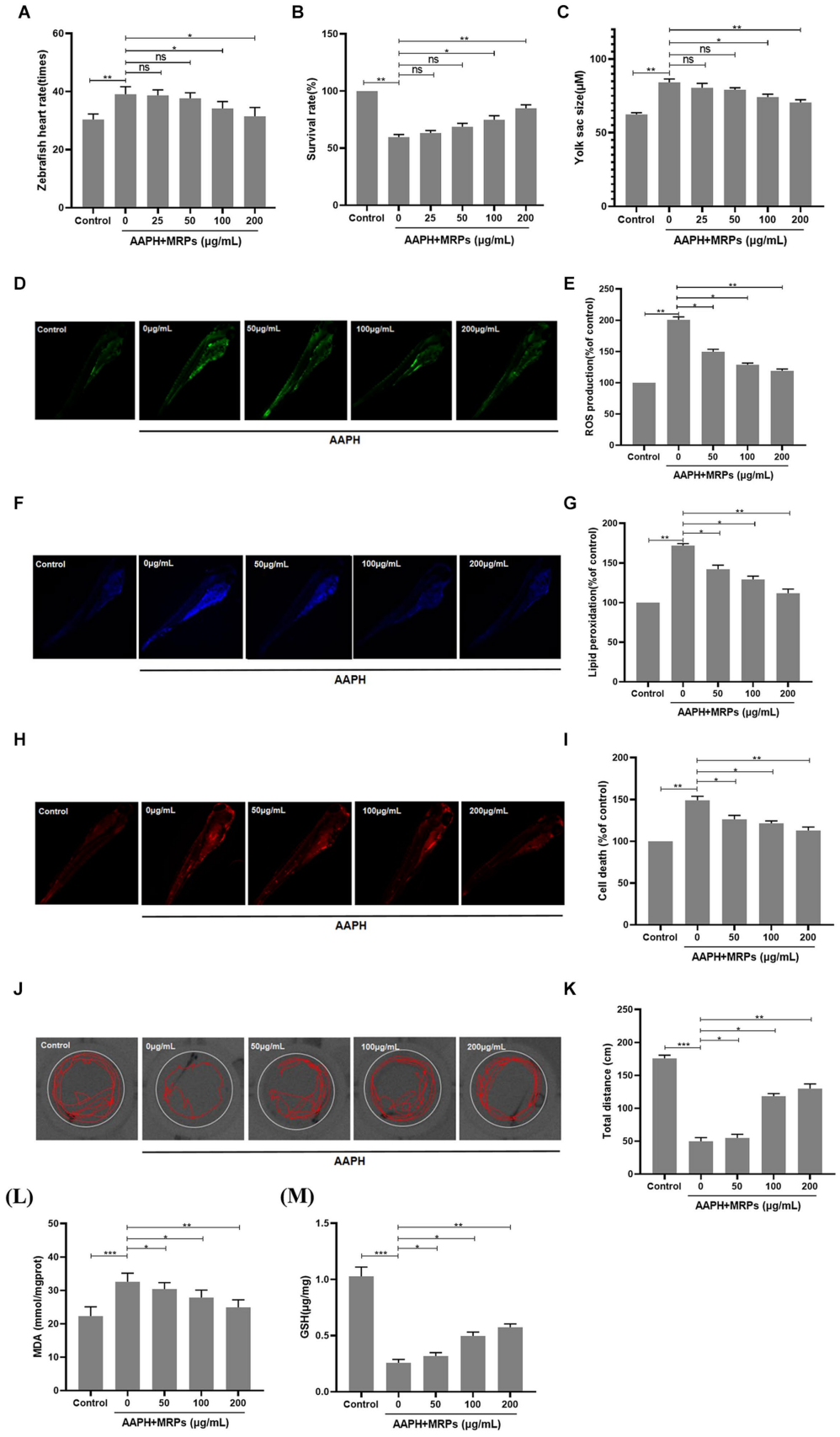

FIGURE 5
Protective effects of MRPs against oxidative stress in zebrafish model. Effect of MRPs on the heart rate **(A)**, survival rate **(B)**, and yolk sac size **(C)** in AAPH-induced zebrafish embryos. Inhibitory effect of MRPs on AAPH-induced ROS production **(D,E)**, lipid peroxidation **(F,G)**, and cell death rate **(H,I)** in

(Continued)

FIGURE 5 (Continued)
zebrafish embryos. They were measured after staining with DCFH-DA, DPPP, and acridine orange followed by image analysis and fluorescence microscopy. **(J,K)** Distance traveled of zebrafish larvae at 96 hpf after exposure to MRPs absence or presence of AAPH. Effect of MRPs on MDA **(L)** and GSH **(M)** in zebrafish. $n = 10$, Data are presented as means ± SD and analyzed by one-way ANOV A followed. * $p < 0.05$, ** $p < 0.01$ and *** $p < 0.001$ vs. AAPH group, ns, not significant.

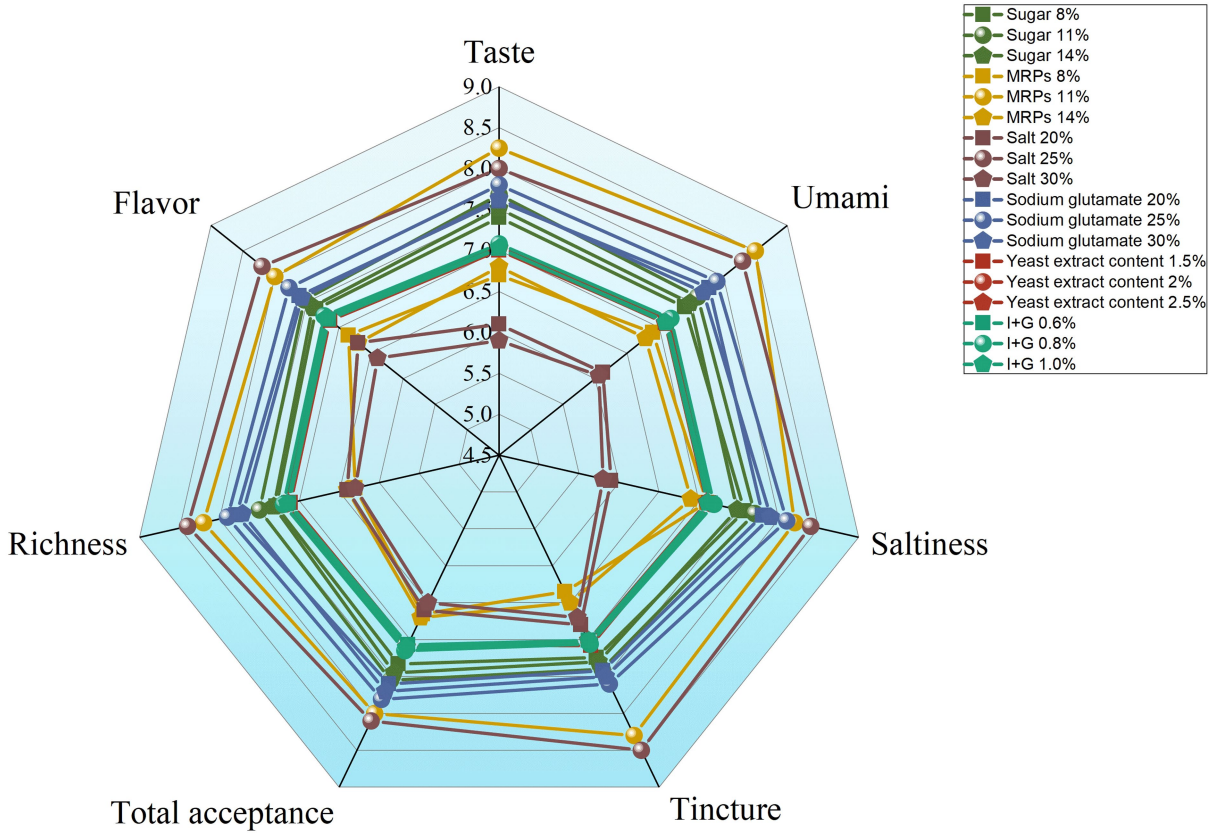

FIGURE 6
Effects of different raw materials on the flavor of *Urechis unicinctus* MRPs seasonings.

TABLE 3 The orthogonal test factors and levels.

Levels	Factors			
	A MRPs (%)	B white sugar (%)	C salt (%)	D sodium glutamate (%)
1	8	8	20	20
2	11	11	25	25
3	14	14	30	30

embryos, which was due to the fact that lipid peroxidation might be a type of cellular harm brought on by free radicals (54). However, MRPs effectively inhibited the formation of this lipid peroxidation. Accordingly, MRPs also exhibited satisfactory effects in inhibiting ROS overproduction and attenuating oxidative damage in a zebrafish model *in vivo*, further validating the antioxidant capacity and nutritional value of MRPs.

As stated previously, MRPs of the *Urechis unicinctus* hydrolysates showed strong aroma and favorable antioxidant effect, which were high-quality raw materials for preparing functional seafood seasonings. Consequently, we utilized MRPs as the raw material to determine the best formula by process optimization and sensory evaluation, and a high-end functional seasoning with a strong aroma and the antioxidant effect was prepared.

TABLE 4 The result of Orthogonal experimental.

Group	Factors				Sensory scores
	A	B	C	D	
1	1	1	1	1	6.15
2	1	2	2	2	8.54
3	1	3	3	3	6.2
4	2	1	2	3	8.02
6	2	3	1	2	7.12
7	3	1	3	2	6.86
8	3	2	1	3	6.34
9	3	3	2	1	7.78
K1	6.963	7.010	6.537	6.943	
K2	7.347	7.260	8.113	7.507	
K3	6.993	7.033	6.653	6.853	
R	0.384	0.250	1.576	0.654	

5 Conclusion

In summary, the Maillard reaction can improve the flavor of *Urechis unicinctus* hydrolysate and enhance its antioxidant property. Next, the MPRs of *Urechis unicinctus* hydrolysates can be utilized for industrial production of functional seafood seasonings and also provide an effective way to realize the high-value utilization of marine resources.

Data availability statement

The original contributions presented in the study are included in the article/Supplementary material, further inquiries can be directed to the corresponding author.

Ethics statement

The animal study was approved by Experimental Animal Ethics Committee of Yantai University. The study was conducted in accordance with the local legislation and institutional requirements.

Author contributions

MD: Conceptualization, Writing – original draft, Formal analysis, Methodology, Software, Validation. WY: Data curation, Formal analysis, Methodology, Resources, Validation, Writing – original draft. ND: Formal analysis, Software, Writing – original draft. MJ: Investigation, Visualization, Writing – original draft. YC: Funding acquisition, Project administration, Resources, Supervision, Writing – review & editing. JG: Funding acquisition, Project administration, Resources, Supervision, Writing – review & editing.

Funding

The author(s) declare financial support was received for the research, authorship, and/or publication of this article. This work was supported by the National Natural Science Foundation of China (32172161), the Natural Science Foundation of Shandong (ZR2022MC217). This work was partly supported by the Center for Mitochondria and Healthy Aging, College of Life Sciences, Yantai University.

Conflict of interest

The authors declare that the research was conducted in the absence of any commercial or financial relationships that could be construed as a potential conflict of interest.

Publisher's note

All claims expressed in this article are solely those of the authors and do not necessarily represent those of their affiliated organizations, or those of the publisher, the editors and the reviewers. Any product that may be evaluated in this article, or claim that may be made by its manufacturer, is not guaranteed or endorsed by the publisher.

Supplementary material

The Supplementary material for this article can be found online at: https://www.frontiersin.org/articles/10.3389/fnut.2024.1325886/full#supplementary-material

References

1. Spence C. The psychology of condiments: a review. *Intern J Gastronomy and Food Sci*. (2018) 11:41–8. doi: 10.1016/j.ijgfs.2017.11.004

2. Wang XY, Xie J, Chen XJ. Applications of non-invasive and novel methods of low-field nuclear magnetic resonance and magnetic resonance imaging in aquatic products. *Front Nutr*. (2021) 8:651804. doi: 10.3389/fnut.2021.800489

3. Sung WS, Park SH, Lee DG. Antimicrobial effect and membrane-active mechanism of Urechistachykinins, neuropeptides derived from *Urechis unicinctus*. *FEBS Lett*. (2008) 582:2463–6. doi: 10.1016/j.febslet.2008.06.015

4. Li JJ, Lu JJ, Asakiya C, Huang KL, Zhou XZ, Liu QL, et al. Extraction and identification of three new *Urechis unicinctus* visceral peptides and their antioxidant activity. *Mar Drugs*. (2022) 20:293. doi: 10.3390/md20050293

5. Kang HK, Lee HH, Seo CH, Park Y. Antimicrobial and immunomodulatory properties and applications of marine-derived proteins and peptides. *Mar Drugs*. (2019) 17:350. doi: 10.3390/md17060350

6. Kim J-S, Lee Y-S. Study of Maillard reaction products derived from aqueous model systems with different peptide chain lengths. *Food Chem*. (2009) 116:846–53. doi: 10.1016/j.foodchem.2009.03.033

7. Nooshkam M, Varidi M, Verma DK. Functional and biological properties of Maillard conjugates and their potential application in medical and food: a review. *Food Res Int*. (2020) 131:109003. doi: 10.1016/j.foodres.2020.109003

8. Fu Y, Zhang Y, Soladoye OP, Aluko RE. Maillard reaction products derived from food protein-derived peptides: insights into flavor and bioactivity. *Crit Rev Food Sci Nutr*. (2020) 60:3429–42. doi: 10.1080/10408398.2019.1691500

9. Song S, Li S, Fan L, Hayat K, Xiao Z, Chen L, et al. A novel method for beef bone protein extraction by lipase-pretreatment and its application in the Maillard reaction. *Food Chem*. (2016) 208:81–8. doi: 10.1016/j.foodchem.2016.03.062

10. Ren GR, Zhao LJ, Sun Q, Xie HJ, Lei QF, Fang WJ. Explore the reaction mechanism of the Maillard reaction: a density functional theory study. *J Mol Model*. (2015) 21:132. doi: 10.1007/s00894-015-2674-5

11. Zhang CL, Alashi AM, Singh N, Chelikani P, Aluko RE. Glycated beef protein hydrolysates as sources of bitter taste modifiers. *Nutrients*. (2019) 11:2166. doi: 10.3390/nu11092166

12. Fu BF, Xu XB, Zhang X, Cheng SZ, El-Seedi HR, Du M. Identification and characterisation of taste-enhancing peptides from oysters *(Crassostrea gigas)* via the Maillard reaction. *Food Chem*. (2023) 424:136412. doi: 10.1016/j.foodchem.2023.136412

13. Xu D, Wang X, Jiang J, Yuan F, Gao Y. Impact of whey protein – beet pectin conjugation on the physicochemical stability of β-carotene emulsions. *Food Hydrocoll*. (2012) 28:258–66. doi: 10.1016/j.foodhyd.2012.01.002

14. Simoes D, Miguel SP, Ribeiro MP, Coutinho P, Mendonca AG, Correia IJ. Recent advances on antimicrobial wound dressing: a review. *Eur J Pharm Biopharm*. (2018) 127:130–41. doi: 10.1016/j.ejpb.2018.02.022

15. Li XD, Teng WD, Liu GM, Guo FY, Xing HZ, Zhu YH, et al. Allicin promoted reducing effect of garlic powder through acrylamide formation stage. *Foods*. (2022) 11:2394. doi: 10.3390/foods11162394

16. van Boekel MA. Formation of flavour compounds in the Maillard reaction. *Biotechnol Adv*. (2006) 24:230–3. doi: 10.1016/j.biotechadv.2005.11.004

17. Cao JR, Yan HX, Liu L. Optimized preparation and antioxidant activity of glucose-lysine Maillard reaction products. *Lwt-Food Science and Technology*. (2022) 161:113343. doi: 10.1016/j.lwt.2022.113343

18. Guérard F, Sumaya-Martinez MT. Antioxidant effects of protein hydrolysates in the reaction with glucose. *Journal of the Oil Chemists' Society*. (2003) 80:467–70. doi: 10.1007/s11746-003-0721-1

19. Hwang IG, Kim HY, Woo KS, Lee J, Jeong HS. Biological activities of Maillard reaction products (MRPs) in a sugar–amino acid model system. *Food Chem*. (2011) 126:221–7. doi: 10.1016/j.foodchem.2010.10.103

20. Vinson JA, Proch J, Zubik L. Phenol antioxidant quantity and quality in foods: cocoa, dark chocolate, and Milk chocolate. *J Agric Food Chem*. (1999) 47:4821–4. doi: 10.1021/jf990312p

21. Long LH, Kwee DCK, Halliwell B. The antioxidant activities of seasonings used in Asian cooking. Powerful antioxidant activity of dark soy sauce revealed using the ABTS assay. *Free Radic Res Commun*. (2000) 32:181–6. doi: 10.1080/10715760000300181

22. Urbaniak A, Szeląg M, Molski M. Theoretical investigation of stereochemistry and solvent influence on antioxidant activity of ferulic acid. *Computational and Theoretical Chemistry*. (2013) 1012:33–40. doi: 10.1016/j.comptc.2013.02.018

23. Shi XM, Wu Q, Ren DD, Wang SY, Xie YF. Research of the determination method of furfurals and furosine in milk and the application in the quality evaluation of milk. *Quality Assurance and Safety of Crops & Foods*. (2022) 14:12–23. doi: 10.15586/qas.v14i1.929

24. Cunha SA, de Castro R, Coscueta ER, Pintado M. Hydrolysate from mussel *Mytilus galloprovincialis* meat: enzymatic hydrolysis, optimization and bioactive properties. *Molecules*. (2021) 26:5228. doi: 10.3390/molecules26175228

25. Zhao F, Qian J, Liu H, Wang C, Wang XJ, Wu WX, et al. Quantification, identification and comparison of oligopeptides on five tea categories with different fermentation degree by Kjeldahl method and ultra-high performance liquid chromatography coupled with quadrupole-orbitrapultra-high resolution mass spectrometry. *Food Chem*. (2022) 378:132130. doi: 10.1016/j.foodchem.2022.132130

26. Wei CK, Thakur K, Liu DH, Zhang JG, Wei ZJ. Enzymatic hydrolysis of flaxseed (*Linum usitatissimum* L.) protein and sensory characterization of Maillard reaction products. *Food Chem*. (2018) 263:186–93. doi: 10.1016/j.foodchem.2018.04.120

27. Li Q, Li X, Ren Z, Wang R, Zhang Y, Li J, et al. Physicochemical properties and antioxidant activity of Maillard reaction products derived from Dioscorea opposita polysaccharides. *Lwt*. (2021) 149:111833. doi: 10.1016/j.lwt.2021.111833

28. Je T, Liu T, Yao Y, Wu N, Du H, Xu M, et al. Changes in physicochemical and antioxidant properties of egg white during the Maillard reaction induced by alkali. *Lwt*. (2021) 143:111151. doi: 10.1016/j.lwt.2021.111151

29. Liu W, Wang H, Pang X, Yao W, Gao X. Characterization and antioxidant activity of two low-molecular-weight polysaccharides purified from the fruiting bodies of Ganoderma lucidum. *Int J Biol Macromol*. (2010) 46:451–7. doi: 10.1016/j.ijbiomac.2010.02.006

30. Hseu YC, Chen SC, Yech YJ, Wang L, Yang HL. Antioxidant activity of Antrodia camphorata on free radical-induced endothelial cell damage. *J Ethnopharmacol*. (2008) 118:237–45. doi: 10.1016/j.jep.2008.04.004

31. Fu Y, Liu J, Hansen ET, Bredie WLP, Lametsch R. Structural characteristics of low bitter and high umami protein hydrolysates prepared from bovine muscle and porcine plasma. *Food Chem*. (2018) 257:163–71. doi: 10.1016/j.foodchem.2018.02.159

32. Djekic I, Lorenzo JM, Munekata PES, Tomasevic I. Review on characteristics of trained sensory panels in food science. *J Texture Stud*. (2021) 52:501–9. doi: 10.1111/jtxs.12616

33. Liu JB, Liu MY, He CC, Song HL, Chen F. Effect of thermal treatment on the flavor generation from Maillard reaction of xylose and chicken peptide. *Lwt-Food Science and Technology*. (2015) 64:316–25. doi: 10.1016/j.lwt.2015.05.061

34. Kang MC, Cha SH, Wijesinghe WA, Kang SM, Lee SH, Kim EA, et al. Protective effect of marine algae phlorotannins against AAPH-induced oxidative stress in zebrafish embryo. *Food Chem*. (2013) 138:950–5. doi: 10.1016/j.foodchem.2012.11.005

35. Kim EA, Lee SH, Ko CI, Cha SH, Kang MC, Kang SM, et al. Protective effect of fucoidan against AAPH-induced oxidative stress in zebrafish model. *Carbohydr Polym*. (2014) 102:185–91. doi: 10.1016/j.carbpol.2013.11.022

36. Gu F-L, Kim JM, Abbas S, Zhang X-M, Xia S-Q, Chen Z-X. Structure and antioxidant activity of high molecular weight Maillard reaction products from casein–glucose. *Food Chem*. (2010) 120:505–11. doi: 10.1016/j.foodchem.2009.10.044

37. Shakoor A, Zhang C, Xie J, Yang X. Maillard reaction chemistry in formation of critical intermediates and flavour compounds and their antioxidant properties. *Food Chem*. (2022) 393:133416. doi: 10.1016/j.foodchem.2022.133416

38. Zhao CJ, Schieber A, Ganzle MG. Formation of taste-active amino acids, amino acid derivatives and peptides in food fermentations - a review. *Food Res Int*. (2016) 89:39–47. doi: 10.1016/j.foodres.2016.08.042

39. Ishibashi N, Arita Y, Kanehisa H, Kouge K, Okai H, Fukui S. Bitterness of leucine-containing peptides. *Agric Biol Chem*. (2016) 51:2389–94. doi: 10.1080/00021369.1987.10868411

40. Lan XH, Liu P, Xia SQ, Jia CS, Mukunzi D, Zhang XM, et al. Temperature effect on the non-volatile compounds of Maillard reaction products derived from xylose-soybean peptide system: further insights into thermal degradation and cross-linking. *Food Chem*. (2010) 120:967–72. doi: 10.1016/j.foodchem.2009.11.033

41. Guan W, Ren X, Li Y, Mao L. The beneficial effects of grape seed, sage and oregano extracts on the quality and volatile flavor component of hairtail fish balls during cold storage at 4 °C. *Lwt*. (2019) 101:25–31. doi: 10.1016/j.lwt.2018.11.024

42. Zhou X, Chong Y, Ding Y, Gu S, Liu L. Determination of the effects of different washing processes on aroma characteristics in silver carp mince by MMSE-GC-MS, e-nose and sensory evaluation. *Food Chem*. (2016) 207:205–13. doi: 10.1016/j.foodchem.2016.03.026

43. Zhao TT, Zhang Q, Wang SG, Qiu CY, Liu Y, Su GW, et al. Effects of Maillard reaction on bioactivities promotion of anchovy protein hydrolysate: the key role of MRPs and newly formed peptides with basic and aromatic amino acids. *Lwt-Food Science and Technology*. (2018) 97:245–53. doi: 10.1016/j.lwt.2018.06.051

44. Refsgaard HHF, Haahr AM, BJJoA JChemistry F. Isolation and quantification of volatiles in fish by dynamic headspace sampling and mass spectrometry. *J Agric Food Chem*. (1999) 47:1114–8.

45. Huang P, Wang Z, Feng X, Kan J. Promotion of fishy odor release by phenolic compounds through interactions with myofibrillar protein. *Food Chem*. (2022) 387:132852. doi: 10.1016/j.foodchem.2022.132852

46. Dini I, Laneri S. Spices, condiments, extra virgin olive oil and aromas as not only flavorings, but precious allies for our wellbeing. *Antioxidants (Basel)*. (2021) 10:868. doi: 10.3390/antiox10060868

47. Wang Z, Zheng L, Li C, Zhang D, Xiao Y, Guan G, et al. Modification of chitosan with monomethyl fumaric acid in an ionic liquid solution. *Carbohydr Polym*. (2015) 117:973–9. doi: 10.1016/j.carbpol.2014.10.021

48. He S, Chen YN, Brennan C, Young DJ, Chang K, Wadewitz P, et al. Antioxidative activity of oyster protein hydrolysates Maillard reaction products. *Food Sci Nutr*. (2020) 8:3274–86. doi: 10.1002/fsn3.1605

49. Liu YP, Sun XH, Jiang WW, Cao XL. Protective effects of dimethylthiourea against hydrogen peroxide-induced oxidative stress in hepatic L02 cell. *Int J Clin Exp Med*. (2019) 12:5114–21.

50. Gao XD, Jia YN, Santhanam RK, Wang YJ, Lu YP, Zhang M, et al. Garlic flavonoids alleviate H_2O_2 induced oxidative damage in L02 cells and induced apoptosis in HepG2 cells by Bcl-2/caspase pathway. *J Food Sci*. (2021) 86:366–75. doi: 10.1111/1750-3841.15599

51. Ko JY, Lee JH, Samarakoon K, Kim JS, Jeon YJ. Purification and determination of two novel antioxidant peptides from flounder fish (*Paralichthys olivaceus*) using digestive proteases. *Food Chem Toxicol*. (2013) 52:113–20. doi: 10.1016/j.fct.2012.10.058

52. Rizwana N, Agarwal V, Nune M. Antioxidant for neurological diseases and Neurotrauma and bioengineering approaches. *Antioxidants*. (2022) 11:72. doi: 10.3390/antiox11010072

53. Finkel T, Holbrook N, Nature JJ. Oxidants, oxidative stress and the biology of ageing. *Nature*. (2000) 408:239.

54. Gegotek A, Skrzydlewska E. Biological effect of protein modifications by lipid peroxidation products. *Chem Phys Lipids*. (2019) 221:46–52. doi: 10.1016/j.chemphyslip.2019.03.011

Frontiers in Nutrition

Explores what and how we eat in the context of health, sustainability and 21st century food science

A multidisciplinary journal that integrates research on dietary behavior, agronomy and 21st century food science with a focus on human health.

Discover the latest Research Topics

See more →

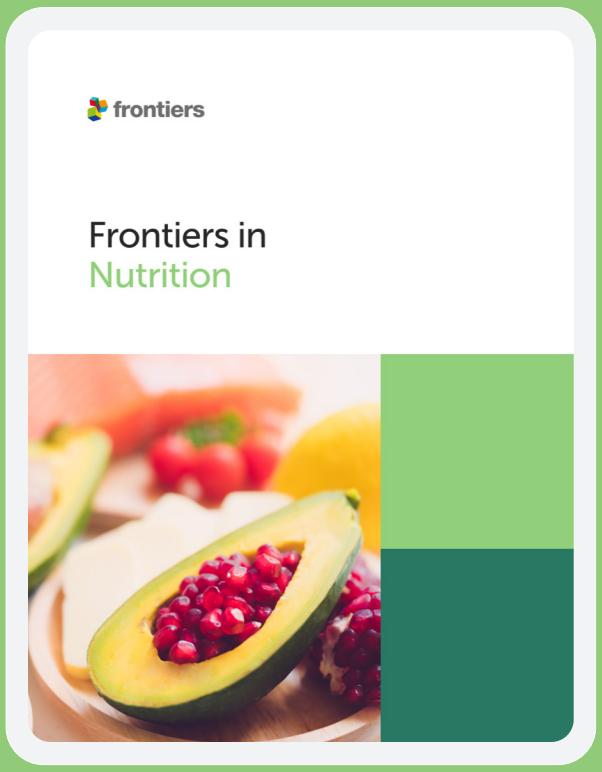

Frontiers

Avenue du Tribunal-Fédéral 34
1005 Lausanne, Switzerland
frontiersin.org

Contact us

+41 (0)21 510 17 00
frontiersin.org/about/contact